General Disclaimer

One or more of the Following Statements may affect this Document

- This document has been reproduced from the best copy furnished by the organizational source. It is being released in the interest of making available as much information as possible.

- This document may contain data, which exceeds the sheet parameters. It was furnished in this condition by the organizational source and is the best copy available.

- This document may contain tone-on-tone or color graphs, charts and/or pictures, which have been reproduced in black and white.

- This document is paginated as submitted by the original source.

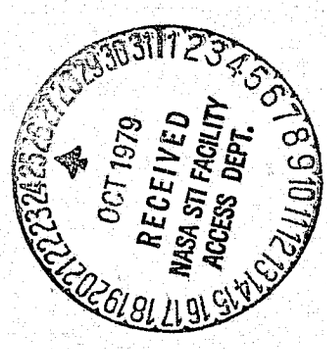
- Portions of this document are not fully legible due to the historical nature of some of the material. However, it is the best reproduction available from the original submission.

Produced by the NASA Center for Aerospace Information (CASI)

Ford Aerospace
955115-Final
Vol 3-(appendix E-N)

(NASA-CR-162371) PHASE 1 OF THE FIRST SOLAR SMALL POWER SYSTEM EXPERIMENT (EXPERIMENTAL SYSTEM NO. 1). VOLUME 3: APPENDIX E - N Final Report (Ford Aerospace and Communications) 187 p HC A09/MF A01 N79-33575

G3/44 Unclas 38929



FOREWORD

This final report documents the technical studies conducted by Ford Aerospace & Communications Corporation, Aeronutronic Division under Contract 955115 to the California Institute of Technology Jet Propulsion Laboratory (JPL) in Pasadena, California. The JPL Technical Manager was Mr. J. R. Womack.

This is a three volume report prepared by the Aeronutornic Division. Subcontractors were the WDL Division of Ford Aerospace & Communications Corporation, Palo Alto, California; United Stirling of Sweden (USS), Malmö, Sweden; Sundstrand Energy Systems, Rockford, Illinois.

The WDL Division was responsible for the concentrator and electrical subsystems. USS provided information on Stirling engines, and Sundstrand supplied information on organic Rankine-Cycle Engines. Additional supporting information was provided by Garrett AiResearch Manufacturing Company, Phoenix, Arizona (closed-cycle Brayton engines); Solar Turbines International, San Diego, California (open-cycle Brayton engines); and Williams Research, Walled Lake, Michigan (open-cycle Brayton engines). Also, the following divisions of the Ford Motor Company provided expertise: Glass Division, Scientific Research Laboratory, and the Manufacturing Planning Group.

The key personnel for the studies documented in this final report are listed below:

- Aeronutronic Division, Ford Aerospace & Communications Corporation

  N. L. Cowden - Program Manager

  R. L. Pons - Technical Manager and Systems Analysis

  T. B. Clark - Optics and Assistant Technical Manager

  D. B. Osborn - Thermodynamics

  E. D. Avetta - Design

  D. C. Jackson - Structures

- WDL Division, Ford Aerospace & Communications Corporation

  H. J. Sund - Subcontract Manager

  I. E. Lewis - Concentrator Subsystem

  J. L. Knorpp - Electrical Subsystem

- United Stirling (USS)

  W. Percival - Consultant to Aeronutronic and Marketing Representative of USS

  Y. Håland - Program Manager for Solar/Stirling Applications

- Sundstrand

  M. Santucci - Principal Investigator, Organic Rankine Engine

- Garrett

  L. Six - Principal Investigator, Closed-Cycle Brayton Engine

- Solar Turbines International

  M. Gramlich

- Williams Research

  R. Mandel

- Ford Motor Company Manufacturing Planning Group

  W. Nagle

T. B. Clark was the editor of these reports.

APPENDIX E

STIRLING ENGINE CONTROL ANALYSIS

Ford Aerospace & Communications Corporation
Aeronutronic Division

Ford Road
Newport Beach, California 92663

TECHNICAL REPORT

TR. NO. 012

SOLAR SMALL POWER SYSTEM (SPS) PROGRAM

TITLE STIRLING ENGINE CONTROL ANALYSIS

PREPARED BY	W. E. Garrigus	ORG NO. L230	CHARGE NO. 2P05-2000
SUPERVISOR APPROVAL	R. E. McCain	DATE 15 December 1978	
PROGRAM ENGINEER APPROVAL	P. L. Pons	TO Distribution	

SUMMARY

This report summarizes the results of meetings held with control equipment suppliers (Basler Corp.), the local electric utility (Southern California Edison) and the engine manufacturer (United Stirling of Sweden), to establish the basic control configuration for the baseline solar SPS. An overall control arrangement is established and various interface requirements are briefly considered.

Distribution

E. D. Avetta
T. B. Clark (2)
N. L. Cowden (2)
H. J. Haskins
D. C. Jackson
I. E. Lewis (WDL)
D. B. Osborn
R. L. Pons
C. C. Wan
L. W. Hau (MTR + 3)

ORIGINAL PAGE IS
OF POOR QUALITY

BACKGROUND

The objectives of the short study reported on in this TR were to examine 1) the special requirements for control of a Stirling cycle engine when employed in a solar application, and 2) the requirements for interfacing a solar-powered engine with an electrical utility grid.

A fuel-powered Stirling engine, as developed by United Stirling-Sweden (USS) for automotive applications, incorporates two separate loops for control of output power (torque and speed) and efficiency. Figure 1 shows the power control loop; engine shaft output is controlled by controlling the pressure and hence the mass of the working fluid* within the engine. It is known as mean pressure level control. The system consists of a high pressure reservoir, a compressor, a servo-driven valve** and associated plumbing that permits the working fluid to be moved into or out of the engine at will. Note that this technique of "inventory" control is characteristic of closed cycle heat engines.

Figure 2 shows the second control loop, which provides for metering both air and fuel flow (modified Bosch K-Jetronic system) to the burner head of the engine in order to keep head temperature (actually tube wall temperature) constant -- and hence maintain constant engine efficiency -- independent of the operation of the power control loop.

SPECIAL SOLAR REQUIREMENTS

It is both impractical and undesirable to try to vary the sun's input to the engine -- as the automotive Stirling varies the amount of fuel burned. The impracticality stems from the difficulty of either shuttering the solar input or of bypassing part of the sodium vapor, e.g., to a condenser and back to the receiver/boiler unit. The undesirability stems from the reduced power output associated with this method of control. It seems obvious, therefore, that the control scheme must be configured to accept all of the solar energy directed to the receiver. One way to accomplish this is to "slave" the existing power control loop to engine head (or receiver) temperature; this arrangement permits output power to "follow" the solar input power curve while maintaining constant system temperature. There are special requirements for system start-up and subsequent grid synchronization, however, as discussed in the following paragraphs. The information presented in these paragraphs is based on extensive discussions with engineering personnel of the Basler Corp. (a major manufacturer and installer of power plant control equipment) and the Southern California Edison Company. Preliminary discussions were also held with engineering personnel representing the engine manufacturer, USS.

---

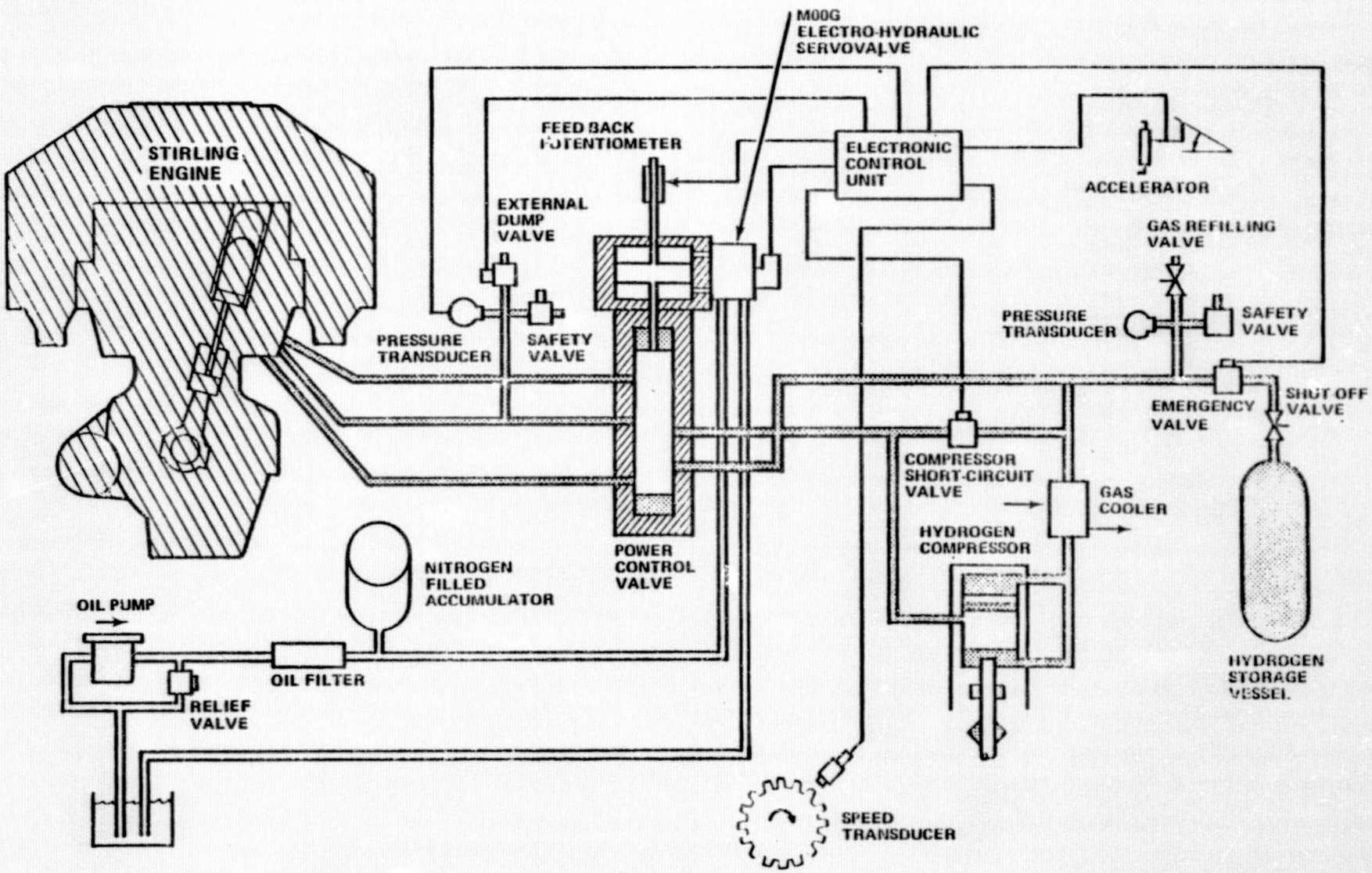
* For a fuel-powered engine, the working fluid is Hydrogen; for the solar application, it is Helium.

** The power control valve is a hydraulic slide valve unit designed and built by USS; it is driven by a Moog Series 76 electro-hydraulic servo valve.

Ford Aerospace &
Communications Corporation
Aeronutronic Division

FIGURE 1.

USS MEAN PRESSURE CONTROL SYSTEM

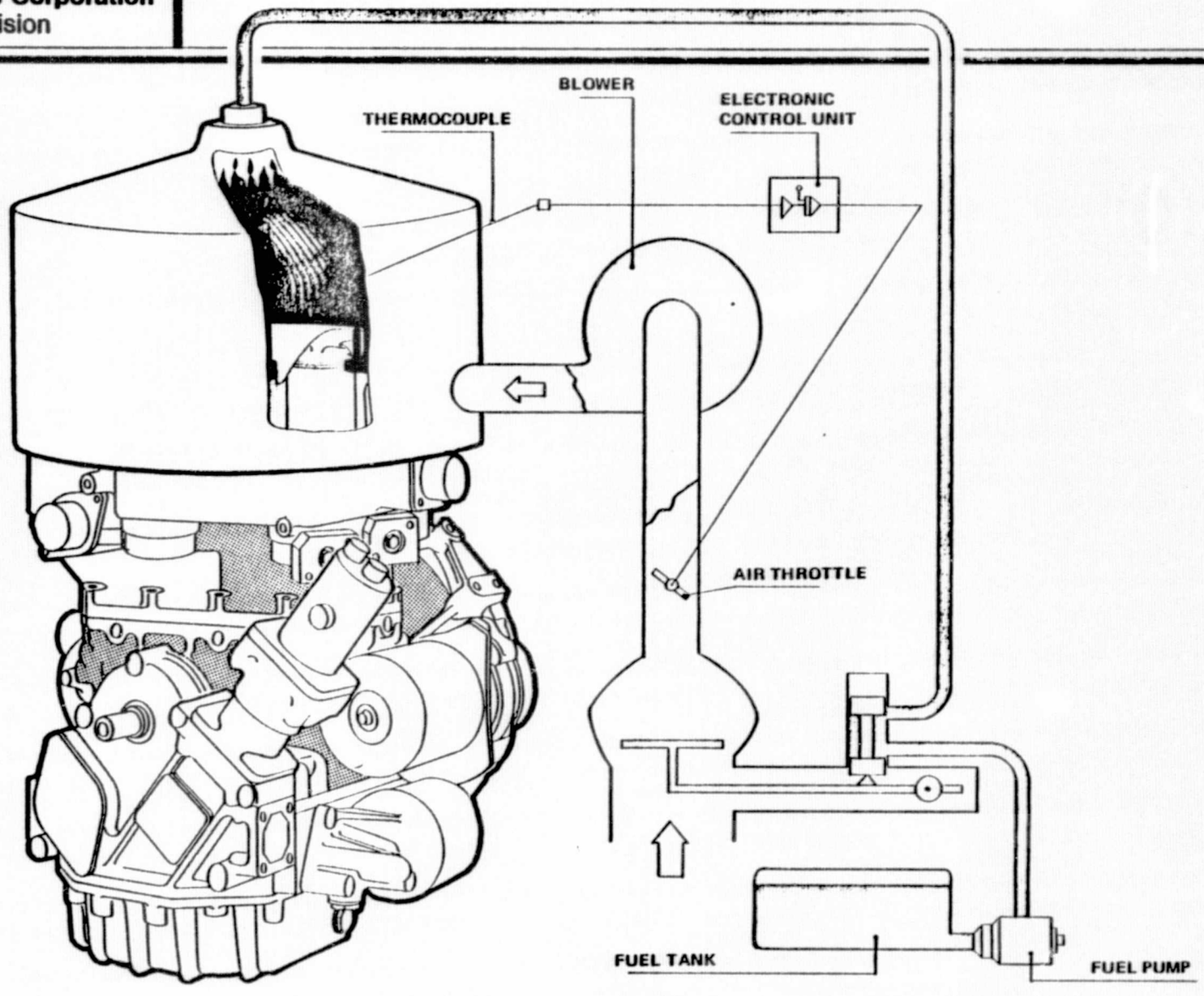


E-3

ORIGINAL PAGE IS
OF POOR QUALITY

FIGURE 2.

AIR/FUEL CONTROL SYSTEM



OVERALL POWER SYSTEM

The block diagram for the overall system is shown typically in Figure 3. Each solar module (collector, Stirling engine and alternator assembly) will have separate automatic and manual override controls to place each alternator "on-line" by actuating a unit power contactor. For maintenance, repair, etc., each set of modules could also have a power contactor (both automatic and manual modes) to place the entire string, e.g., line "A" of Figure 3, on the grid. (The line power contactors are an optional feature.) Also, the energy storage system will be controlled to supply stored energy per overall system requirements. The microprocessor will provide automatic control for all modules except for the automatic "on-line" and "off-line" control equipment built into each module. Energy delivery sensing and recording equipment will be supplied by the utility company. The master control and transfer unit will include a mimic bus and status indicators. All alternators will operate in the "scramble" mode (each alternator independently "scrambles" to get onto the utility grid as soon as it can) and each alternator voltage regulator will operate with parallel droop compensation. All alternators are delivering power to an "infinite" bus, i.e., the voltage and frequency are independent of the solar system power level.

STIRLING ENGINE OPERATION

As mentioned above, it is necessary that the engine remove power from the receiver at essentially the same rate as the net solar input to the receiver. This automatically assures constant temperature operation, which in turn provides high overall system efficiency and minimizes the deleterious thermo-structural effects of thermal cycling. The only direct means for controlling engine output is through the existing power control subsystem. This is accomplished by driving the power control valve so as to satisfy the requirements for different modes of operation, e.g., 1) start-up, 2) grid synchronization, 3) on-line operation and 4) emergency shutdown. A preliminary approach to establishing the control sequences and associated hardware is given below. The approach is predicated on the following observations:

- The combination of receiver and heat transport components comprise a very slow response system (typically 1 to 2 minutes to show significant temperature change due to large step changes in either input solar flux or in power removed by the engine)

- The engine/alternator combination is a comparatively fast response system (idle to full power in less than 1 second)

- It is undesirable to try to pull high power from the engine at head temperatures less than about 100°C-200°C below steady-state operating temperature. In a closed system as employed the rapid drop in sodium vapor pressure and density with lowered temperature results in flow choking in the vapor pipe connecting the receiver/boiler to the head of the engine. An unreasonably large increase in pipe diameter would be required to avoid choking at the vapor mass flow rates corresponding to operation near rated power.

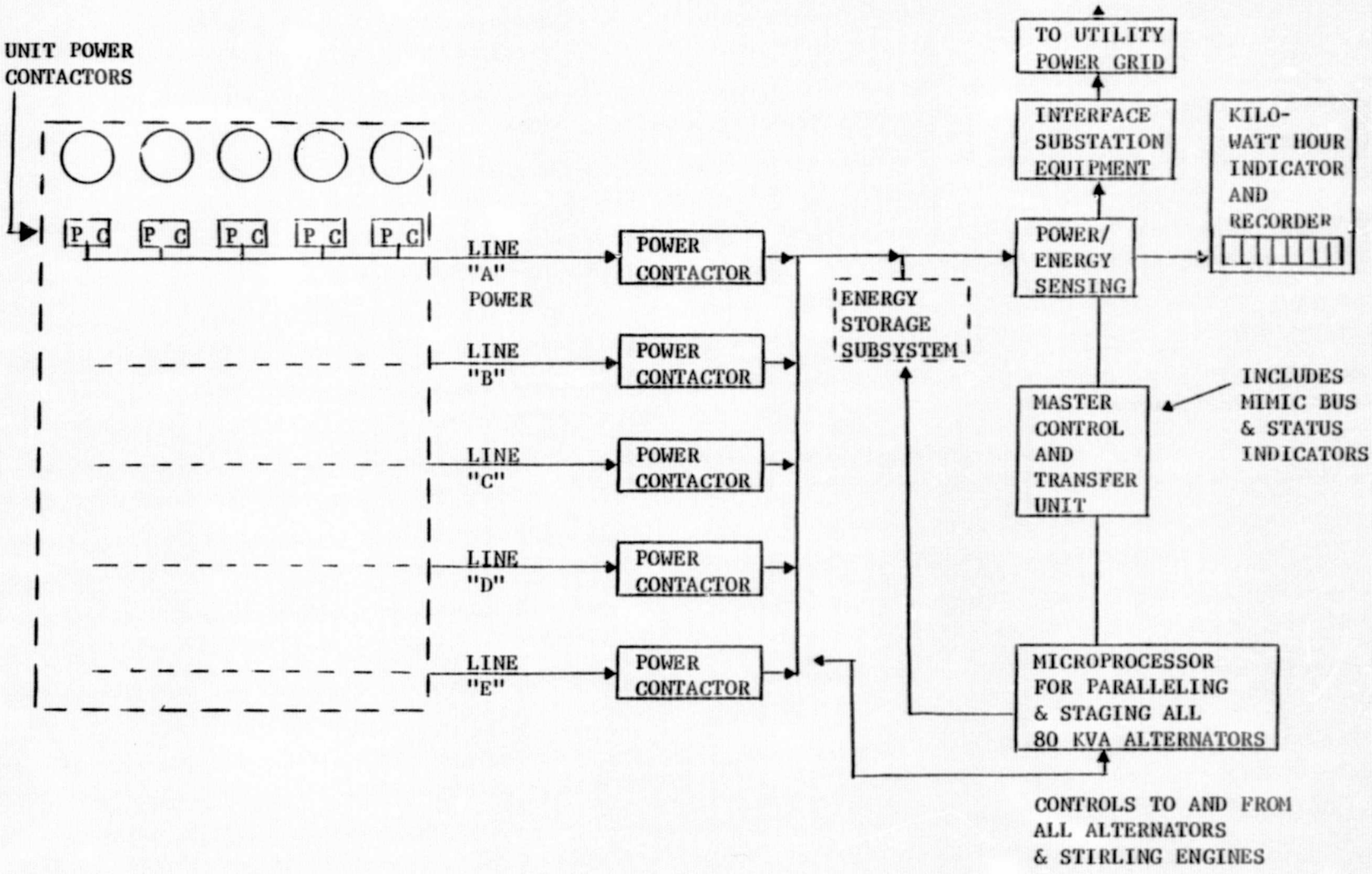


FIGURE 3. OVERALL SYSTEM CONFIGURATION

- For a system with a large number of modules, it is desirable to get all engines up to speed and quickly locked onto the utility grid at low power level, then bring each engine up to full power as soon as the operating temperature range is reached.

Careful consideration of these points suggests the following sequence:

1. Start each engine as soon as there is sufficient temperature and input solar flux for self-sustained operation. The engine will operate (unloaded) at idle speed, developing sufficient power to overcome internal work (friction and compression) as well as the drag of the alternator.

2. Move the power control valve to increase Helium pressure in the engine, thereby increasing engine torque and speed until alternator output frequency, voltage and phase are matched to grid values. Close line switch (contactor) and lock onto grid at lower power level. The grid will hold the engine at essentially constant speed.

3. When engine head temperature reaches the proper value, move the power control valve further and increase engine torque (speed is constant) until the energy withdrawn from the receiver matches the net input from the sun. As the solar power input increases or decreases, modulate the power control valve to maintain constant temperature (within the appropriate control band).

4. In the event of an emergency, e.g., sudden unloading of the engine, overspeed damage would be avoided by quickly moving the power control valve so as to release the working fluid from the engine to the reservoir, thereby shutting the engine down.

Implementation of this sequence of operation is proposed as follows:

Start-up

At shut-down on the previous day, the remotely-actuated blocking valve was closed to prevent heat leak to the engine overnight via the sodium vapor line. Also, most of the Helium was evacuated from the engine to minimize seal leakage overnight. When the sun reaches the minimum elevation angle achievable with the collector, identifiable either by a sun-tracking signal or by signal from a programmable timer, 1) the module is moved into position, 2) the cover of the cavity receiver is rotated into the stowed position (letting the focussed solar beam into the aperture), 3) the power control valve is moved to permit engine pressurization with Helium to 30-50 atm, and 4) the blocking valve is opened to permit the still-hot* sodium vapor to warm up the vapor pipe and the engine heater head assembly.

*Normal nighttime conditions serve to keep the sodium temperature in the receiver well above 250°C; for extended bad weather, however, the sodium can freeze and the engine should not be started until the sodium is melted and raised to at least 250°C.

Upon receipt of sensor signals that 1) verify that head temperature is $\geq 250^{\circ}C$, 2) verify that the sun is putting at least "threshold" energy into the receiver and 3) verify engine Helium pressure level, the starter motor is engaged.

With the power control valve set in the idle power position, the engine will come up to 750 rpm idle speed in approximately 6 seconds and the starter motor will automatically disengage. Engine speed will hold constant at 750 rpm by action of a shaft governor which modulates the power control valve; it is part of the existing power control system. The engine is now ready to be placed on-line while the sun continues to warm up the receiver.

Synchronization

When the head temperature reaches a pre-selected value ($\sim 500^{\circ}C$), the power control valve is placed under command of the grid synchronizer (typically a Basler PRS-370 and associated equipment) which moves the valve to increase Helium pressure within the engine, causing a simultaneous increase in engine shaft torque and speed (increased power). Once the correct speed is reached, the synchronizer "dithers" the valve (and thus engine speed) to obtain correct phase; upon verification of voltage, frequency and phase match with the grid, the synchronizer activates a unit power contactor and the system is locked onto the grid, with the engine speed held essentially constant and the power valve in a "minimum" power setting. With this action, the synchronizer releases control of the power valve to the engine head temperature sensor, as shown in Figure 4, and the system is now ready for normal on-line operation*.

On-Line Operation

Engine heater head temperature will continue to rise since the net solar input power is much greater than the power removed by the engine. The engine power setting will remain at the "minimum" position until the temperature rises to a pre-determined value, e.g., above the steady state operating point but within the temperature deadband. At this point the temperature controller moves the power valve to bring the engine up to a torque level such that more energy is removed from the receiver than is supplied by the sun and the temperature will begin to drop. From this point on the power valve is modulated to hold temperatures within the control band as the solar flux varies during the day. Figure 5 shows temperature, speed and torque histories for a typical starting sequence.

Emergency Shutdown

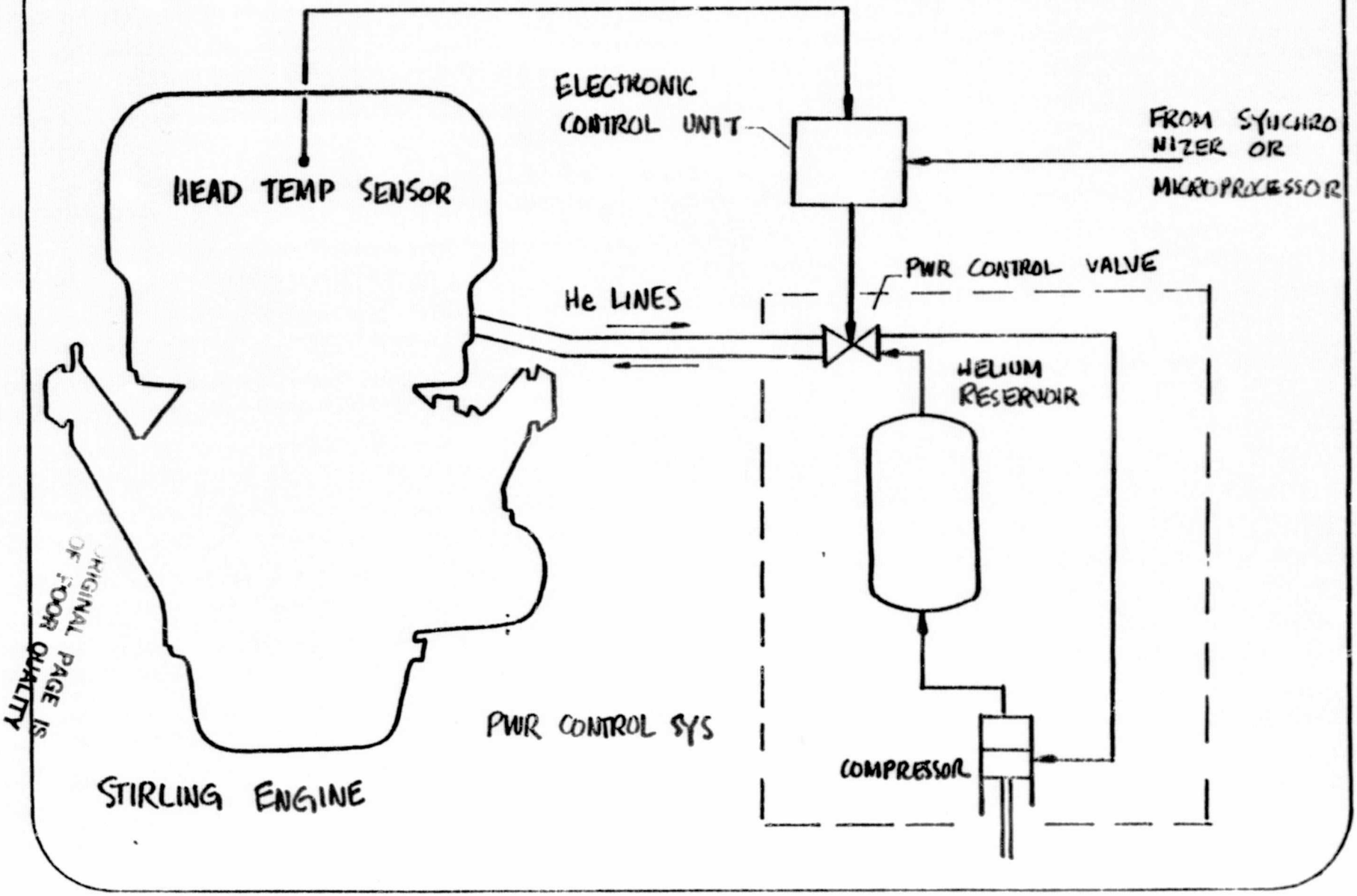
As indicated previously, an overspeed sensor is keyed to the engine drive shaft and switches the engine power control valve into a "dump" position so that the working fluid is rapidly removed from the engine and the power is

*Further FACC power control subsystem analyses suggest that an alternate approach employing the central microprocessor for sequential synchronization is less costly. The actual synchronization procedure, however, is unchanged. Documentation of the results of these analyses is forthcoming.

Ford Aerospace & Communications Corporation

FIGURE 4.

SOLAR- STIRLING CONTROL SCHEME

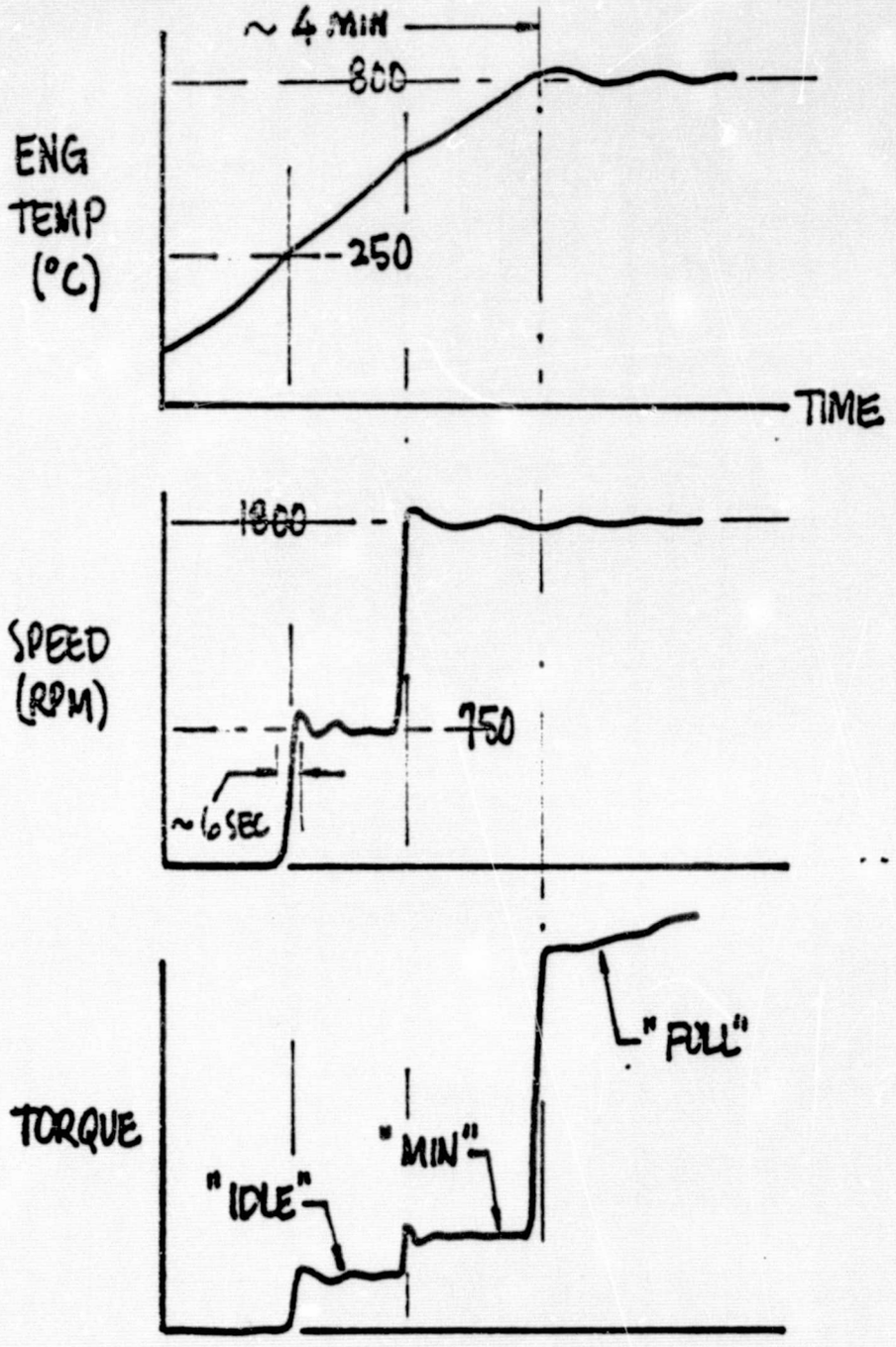


ORIGINAL PAGE IS OF POOR QUALITY

FIGURE 5

Ford Aerospace & Communications Corporation

SOLAR STARTING SEQUENCE (TYPICAL)



reduced to idle level (or zero) to prevent damage in the event of inadvertent, sudden loss of load from the grid. This is similar to the "short-circuit" feature currently incorporated in the automotive power control. Other events would occur simultaneously with the power dump operation, e.g., the concentrator azimuth/elevation drive system would be signalled to defocus the complete module and the unit power contactor would open to make certain that the alternator is off-line.

United Stirling has indicated that it may be desirable to modify the existing "short-circuit" technique if engine shutdown in ~ 20 seconds is acceptable. Furthermore, since the solar operation does not have the numerous start/stop characteristics of the automotive operation, some power can be saved by adding a small low-pressure reservoir on the suction side of the compressor, and running the compressor only intermittently, i.e., just to keep the high pressure reservoir charged up (typical of air brake operation on trucks).

Engine load is supplied by the alternator, whose operation is described in the following paragraphs.

ALTERNATOR

The operation of the alternator is considered in terms of its operating modes, control equipment/operation and its interfaces, as described below:

1. Basic Operation

The alternator is directly connected* to the Stirling engine; a shaft coupling will be provided for assembly/disassembly as required. The power input to the alternator is thus the power output of the Stirling engine which is proportional to the product of Torque X Speed. As previously stated, once the alternator is connected to the utility grid its speed is held fixed by the grid since speed is proportional to frequency. Thus, as the engine power output is varied by the control system to accommodate varying solar flux, only the shaft torque will vary. The alternator power output is in turn proportional to the product of Voltage X Current since its output voltage is held fixed by the utility grid voltage, the current will vary in proportion to the input torque variation.

2. Controls

Alternator/engine control arrangements are shown in Figure 6. A number of synchronizer circuits are available to synchronize the alternator with the electric utility grid before connecting to it. The Basler PRS 370 will provide the proper phase matching functions between the alternator and the line by controlling the speed of the Stirling engine, as discussed previously; its

*System studies indicate optimum engine speed is 1800 rpm, which is the selected value for the alternator; thus, no gearbox is necessary.

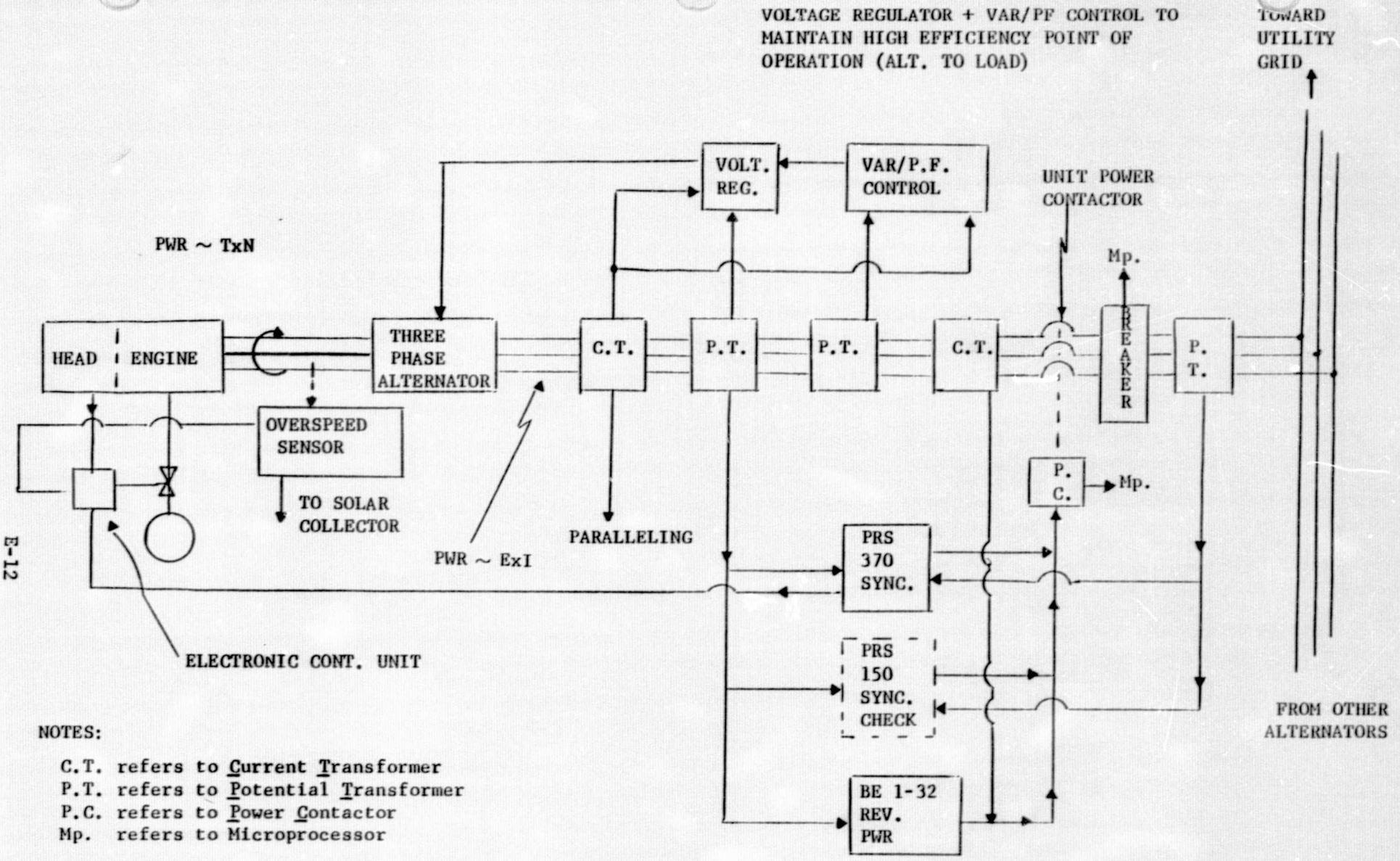


FIGURE 6. ALTERNATOR/ENGINE CONTROL CIRCUITS

approximate cost is $520. The Basler PRS 150 Sync Check, at an additional cost of $918, may be desirable. It will not allow the alternator on-line unless both phase and voltage are within close tolerances.

Southern California Edison requires Volt-Amperes Reactive (VAR) control to minimize VAR losses in the electrical system. The alternator and the load usually have some inductive reactances which result in load conditions having both in-phase power and reactive power as shown in Figure 7 below:

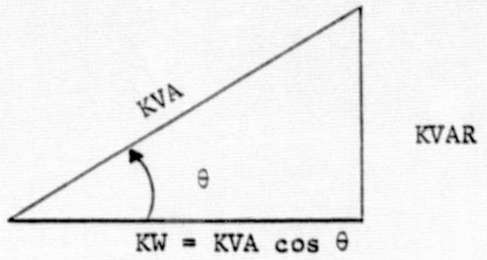


FIGURE 7. KW-KVA TRIANGLE

The horizontal leg of the triangle represents true electrical power (KW) delivered; the vertical leg is proportional to the kilovolt-ampere product and represents reactive power. The cosine of the angle, θ, is the power factor; to prevent excessive VAR losses, the power factor must be kept above approximately 0.8. When the alternator is connected to the utility grid, this is accomplished by varying the alternator field to control the KVAR/KW ratio. Basler makes VAR control circuits for most alternators. They can supply an existing VAR control as well as a voltage regulator to go in the alternator circuit as shown previously in Figure 6.

A reverse power control circuit is also required to prevent utility grid power from entering the alternator. A Basler BE-1-32 unit (or equivalent) must be included.

3. Multiple Alternator Operation

As discussed previously, it is desirable to connect the alternator to the grid as quickly as possible to provide load for the engine. By operating all alternators in the scramble mode, each alternator will go "on-line" as soon as it is rotating at the required speed (frequency) and phase. This is the normal mode for utility operation where the alternators are being operated into an "infinite" bus. For example, at the San Onofre Nuclear Plant, 12 steam turbine-electric generating units -- at 50 MW each -- are "scrambled" onto the SCE/SDGE grid, without introducing dynamic instability in the grid.

The voltage regulators will be connected in the parallel droop compensation mode. In this mode, the regulator circuits have interconnections between all alternators. Without these circuits, one or more alternators might have excessive currents in the windings resulting in an overload condition.

4. Utility Interface

The utility interface will be as indicated in Figure 8. The utility will provide sensing circuits as indicated and the power contactors will be opened at any abnormal operation. SCE indicates that there may be no warning before they disconnect, so it is essential that we be able to de-focus the solar collectors sufficiently fast to prevent damaging temperature overshoot in the receiver and in the engine heater head.

The solar power system will need lightning protection; SCE would provide this protection in their package, if necessary; further analysis of this issue is required.

In consideration of Phase II of the program, SCE indicated that SPS power -- from one or more test units -- could be worked into the Aeronutronic plant electrical grid if desired. The special interface equipment would cost roughly $200 per month.

CONCLUSIONS

A preliminary analysis of the SPS control requirements has been made and an initial system mechanization identified. More detailed analysis is required to definitize the system. For example, the following information is required:

1. Transfer characteristics of the current Stirling engine power control valve

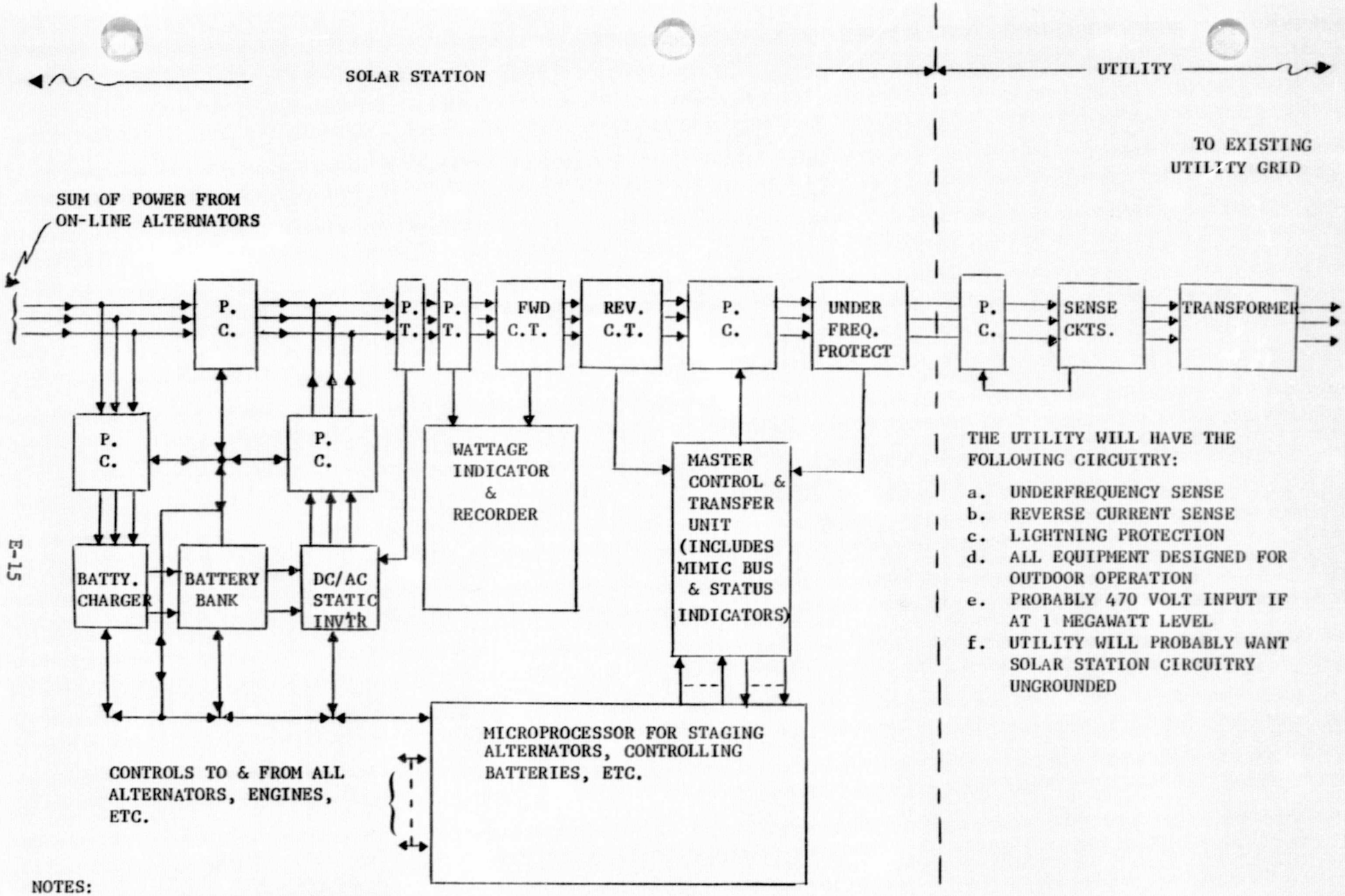
2. Engine head temperature sensor characteristics

3. Data requirements for the microprocessor

4. Alternator characteristics

5. Other interface data, e.g., the energy storage system, the master control and transfer unit (including the mimic bus and status indicators), the energy indicator and recorder, the energy transfer unit

Also, additional analysis should be carried out to address the control requirements for accommodating engine operation during transient cloud passage.



THE UTILITY WILL HAVE THE FOLLOWING CIRCUITRY:

a. UNDERFREQUENCY SENSE
b. REVERSE CURRENT SENSE
c. LIGHTNING PROTECTION
d. ALL EQUIPMENT DESIGNED FOR OUTDOOR OPERATION
e. PROBABLY 470 VOLT INPUT IF AT 1 MEGAWATT LEVEL
f. UTILITY WILL PROBABLY WANT SOLAR STATION CIRCUITRY UNGROUNDED

NOTES:
C.T. referrs to Current Transformer
P.T. refers to Potential Transformer
P.C. refers to Power Contactor
Mp. refers to Microprocessor

FIGURE 8. UTILITY INTERFACE

APPENDIX F

BRAYTON CYCLE PERFORMANCE MODELS

Part I - Closed Cycle - page F-1

Part II - Open Cycle - page F-21

Ford Aerospace & Communications Corporation
Aeronutronic Division

Ford Road
Newport Beach, California 92663

TECHNICAL REPORT

TR. NO. 3PS-014

SOLAR SMALL POWER SYSTEM (SPS) PROGRAM

TITLE CLOSED BRAYTON CYCLE PERFORMANCE MODEL

PREPARED BY	T. L. Pons	ORG NO. L280	CHARGE NO. 2P05-2000
SUPERVISOR APPROVAL	W. C. Barnum	DATE 05 January 1979	
PROGRAM ENGINEER APPROVAL	R. L. Pons	TO Distribution	

SUMMARY

The Garrett CCPS-40 Gas Turbine is mathematically modeled to permit determination of annualized SPS power output and to identify working fluid mass flow rates required for sizing the solar receiver.

DISTRIBUTION

E. D. Avetta
W. C. Barnum
T. B. Clark
N. L. Cowden (2)
R. M. Grabow
H. J. Haskins
D. C. Jackson
I. E. Lewis (WDL)
R. A. Maxwell
D. B. Osborn
R. M. Taylor
H. R. Wahlin
C. C. Wan
D. J. Corn (3 + MTR)

BACKGROUND

This report summarizes results of a preliminary analysis carried out for a closed Brayton cycle engine -- specifically the Garrett CCPS-40-1 Gas Turbine shown in Figure 1 -- as an initial step in evaluating its applicability to the solar SPS concept. The basic objectives of the analysis were 1) to determine engine output (shaft) power, P_o, as a function of input power, P_i, and ambient temperature, T_a, and 2) to establish working fluid mass flow requirements. Objective (1) was formulated to permit determination of annualized SPS power output; objective (2) was formulated to permit sizing of the solar receiver.

Selection of a closed cycle engine for initial study was predicated on a recommendation by Garrett personnel for the following reasons:

1) The engine can be operated at constant speed and constant turbine inlet temperature (TIT) over the entire power range. Power variation is achieved by inventory control, i.e. by varying the amount of working fluid in the engine. Engine efficiency is nearly constant over the power range. Without an expensive infinitely-variable ratio gear box, an open-cycle engine would require TIT variation for power control at constant speed and part-load efficiency would be substantially reduced.
2) By operating at high working fluid pressure, effectiveness of the heat exchangers is improved, resulting in smaller, lighter, less costly units than would be required by an open cycle machine.

APPROACH

The approach taken here employs well-established theoretical cycle analysis to generate an equation relating P_i, P_o and T_a. The cycle analysis, however, is modified to accommodate component performance data derived from tests conducted by the U. S. Navy on the CCPS-40 engine as reported in Reference 1.

Performance estimates are also made for the CCPS-40 engine with future improved component efficiencies as suggested by Garrett.

ANALYSIS

As derived in the Appendix, a generalized efficiency equation for the CCPS-40 engine is

$$\eta_E = \left[\frac{\eta_t \xi_t - \frac{\xi_c}{\eta_c}\left(\frac{T_a}{T_4}\right)\left(\frac{T_1}{T_a}\right)\left(\frac{\dot{m}_c}{\dot{m}_t}\right)}{1 - \epsilon_1 \tau_t - (1-\epsilon_1)\tau_c\left(\frac{T_a}{T_4}\right)\left(\frac{T_1}{T_a}\right)} \right] \psi \qquad (1)$$

where

η_t = Turbine efficiency

η_c = Compressor efficiency

$\xi_t = 1 - (\beta R_c)^{-K}$ and $\tau_t = 1 - \eta_t \xi_t$

$\xi_c = R_c^{K} - 1$ and $\tau_c = 1 + \xi_c/\eta_c$

R_c = Compressor pressure ratio

β = Pressure drop parameter = R_t/R_c

R_t = Turbine pressure ratio

$k = \frac{\gamma-1}{\gamma}$, $\gamma = C_p/C_v$ = Ratio of specific heats = 1.667 for Argon

T_a = Ambient temperature, ^oK

T_4 = TIT, ^oK

T_1 = Compressor inlet temperature, ^oK

$\dot{m}_c$ = Compressor mass flow rate, Kg/sec

$\dot{m}_t$ = Turbine mass flow rate, Kg/sec

ψ = Correction factor

and

$$\frac{T_1}{T_a} = \frac{\varepsilon_2 + (1-\varepsilon_2)\ \tau_t \left(\frac{T_4}{T_a}\right)\ (1-\varepsilon_1)}{1-\varepsilon_1\ (1-\varepsilon_2)\ \tau_c} \qquad (2)$$

where

ε_1 = Recuperator effectiveness (high pressure side)

ε_2 = Cooler effectiveness (working fluid side)

Note that Equation (1) includes an allowance for bleeding some of the working fluid (Argon) off of the compressor discharge in order to cool the bearings, as reported in Reference 1. Also, the factor ψ is introduced to accommodate the influence of mechanical/thermal losses and Argon leakage; comparison with the test data of Reference 1 indicates that $\psi = 0.93$ gives good data correlation.

- Compressor Pressure Ratio

Figure 2 shows engine efficiency as a function of compressor pressure ratio, R_c, for the CCPS-40 engine as it is presently configured, with the

following parameters and component efficiencies corresponding to a nominal power output of 25 KW:

$\eta_c = 0.757$ $\quad\quad$ $\beta = 0.935$

$\eta_t = 0.872$ $\quad\quad$ TIT = 816°C (1500 F)

$\varepsilon_1 = 0.895$ $\quad\quad$ $T_a = 44.6°C$ (112 F)*

$\varepsilon_2 = 0.960$

Figure 2 shows that maximum efficiency occurs in the vicinity of $R_c = 2$; according to Reference 1 the nominal R_c for the CCPS-40 engine is 1.89. Subsequent performance calculations have all been carried out at this value, assumed invariant with changes in working fluid pressure/mass flow.

- Effect of Component Performance

Reference 1 provides test data on compressor and turbine efficiencies as well as on recuperator and cooler effectiveness. The smoothed data for these parameters are given in Figure 3, corresponding to the following curve fits:

$$\eta_c = 0.77 - .0005\ P_o \tag{3}$$

$$\eta_t = 0.0683 + 0.6941\ (P_o)^{.046} \tag{4}$$

$$\varepsilon_1 = 0.9249 - 7.917\ (10)^{-5}\ (P_o)^{1.79} \tag{5}$$

$$\varepsilon_2 = 0.98015 - 1.3474\ (10)^{-9}\ (P_o)^{5.06} \tag{6}$$

Substitution of Equations (3) - (6) into Equation (1) yields engine efficiency vs. output power as shown in Figure 4. The comparison with the test data of Reference 1 is well within $\pm$ 10% over the entire power range. The data are replotted in Figure 5 as P_o vs. P_i; Equation (1) is seen to correlate the test data quite well.

- Generalized Performance

It is assumed that TIT will not exceed 816°C (1500°F) for the foreseeable future, primarily due to materials limitations; for $R_c = 1.89$, $\beta = 0.935$ and $\dot{m}_c/\dot{m}_t = 1.033$, Equation (1) for CCPS-40 engine efficiency becomes:

---

*This value corresponds to hottest Barstow day when solar insolation is 800 w/m^2.

$$\eta_E = \left[\frac{(0.204)\eta_t - \frac{(0.3)}{\eta_c}\left(\frac{T_a}{T_4}\right)\left(\frac{T_1}{T_a}\right)}{1 - \varepsilon_1\tau_t - (1-\varepsilon_1)\,\tau_c\left(\frac{T_a}{T_4}\right)\left(\frac{T_1}{T_a}\right)} \right] 0.93 \qquad (7)$$

where

$$\tau_t = 1 - \eta_t\xi_t = 1 - (0.204)\eta_t$$

$$\tau_c = 1 + \xi_c/\eta_c = 1 + 0.291/\eta_c$$

Equation (7) is plotted in Figure 6 for ambient temperatures of 10°C, 30°C, and 50°C. A curve fit to these data yields:

$$P_o = [0.30375 - .001275(T_a)]\,(P_i + 6) - 1 \qquad (8)$$

where

$T_a \sim {}^{o}C$

$P_o, P_i \sim KW$

Equation 8 thus provides the desired relationship between P_i, T_a and P_o.

- Mass Flow Rate

The power generated by the turbine, P_t, is:

$$P_t = \dot{m}_t\eta_t\, C_p\, T_4\xi_t\psi, \ \frac{K\text{-cal}}{sec} \qquad (9)$$

where

$\dot{m}_t \sim$ Kg/sec

$C_p \sim 0.124$ K-cal/Kg°K

$T_4 \sim {}^{o}K$

and the power consumed by the compressor, P_c, is

$$P_c = \frac{\dot{m}_c C_p T_1 \xi_c \psi}{\eta_c} \quad , \quad \frac{\text{K-cal}}{\text{sec}} \tag{10}$$

The net power output is thus $P_o = P_t - P_c$ or:

$$P_o = (4.188)\, \dot{m}_c C_p T_a \left\{ \eta_t \left(\frac{T_4}{T_a}\right) \xi_t \left(\frac{\dot{m}_t}{\dot{m}_c}\right) - \frac{1}{\eta_c}\left(\frac{T_1}{T_a}\right) \xi_c \right\} \psi \ , \ \text{KW} \tag{11}$$

Equation (11) permits solution of the mass flow rate, $\dot{m}_c$, as a function of P_o and T_a, for the proscribed $T_4 = 816^{\circ}C$, $R_c = 1.89$, $\beta = 0.935$ and the curve fits given by Equations (3) - (6). Typical results are shown in Figure 7; mass flow rate is nearly linear with output power.

POTENTIAL PERFORMANCE IMPROVEMENTS

If TIT is held to 816°C for the foreseeable future, improvements in engine performance must come from improvements in the various components. The "schedule" for such improvements is obviously speculative since there are significant cost implications. We assume, however, that for the near future, i.e. ca 1982, the most expeditious thing to do is 1) to improve recuperator effectiveness, ε_1, by increasing heat exchanger surface area and 2) to increase β by increasing flow passage size wherever possible, particularly in the interconnecting ducts. Both types of improvements obviously require engine repackaging. The performance gains corresponding to estimated values of $\varepsilon_1 = 0.93$ and $\beta = 0.95$ are shown in Figure 8 for a nominal power output of 25 KW. Peak efficiency is increased from 25.1% to 28.4%.

For the far term, ca 1990, the rotating group could be redesigned; the additional performance gain achieved by going to estimated values of $\eta_c = 0.85$ and $\eta_t = 0.92$ are also shown in Figure 8; max $\eta_E = 36.7\%$.

CONCLUSIONS/RECOMMENDATIONS

A simple expression has been derived which will permit determination of the annual power output of a solar-driven closed Brayton cycle engine, specifically the Garrett CCPS-40 engine. Working fluid mass flow rates have also been determined to permit sizing the solar receiver.

Estimates of improvements in component performance with further development have also been made and the effect on engine performance has been evaluated at a single power point. It is recommended that performance expressions similar to the aforementioned one be generated over the complete power range to ascertain the annualized performance change with the estimated component improvements.

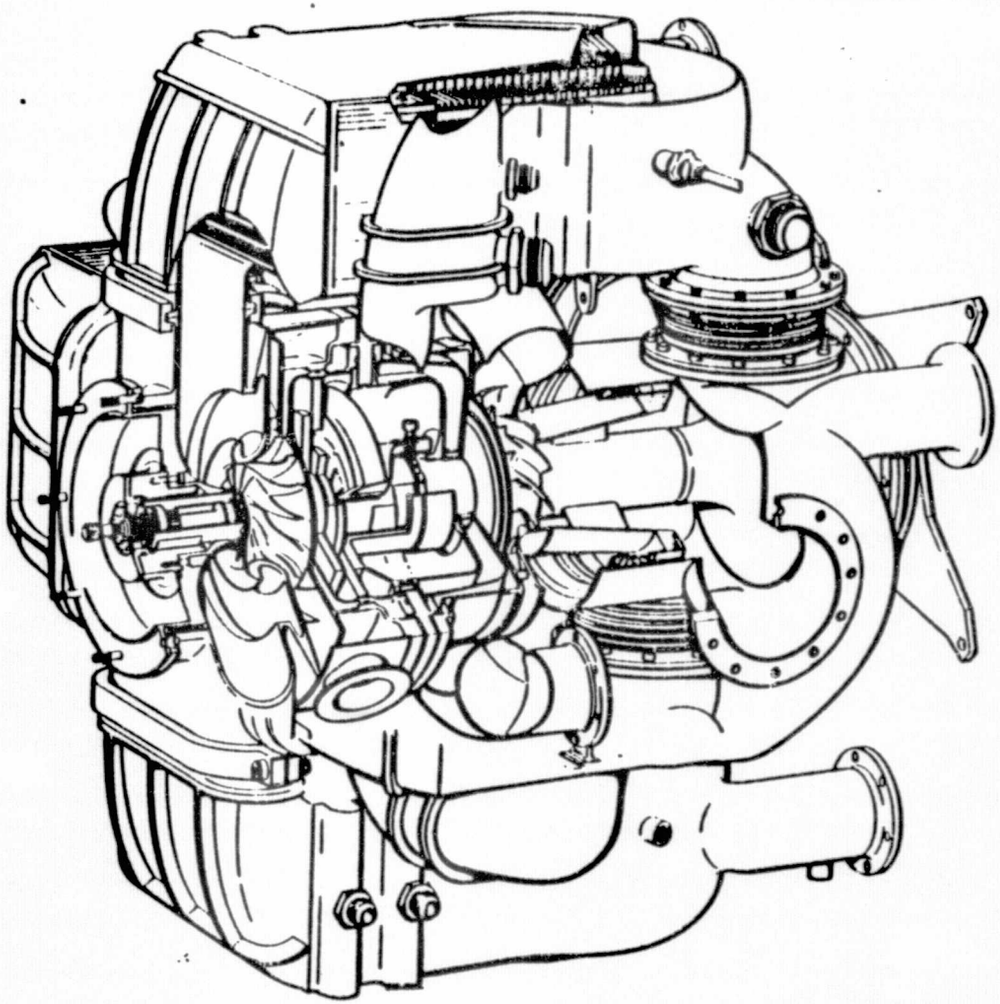
It is also recommended that similar analyses be carried out for the open Brayton cycle engine before final judgements are made regarding the optimum SPS engine selection.

REFERENCE

1) Duvall, Gordon D., "Operational Evaluation of a Closed Brayton Cycle Laboratory Engine", 11th Intersociety Energy Conversion Engineering Conference, 1976.

FIGURE 1

CCPS 40-1 CLOSED CYCLE ENGINE



ORIGINAL PAGE IS
OF POOR QUALITY

FIG. 2 **BASELINE ENGINE PERFORMANCE**

CCPS-40

TIT = 816 C (1500 F) η_c = 0.757

T_a = 44.6 C (112 F) η_t = 0.872

β = 0.935 ϵ_1 (RECUP) = 0.895

P_0 = 25 KW ϵ_2 (COOLER) = 0.960

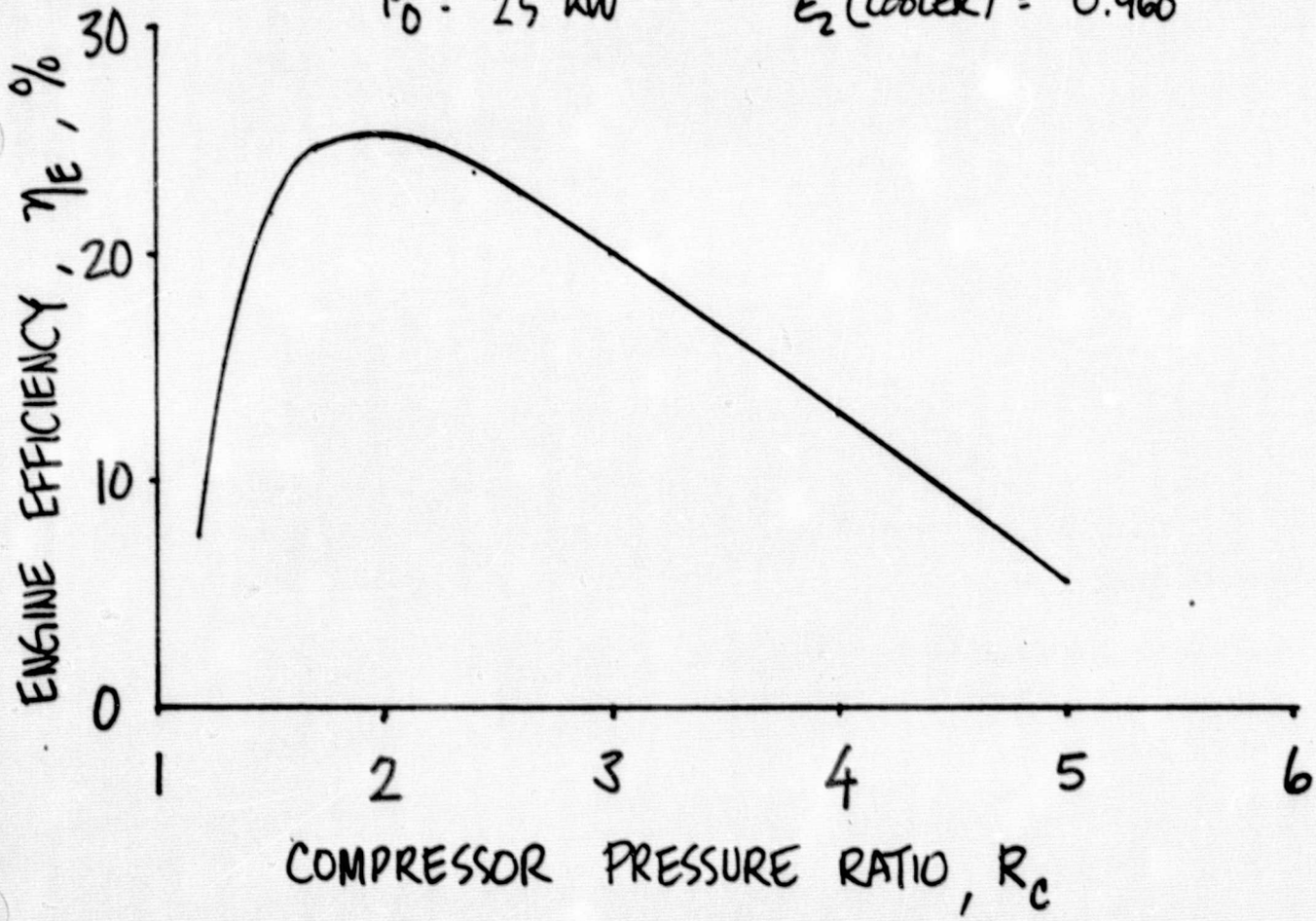
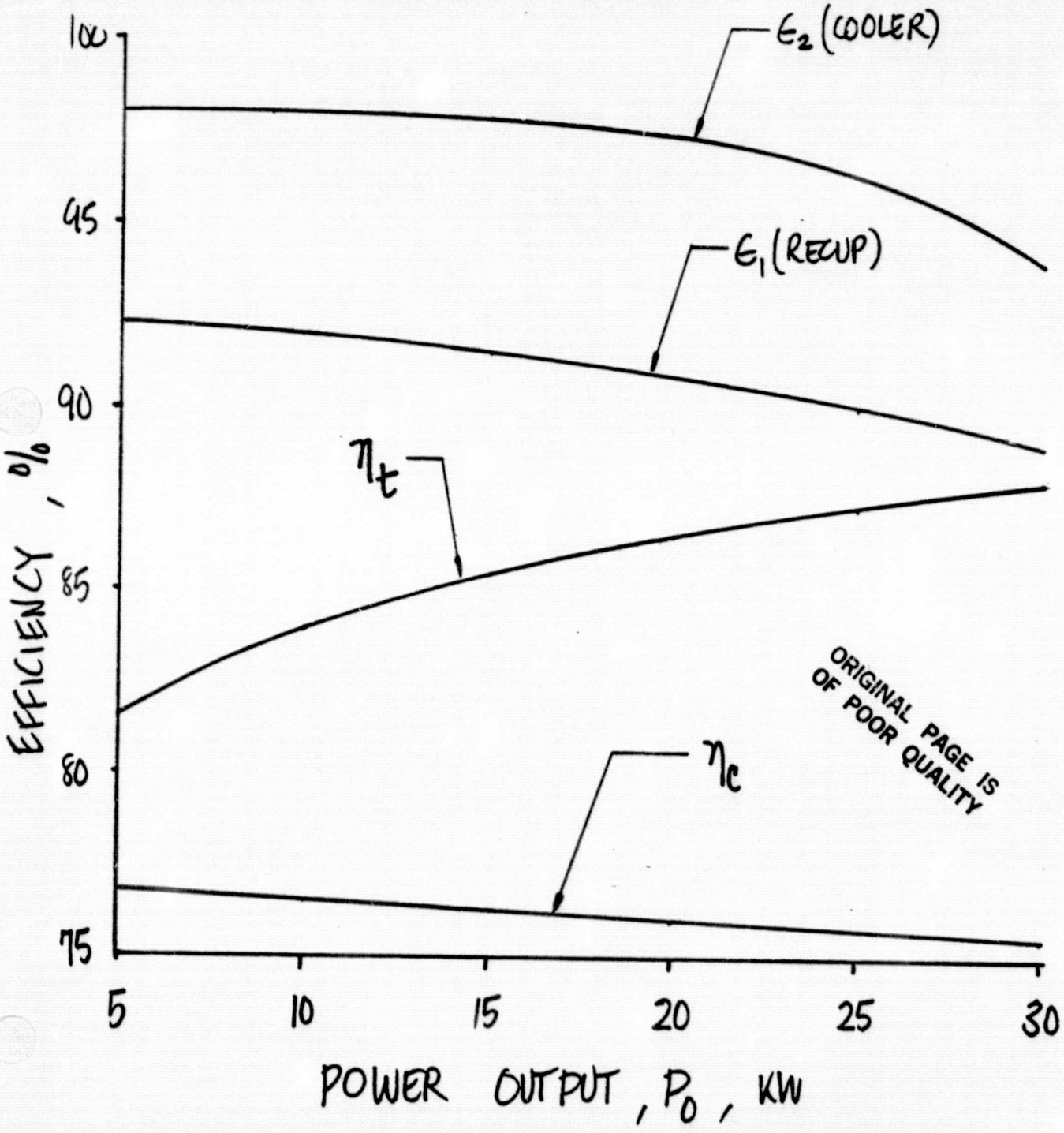


FIG. 3 COMPONENT EFFICIENCIES



ORIGINAL PAGE IS
OF POOR QUALITY

FIG 4 TEST DATA CORRELATION

$R_C = 1.89$

$\beta = 0.935$

3.2% BLEED

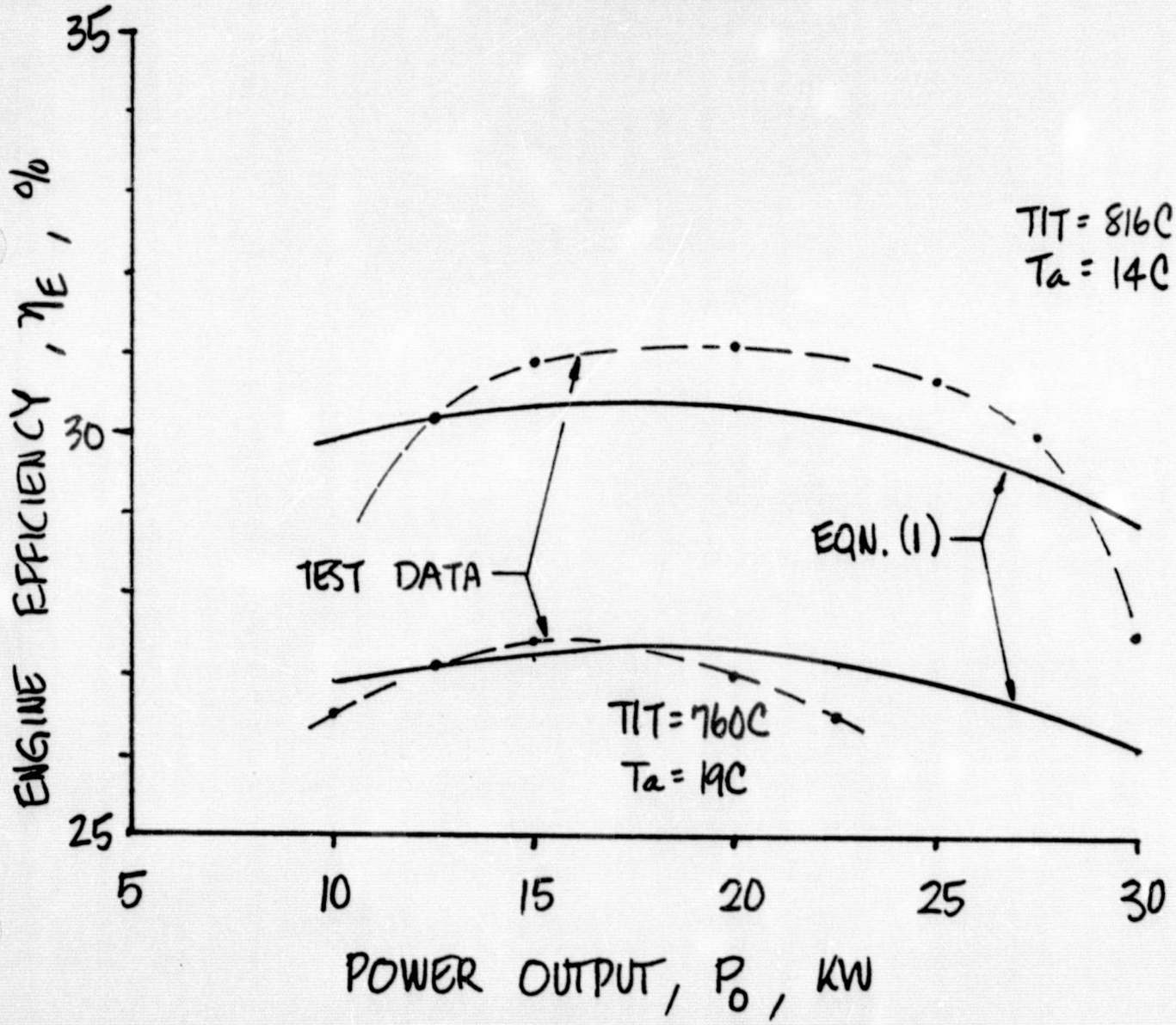


FIG. 5 **POWER DATA COMPARISON**

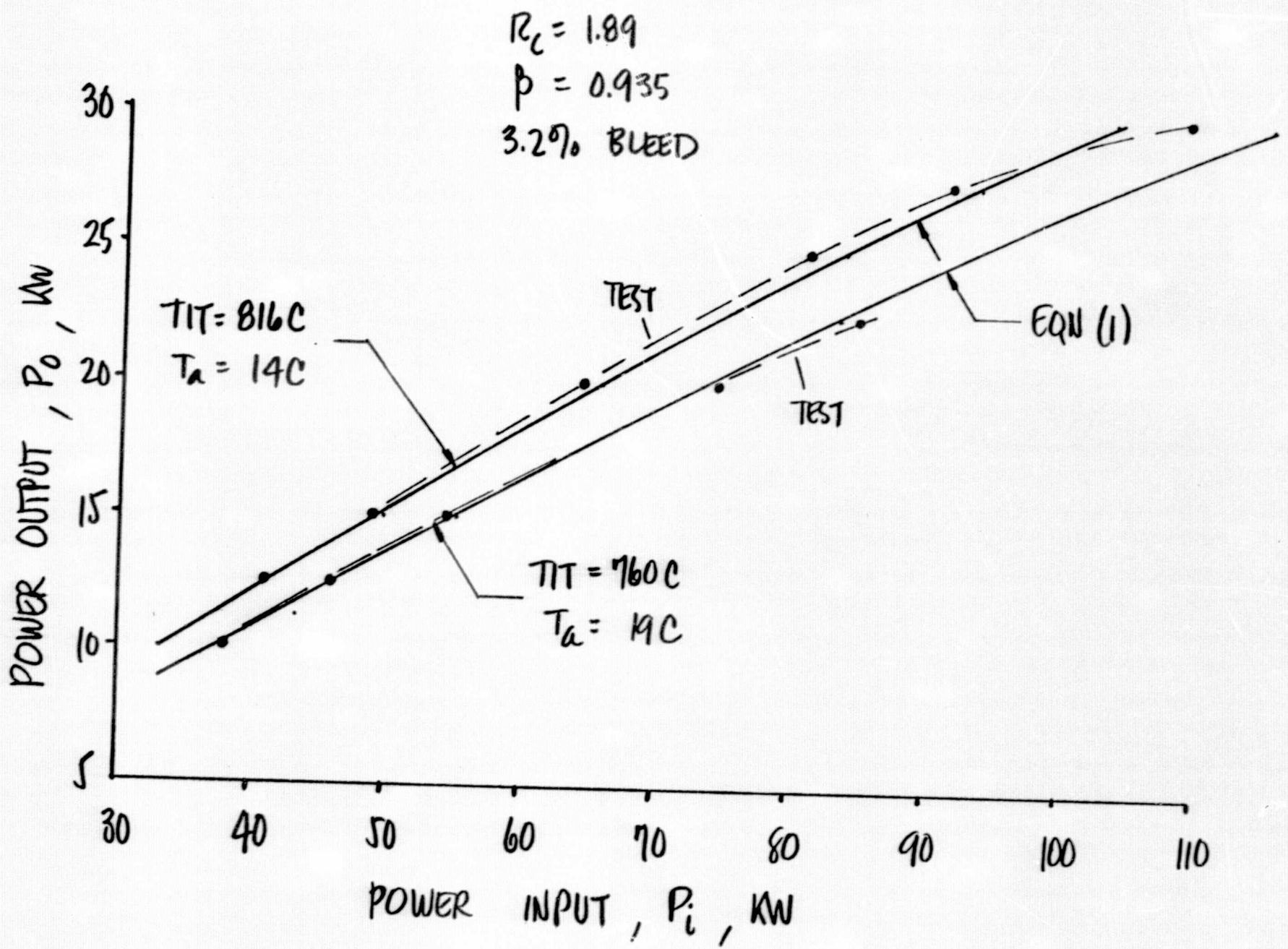


FIG. 6 EFFECT OF AMBIENT TEMPERATURE

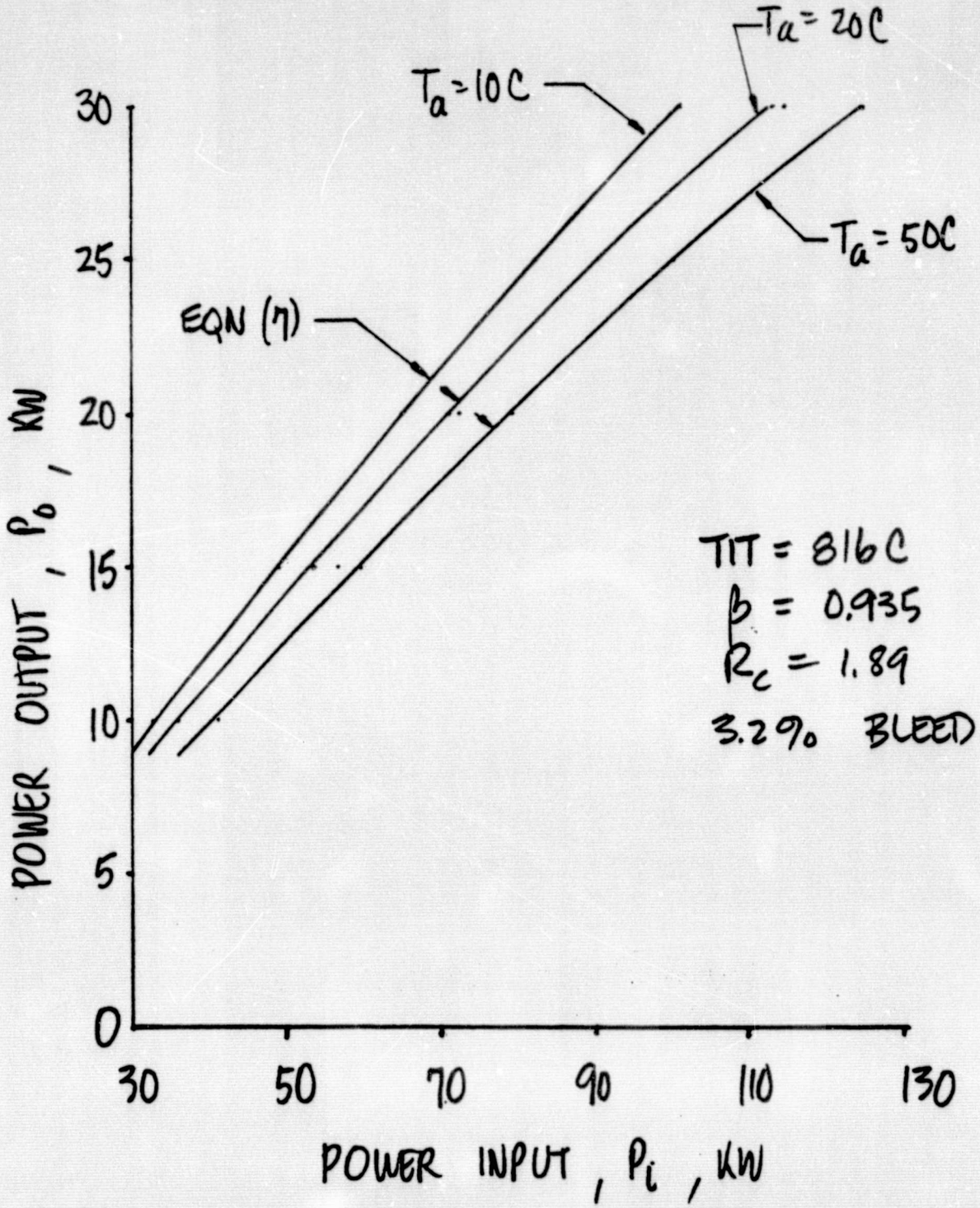


FIG. 7 **COMPRESSOR MASS FLOW**

- CCPS-40 ENGINE
- ARGON

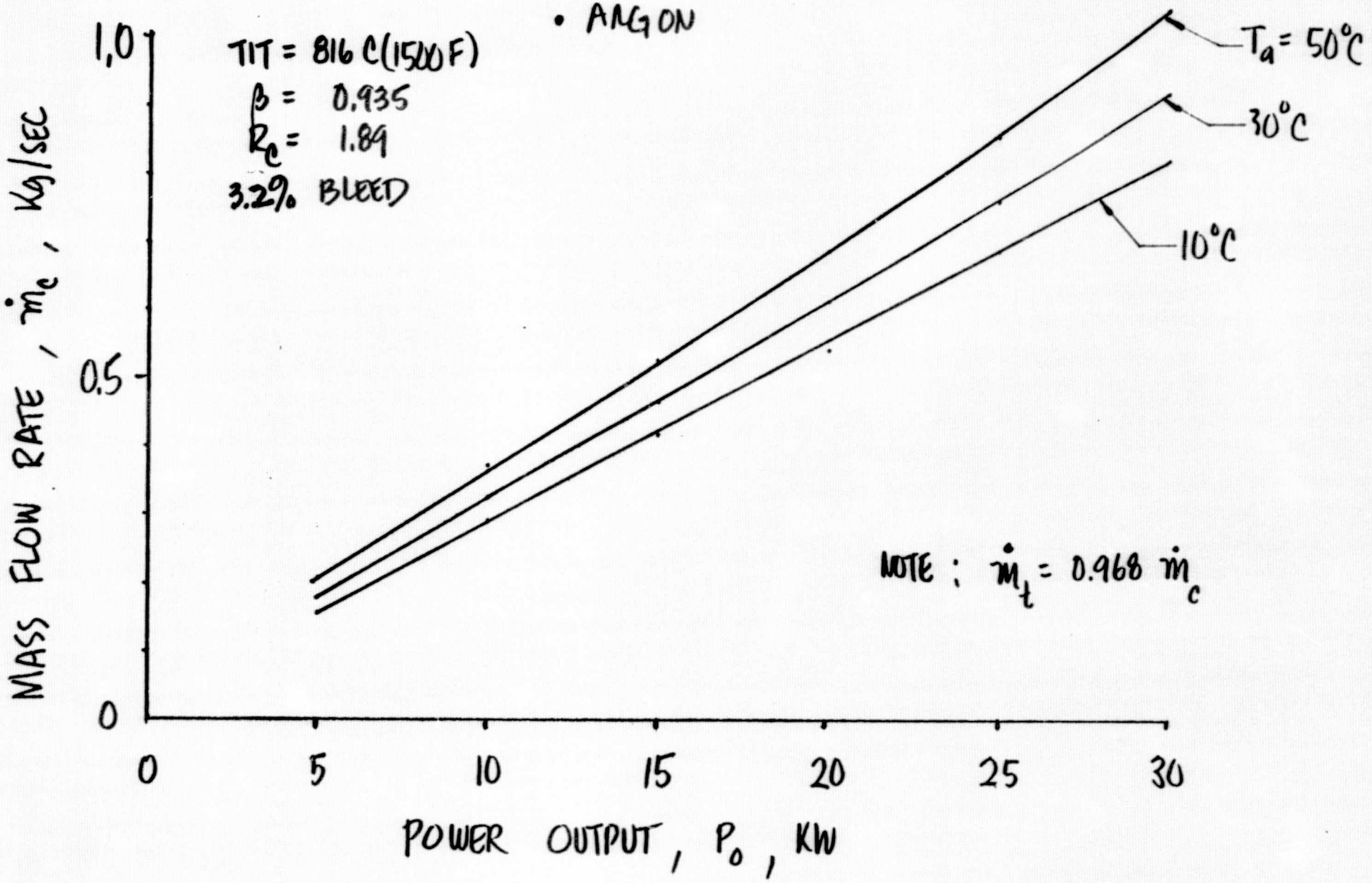
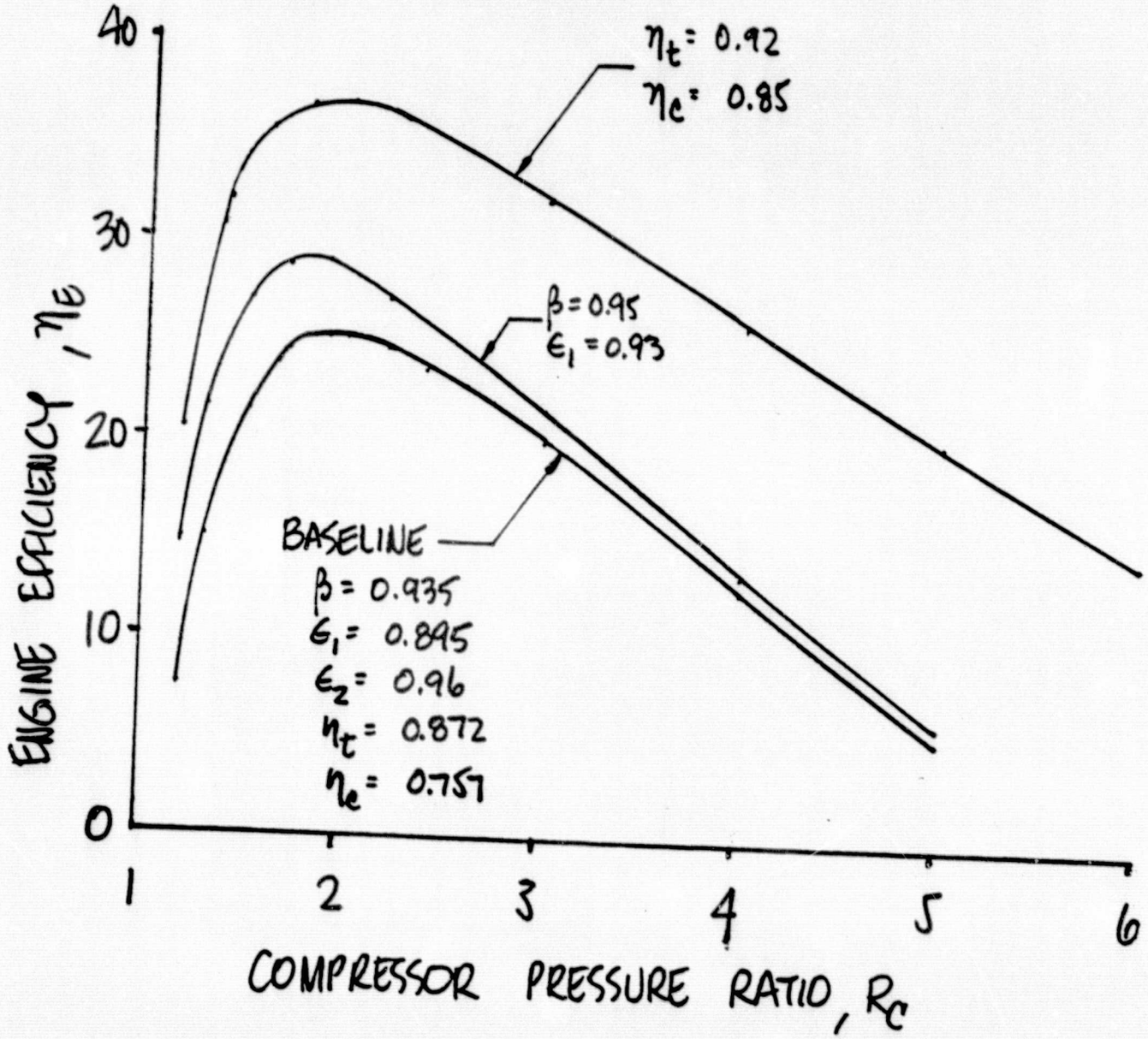


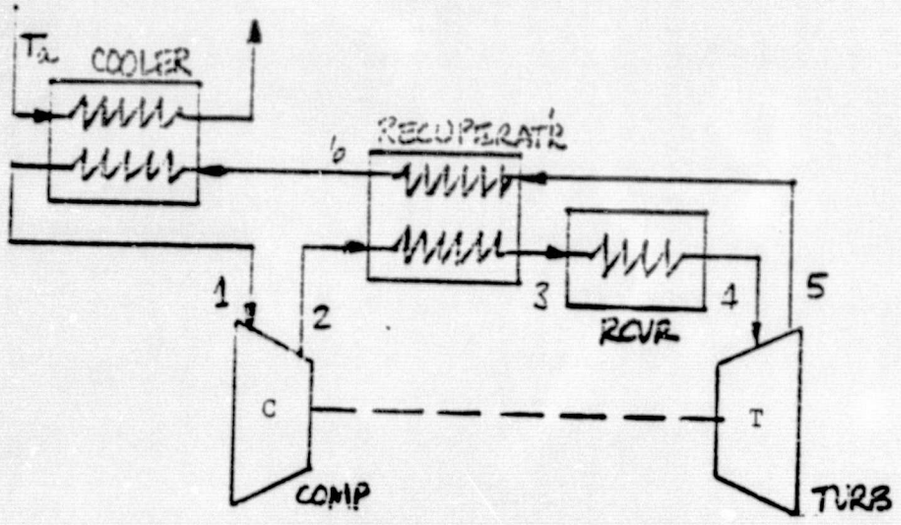
FIG. 8 **ENGINE GROWTH CAPABILITY**

CCPS40-1 (ARGON)

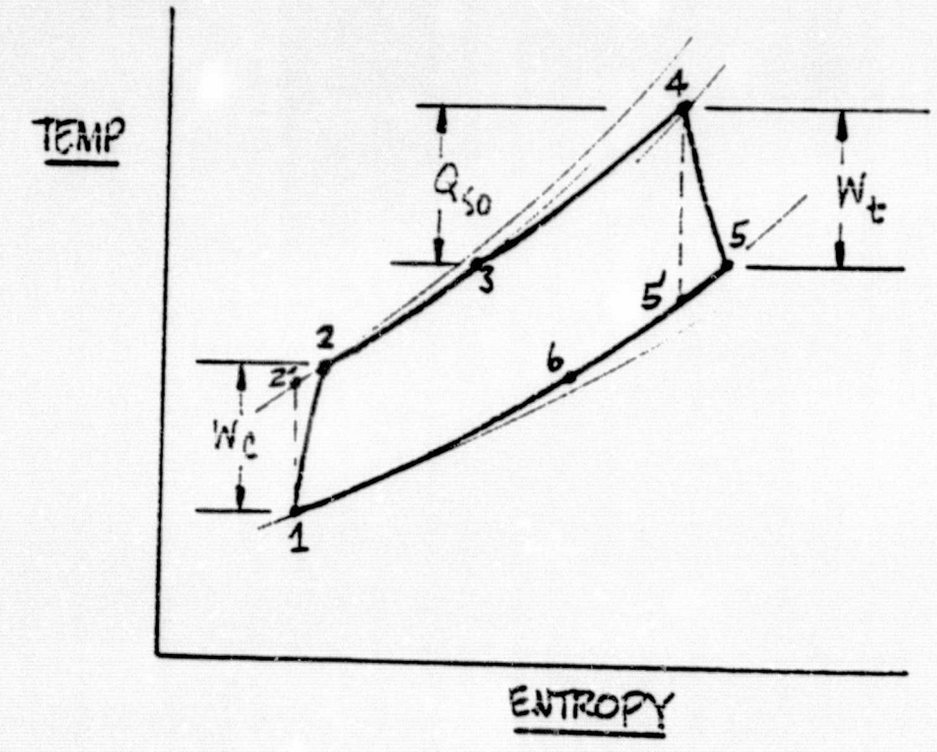
T_a = 44.6 C (112 F)



ENGINE SCHEMATIC



T-S DIAGRAM



- COMPRESSOR WORK POWER, P_C

$$P_c = \frac{\dot{m}_c C_p (T_2' - T_1)}{\eta_c} = \frac{\dot{m}_c C_p T_a}{\eta_c} \left(\frac{T_1}{T_a} \right) \left[\left(\frac{P_2}{P_1} \right)^k - 1 \right]$$

$$= \frac{\dot{m}_c C_p T_a}{\eta_c} \left(\frac{T_1}{T_a} \right) \xi_c \qquad \text{(A1)}$$

WHERE $\xi_c = R_c^k - 1$, $R_c = \frac{P_2}{P_1}$

- TURBINE POWER, P_t

$$P_t = \dot{m}_t \eta_t C_p (T_4 - T_5') = \dot{m}_t \eta_t C_p T_4 \left(1 - \frac{T_5'}{T_4}\right)$$

WHERE $$\frac{T_5'}{T_4} = \left(\frac{P_4}{P_5}\right)^{-k} = (\beta R_c)^{-k}$$

AND $$\beta = \left(\frac{P_3}{P_2}\right)\left(\frac{P_4}{P_3}\right)\left(\frac{P_1}{P_6}\right)\left(\frac{P_6}{P_5}\right)$$

$$= \frac{P_4/P_5}{P_2/P_1} = R_t/R_c$$

SO $$P_t = \dot{m}_t \eta_t C_p T_4 \xi_t \qquad \text{(A2)}$$

WHERE $$\xi_t = 1 - (\beta R_c)^{-k}$$

- SOLAR INPUT, Q_{so}

$$Q_{so} = \dot{m}_t C_p (T_4 - T_3) = \dot{m}_t C_p T_4 \left(1 - \frac{T_3}{T_4}\right) \qquad \text{(A3)}$$

BUT $$\epsilon_1 = \frac{T_3 - T_2}{T_5 - T_2}$$

SO $$T_3/T_5 = \frac{T_2}{T_5}(1 - \epsilon_1) + \epsilon_1$$

AND $$T_3/T_4 = \frac{T_2}{T_4}(1-\epsilon_1) + \epsilon_1 \left(\frac{T_5}{T_4}\right)$$

WHERE $$= (1-\epsilon_1)\,\tau_c \left(\frac{T_1}{T_a}\right)\left(\frac{T_a}{T_4}\right) + \epsilon_1 \tau_t \qquad \text{(A4)}$$

WHERE $\tau_c = T_2/T_1$, $\tau_t = T_5/T_4$

Substitution of (A4) into (A3) gives

$$Q_{so} = \dot{m}_t C_p T_4 \left[1 - (1-\varepsilon_1)\, \tau_c \left(\frac{T_1}{T_a} \right) \left(\frac{T_a}{T_4} \right) - \varepsilon_1 \tau_t \right] \qquad \text{(A5)}$$

T_1/T_a must now be determined in order to evaluate Equations (A1) and (A5) only in terms of R_c, T_a and T_4:

$$\varepsilon_2 = \frac{T_6 - T_1}{T_6 - T_a}, \quad \text{SO} \quad \frac{T_1}{T_a} = \frac{T_6}{T_a} (1-\varepsilon_2) + \varepsilon_2$$

$$\text{OR} \qquad \frac{T_1}{T_a} = (1-\varepsilon_2) \left(\frac{T_6}{T_5} \right) \left(\frac{T_4}{T_a} \right) \tau_t + \varepsilon_2 \qquad \text{(A6)}$$

From heat balance on the recuperator,

$$T_5 - T_6 = T_3 - T_2, \quad \text{SO} \quad \frac{T_6}{T_5} = 1 - \frac{T_3}{T_5} + \frac{T_2}{T_5}$$

$$\text{OR} \qquad \frac{T_6}{T_5} = 1 - \left(\frac{1}{\tau_t} \right) \left(\frac{T_3}{T_4} \right) + \tau_c \left(\frac{T_1}{T_a} \right) \left(\frac{T_a}{T_4} \right) \left(\frac{1}{\tau_t} \right) \qquad \text{(A7)}$$

Substitution of Equation (A4) into (A7) yields:

$$\frac{T_6}{T_5} = \left\{ 1 - \left(\frac{1}{\tau_t} \right) \left[(1 - \varepsilon_1)\, \tau_c \left(\frac{T_1}{T_a} \right) \left(\frac{T_a}{T_4} \right) + \varepsilon_1 \tau_t \right] + \tau_c \left(\frac{T_1}{T_a} \right) \left(\frac{T_a}{T_4} \right) \left(\frac{1}{\tau_t} \right) \right\} \qquad \text{(A8)}$$

Substitution of Equation (A8) into (A6) yields:

$$\left(\frac{T_1}{T_a} \right) = \frac{\varepsilon_2 + (1-\varepsilon_2)\, \tau_t \left(\frac{T_4}{T_a} \right) (1-\varepsilon_1)}{1 - \varepsilon_1 (1-\varepsilon_2) \tau_c} \qquad \text{(A9)}$$

WHERE

$$\tau_c = \frac{T_2}{T_1} = 1 + \frac{1}{\eta_c} \left(\frac{T_2'}{T_1} - 1 \right) = 1 + \frac{1}{\eta_c} \left(R_c^{\,k} - 1 \right)$$

$$= 1 + \xi_c / \eta_c$$

$$\tau_t = \frac{T_5}{T_4} = 1 - \eta_t \left(1 - \frac{T_5'}{T_4}\right) = 1 - \eta_t \left[1 - (\beta R_c)^{-k}\right]$$

$$= 1 - \eta_t \xi_t$$

Equation (A9) thus becomes:

$$\left(\frac{T_1}{T_a}\right) = \frac{\varepsilon_2 + (1 - \varepsilon_2)(1 - \varepsilon_1)\left(\frac{T_4}{T_a}\right)(1 - \eta_t \xi_t)}{1 - \varepsilon_1(1-\varepsilon_2)(1 + \xi_c/\eta_c)} \qquad \text{(A10)}$$

- CYCLE EFFICIENCY, η_{CY}

$$\eta_{CY} = \frac{P_t - P_c}{Q_{so}}$$

$$= \frac{\dot{m}_t \eta_t C_p T_4 \xi_t - \dot{m}_c \frac{C_p T_a}{\eta_c}\left(\frac{T_1}{T_a}\right)\xi_c}{\dot{m}_t C_p T_4 \left[1 - (1-\varepsilon_1)\left(1 + \frac{\xi_c}{\eta_c}\right)\left(\frac{T_1}{T_a}\right)\left(\frac{T_a}{T_4}\right) - \varepsilon_1 (1 - \eta_t \xi_t)\right]}$$

SO,

$$\eta_{CY} = \frac{\eta_t \xi_t - \frac{\xi_c}{\eta_c}\left(\frac{T_a}{T_4}\right)\left(\frac{T_1}{T_a}\right)\left(\frac{\dot{m}_c}{\dot{m}_t}\right)}{1 - \varepsilon_1 (1-\eta_t \xi_t) - (1-\varepsilon_1)\left(1 + \frac{\xi_c}{\eta_c}\right)\left(\frac{T_a}{T_4}\right)\left(\frac{T_1}{T_a}\right)} \qquad \text{(A11)}$$

WHERE

$$\xi_t = 1 - (\beta R_c)^{-k}$$

$$\xi_c = R_c^{\,k} - 1$$

Equations (A11) and (A10) now fully define the cycle efficiency in terms of the variables T_a, T_4, ε_1, ε_2, β and R_c. Engine efficiency can be written as

$$\eta_E = \eta_{CY} (\psi)$$

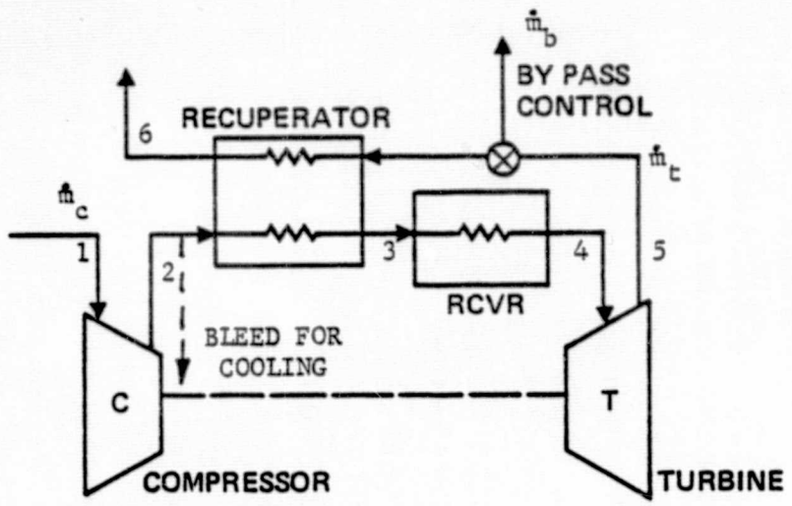
where ψ is a correction factor (~ 0.93 for the CCPS-40 engine) to account for mechanical/thermal losses and the effect of working fluid leakage.

PART 2

OPEN CYCLE PERFORMANCE MODEL

ENGINE SCHEMATIC

The engine analyzed herein is shown in the following sketch.



- HEAT BALANCE FOR THE RECUPERATOR

$$\dot{m}_t(T_3 - T_2) = (\dot{m}_t - \dot{m}_b)(T_5 - T_6)$$

$$\therefore\ T_3 - T_2 = (1 - \delta)(T_5 - T_6)$$

where

$$\delta = \alpha M$$

$$\alpha = \frac{\dot{m}_b}{\dot{m}_c} = \text{By-pass ratio}$$

$$M = \frac{\dot{m}_c}{\dot{m}_t} = \text{Bleed ratio}$$

but

$$\varepsilon_H = \frac{T_5 - T_6}{T_5 - T_2}$$

so

$$T_3 - T_2 = \varepsilon_H(1 - \delta)\left[\left(\frac{T_5}{T_4}\right) T_4 - T_2\right]$$

or

$$T_3 - T_2 = \varepsilon_H(1 - \delta)(\tau_t T_4 - T_2) \qquad \text{(B1)}$$

- SOLAR INPUT, Q_{so}

$$Q_{so} = P_i = \dot{m}_t C_p (T_4 - T_3)$$

$$\therefore T_3 = T_4 - \frac{P_i}{\dot{m}_t C_p} \qquad \text{(B2)}$$

Combining equations (B1) and (B2) and solving for TIT:

$$T_4 - \frac{P_i}{\dot{m}_t C_p} - T_2 = \varepsilon_H(1 - \delta)(\tau_t T_4 - T_2)$$

$$T_4[1 - \varepsilon_4(1 - \delta)\tau_T] = T_2[1 - \varepsilon_H(1 - \delta)] + \frac{P_i}{\dot{m}_t C_p}$$

thus

$$T_4 = \frac{\tau_c[1 - \varepsilon_H(1 - \delta)]T_1 + \frac{P_i}{\dot{m}_t C_p}}{[1 - \varepsilon_H(1 - \delta)\tau_t]}$$

for

$$P_i < P_{i_r}, \quad \alpha = 0 \quad \therefore \quad \delta = 0$$

and

$$T_4 = \frac{\tau_c(1 - \varepsilon_H)T_1 + \frac{P_i}{\dot{m}_t C_p}}{(1 - \varepsilon_H \tau_t)}$$

Now,

$$P_{o_r} = (P_t - P_c)_r = \frac{\dot{m}_c C_p T_1}{M}\left[\eta_t \xi_t \left(\frac{T_4}{T_1}\right)_r - \frac{\xi_c M}{\eta_c}\right] \tag{B3}$$

$$\therefore T_4 = \frac{\tau_c(1 - \varepsilon_H)T_1 + \frac{P_i}{P_{o_r}}\left[\eta_t \xi_t \left(\frac{T_4}{T_1}\right)_r - \frac{\xi_c M}{\eta_c}\right]}{1 - \varepsilon_H \tau_t}$$

but

$$\frac{P_i}{P_{o_r}} = \frac{P_i}{P_{i_r}}\left(\frac{1}{\eta_{E_r}}\right)$$

so

$$T_4 = \frac{\tau_c(1 - \varepsilon_H)T_1 + \left(\frac{P_i}{P_{i_r}}\right)\left(\frac{1}{\eta_{E_r}}\right)\left[\eta_t \xi_t \left(\frac{T_4}{T_1}\right)_r - \frac{\xi_c M}{\eta_c}\right]}{(1 - \varepsilon_H \tau_t)} \tag{B4}$$

Equation (B4) can be used to determine

$$\text{TIT} = T_4 = \text{fn}\left(\frac{P_i}{P_{i_r}}\right) \quad \text{for} \quad \left(\frac{P_i}{P_{i_r}}\right) \leq 1$$

- ENGINE EFFICIENCY, η_E

$$\eta_E = \frac{P_t - P_C}{Q_{so}} \tag{B5}$$

$$\eta_E = \frac{\left[\eta_t \varepsilon_t \left(\frac{T_4}{T_1}\right) - \frac{\xi_c M}{\eta_c}\right] \psi}{\left(\frac{T_4}{T_1}\right)\left[1 - \tau_t \varepsilon_c (1 - \delta)\right] - \tau_c \left[1 - \varepsilon_c (1 - \delta)\right]} \tag{B6}$$

where

$\varepsilon_c = \varepsilon_H = fn(\alpha)$ (See Recuperator Effectiveness Derivation below)

Thus

$$\left(\frac{P_o}{P_{o_r}}\right) = \frac{\eta_E}{\eta_{E_r}} \left(\frac{P_i}{P_{i_r}}\right) \tag{B7}$$

Substituting appropriate constants into equation (B7) give the following expressions:

$$\left(\frac{P_o}{P_{o_r}}\right) = 2.31 \left(\frac{P_i}{P_{i_r}}\right) - 0.00412 T_1 \quad \text{for} \quad \left(\frac{P_i}{P_{i_r}}\right) \leq 1 \tag{B8}$$

where

P_{o_r} = Specified output power, kW

$P_{i_r} = \frac{P_{o_r}}{\eta_{E_r}}$ where $\eta_{E_r} = 0.28123$

T_1 = Ambient temperature, ^oK

and

$$\left(\frac{P_{o_m}}{P_{o_r}}\right) = 2.31 \left(\frac{P_i}{P_{i_r}}\right)_x - (0.00412)T_1$$

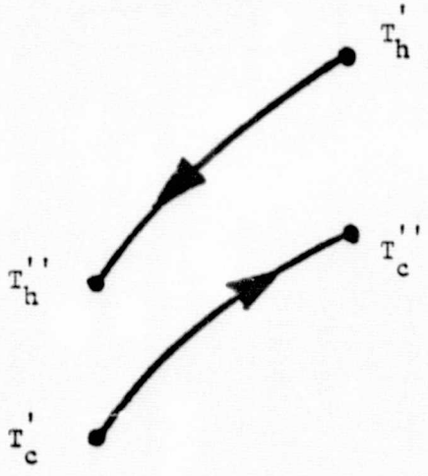
where

$$\left(\frac{P_i}{P_{i_r}}\right)_x = 1.1781 - 0.0005604(T_1)$$

$$\therefore \left(\frac{P_o}{P_{o_r}}\right) = 2.7214 - 0.0054145T_1 \quad \text{for} \quad \left(\frac{P_i}{P_{i_r}}\right) > 1 \tag{B9}$$

Equations (B8) and (B9) have been used to model the open-cycle Brayton engine using program SPEE1 with the Barstow solar data.

- RECUPERATOR EFFECTIVENESS DERIVATION



$$\varepsilon_{max} = \frac{1 - \exp\left[-\text{NTU}\left(1 - \frac{C_{min}}{C_{max}}\right)\right]}{1 - \left(\frac{C_{min}}{C_{max}}\right)\exp\left[-\text{NTU}\left(1 - \frac{C_{min}}{C_{max}}\right)\right]}$$

where

$$NTU = \frac{UA}{C_{min}}$$

$$C = \dot{m}C_p$$

In this case

$$C_{min} = C_{hot}$$

$$C_{max} = C_{cold}$$

$$\therefore \frac{C_{min}}{C_{max}} = \frac{C_h}{C_c} = \frac{\dot{m}_h}{\dot{m}_c} = 1 - \alpha$$

since

$$C_{P_{hot}} = C_{P_{cold}}$$

$$\therefore \varepsilon_{max} = \varepsilon_c = \frac{1 - \exp(-(NTU)\alpha)}{1 - (1 - \alpha)\exp(-(NTU)\alpha)}$$

but

$$\varepsilon_c = \frac{C_c(T_c'' - T_c')}{C_h(T_h' - T_c')}$$

$$= \frac{1}{(1 - \alpha)}\left(\frac{T_c'' - T_c'}{T_h' - T_c'}\right) \equiv \left(\frac{T_h' - T_h''}{T_h' - T_c'}\right) = \varepsilon_h$$

$$\therefore \varepsilon_c \equiv \varepsilon_h$$

APPENDIX G

DETERMINATION OF STATION-KEEPING POWER

APPENDIX G

DETERMINATION OF STATION-KEEPING POWER

All system calculations carried out to date include an allowance for the parasitic power required to operate the SPS. The station power requirement is comprised of 1) the power needed to operate each collector and 2) the power to operate and environmentally condition the control building. These loads were evaluated for both the no-storage case and the case of battery storage; the analysis is incorporated in TR-E-4 which is part of this Appendix. The results of TR-E-4 have been modified to accommodate more recent system design changes. For example, the original storage energies of 648 and 7848 kWh no longer correspond to the energies associated with annualized capacity factors (ACF) of 0.4 and 0.7, respectively. The data of TR-E-4 have been generalized to scale to any level of storage energy required, as described below.

1. NO STORAGE

The average daily collector load is given in TR-E-4 as 14.85 kWh but this value includes power for engine control as well as the engine starting battery charger. If these values are removed (they are already incorporated in the quoted USS P-75 engine performance) and an average operating day of ~8 hours employed instead of the quoted 10.14 hours, total collector power (at the grid) can be represented by:

$$P_{COLL} \cong 1.5\ N_o, \qquad \text{kW} \tag{1}$$

where N_o is the number of collectors.

The building load -- which is primarily for air conditioning the 680 ft^2 structure -- is given as 125.27 kWh/day in TR-E-4, but this conservative analysis was carried out for summer heating conditions. For yearly average conditions and an approximate 8 hour operating day, the building power requirement can be expressed more accurately as

$$P_{BLDG} \cong 8 \text{ kW} \tag{2}$$

The station power requirement without storage is thus:

$$P_o(STA) = 1.5\ N_o + 8, \qquad \text{kW} \tag{3}$$

Equation (3) is incorporated in the computation of system output based on the 15 minute Barstow site tapes.

2. BATTERY STORAGE

The station power must be increased to accommodate the increased building loads associated with the addition of batteries. The <u>added</u> station power is:

$$E_1 = C_1 \bar{E}_b D_{yr} \quad (4)$$

where

E_1 = Added daily energy to building.

C_1 = Constant derived from data of TR-E-4, $\tilde{=}$ 0.177 (1/hr).

$\bar{E}_b$ = Average daily energy delivered to the grid from batteries, kWh.

D_{yr} = Number of operating days per year.

Figure G-1 presents the additional building energy required for battery storage as a function of the battery energy delivered to the grid. The summer operation data from TR-E-4 was used to size the air conditioning units. This ensures that proper environmental conditions exist within the storage building during hot days. However, these data are not appropriate for cooler days since the air conditioning equipment will be operated much less frequently (or not at all). Thus, the data of TR-E-4 have been adjusted to reflect the average annual energy requirements for the building (dashed line in Figure G-1). Approximately 17.7 percent of the energy delivered from battery storage to the grid is required to condition the storage building on an average annual basis. This percentage corresponds to the constant C given in Equation (4).

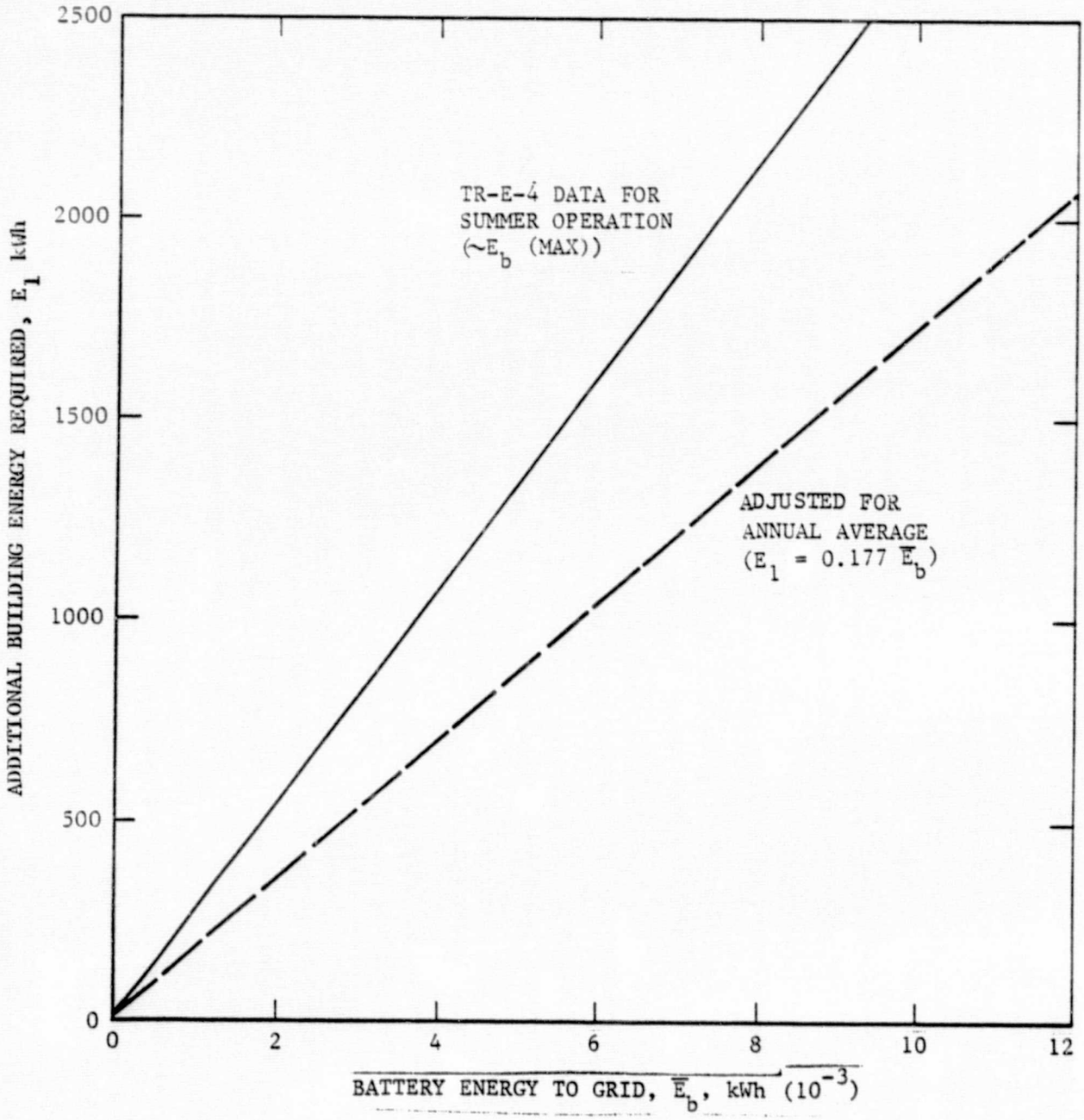


FIGURE G-1. ADDITIONAL ENERGY REQUIRED TO COOL BUILDING FOR BATTERY STORAGE

94-2-184

Ford Aerospace &
Communications Corporation
Aeronutronic Division

Ford Road
Newport Beach, California 92663

TECHNICAL REPORT

TR. NO. E-4 (Rev. 1)

SOLAR SMALL POWER SYSTEM (SPS) PROGRAM -

TITLE POWER AND ENERGY REQUIREMENTS--STATION AUXILIARIES

PREPARED BY	J. Knorpp	ORG NO. 3T7450	CHARGE NO. C398.ELEC
SUPERVISOR APPROVAL	J. Knorpp	DATE 3/16/79	
PROGRAM ENGINEER APPROVAL		TO	

SUMMARY

Station auxiliary device loads have been analyzed and found to fall in two classes; i.e., those directly associated with a collector and those associated with the control building.

Collector auxiliary device power requirements have been found to be primarily a function of collector engine cooling requirements and for a collector in the 40-80 kW size range would be approximately 1.6 kW (per collector).

Control building auxiliary device power requirements have been found to be a complex function of site environment, station operating schedule and energy storage requirements. Power requirements for these loads for the no storage, 648 kWh* storage (typical for 0.4 capacity factor station), 7,848 kWh* storage (typical for 0.7 capacity factor station) would be approximately (14 kW)/n, (32 kW)/n and 254 kW)/n, respectively, where "n" is the number of collectors in the collection field.

Rev. 1:

1. Heat dissipation of building lights test equipment and outlets deleted from air conditioning equipment energy demand calculations based on plans for un-attended station operation.
2. Revised air conditioning equipment power requirements incorporated.

* Due to system design changes, these figures for the P-75 engine are now 2,132 and 13,625 kWh, respectively. The storage values for the P-40 engine are 2,534 and 14,176 kWh, respectively.

ORIGINAL PAGE IS
OF POOR QUALITY

1.0 GENERAL CONSIDERATIONS

Station auxiliaries, such as collector engine cooling fans, the power control microprocessor, tracking drive units and control building air conditioning equipment are necessary for station operation, but consume energy which must be subtracted from the gross station generating capacity to determine the net station output. These auxiliaries fall in two classes; i.e., those directly associated with the collectors and those associated with the control building and its installed equipment.

Power requirements for the auxiliaries associated with any single collector are primarily a function of heat engine size and efficiency. Energy requirements are a function of the foregoing factors and collector operating time, which has been assumed to average 10.14 hours per day, based on data provided in Table 1 of Reference 1.* Both energy and power requirements may be calculated in a fairly direct manner.

Power and energy requirements for control building ancilliaries are recursive in nature and require assumption of a station operating schedule to calculate absolute values. For purposes of this report it has again been assummed that the period of direct energy collection will average 10.14 hours per day. In those cases where storage is provided, it has also been assummed that the batteries will be recharged in the eight-hour period centered on the solar meridian and that they will be discharged through the inverter to the utility grid in the period immediately following the period of direct collection. Reasonable variations in the above described station operating schedule will not significantly affect the results presented.

2.0 COLLECTOR AUXILIARIES

Connected loads directly associated with a collector of 40-80 kW output rating are estimated to be as follows:

P_{fp}	=	0.99	kW	(1 HP engine cooling fan & pump)
P_{ec}	=	0.10	kW	(engine control system)
P_{bc}	=	0.05	kW	(engine starting battery charger)
P_{dc}	=	1.10	kW	(collector declination drive)
P_{ha}	=	4.40	kW	(collector hour-angle drive)
P_{pc}	=	0.10	kw	(power control assembly)
P_C	=	6.74	kW	(collector total)

* The more recent Barstow-based analysis shows that average operating time is approximately 8 hrs/day.

COLLECTOR AUXILIARIES continued:

Energy requirements of each auxiliary device are a function of its power requirement and its operating duty cycle. The engine cooling fan & pump motor will (for example) operate continuously while the collector is in service and for a 0.25 hour cool-down period immediately following the period of operation. This would give a duty cycle of (10.14 + 0.25)/24 or 0.4329. Duty cycles for other auxiliary devices have been calculated on the basis of estimated device utilization and tabulated below with the resulatant energy requirements.

	Power (kW)		Duty Cycle		Hrs/Day		Energy Rqmts.
E_{fp} =	0.99	X	0.4329	X	24	=	10.29 kWh
E_{ec} =	0.10	X	0.4225	X	24	=	1.01
E_{bc} =	0.05	X	1.0000	X	24	=	1.24
E_{dc} =	1.10	X	0.00758	X	24	=	0.20
E_{ha} =	4.40	X	0.0104	X	24	=	1.10
E_{pc} =	0.10	X	0.4225	X	24	=	1.01
Total Average Daily Energy Per Collector					E_C	=	14.85 kWh

For an average daily collection period of 10.14 hours and a generator efficiency of 0.9, the average power required from the output shaft of each collector engine would be:

$$P_c' = \frac{14.85}{(10.14)(0.90)} = 1.63 \text{ kW}$$

Since the energy requirement of the major user (E_{fp}) is nearly directly proportional to collector operating time, P_c' will be nearly independent of operating time and thus will not vary significantly throughout the year. For smaller collector engines with an output rating in the range of 20-40 kW, all auxiliary loads would be the same except the engine cooling fan and pump motor which would be proportionally sized down to 1/2 HP and would draw 0.59 kW. By calculations similar to the above, it can be shown that the average power requirement would be 1.17 kW per collector.

COLLECTOR AUXILLARIES continued:

For larger collector engines with an output rating in the range of 80-120 kW, all auxiliary loads would again be the same except the engine cooling fan and pump motor which would be proportionally sized up to 2 HP and would draw 2.00 kW. Again, by calculations similar to above, it can be shown that the average power requirement would be 2.78 kW per collector.

3.0 CONTROL BUILDING AUXILLARIES

Power requirements for control building auxiliary loads are a strong function of energy storage requirements, which in turn are a function of required station capacity factor and the percentage of capacity factor which can be satisfied from direct generation. It is therefore necessary to consider three major cases; i.e., the no storage case, the 0.4 capacity factor case and the 0.7 capacity factor case.

For all three cases, it has been assumed that a well-constructed and well-insulated building, having 60#/sq. ft. wall construction, 20#/sq. ft. roof construction and an insulation "U" factor of 0.1, will be provided to house the station power control, storage (where used) and distribution equipment. Design ambient conditions have been assumed to be as follows, based on technical equipment requirements and typical site conditions, as delineated in the Barstow weather data.

Inside Temperature:		$25^{\circ} \pm 8^{\circ}C$	
Outside Summer	:	$46.1^{\circ}C$	dry bulb
		$25.0^{\circ}C$	wet bulb
Outside Winter	:	$1.7^{\circ}C$	dry bulb
Daily Range	:	$20.7^{\circ}C$	

The general calculation procedure used has been to assume that (for each case) a building of the configuration shown in the 3rd Progress Review Meeting will be oriented on the site to minimize solar exposure. Solar and transmission heat gain has then been calculated and totalled for the four wall and roof exposures(it has also been averaged over the floor area as a convience for rapidly considering the effect of changes in building size).

CONTROL BUILDING AUXILLARIES continued:

Heat dissipation has then been calculated and tabulated for all station auxiliaries in each room. Heat dissipation from the main power switchboard and storage subsystem components (where applicable) for the various modes of operation have then been calculated, tabulated and summed with the aforementioned heat loads to compute the required size (s) for the air conditioning equipment. Air conditioning equipment power requirements are then determined for each mode of operation based on the percentage of the installed capacity actually being used. This power is added to the other power flowing through the main switchboard and heat dissipation from the switchboard is re-calculated and re-totalled with the other heat loads to determine an adjusted value for building heat load and percentage of air conditioning capacity in use and hence a duty cycle for the air conditioning equipment. Although further iterations would improve the mathematical precision of the result, the single iteration undertaken assures that the accuracy of the result will be determined by the accuracy of the input data assumptions.

3.1 No Storage Case:

A building of approximately 680 square feet (20' x 34') will be required to house the power control & distribution equipment, a small maintenance shop and a rest room. Based on the above stated design conditions, building heat loads would be as follows:

Bldg. Heat Gain	680 sq. ft.	x	15.0	Btuh/sq.ft.	=	10,200 Btuh
Lighting	1,300W	x	3.41	Btu/watt hr.	=	4,433 *
Outlets	1,200W	x	3.41	Btu/watt hr.	=	4,092 *
Control equip.	1,900W	x	3.41	Btu/watt hr.	=	6,479
Main Switchboard	3,131W	x	3.41	Btu/watt hr	=	10,677
People	2	x	215	Btuh/person	=	430 *
Total Sensible Heat						36,311 Btuh

* Used for air conditioning unit capacity calculation, but not for energy calculation due unattended nature of station operation.

3.1 No Storage Case continued:

The control room cooling requirement could (typically) be satisfied by a Pomona Air ACC-300 cooling unit and a Bohn RDD-5 air-cooled condenser. The cooling requirement in each of the smaller rooms could be satisfied by a Carrier KK0051. The total connected load of all of the above units would be 14.10 kW.

Connected loads in the control building are estimated to be as follows:

P_{mp}	=	0.76 kW	(microprocessor)
P_{ct}	=	0.14 kW	(CRT terminal)
P_{ad}	=	1.00 kW	(A-D converters)
P_{cl}	=	0.80 kW	(control room lights)
P_{ml}	=	0.40 kW	(maintenance shop lights)
P_{rl}	=	0.10 kW	(rest room lights)
P_{to}	=	1.20 kW	(test equip. & outlets)
P_{ac}	=	14.10 kW	(air-conditioning equip.)
P_B	=	18.50	(building total)

Energy requirements for the above loads are a function of the power requirement of each load and its operating duty cycle. In this case, it has been assumed that the microprocessor will operate 24 hours per day and that the other technical loads will operate 10.14 hours out of the 24-hour day. Lighting is assumed to be required an average of 4 hours per week and test equipment and outlet power is assumed to be required 2 hours per week. The air conditioning equipment will operate 56% of the time during 10.14 operating day and will be shut down during the nonoperating period to conserve energy. Under these conditions energy requirements would be as follows:

		Power(kW)		Duty Cycle		Hrs/Day		Energy Rqmts.
E_{mp}	=	0.76	X	1.0000	X	24	=	18.24 kWh
E_{ct}	=	0.14	X	0.4225	X	24	=	1.42
E_{ad}	=	1.00	X	0.4225	X	24	=	10.14
E_{cl}	=	0.80	X	0.0238	X	24	=	0.46
E_{ml}	=	0.40	X	0.0238	X	24	=	0.23
E_{rl}	=	0.10	X	0.0238	X	24	=	0.06
E_{to}	=	1.20	X	0.0119	X	24	=	0.34
E_{ac}	=	14.10	X	0.2789	X	24	=	94.38
		Total Daily Energy Requirement					E_B =	125.27 kWh

No Storage Case continued:

The average power requirement for the building auxiliary equipment loads during a 10.14 hour operating day would be:

$$P_B' = \frac{125.27}{10.14} = 12.35$$

If there are 'n' collectors in the collection field, the average auxiliary equipment power required at the engine output shaft of each collector during the operating day would be:

$$P_B'' = \frac{12.35}{n(0.997)(0.981)(0.900)} = \frac{14.03}{n} \text{ kW}$$

The above requirement is additive to the requirement for collector auxiliary equipment power requirements defined in paragraph 2.0. It includes no allowance for perimeter (or other) site security lighting.

3.2 0.4 Capacity Factor Storage Case:

Power requirements for control building auxiliary equipment loads for the 0.4 capacity factor case are a strong function of the stored energy requirement, which is equal to the total energy requirement less the amount of energy available from direct generation. Computations in this section assume that a capacity factor of 0.373 will be achieved from direct generation per Table 4 of Reference 1. Any significant variations in this value will affect required battery ampere-hour capacity, building size, collector and inverter operating time, air conditioning equipment size and energy requirements. They will have a significant effect on building related auxiliary equipment power and energy requirements. Average daily stored energy delivery to the utility grid for a station having a direct generation capacity factor of 0.373 would be:

$$E_S = \frac{(1.0)(10^3)(8760)(0.400-0.373)}{365} = 648 \text{ kWh}$$

The total storage capacity required to deliver this amount of energy would be:

$$E_{batt} = \frac{648}{(\eta_{HV})(\eta_T)(\eta_I)} = \frac{648}{(0.999)(0.98)(0.94)} = 704.1 \text{ kWh}$$

where η_{HV}, η_T and η_I are the efficiencies of the HV connection equipment, LV-HV transformer and inverter, respectively.

A building to house the storage subsystem of this size, in addition to the basic power control and distribution equipment, a maintenance shop and rest room would require a floor area of approximately 3,072 square feet.

3.2 0.4 Capacity Factor Storage Case continued:

Technical equipment heat loads within the building will vary significantly during a typical day's operation depending on whether the storage subsystem is in a float, charge, or discharge mode.

In the float charge mode, which last 2.14 hours of the typical operating day, the building heat loads would be as follows:

Bldg. Heat Gain	3,072 sq.ft.	X	10.00 Btuh/sq.ft.	=	30,720 Btuh
Lighting	3,900W	X	3.41 Btu/watt hr.	=	13,299 *
Outlets	1,500W	X	3.41 Btu/watt hr.	=	5,115 *
Control Equipment	1,900W	X	3.41 Btu/watt hr.	=	6,479
Main Switchboard	3,071W	X	3.41 Btu/watt hr.	=	10,472
Converters	400W	X	3.41 Btu/watt hr.	=	1,364
Inverters	400W	X	3.41 Btu.watt hr.	=	1,364
Battery	0	X	3.41 Btu/watt hr.	=	0
People	2	X	215 Btuh/person	=	430 *
			Total Sensible Heat		69,243 Btuh

In the charge mode, which would last 8.0 hours of the typical operating day, the basic building heat loads would be increased by the converter and battery heat losses. The total sensible heat load for this mode of operation is summarized below.

Bldg. Heat Gain	3,072 sq. ft.	X	10.0 Btuh/sq.ft.	=	30,720 Btuh
Lighting	3,900W	X	3.41 Btu/watt hr.	=	13,299 *
Outlets	1,500W	X	3.41 Btu/watt hr.	=	5,115 *
Control Equipment	1,900W	X	3.41 Btu/watt hr.	=	6,479
Main Switchboard	3,414W	X	3.41 Btu/watt hr.	=	11,642
Converters	3,200W	X	3.41 Btu/watt hr.	=	10,912
Inverters	400W	X	3.41 Btu/watt hr.	=	1,364
Battery	10,360W	X	3.41 Btu/watt hr.	=	35,328
People	2	X	215 Btuh/person	=	430 *
			Total Sensible Heat		115,289 Btuh

* Used for air conditioning unit capacity calculation, but not for energy calculation due unattended nature of station operation.

3.2 0.4 Capacity Factor Storage Case continued:

In the discharge mode, which would last 0.93 hours of a typical operating day, the inverter and storage battery losses would contribute to the total sensible heat. Air conditioning requirements during this period would therefore be as follows:

Bldg. Heat Gain	3,072 sq. ft.	X	10.0	Btuh/sq.ft.	=	30,720 Btuh
Lighting	3,900W	X	3.41	Btu/watt hr.	=	13,299 *
Outlets	1,500W	X	3.41	Btu/watt hr.	=	5,115 *
Control Equipment	1,900W	X	3.41	Btu/watt hr.	=	6,479
Main Switchboard	2,422W	X	3.41	Btu/watt hr.	=	8,259
Converters	400W	X	3.41	Btu/watt hr.	=	1,364
Inverters	45,640W	X	3.41	Btu/watt hr.	=	155,632
Battery	45,120W	X	3.41	Btu/watt hr.	=	153,859
People	45,120W	X	215	Btuh/person	=	430 *
				Total Sensible Heat		375,157 Btuh

As can be seen from the above tabulations, there is an approximate 5:1 variation in total heat load encompassed by the various operating modes. Both the control room and battery room cooling requirements could be satisfied by separate air conditioning systems consisting of a Pomona ACC-500/Bohn RDD-9 combination supplemented by two Trane SACA 754 units, all operating under staged thermostatic control. Cooling requirements of the two smaller rooms could be satisfied, as before, by two Carrier KK0051 units. Based on the foregoing, connected loads in the control building are estimated to be:

P_{mp}	=	0.76 kW	(microprocessor)
P_{ct}	=	0.14	(CRT terminal)
P_{ad}	=	1.00	(A-D converters)
P_{cl}	=	1.80	(control room lights)
P_{bl}	=	1.60	(battery room lights)
P_{ml}	=	0.40	(maintenance shop lights)
P_{rl}	=	0.10	(rest room lights)
P_{to}	=	1.50	(test equip. & outlets)
P_{ac}	=	93.09	(air conditioning equip)
P_B	=	100.39 kW	(building total)

3.2 0.4 Capacity Factor Storage Case continued:

Energy requirements for the above loads are, again, a function of the power requirement and duty cycle of each load. Based on an assumed mode of station operation which would result in direct generation and power delivery to the grid for 10.14 hours, battery charging for 8.00 hours and delivery of power from storage to the grid for 0.93 hours, the average daily auxiliary equipment energy requirement would be as follows:

	Power(kW)		Duty Cycle		Hrs/Day		Energy Rqmts.
E_{mp}	= 0.76	X	1.0000	X	24	=	18.24 kWh
E_{ct}	= 0.14	X	0.4225	X	24	=	1.42
E_{ad}	= 1.00	X	0.4225	X	24	=	10.14
E_{cl}	= 1.80	X	0.0238	X	24	=	1.03
E_{bl}	= 1.60	X	0.0238	X	24	=	0.91
E_{ml}	= 0.40	X	0.0238	X	24	=	0.23
E_{rl}	= 0.10	X	0.0238	X	24	=	0.06
E_{to}	= 1.50	X	0.0119	X	24	=	0.43
E_{acf}	= 93.09	X	0.0102	X	24	=	22.79
E_{acc}	= 93.09	X	0.0731	X	24	=	163.32
E_{acd}	= 93.09	X	0.0314	X	24	=	70.15
						Total Daily Energy Requirement =	288.72 kWh

The average auxiliary equipment power requirement for the building loads during a 10.14 hour operating day would be:

$$P_B' = \frac{288.72}{10.14} = 28.47 \text{ kW}$$

If there are "n" collectors in the collection field, the average power required at the engine output shaft of each collector would be:

$$P_B'' = \frac{28.47}{n(0.997)(0.981)(0.90)} = \frac{32.34}{n} \text{ kW}$$

The above requirement is additive to the requirement for collector auxiliary equipment power requirements defined in paragraph 2.0. It includes no allowance for perimeter (or other) site security lighting.

3.3 0.7 Capacity Factor Storage Case:

Power requirements for control building auxiliary equipment loads for the 0.7 capacity factor case are also a strong function of the stored energy requirement, which is equal to the total energy requirement less the amount of energy available from direct generation.

Computations in this section assume that a capacity factor of 0.373 will be achieved from direct generation per Table 4 of Reference 1. Any significant variations in this value will affect required battery ampere-hour capacity, building size, collector and inverter operating time, air conditioning equipment size and energy requirements. They will have a significant effect on building related auxiliary equipment power and energy requirements. Average daily stored energy delivery to the utility grid for a station having a direct generation capacity factor of 0.373 would be:

$$E_S = \frac{(1.0)(10^3)(8760)(0.700-0.373)}{365} = 7,848 \text{ kWh}$$

The total storage capacity required to deliver this amount of energy would be:

$$E_{batt} = \frac{7,848}{(\eta_{HV})(\eta_T)(\eta_I)} = \frac{7,848}{(0.999)(0.98)(0.94)} = 8,528 \text{ kWh}$$

Where η_{HV}, η_T and η_I are the efficiencies of the HV connection equipment, LV-HV transformer and inverter, respectively.

A building to house the storage subsystem of this size, in addition to the basic power control and distribution equipment, a maintanance shop and rest room would require a floor area of approximately 8,448 square feet. Technical equipment heat loads within the building will vary significantly during a typical day's operation depending on whether the storage subsystem is in a float, charge, or discharge mode.

In the float charge mode, which would last 2.14 hours of the typical operating day, the building heat loads would be as follows:

3.3 0.7 Capacity Factor Storage Case continued:

Bldg. Heat Gain	8,448 sq.ft.	X	8.50	Btuh/sq.ft.	=	71,808 Btuh
Lighting	8,500W	X	3.41	Btu/watt hr.	=	28,985 *
Outlets	1,800W	X	3.41	Btu/watt hr.	=	6,138 *
Control Equipment	1,900W	X	3.41	Btu/watt hr.	=	6,479
Main Switchboard	3,152W	X	3.41	Btu/watt hr.	=	10,748
Converters	400W	X	3.41	Btu/watt hr.	=	1,364
Inverters	400W	X	3.41	Btu/watt hr.	=	1,364
Battery	0	X	3.41	Btu/watt hr.	=	0
People	2	X	215	Btuh/person	=	430 *
				Total Sensible Heat		127,316 Btuh

In the charge mode, which would last 8.0 hours of the typical operating day, the basic building heat loads would be increased by the converter and battery heat losses. The total sensible heat load for this mode of operation is summarized below.

Bldg Heat Gain	8,448 sq.ft.	X	8.5	Btuh/sq.ft.	=	71,808 Btuh
Lighting	8,500W	X	3.41	Btu/watt hr.	=	28,985 *
Outlets	1,800W	X	3.41	Btu/watt hr.	=	6,138 *
Control Equipment	1,900W	X	3.41	Btu/watt hr.	=	6,479
Main Switchboard	7,513W	X	3.41	Btu/watt hr.	=	25,619
Converters	38,780W	X	3.41	Btu/watt hr.	=	132,240
Inverters	400W	X	3.41	Btu/watt hr.	=	1,364
Battery	125,400W	X	3.41	Btu/watt hr.	=	427,614
People	2	X	215	Btuh/person	=	430 *
				Total Sensible Heat		700,677 Btuh

In the discharge mode, which would last 11.21 hours of a typical operating day, the inverter and storage battery losses would contribute to the total sensible heat. Air conditioning requirements during this period would therefore be as follows:

* Used for air conditioning unit capacity calculation, but not for energy calculation due unattended nature of station operation.

3.3 0.7 Capacity Factor Storage Case continued:

Bldg Heat Gain	8,448 sq.ft.	X	8.5	Btuh/sq.ft.	=	71,808 Btuh
Lighting	8,500W	X	3.41	Btu/watt hr.	=	28,985 *
Outlets	1,800W	X	3.41	Btu/watt hr.	=	6,138 *
Control Equipment	1,900W	X	3.41	Btu/watt hr.	=	6,479
Main Switchboard	2,513W	X	3.41	Btu/watt hr.	=	8,569
Converters	400W	X	3.41	Btu/watt hr.	=	1,364
Inverters	45,640W	X	3.41	Btu/watt hr.	=	155,632
Battery	45,120W	X	3.41	Btu/watt hr.	=	153,859
People	2	X	215	Btuh/person	=	430 *
				Total Sensible Heat		433,264 Btuh

As can be seen from the above tabulations, there is an approximate 6:1 variation in total heat load encompassed by the various operating modes. The control room cooling requirement could be satisfied by two Pomona ACC-800-2/Bohn RDD-16 combinations. The battery room would require three Pomona ACC-1500-2/Bohn RDD-27 combinations. All units would operate under staged thermostatic control. Cooling requirements of the two smaller rooms could be satisfied, as before, by two Carrier KK0051 units. Based on the foregoing, connected loads in the control building are estimated to be:

P_{mp}	= 0.76 kW		(microprocessor)
P_{ct}	= 0.14		(CRT terminal)
P_{ad}	= 1.00		(A-D converters)
P_{cl}	= 1.80		(control room lights)
P_{bl}	= 7.20		(battery room lights)
P_{ml}	= 0.40		(maintenance shop lights)
P_{rl}	= 0.10		(rest room lights)
P_{to}	= 1.80		(test equip. & outlets)
P_{ac}	= 175.73		(air conditioning equip)
P_B	= 188.93		(building total)

* Used for air conditioning unit capacity calculation, but not for energy calculation due unattended nature of station operation.

3.3 0.7 Capacity Factor Storage Case continued:

Energy requirements for the above loads are, again, a function of the power requirement and duty cycle of each load. Based on an assumed mode of station operation which would result in direct generation and power delivery to the grid for 10.14 hours, battery charging for 8.00 hours and delivery of power from storage to the grid for 11.21 hours, the average daily auxiliary equipment energy requirement would be as follows:

	Power(kW)		Duty Cycle		Hrs/Day		Energy Rqmts.
E_{mp}	= 0.76	X	1.0000	X	24	=	18.24 kWh
E_{ct}	= 0.14	X	0.4225	X	24	=	1.42
E_{ad}	= 1.00	X	0.4225	X	24	=	10.14
E_{cl}	= 1.80	X	0.0238	X	24	=	1.03
E_{bl}	= 7.2	X	0.0238	X	24	=	4.11
E_{ml}	= 0.40	X	0.0238	X	24	=	0.23
E_{rl}	= 0.10	X	0.0238	X	24	=	0.06
E_{to}	= 1.80	X	0.0119	X	24	=	0.51
E_{acf}	= 175.73	X	0.0113	X	24	=	47.66
E_{acc}	= 175.73	X	0.2624	X	24	=	1106.67
E_{acd}	= 175.73	X	0.2565	X	24	=	1081.79
	Total Daily Energy Requirement E_B'					=	2271.86 kWh

The average auxiliary equipment power requirement for the building loads during a 10.14 hour operating day would be:

$$P_B' = \frac{2271.86}{10.14} = 224.05$$

If there are "n" collectors in the collection field, the average power required at the engine output shaft of each collector would be:

$$P_B'' = \frac{224.05}{n(0.997)(0.981)(0.90)} = \frac{254.53}{n} \text{ kW}$$

The above requirement is additive to the requirement for collector auxiliary equipment power requirements defined in paragraph 2.0. It includes no allowance for perimeter (or other) site security lighting.

3.4 Energy Requirements for Security Lighting:

Perimeter security lighting (if required) for the 0.4 capacity factor station would typically consist of 32 175W halogen lamps for which power requirements would be:

$$P_L = 32 \times 0.175 = 5.6 \text{ kW}$$

And for an annual average daily sunset to sunrise period of 11.93 hours would require:

$$E_L = 5.6 \times 11.93 = 66.8 \text{ kWh}$$

If there "n" collectors in the collection field, the average power required at the engine output shaft would be:

$$P_L' = \frac{66.8}{n(0.997)(0.981)(0.90)(10.14)} = \frac{7.48}{n} \text{ kW}$$

3.5 Cold Weather Heating Requirements:

Cold weather heating has not been specificially addressed in the preceding paragraphs, since excess heat will be available during all periods of equipment operation and all equipment items are suitable for a non-operating temperature environment of 0°C, which is less than the minimum listed in the weather data for the typical site location.

Heat balance calculations should, however, be made for sites having a lower temperature minimum to determine whether heat dissipation from the installed equipment and re-radiation from the thermal mass of the building structure will maintain the building interior above 0°C or whether supplemental heating will be required.

REFERENCES

1. Pons, R.L., "Preliminary System Performance Analysis", Technical Report No. SPS-007, dated 27 September 1978.

APPENDIX H

LIFE CYCLE COST EQUATIONS

LIFE CYCLE COST EQUATIONS*

This Appendix presents a summary of the life cycle cost (LCC) equations used for the system energy cost analyses. An effective energy "price" is required in order to recover the costs associated with the purchase, installation, operation and maintenance of a utility-owned solar electric system. This energy "price" is expressed in terms of the levelized busbar energy cost ($\overline{BBEC}$). The methodology for determining $\overline{BBEC}$ is presented below.

(a) Present Value of Capital Investment (CI_{pv})

$$CI_{pv} = (1 + g_c)^p \Sigma_t \left[\frac{1 + g_c}{1 + k}\right]^j CI_t \qquad (1)$$

where:

CI_t = Capital outlay in year t

g_c = Escalation rate for capital costs (0.06)

k = Cost of capital (0.086)

$p = Y_{co} - Y_p$

Y_{co} = First year of commercial operation (1988 for SPS example)

Y_p = Price year for cost information (1978)

$j = Y_t - Y_{co} + 1$

Y_t = Year of given investment outlay

(b) Annualized System Resultant Cost, $\overline{AC}$
(without fuel costs or operating costs)

$$\overline{AC} = (1+g)^{-d} [\overline{FCR} \cdot CI_{pv} + CRF_{k,N} MNT_{pv}] \qquad (2)$$

$$= 0.08739\ CI_{pv} + 0.04773\ MNT_{pv}$$

*Obtained from: "The Cost of Energy from Utility Owned Solar Electric System", JPL Report 5040-79, ERDA/JPL 1012-76/3, June 1976

where:

g = Rate of general inflation (0.06)

d = $Y_{co} - Y_b$ = 1988 - 1978 = 10

Y_b = Base year = 1978

$\overline{FCR}$ = Annualized Fixed Charge Rate (0.1565)

$CRF_{k,N}$ = Capital Recovery Factor (0.0939)

MNT_{pv} = Present value of recurring maintenance costs

(c) Present Value of Maintenance Costs, MNT_{pv} for uniform growth,

$$MNT_{pv_1} = (1 + g_m)^p \left[\frac{1 + g_m}{k - g_m}\right] \left\{1 - \left[\frac{1 + g_m}{1 + K}\right]^N\right\} X_o \qquad (3)$$

$$= 47.274\ X_o$$

where:

g_m = Escalation rate for maintenance costs (0.07)

N = System operating lifeline (30 years)

X_o = Recurrent costs ($)

for non-uniform growth,

$$MNT_{pv_2} = (1 + g_m)^p \Sigma_j \left[\frac{1 + g_m}{1 + K}\right]^j X_t \qquad (4)$$

$$= 1.96715\ (0.98527)^j\ X_t$$

(d) Levelized Busbar Energy Costs, $\overline{BBEC}$

$$\overline{BBEC} = \frac{\overline{AC}}{MWH_A} \qquad (5)$$

where:

MWH_A = ACF x 8760* = actual plant output

ACF = Annualized capacity factor, including allowance for unscheduled maintenance

so:

$$\overline{BBEC}_C = 9.9759(10)^{-6}\ \overline{AC}_c \text{ (for leap year)} \quad (6)$$

and:

$$\overline{BBEC}_M = \overline{OM} = 5.4491(10)^{-6} \cdot \overline{AC}_M \text{ (for leap year)} \quad (7)$$

where:

$(\ )_C$ = Due to capital expenditures

$(\ )_M$ = Due to maintenance expenditures

so:

$$\overline{BBEC} = 9.9759(10)^{-6}\ \overline{AC}_c + 5.4491(10)^{-6}\ \overline{AC}_M \quad (8)$$

* = 8784 for leap year

APPENDIX I

RELIABILITY PREDICTIONS FOR THE SPS

Ford Aerospace &
Communications Corporation
Aeronutronic Division

Ford Road
Newport Beach, California 92663

TECHNICAL REPORT

TR. NO. SPS-020 (Revision A)

SOLAR SMALL POWER SYSTEM (SPS) PROGRAM

TITLE: RELIABILITY PREDICTIONS FOR THE SPS

PREPARED BY	A. Imamura	ORG NO. J230	CHARGE NO. 2P05
SUPERVISOR APPROVAL	W. S. Mathisen	DATE 10 April 1979	
PROGRAM ENGINEER APPROVAL	R. L. Pons	TO Distribution	

SUMMARY

This TR supercedes TR SPS-020 dated 12 March 1979 and revises the predicted cumulative mean-time-between-failure (CMTBF), cumulative mean-time-to-repair (CMTTR) and availability for the baseline solar SPS having a plant size of 1 megawatt electrical (MWe) output with an annual capacity factor (ACF) of 0.4.

In addition, this TR also includes the predicted CMTBF, CMTTR and availability for additional plant sizes of 0.5 and 10.0 MWe with ACF's of 0.36, 0.4 and 0.7, comprising eight additional solar SPS's.

DISTRIBUTION

E. D. Arvetta
F. P. Boda
V. L. Chantler
T. B. Clark
N. L. Cowden
D. C. Jackson
J. M. Klaarenbeek
I. -. Krell
I. E. Lewis (WDL)
V. S. Mathisen
D. B. Osborn
R. L. Pons
W. L. Smallwood
C. C. Wan
D. J. Corn (3+Mstr)

ORIGINAL PAGE IS
OF POOR QUALITY

RELIABILITY PREDICTIONS FOR THE BASELINE SYSTEM AND OTHER SYSTEMS

1. INTRODUCTION

This technical report (TR) revises the predicted cumulative mean-time-between-failure (CMTBF), cumulative mean-time-to-repair (CMTTR) and availability of full rated output during the scheduled power delivery time for the baseline Solar Small Power System (SPS) having a plant size of 1.0 megawatt electrical (MWe) output with an annual capacity factor (ACF) of 0.4.

This TR also includes the predicted CMTBF, CMTTR and availability for additional plant sizes of 0.5 and 10.0 MWe with ACF's of 0.36, 0.4 and 0.7 comprising eight additional Solar SPS's.

2. PREDICTION SUMMARY

Availability is defined as the probability that a system will operate as required by its design at any point in time and considers only operating time (uptime) and downtime, thus excluding idle time. Downtime refers to the corrective (unscheduled) maintenance action time required to return the system, subsystem, equipment or item to the operational state. Availability, derived by the ratio of the system CMTBF to the sum of system CMTBF and CMTTR, corresponds to the uptime probability.

The data presented herein are structured primarily to focus on the areas where corrective (unscheduled) maintenance will be required during the solar SPS operation. Table I summarizes the results of the reliability and availability prediction for the baseline system as well as the eight other systems considered.

The data presented in Table II summarize the predicted subsystem failures and the corresponding subsystem failure distribution in percent to identify the subsystems where failures are most likely to occur over the system power output duration, T_o.

The data presented in Table III summarize the predicted cumulative subsystem downtime in hours resulting from system operation over the time duration, T_o. The downtime distribution in percent for each subsystem is presented to identify the subsystem that drastically affects system availability or uptime.

3. CONCLUSIONS

The following conclusions are based on data presented in Tables I, II and III.

3. CONCLUSIONS - (continued)

- The cumulative system failure and the system downtime increase with the solar SPS complexity (ref. Table I).

- The system complexity has definite effect on the CMTBF (ref. Table I). The CMTBF for the baseline system is 222 hours.

- The availability is relatively insensitive to the ACF's considered for a given plant size (ref. Table I). The availability of the baseline system is 0.9868.

- The collector and power subsystems of systems with ACF of 0.36 have the highest failure percentages due to the absence of power storage capability (ref. Table I).

- The collector and power conversion subsystems of any solar SPS will contribute to more than 60 percent of the annual failures (ref. Table II). For the baseline system, the collector and power conversion subsystems will fail approximately 10 times during the year, corresponding to 70.3 percent of the annual number of expected system failures.

- More than 85 percent of the system downtime is due to the collector and power conversion subsystems (ref. Table III). For the baseline system, its collector and power conversion subsystem dowtime is approximately 38 hours per year, corresponding to 89.9 percent of the annual system downtime.

- The prediction data indicate that ease of maintenance, repair or replacement must be designed into the system to reduce downtime. Modularization of items with relatively high failure rates and downtime should be considered to enhance accessibility, handling and quick replacement in the event of a failure.

- Provision to switch-in a standby subsystem should be a consideration in the design to negate the effects of long downtime due to repair or replacement. The downtime for this consideration is the time it takes the subsystem to switch-in and to attain operational status. This approach can drastically increase subsystem availability in areas where the frequency of failure occurrence and the corresponding downtime are relatively high.

4. ANALYSIS

The solar SPS analyses are based on information provided by Engineering on nine different system configurations encompassing plant sizes of

TABLE I. SYSTEM RELIABILITY AND AVAILABILITY PREDICTION SUMMARY

--SYSTEM DESCRIPTION--			Power Output	PREDICTION				
Plant Size	ACF	Storage	Duration (Hours)	Cumulative Failures	Downtime (Hours)	CMTBF (Hours)	CMTTR (Hours)	Full Rated Availability
0.5MWe	0.36	No	2838	6.09	19.51	466	3.20	0.9931
0.5MWe	0.40	Yes	3168	8.03	22.85	395	2.85	0.9928
0.5MWe	0.70	Yes	5544	17.61	47.82	315	2.72	0.9914
1.0MWe	0.36	No	2838	11.06	37.63	257	3.40	0.9869
*1.0MWe	0.40	Yes	3168	14.29	42.32	222	2.96	0.9868
1.0MWe	0.70	Yes	5544	32.53	91.54	170	2.81	0.9837
10.0MWe	0.36	No	2838	100.8	366.6	28	3.64	0.8849
10.0MWe	0.40	Yes	3168	131.9	412.5	24	3.13	0.8846
10.0MWe	0.70	Yes	5544	305.9	896.4	18	2.93	0.8600

* Baseline System Calculations:

$$\text{CMTBF} = \frac{3168 \text{ Hours}}{14.29 \text{ Failures}} = 222 \text{ hours between failures}$$

$$\text{CMTTR} = \frac{42.32 \text{ Hours}}{14.29 \text{ Failures}} = 2.96 \text{ hours to repair}$$

$$\text{Availability} = \frac{\text{CMTBF}}{\text{CMTBF} + \text{CMTTR}} = \frac{222}{222 + 2.96} = 0.9868$$

TABLE II. PREDICTED SUBSYSTEM FAILURES AND FAILURE DISTRIBUTION

Plant Size	ACF	Data	SUBSYSTEM FAILURES AND DISTRIBUTION: Collector	Power Conversion	Transport/ Distribution	Computer Control	Storage	System Total
0.5MWe	0.36	Failures	2.32	2.45	0.27	1.05	---	6.09
		Distribution	38.1%	40.3%	4.4%	17.2%	---	100%
0.5MWe	0.40	Failures	2.56	2.72	0.36	1.17	1.22	8.03
		Distribution	31.8%	33.9%	4.5%	14.6%	15.2%	100%
0.5MWe	0.70	Failures	5.39	5.71	1.14	2.06	3.31	17.61
		Distribution	30.6%	32.4%	6.5%	11.7%	18.8%	100%
1.0MWe	0.36	Failures	4.62	4.90	0.49	1.05	---	11.06
		Distribution	41.8%	44.3%	4.4%	9.5%	---	100%
*1.0MWe	0.40	Failures	4.87	5.17	0.63	1.17	2.45	14.29
		Distribution	34.1%	36.2%	4.4%	8.2%	17.1%	100%
1.0MWe	0.70	Failures	10.52	11.16	2.19	2.06	6.60	32.53
		Distribution	35.3%	37.5%	4.2%	0.9%	22.1%	100%
10.0MWe	0.36	Failures	46.2	49.0	4.6	1.0	---	100.8
		Distribution	45.8%	48.6%	4.6%	1.0%	---	100%
10.0MWe	0.40	Failures	48.7	51.7	5.8	1.2	24.5	131.9
		Distribution	36.9%	39.2%	4.4%	0.9%	18.6%	100%
10.0MWe	0.70	Failures	105.2	111.6	21.0	2.1	66.0	305.9
		Distribution	34.4%	36.5%	6.9%	0.7%	21.5%	100%

*Baseline System

TABLE III. PREDICTED SUBSYSTEM DOWNTIME AND DISTRIBUTION

----SYSTEM----			----------SUBSYSTEM DOWNTIME (DT) AND DISTRIBUTION ----------					
Plant Size	ACF	Data	Collector	Power Conversion	Transport/ Distribution	Computer Control	Storage	System Total
0.5MWe	0.36	DT (Hours)	8.29	9.80	0.37	1.05	---	19.51
		Distribution	42.5%	50.2%	1.9%	5.4%	---	100%
0.5MWe	0.40	DT (Hours)	9.09	10.88	0.43	1.17	1.28	22.85
		Distribution	39.8%	47.6%	1.9%	5.1%	5.6%	100%
0.5MWe	0.70	DT (Hours)	19.16	22.84	0.93	2.06	2.83	47.82
		Distribution	40.1%	47.8%	1.9%	4.3%	5.9%	100%
1.0MWe	0.36	DT (Hours)	16.50	19.60	0.48	1.05	---	37.63
		Distribution	43.8%	52.1%	1.3%	2.8%	---	100%
*1.0MWe	0.40	DT (Hours)	17.35	20.68	0.56	1.17	2.56	42.32
		Distribution	40.1%	48.9%	1.3%	2.8%	6.0%	100%
1.0MWe	0.70	DT (Hours)	37.41	44.64	1.81	2.06	5.62	91.54
		Distribution	40.8%	48.8%	2.0%	2.3%	6.1%	100%
10.0MWe	0.36	DT (Hours)	165.0	196.0	4.6	1.0	---	366.6
		Distribution	45.0%	53.4%	1.3%	0.3%	---	100%
10.0MWe	0.40	DT (Hours)	173.5	206.8	5.4	1.2	25.6	412.5
		Distribution	42.1%	50.1%	1.3%	0.3%	6.2%	100%
10.0MWe	0.70	DT (Hours)	374.1	446.4	17.6	2.1	56.2	896.4
		Distribution	41.7%	49.8%	2.0%	0.2%	6.3%	100%

* Baseline System

4. ANALYSIS - (continued)

0.5, 1.0 and 10.0 MWe, each plant size considered for ACF's of 0.36, 0.4 and 0.7.

4.1 RELIABILITY MODEL

The basic reliability model of the solar SPS is configured as a series model illustrated by the block diagrams of Figure 1. The basic difference between Figure 1A and 1B is the presence of the storage subsystem for the ACF's indicated. The main difference among the systems analyzed is the variation in complexity of the subsystem as summarized by Table IV for (N) number or quantity of item per subsystem.

4.2 ASSUMPTIONS AND CONDITIONS

The annual solar SPS operational or rated power output duration is determined by the ACF (see 4.3.1). Failure occurrence during this time duration will require corrective maintenance action to restore the system to full operational status by replacing, repairing or adjusting the component or subsystem which caused interruption of service.

Preventive maintenance is performed at regular intervals when the SPS is not delivering scheduled power in order to maintain the system in a condition consistent with its designed level of performance, reliability, and where applicable, safety.

Preventive maintenance typically involves servicing, inspections and minor or major overhauls during which

a. regular care is provided to the normally operating subsystems and components which require such attention (lubrication, cleaning, adjustments, alignment, etc.),

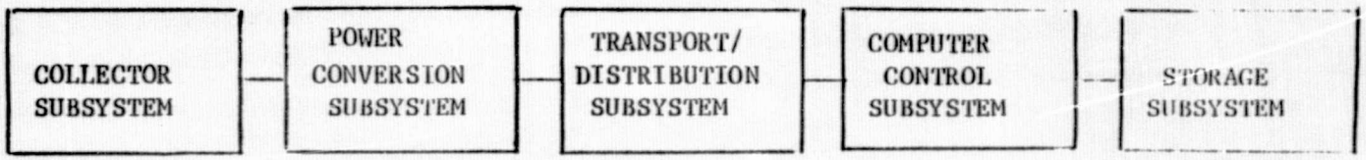
b. periodic functional check is performed to ascertain the integrity of the subsystem,

c. marginal or erratic components and subsystems are repaired or removed and replaced, and

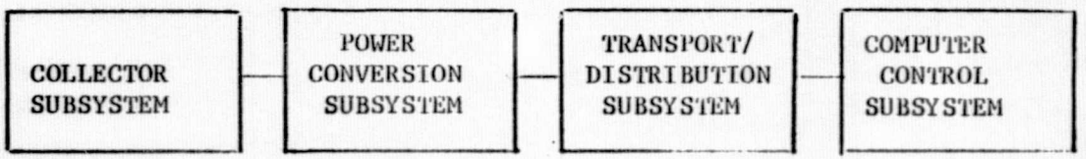
d. components which are nearing wearout condition are replaced or overhauled.

4.3 DEFINITIONS, EQUATIONS AND CALCULATIONS

The following definitions and equations were established and used to calculate the various reliability parameters.



A. Model applicable to the Solar SPS with ACF of 0.4 and 0.7.



B. Model applicable to the Solar SPS with ACF of 0.36.

Figure I. Basic Reliability Model Block Diagrams.

ORIGINAL PAGE IS OF POOR QUALITY

TABLE IV. PREDICTED FAILURE RATE SUMMARY
BASED ON
PLANT SIZE AND ACF COMPLEXITY

SUBSYSTEM/ITEM	SINGLE ITEM BASIC FAILURE RATE	PLANT SIZE AND ANNUAL CAPACITY FACTOR (ACF)																	
		PLANT SIZE = 0.5 MWe						PLANT SIZE = 1.0 MWe						PLANT SIZE = 10.0 MWe					
		ACF = 0.36 No STORAGE		ACF = 0.40 WITH STORAGE		ACF = 0.70 WITH STORAGE		ACF = 0.36 No STORAGE		ACF = 0.40 WITH STORAGE		ACF = 0.70 WITH STORAGE		ACF = 0.36 No STORAGE		ACF = 0.40 WITH STORAGE		ACF = 0.70 WITH STORAGE	
	λ	N	Nλ	N	Nλ	N	Nλ	N	Nλ	N	Nλ	N	Nλ	N	Nλ	N	Nλ	N	Nλ
1. COLLECTOR																			
A. STRUCTURE	0.37	9	3.33	10	3.70	21	7.77	18	6.66	19	7.03	41	15.17	180	66.60	190	70.30	410	151.70
B. DRIVE CONTROLS	60.90	9	548.10	10	609.0	21	1278.9	18	1096.2	19	1157.10	41	2496.9	180	10,962	190	11,571	410	24,969
C. MIRRORED PANEL SET	12.50	9	112.5	10	125.0	21	262.5	18	225	19	237.50	41	512.5	180	2,250	190	2,375	410	5,125
D. RECEIVER/VAPOR PIPE	16.70	9	150.3	10	167.0	21	350.7	18	300.6	19	317.30	41	684.7	180	3,006	190	3,173	410	6,847
COLLECTOR SUBSYSTEM TOTAL			814.23		904.7		1899.87		1628.46		1718.93		3709.27		16,284.6		17189.3		37,282
2. POWER CONVERSION																			
A. ENGINE + ACCESSORIES	77.50	9	697.5	10	775	21	1627.5	18	1395	19	1472.5	41	3177.5	180	13950	190	14725	410	31775
B. ALTERNATOR + ACCESSORIES	18.35	9	165.15	10	183.5	21	385.35	18	330.3	19	348.65	41	752.35	180	3303	190	3486.5	410	7523.5
POWER CONVERSION SUBSYS TOTAL			862.65		958.5		2012.85		1726.3		1821.15		3929.85		17,253		18211.5		39,298.5
3. TRANSPORT/DISTRIBUTION																			
1. MAIN SWITCHBOARD *	2.88	30	86.4	36	103.68	69	198.72	57	164.16	66	190.08	132	380.16	543	1563.84	603	1736.64	1263	3637.44
2. HV TRANSFORMER	5.70	1	5.7	1	5.7	1	5.7	1	5.7	1	5.7	2	11.4	10	57	10	57	20	114
3. HV SWITCH	1.60	1	1.6	1	1.6	1	1.6	1	1.6	1	1.6	2	3.2	10	16	10	16	20	32
TRANS/DIST SUBSYS TOTAL			93.7		110.98		206.02		171.46		197.38		394.76		1636.84		1809.64		3,783.44
4. COMPUTER CONTROL																			
A. COMPUTER + ACCESSORIES	155.50	1	155.50	1	155.50	1	155.50	1	155.50	1	155.50	1	155.50	1	155.50	1	155.50	1	155.50
B. FAN/AIR CONDITIONER	216.00	1	216.00	1	216.00	1	216.00	1	216.00	1	216.00	1	216.00	1	216.00	1	216.00	1	216.00
COMP CONTROL SUBSYS TOTAL			371.5		371.5		371.5		371.5		371.5		371.5		371.5		371.5		371.5
5. STORAGE																			
A. FAN/AIRCONDITIONER	216.00	0	0	1	216.0	1	216.0	0	0	2	432	2	432	0	0	20	4320	20	4320
B. AC TO DC CONVERTER	101.00	0	0	1	101.0	1	101.0	0	0	2	202	2	202	0	0	20	2020	20	2020
C. BATTERY BANK	69.70	0	0	1	69.7	4	278.8	0	0	2	139.4	8	557.6	0	0	20	1394	80	5576
D. DC TO AC INVERTER	100.00	0	0	1	100.0	1	100.0	0	0	2	200	2	200	0	0	20	2000	20	2000
STORAGE SUBSYSTEM TOTAL			0		487.7		687.8		0		969.4		1375.6		0		9414		13,136
SYSTEM FAILURE RATE			2,142.08		2,832.38		5,186.04		3,896.72		5,078.36		9,796.98		35,545.94		47,315.94		111,651.44

* N AND λ FOR THE SWITCHBOARD ARE BASED ON THE QUANTITY AND FAILURE RATE OF POWER CIRCUIT BREAKERS.

MWe = MEGAWATT ELECTRICAL.

N = NUMBER OR QUANTITY OF ITEM.

λ = FAILURES PER MILLION HOURS = FAILURE RATE.

4.3.1 ANNUAL CAPACITY FACTOR. The ACF is defined by the ratio:

$$ACF = \frac{T_o}{T_b}$$

where: T_o = total time a given system delivers rated power output per year, and

T_b = time base of 330 calendar days or, 7920 hours per year.

For ACF's of 0.36, 0.4 and 0.7, the corresponding T_o's are 2838, 3168 and 5544 hours, respectively.

On a daily basis, the power delivery time breakdowns listed below relative to solar or storage source are assumed for the different ACF's. The time durations as shown form the basis of item operational time of Table V.

	-----Time (Hours)------		
ACF	Solar Source	Storage Source	Total Time
0.36	8.6	None	8.6
0.40	8.6	1.0	9.6
0.70	8.6	8.2	16.8

4.3.2 FAILURE AND FAILURE RATE. Failure is defined as the inability of a part, a component or an equipment to perform as specified, or a system to continue operation as required, resulting in repair, removal or replacement action.

Failure rate, the number of failure occurrences per unit time, is generally expressed in terms of failures per million operating hours. The single item failure rates (λ) tabulated in Table IV were estimated by using parts count, equipment similarity and complexity assessment techniques. The basic failure data for the drive controls of the collector subsystem were provided by WDL Division of FACC, based on their field experiences. Other sources of the basic part/component failure rates were the following:

Part/Component	Data Source
a. Electronic	MIL-HDBK-217B, "Military Standardization Handbook, Reliability Prediction of Electronic Equipment", dated 9-20-74; Notice 1, dated 9-7-76; Note 2, dated 3-17-78.

4.3.2 FAILURE AND FAILURE RATE. - (continued)

Part/Component	Data Source
b. Nonelectronic, mechanical, etc.	NPRD-1, "Nonelectronic Parts Reliability Data", Summer 1978, ITT Research Institute/ Rome Air Development Center (RADC)
c. Nonelectronic, mechanical, etc.	RADC-TR-75-22, "Nonelectronic Reliability Notebook", dated January 1975, RADC.
d. Mechanical Piece Part	T-70-48891-007, "Handbook of Piece Part Failure Rates", (HPPF), dated 6-22-70, Martin Marietta, Denver Division, GIDEP Access No. E031-1273.

The total item failure rate (λ_I) is defined by the expression

$$\lambda_I = N\lambda$$

where: N = quantity of a given item
λ = single item failure rate.

The total expected item failure quantity per year is determined by the expression

$$F = \lambda_I t_o$$

where: λ_I = total item failure rate

t_o = total item operating time per year, determined by the ACF.

Tables IV and V tabulate the calculated results for $\lambda_I = N\lambda$ and Table V contains the results for F.

4.3.3 DOWNTIME OR RECOVERY TIME. Downtime is the time it takes to restore system operation after an in-service failure or malfunction. The cumulative downtime per year for a given item is determined by

$$T_d = F \times t_r$$

where: F = number of item failures per year
t_r = downtime or recovery time per failure.

The calculated results of the cumulative downtime for the subsystems and items are summarized in Table V.

TABLE V-1. PREDICTED ITEM FAILURE COUNT AND DOWNTIME (ACF - 0.36)

SUBSYSTEM/ITEM	t_o	t_r	PLANT SIZE = 0.5MWe λ_I	F	Fx t_r	PLANT SIZE = 1.0MWe λ_I	F	Fx t_r	PLANT SIZE = 10.0MWe λ_I	F	Fx t_r
1. COLLECTOR											
A. Structure	2838	24.0	3.3	0.01	0.24	6.6	0.02	0.48	66.6	0.2	4.8
B. Drive Controls	2838	2.0	548.1	1.56	3.12	1096.2	3.11	6.22	10962.0	31.1	62.2
C. Mirrored Panel Set	2838	8.0	112.5	0.32	2.56	225.0	0.64	5.12	2250.0	6.4	51.2
D. Receiver/Vapor Pipe	2838	5.5	150.3	0.43	2.37	300.6	0.85	4.68	3006.0	8.5	46.8
COLLECTOR TOTAL				2.32	8.29		4.62	16.50		46.2	165.0
2. POWER CONVERSION											
A. Engine and Access.	2838	4.0	697.5	1.98	7.92	1395.0	3.96	15.84	13950.0	39.6	158.4
B. Alternator & Acces.	2838	4.0	165.2	0.47	1.88	330.3	0.94	3.76	3303.0	9.4	37.6
POWER CONV. TOTAL				2.45	9.80		4.90	19.60		49.0	196.0
3. TRANSPORT/DISTRIB.											
A. Main Switchboard	2838	0.5	86.4	0.25	0.13	164.2	0.47	0.24	1563.8	4.4	2.2
B. HV Transformer	2838	12.0	5.7	0.02	0.24	5.7	0.02	0.24	57.8	0.2	2.4
C. HV Switch	2838	1.5	1.6	0.00	0.00	1.6	0.00	0.00	16.0	0.0	0.0
TRANS/DISTR. TOTAL				0.27	0.37		0.49	0.48		4.6	4.6
4. COMPUTER CONTROL											
A. Computer & Access.	2838	1.0	155.5	0.44	0.44	155.5	0.44	0.44	155.5	0.4	0.4
B. Fan/Air Cond.	2838	1.0	216.0	0.61	0.61	216.0	0.61	0.61	216.0	0.6	0.6
COMPUTER CONTROL TOTAL				1.05	1.05		1.05	1.05		1.0	1.0
SYSTEM TOTAL				6.09	19.51		11.06	37.63		100.8	366.6

Legend:

t_o = item operating hour in hours per year.

t_r = estimated item recovery time per failure = downtime in hours.

λ_I = item base failure rate in failures per million hours for a given plant size and ACF (See Table IV) = $N\lambda$

F = $(\lambda)(t_o)$ = failure quantity over the t_o duration.

Fxt_r = item downtime over the t_o duration.

TABLE V-2. PREDICTED ITEM FAIL[illegible] COUNT AND DOWNTIME (ACF = 0.40)

SUBSYSTEM/ITEM	t_o	t_r	PLANT SIZE = 0.5MWe λ_I	F	Fx t_r	PLANT SIZE = 1.0MWe λ_I	F	Fx t_r	PLANT SIZE - 10.0MWe λ_I	F	Fx t_r
1. COLLECTOR											
A. Structure	2838	24.0	3.7	0.01	0.24	7.0	0.02	0.48	70.3	0.2	4.8
B. Drive Controls	2838	2.0	609.0	1.73	3.46	1157.1	3.28	6.56	11571.0	32.8	65.6
C. Mirrored Panel Set	2838	8.0	125.0	0.35	2.80	237.5	0.67	5.36	2375.0	6.7	53.6
D. Receiver/Vapor Pipe	2838	5.5	167.0	0.47	2.59	317.3	0.90	4.95	3173.0	9.0	49.5
COLLECTOR TOTAL				2.56	9.09		4.87	17.35		48.7	173.5
2. POWER CONVERSION											
A. Engine & Access.	2838	4.0	775.0	2.20	8.80	1472.5	4.18	16.72	14725.0	41.8	167.2
B. Alternator & Access.	2838	4.0	183.5	0.52	2.08	348.7	0.90	3.96	3486.5	9.9	39.6
POWER CONV. TOTAL				2.72	10.88		5.17	20.68		51.7	206.8
3. TRANSPORT/DISTRIB.											
A. Main Switchboard	3168	0.5	103.7	0.33	0.17	190.1	0.60	0.30	1736.6	5.5	2.8
B. HV Transformer	3168	12.0	5.7	0.02	0.24	5.7	0.02	0.24	57.0	0.2	2.4
C. HV Switch	3168	1.5	1.6	0.01	0.02	1.6	0.01	0.02	16.0	0.1	0.2
TRANS/DISTR. TOTAL				0.36	0.43		0.63	0.56		5.8	5.4
4. COMPUTER CONTROL											
A. Computer & Access.	3168	1.0	155.5	0.49	0.49	155.5	0.49	0.49	155.5	0.5	0.5
B. Fan/Air Cond.	3168	1.0	216.0	0.68	0.68	216.0	0.68	0.68	216.0	0.7	0.7
COMPUTER CONT. TOTAL				1.17	1.17		1.17	1.17		1.2	1.2
5. STORAGE											
A. Fan/Air Cond.	3168	1.0	216.0	0.68	0.68	432.0	1.37	1.37	4320.0	13.7	13.7
B. AC to DC Conv.	2838	1.5	101.0	0.29	0.44	202.0	0.57	0.86	2020.0	5.7	8.6
C. Battery Bank	3168	0.5	69.7	0.22	0.11	139.4	0.44	0.22	1394.0	4.4	2.2
D. DC to AC Inverter	330	1.5	100.0	0.03	0.05	200.0	0.07	0.11	2000.0	0.7	1.1
STORAGE TOTAL				1.22	1.28		2.45	2.56		24.5	25.6
SYSTEM TOTAL				8.03	22.85		14.29	42.32		131.9	412.5
						BASELINE SYSTEM					

TABLE V-3. PREDICTED ITEM FAILURE COUNT AND DOWNTIME (ACF = 0.70)

SUBSYSTEM/ITEM	t_o	t_r	PLANT SIZE = 0.5MWe λ_I	F	Fx t_r	PLANT SIZE = 1.0MWe λ_I	F	Fx t_r	PLANT SIZE - 10.0MWe λ_I	F	Fx t_r
1. COLLECTOR											
A. Structure	2838	24.0	7.8	0.02	0.48	15.2	0.04	0.96	151.7	0.4	9.6
B. Drive Controls	2838	2.0	1278.9	3.63	7.26	2496.9	7.09	14.18	24969.0	70.9	141.8
C. Mirrored Panel Set	2838	8.0	262.5	0.74	5.92	512.5	1.45	11.60	5125.0	14.5	116.0
D. Receiver/Vapor Pipe	2838	5.5	350.7	1.00	5.50	684.7	1.94	10.67	6847.0	19.4	106.7
COLLECTOR TOTAL				5.39	19.16		10.52	37.41		105.2	374.1
2. POWER CONVERSION											
A. Engine and Access.	2838	4.0	1627.5	4.62	18.48	3177.5	9.02	36.08	31775.0	90.2	360.8
B. Alternator & Acces.	2838	4.0	385.4	1.09	4.36	752.4	2.14	8.56	7523.5	21.4	85.6
POWER CONV. TOTAL				5.71	22.84		11.16	44.64		111.6	446.4
3. TRANSPORT/DISTRIB.											
A. Main Switchboard	5544	0.5	198.7	1.10	0.55	380.2	2.11	1.06	3637.4	20.2	10.1
B. HV Transformer	5544	12.0	5.7	0.03	0.36	11.4	0.06	0.72	114.0	0.6	7.2
C. HV Switch	5544	1.5	1.6	0.01	0.02	3.2	0.02	0.03	32.0	0.2	0.3
TRANS/DISTR. TOTAL				1.14	0.93		2.19	1.81		21.0	17.6
4. COMPUTER CONTROL											
A. Computer & Access.	5544	1.0	155.5	0.86	0.86	155.5	0.86	0.86	155.5	0.9	0.9
B. Fan/Air Cond.	5544	1.0	216.0	1.20	1.20	216.0	1.20	1.20	216.0	1.2	1.2
COMPUTER CONT. TOTAL				2.06	2.06		2.06	2.06		2.1	2.1
5. STORAGE											
A. Fan/Air Cond.	5544	1.0	216.0	1.20	1.20	432.0	2.40	2.40	4320.0	24.0	24.0
B. AC to DC Conv.	2838	1.5	101.0	0.29	0.44	202.0	0.57	0.86	2020.0	5.7	8.6
C. Battery Bank	5544	0.5	278.8	1.55	0.78	557.6	3.09	1.55	5576.0	30.9	15.5
D. DC to AC Inverter	2706	1.5	100.0	0.27	0.41	200.0	0.54	0.81	2000.0	5.4	8.1
STORAGE TOTAL				3.31	2.83		6.60	5.62		66.0	56.2
SYSTEM TOTAL				17.61	47.82		32.53	91.54		305.9	896.4

4.3.4 CUMULATIVE-MEAN-TIME-BETWEEN-FAILURE. The CMTBF is defined by the expression

$$CMTBF = \frac{T_o}{\Sigma F}$$

where: T_o = total time a given system delivers rated power output per year as determined by the ACF, and

ΣF = cumulative number of failures that are expected to occur during system operation for a year.

The CMTBF for the nine systems are tabulated in Table I.

4.3.5 CUMULATIVE MEAN-TIME-TO-RECOVERY. The CMTTR is defined by the expression

$$CMTTR = \frac{\Sigma T_d}{\Sigma F} = \frac{\Sigma(Fxt_r)}{\Sigma F}.$$

The CMTTR for the nine systems are tabulated in Table I.

4.3.6 SYSTEM AVAILABILITY. The system availability or up time probability is defined by the expression

$$A = \frac{CMTBF}{CMTBF + CMTTR}.$$

The system availability results are tabulated in Table I.

APPENDIX J

STUDY OF RECEIVER INSULATION MATERIALS

APPENDIX J

STUDY OF RECEIVER INSULATION MATERIALS

Table J-1 presents some of the physical and cost data for various thermal insulations investigated for SPS. The table was limited to high temperature, low thermal conductivity, low cost and lightweight insulations. These insulators are typically ceramic blankets made from high purity alumina-silica fibers, and the data were obtained from several vendors. The insulation cost is listed in terms of dollars per board foot (1" x 12" x 12"). This cost is the "best" quotation price obtained for a purchase of 5,000 (or more) board feet of insulation. This cost can be reduced by purchasing insulation in greater quantities and by purchasing directly from the manufacturers.

Thermal conductivities of the insulators are presented as a function of mean insulation temperature in Figure J-1. The thermal conductivities for the ceramic blankets at the mean temperature (~375°C) of the receiver subsystem are approximately 0.06 to 0.08 W/m-°C. The thermal conductivity of the Johns-Manville Min-K is approximately one-half that of the other insulators, however, it is more appropriate to compare thermal insulators on a "performance-cost" basis. Insulation performance-cost is simply the product of the thermal conductivity and the cost per volume. Figure J-2 presents this factor for several candidate materials as a function of the mean insulation temperature. The "Cerawool"* and "Durablanket" insulations are the least expensive ceramic blankets in the 8#/ft^3 (128 kg/m^3) densities. The Cerawool blanket has been selected for the baseline since it has slightly lower conductivity. Although less expensive, the lower density insulations such as the "Duraback" blanket are not recommended since they are easily compressed to a less effective thickness. The performance-cost of the Cerawool blanket is approximately 35$-W/m^4-°C. Although it has a very low thermal conductivity, the performance-cost of the Min-K is about 1350$W/m^4-°C, which makes it prohibitively expensive.

---

* Manufacturers of these trade-name insulations are listed in Table J-1.

TABLE J-1: INSULATION DATA

	INSULATION	CHEMICAL COMPOSITION	MAXIMUM SERVICE TEMPERATURE	DENSITY	COST
1	Cerawool[A]	40% Al_2O_3, 51% S_iO_2	1600°F (871°C)	8#/ft^3 (128 kg/in^3)	1.08 $/BDft
2	Cerablanket[A]	47% Al_2O_3, 53% S_iO_2	2400 (1316)	8 (128)	1.42
3	Cerafelt[A]	46% Al_2O_3, 54% S_iO_2	2400 (1316)	8 (128)	1.70
4	Cerachrome[A]	41% Al_2O_3, 55% S_iO_2	2600 (1427)	8 (128)	3.04
5	Durablanket[B]	48% Al_2O_3, 52% S_iO_2	2300 (1260)	8 (128)	1.14
6	Duraback[B]	40% Al_2O_3, 57% S_iO_2	1700 (927)	4 (64)	0.43
7	Lo-Con Blanket[B]	52% Al_2O_3, 48% S_iO_2	2300 (1260)	6 (96)	1.08
8	Mineral Wool[C]		1000 (538)	8 (128)	0.15
9	Krawool[D]	45% Al_2O_3, 52% S_iO_2	2300 (1260)	8 (128)	1.65
10	Fiberglass TIW-I[E]		1000 (538)	- --	0.09
11	Min-K[A]		1800 (982)	16 (256)	84.00

A. Johns-Manville
B. Carborundum Company
C. Holmes Ltd.
D. Babcock & Wilcox Company
E. Owens-Corning Fiberglass Corporation

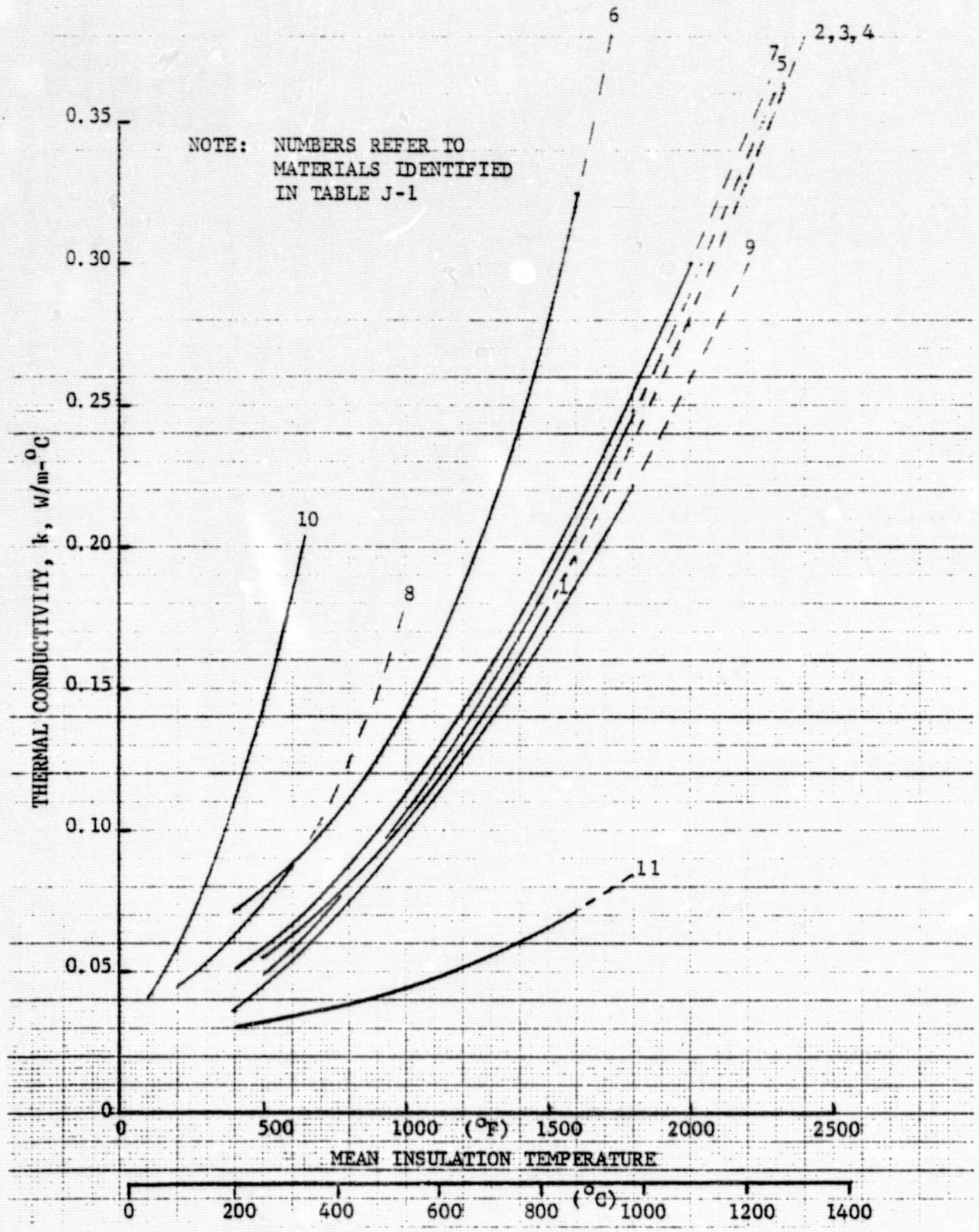


FIGURE J-1. THERMAL CONDUCTIVITY OF INSULATION MATERIALS

E IS OF POOR QUALITY

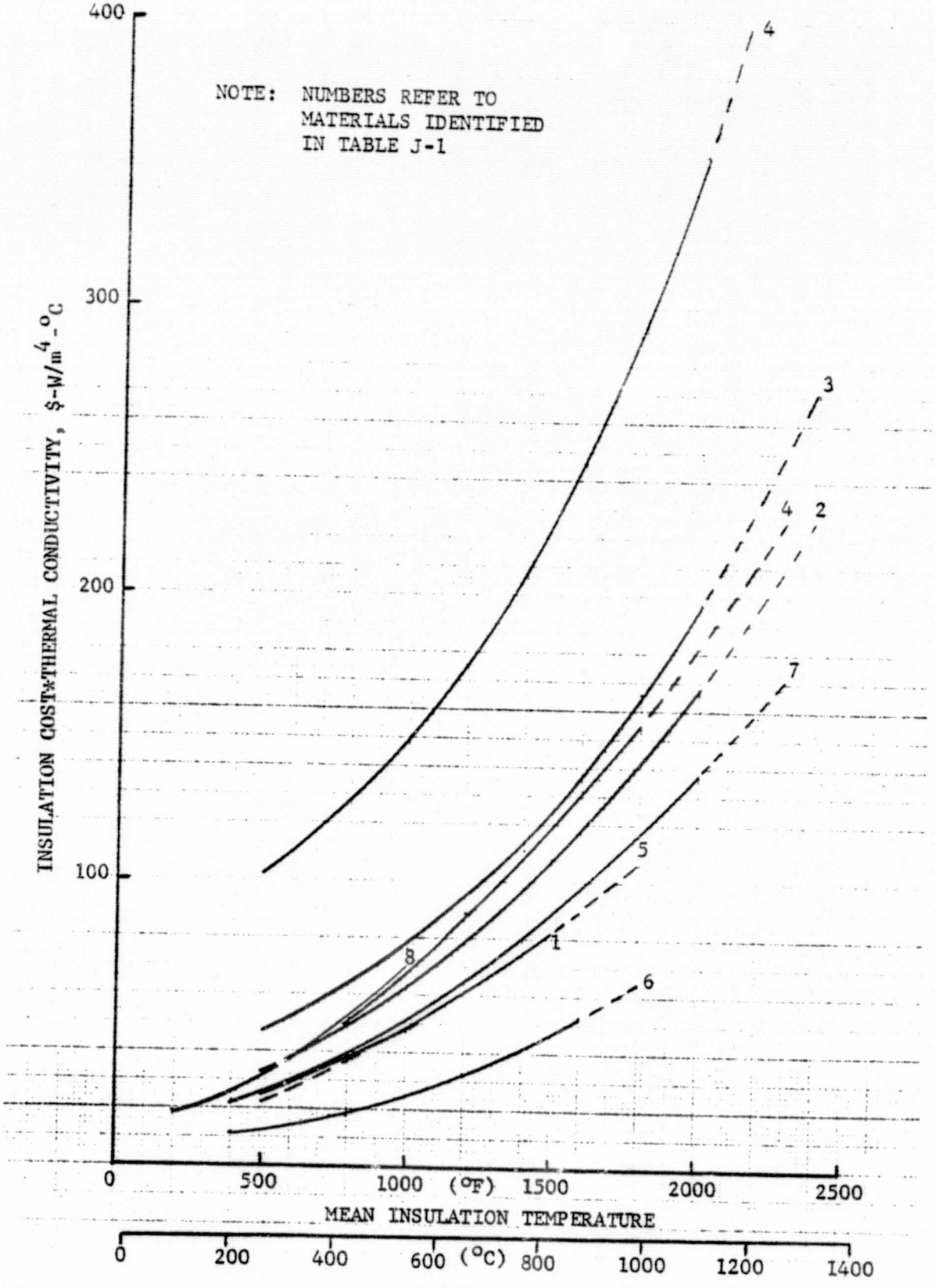


FIGURE J-2. PERFORMANCE-COST OF INSULATION MATERIALS

ORIGINAL PAGE IS OF POOR QUALITY

APPENDIX K

BUFFER STORAGE MATERIALS AND COMPARISON

APPENDIX K

BUFFER STORAGE MATERIALS AND COMPARISON

1. MATERIALS

Buffer storage is composed of a material capable of absorbing and releasing large amounts of heat over the proper temperature range. Storage capacity can be in the form of sensible heat, latent heat, heat of reaction, or various combinations thereof. The work of Schröder at the Philips Aachen Lab (Germany) demonstrates that the most practical solution at the present time for Stirling engine applications is a combination of sensible energy of the solid and liquid phases plus latent heat of fusion of certain high-melting-point salts (Reference K-1). This is verified to some extent by a Sandia study (Reference K-2) in which some additional compounds were identified which may have some cost advantages.

Investigation of the basic laws of chemistry shows that the highest sensible heat capacities and heats of fusion per unit weight and volume will be obtained in substances having a close molecular packing of small and light elements. (Reference K-3). In addition to high thermal capacity, a storage material should satisfy several other criteria:

(1) The melting point must be within the operating temperature range of the engine, which should be as high as possible for maximum power plant efficiency (i.e., ~800°C for the existing USS Stirling engines).

(2) The material must be chemically stable and non-corrosive or have additives to eliminate corrosion.

(3) Low cost, especially for large-scale applications.

(4) The vapor pressure should be low at the maximum temperatures.

(5) The material should not be highly flammable or toxic.

The first criterion sets a fusion point of the buffer store in the range of roughly 750-850°C (1380-1560°F). It is usually desirable to run a Stirling engine at a high constant heater head temperature as much as possible since the engine operates less efficiently at lower heat temperatures. Since this can occur only at the stores fusion point if the engine is running exclusively from the buffer heat storage, it is desirable to have a large heat of fusion. The lower temperature limit at which the buffer storage is effective is dictated by the heat transfer characteristics of the medium which transports the energy from the store to the engine.

Studies documented in References K-1 and K-5 have shown that the fluorides of lithium, sodium, and magnesium have higher total heat capacities than any

other practical materials. However, the high melting point of most pure fluorides (except LiF and BeF_2) makes it necessary to employ lower melting point eutectic mixtures to obtain the desired performance over the selected operating temperature range. Other properties of fluoride-type materials are also as good as, or better than, most other potential heat store candidates, particularly for the lithium-based compounds. Unfortunately, the current price of lithium compounds appears to make them non-competitive on a cost basis for large-scale application, and beryllium compounds are excluded on the basis of cost and toxicity. Other potential candidates, particularly from a cost standpoint, are basically in the chloride group (Reference K-2). The following high temperature heat store salts were selected for comparison from a much larger list of candidates.

Fluorides: LiF, and eutectics of LiF/MgF_2, NaF/MgF_2, or $LiF/NaF/MgF_2$

Chlorides: NaCl, $NaCl/CaCl_2$ eutectic, $NaCO_3/KCl$ eutectic and $CaCl_2$

Carbonates: K_2CO_3/Na_2CO_3 eutectic

Fluorides. Table K-1 lists some of the properties of candidate fluorides. LiF has the highest heat of fusion of all the materials on a weight basis but contains a large amount of scarce and expensive lithium. An eutectic mixture of 67% LiF/33% MgF_2 (mole percent) contains only 12.1 percent lithium, costs about one-fourth that of LiF, and has a volumetric heat of fusion even higher than LiF (or even LiH). The third mixture shown in the table contains no lithium and is one of the more cost effective candidates, as well as having other favorable properties as outlined below. The low production cost of the NaF/MgF_2 material is due to the fact that fertilizer manufacturers have been throwing away fluoride-bearing compounds (mostly in the form of H_2SiF_6) for a number of years as waste products. Philips has obtained cost quotes for the production of material No. 3 of $0.15/kg in large quantities from LaPorte Company in England. This quote includes the recovery of fluorine and combining it with common sodium and magnesium (or other elements as desired). The production cost of this material in the U.S. is also projected to be about $0.15/kg.*, provided fluorine can be obtained from H_2SiF_6, which is now an undesirable waste product and is usually dumped in a land fill. Today the price of NaF or NaF/MgF_2 is about $0.70/kg* because the source of the flourine is expensive hydrofluoric acid, and production is relatively small. The fourth material is typical of a relatively low melt temperature fluoride eutectic, and is included only for reference since the cost will likely be too high and the melting point too low compared to material No. 3.

---

*Personal communication with Dr. J. Eichelberger of the Pennwalt Corp.

TABLE K-1. REPRESENTATIVE PROPERTIES OF CANDIDATE HEAT STORE MATERIALS
(Sources: References K-1, K-2, K-5, K-7)

No.	Composition, Mole %	Melting Point °C	Melting Point (°F)	ΔHf, Heat of Fusion kW-sec/kg	ΔHf, Heat of Fusion (BTU/lb)	Heat Capacity; 450-850°C kW-sec/kg	Heat Capacity; 450-850°C (BTU/lb)	Density at Melt, g/cm³ Solid	Density at Melt, g/cm³ Liquid	Approx. Cost $/kg	Comments
1	LiF	848	(1558)	930[1]	(400)	1885	(811)	-	1.83	20-22	Too expensive
2	67 LiF/33 MgF_2	746	(1375)	910	(390)	1640	(705)	2.63	2.31	4.98[2]	Too expensive
3	75 NaF/25 MgF_2	832	(1530)	636	(273)	1275	(548)	2.69	2.19	0.15[3]	Final candid.
4	46LiF/44 NaF/ 10 MgF_2	632	(1170)	686	(295)	1260	(542)	2.61	2.10	-	Probably too expensive, melts too low
5	NaCl	800[4]	(1472)	479	(206)	1020	(439)	1.96	1.55	See Text	Possible candid. but low ρ
6	48 NaCl/52 $CaCl_2$	500	(932)	281	(121)	720	(309)	-	-	0.073[5]	Melts too low
7	50 Na_2CO_3/50KCl	588	(1090)	268	(115)	830	(357)	-	-	0.11[5]	Melts too low
8	$CaCl_2$	772	(1422)	255	(110)	650	(280)	2.09?	2.08	See Text	Possible candidate but low heat capacity
9	44 K_2CO_3/56 Na_2CO_3	710	(1310)	159	(68)	Not evaluated, judged to be low		-	-	-	Heat capacity too low

(1) Given as 1046 kW-sec/kg (450 BTU/lb) in some references.

(2) Reference K-6; unknown quantity and impurity level.

(3) Projected production costs (see text).

(4) Reference K-7; other references give melt point as high as 808°C.

(5) Reference K-3; unknown quantity and impurity level. See text for comments.

Additional advantages of the fluoride-type compounds are as follows. First, the densities of the materials near the melt are considerably higher than chlorides or other competing compounds. This is a significant advantage for packaging. Also, the vapor pressure is low (less than 1 Torr up to 900°C), they have high chemical stability, and a thermal conductivity which is higher than most other types of storage materials (solid conductivities range from about 4 to 8 W/m-°C). However, the conductivity is still relatively low, which necessitates a package with a large surface area and a low heat transfer rate in order to avoid excessive temperature gradients in the salt during the periods when it is solidified. Measurements have shown that the expansion coefficients are nearly linear and there is no phase change in the solid state. The densities of the individual solid fluorides differ from one another and from the densities of the eutectic melts by less than 20 percent. No supercooling is evident, so that there is little tendency for the phases to separate by sedimentation. Because of their high chemical stabilities, the fluorides are rather inert and show little corrosive action on stainless steel. When a small amount of aluminum is added to the fluoride melt as a corrosion inhibitor, no corrosion has been observed on 18-8 type stainless steel after well over 1000 hours of operation at 850°C in the Philips Eindhoven (Holland) Laboratory. An inert atmosphere is required at these conditions.

Chlorides. Materials 5 through 8 in Table K-1 list some typical chlorides. The two eutectic compositions (Nos. 6 and 7) have far too low a melting (fusion) temperature, and are not considered further. Both sodium chloride (No. 5) and calcium chloride (No. 8) have melting points in the proper range. They have heat capacities somewhat below material No. 3, especially for calcium chloride. Other comparative disadvantages include: lower densities, apparently lower thermal conductivity (although good data are lacking), and the lack of practical experience in their use as a high temperature buffer store.

There are potential corrosion problems with chlorides unless pure, anhydrous grades are used in an inert atmosphere. An initial examination indicates that USP grade NaCl should be used pending corrosion studies of less pure grades. No water should be present, although if some occurs, it may not be too great a problem to drive it off by heating. Anhydrous grade $CaCl_2$ must be used, again, pending further tests since wet $CaCl_2$ is expected to have corrosion problems with stainless steel containers. Heating is not a good way to dry $CaCl_2$ since oxides tend to form which are also quite corrosive.

The cost of NaCl and $CaCl_2$, derived from Reference K-2 is between 7 and 9¢/kg. This is as low a cost as can be expected for any chemical compound, thus these materials may have a cost advantage for use as heat stores. They will maintain this advantage over, say, material No. 3 as long as they cost less than approximately ½ to 1/3 that of NaF and MgF_2. However, it appears that 7-9¢/kg is too optimistic for the high purity grades needed to assure that corrosion is not a problem. The costs in 1976 for the Los Angeles area are as follows:

Material	Grade	Total Amounts	Containers	Cost
NaCl	USP	Truckload (24,000 lbs.)	350 lb. drums	$0.37/kg
$CaCl_2$	Anhydrous	Truckload (24,000 lbs.)	350 lb. drums	$0.64/kg

Both materials are available in less pure grades (technical grades) in freightcar lots or greater at much lower prices, but these grades are not recommended until the corrosive nature is actually tested at the proper temperature range and/or pre-treatment techniques are investigated.

Carbonates. The ninth material identified is a eutectic of potassium carbonate and sodium carbonate. A very low heat of fusion makes this material undesirable for buffer store applications compared to the other leading candidates.

Material Comparisons. Figure K-1 shows a comparison plot of the heat store capacity of several typical materials over the selected temperature range. In most cases the sensible energy and the latent heat of fusion are roughly equal, and the heat store would have to be correspondingly larger if sensible energy were not used. As discussed previously, the recommended temperature range is dictated by the heat transport capability of the heat transfer fluid on the low side, and the temperature limits of the Stirling engine on the upper end.

Figure K-2 presents the cost of heat store capacity for selected materials, neglecting container and all other non-heat-store-material costs. The results for mixtures No. 6 and 7 are based on the costs derived from Reference K-2 which appear to be quite optimistic. However, note that materials No. 6 and 7 are not candidate materials because of their low fusion point, but the plots demonstrate the potential cost/storage energy relationship of chlorides if they could be purchased in the 7-11¢/kg range. Material No. 3 is quite competitive on a projected production cost basis of 15¢/kg., especially considering its other advantages. One of the best materials from strictly a total heat capacity standpoint, LiF/MgF_2, is very poor on a cost comparison because of the $4.98/kg figure.

In some cases it may be advantageous to change the fusion point of the storage material to a slightly lower value than exhibited by a single, pure compound. This is achievable with a non-eutectic mixture, and range of fusion temperatures is exhibited, rather than a single value. There are some well-known problems associated with the precipitation of different compounds at different temperatures for some mixtures, but their suitability should be investigated further.

For example, the $NaCl/CaCl_2$ phase diagram shows that a mixture of 80 NaCl/20 $CaCl_2$ (mass fraction) will begin to precipitate almost pure NaCl (actually, a solid solution of $CaCl_2$ in NaCl) at ~760°C (1400°F). As this separates

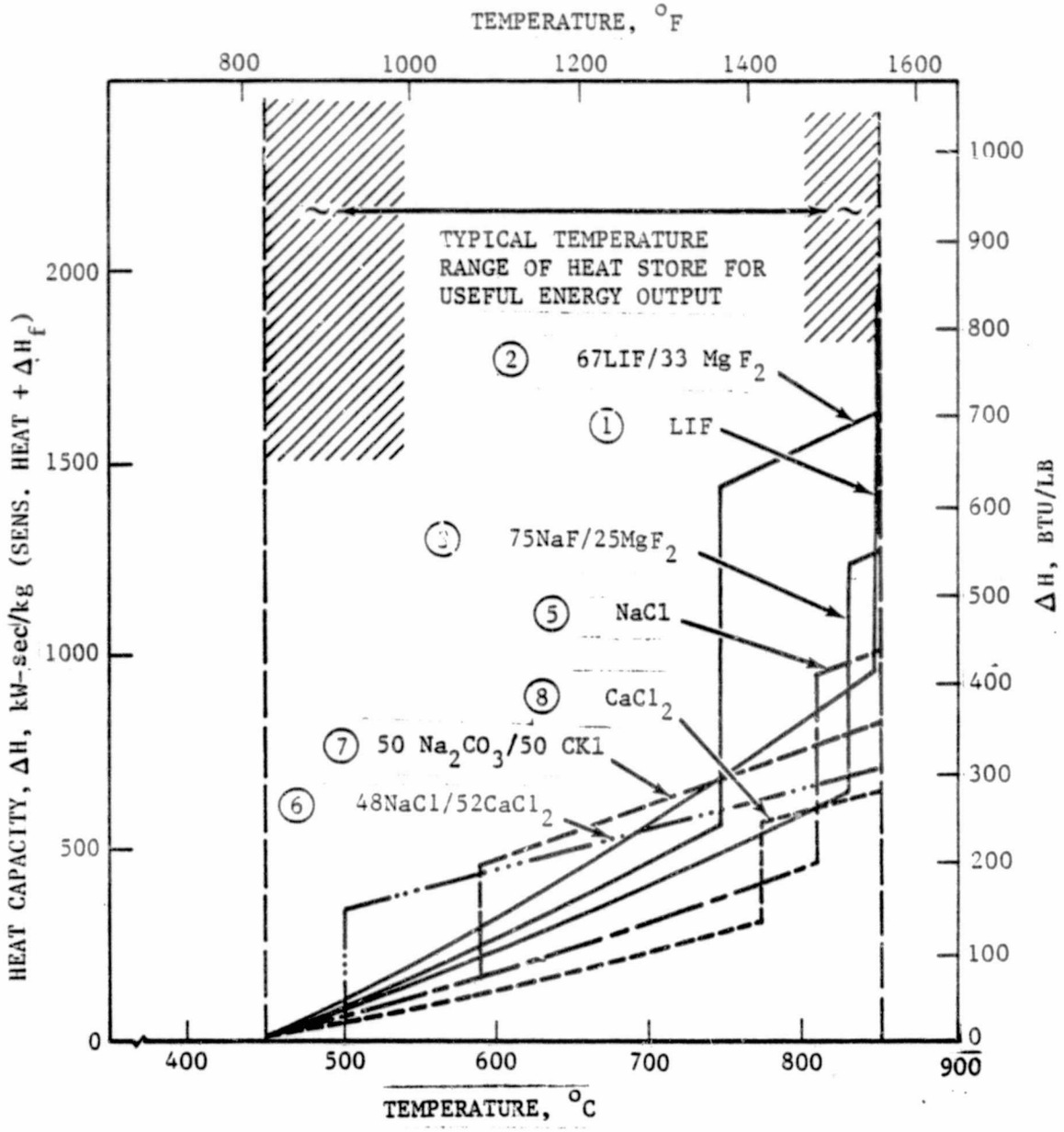


FIGURE K-1. HEAT STORE CAPACITY OF TYPICAL MATERIALS

94-2-182

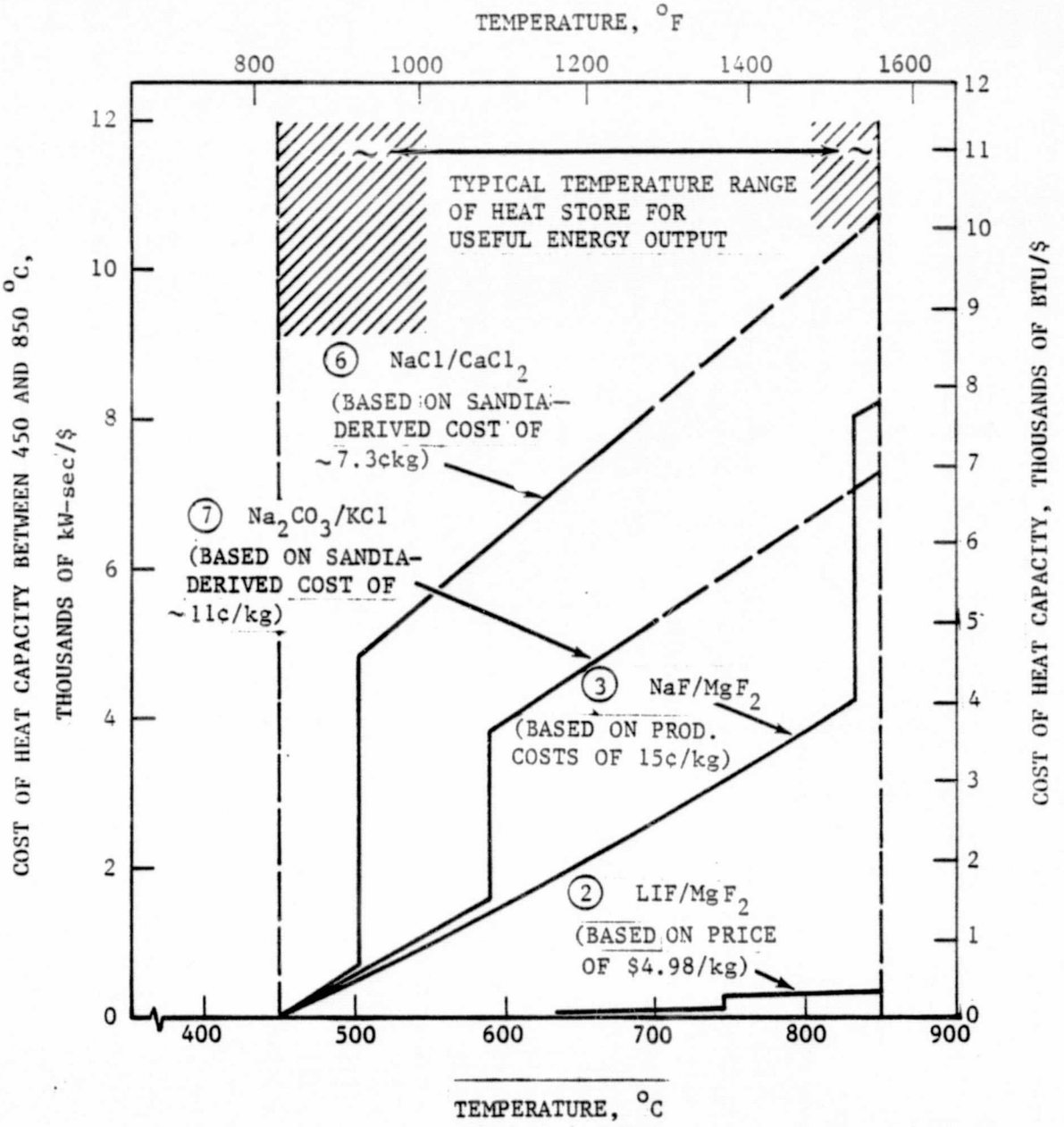


FIGURE K-2. COST OF HEAT STORE CAPACITY FOR SELECTED MATERIALS

94-2-183

C-2

from the remaining liquid, the liquid will become richer in $CaCl_2$. The solid solution will continue to separate until the peritectic temperature and composition are reached (~600°C and ~60 mole percent NaCl). At this temperature the liquid will react with the precipitated solid solution to form the compound $4NaCl \cdot CaCl_2$ until the melt is completely solidified. Thus, fusion starts at ~760°C and is completed at ~600°C for this particular mixture.

In summary, the leading candidates for the high temperature energy storage material are in current order of preference:

1. 75 NaF/25 MgF_2
2. NaCl
3. $CaCl_2$
4. Non-eutectic mixtures of NaCl and $CaCl_2$

Considerably more systems and cost analyses will be required to verify these initial choices

2. ENCAPSULATION

The buffer storage system must efficiently transfer heat from the heat store material to the heat transfer or working fluid (and from the working fluid into the mixture during charging). N. V. Philips has investigated this problem in terms of various encapsulation techniques and determined that a good design is one that has a large number of long, slender, thin-wall stainless steel containers which are filled with the store material and sealed. These containers are in turn enclosed by liquid sodium within the receiver pool. A photograph of a partial assembly of a laboratory heat store showing the individual containers, or canisters, is presented in Figure K-3. When the mixture is liquid it occupies almost the entire volume in the canister except for a small volume of inert argon gas. When the mixture solidifies there is a slight argon over-pressure so that the container will not collapse. Figure K-4 shows a cross-section of a canister filled with solidified lithium fluoride, and Figure K-5 shows the external view of the tank which holds the canisters. The tank insulation is partially removed to show the external configuration and the many temperature and pressure instrumentation leads.

During charging, energy from the solar heated sodium pool melts the eutectic salt. Whenever solar power is not received (and the salt is charged), the latent heat of fusion is released into the pool thereby vaporizing sodium to continue engine operation.

3. COST OF BUFFER STORAGE

The cost of buffer storage is obviously a function of the material which is selected -- not only because of the store material cost, but also because of

its heat capacity and density characteristics. For example, Table K-1 shows that the heat capacity of NaF/MgF_2 is 25 percent better than NaCl, and the density of the solid at the melt point is 37 percent higher (41 percent higher for the liquid phase). Therefore, NaCl will require a 70 percent increase in store volume compared to the baseline material for the same energy storage (assuming other conditions are equal). It is obvious that the baseline material can be a factor of 2 or 3 more expensive on a weight basis than common salt and still be competitive. Another important cost factor is the design and fabrication of the canisters. Low density, lower heat capacity materials require larger or additional containers, thus increased containerization costs.

ORIGINAL PAGE IS
OF POOR QUALITY

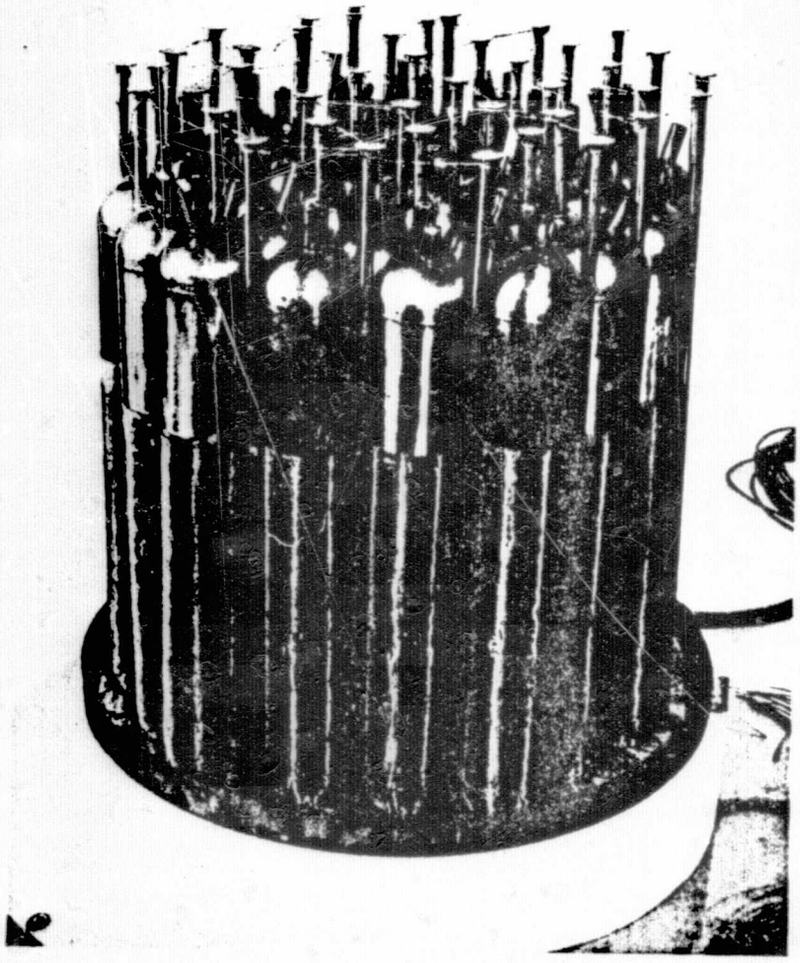


FIGURE K-3. PARTIAL ASSEMBLY OF PHILIPS HEAT STORE SHOWING CONTAINERS FILLED WITH STORE MATERIALS

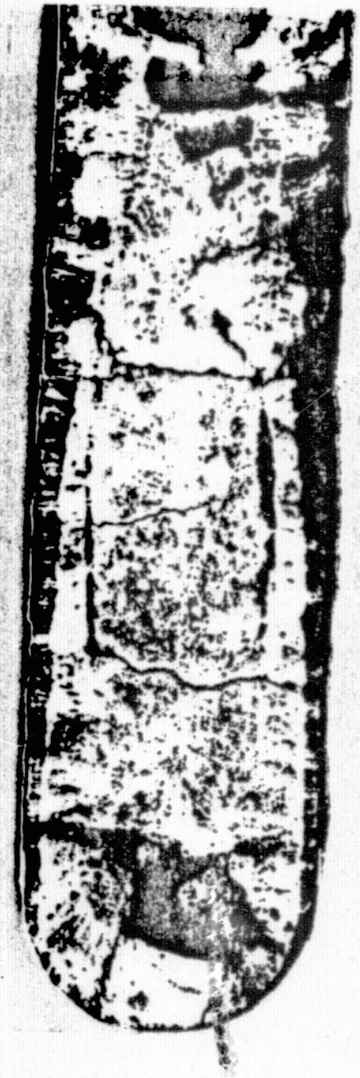


FIGURE K-4. CUT-AWAY OF A CANISTER SHOWING SOLIDIFIED HEAT STORE MATERIAL (LITHIUM FLUORIDE)

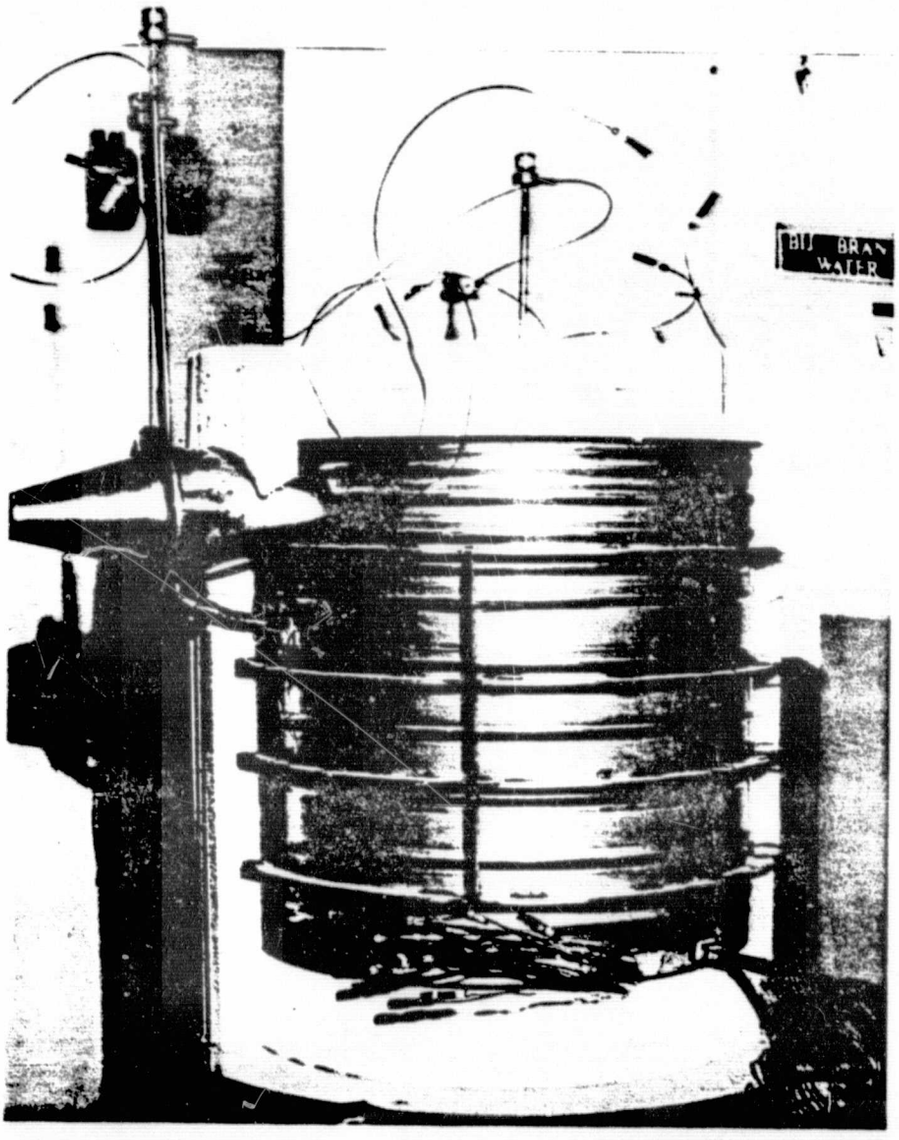


FIGURE K-5. PHOTOGRAPH OF PHILIPS HEAT STORE TANK AND PARTIAL INSULATION COVERING.

ORIGINAL PAGE IS
OF POOR QUALITY

APPENDIX K

REFERENCES

K-1 Schroder, J., "Thermal Energy Storage and Control," ASME Paper 74-WA/OcT-1, 1974.

K-2 Bramlette, T. T., et.al., "Survey of High Temperature Thermal Energy Storage," Sandia Laboratories Energy Report SAND75-8063, March 1976.

K-3 Schroder, J., "Thermal Energy Storage Using Fluorides of Alkali and Alkaline Earth Metals," paper presented at 148 Meeting of the Electro-Chemical Society, Dallas, Texas, 1975.

K-4 Pons, R. L., "Stirling Engine Performance Model," TR-SPS-001, August 16 1978, Ford Aerospace & Communications Corporation, Aeronutronic Division, Newport Beach, CA.

K-5 Eichelberger, J. L., "Final Report -- Investigation of Metal Fluoride Thermal Energy Storage Materials, Phase I -- Study of Availability, Cost, and Components," U.S. ERDA Contract No. EY-76-C-02-2990*000, December, 1976, Pennwalt Corporation, King of Prussia, PA.

K-6 Martin, W. R., "The Free-Displacer, Free-Piston Stirling Engine - Potential Energy Conserver," IECEC -75 Record, Paper No. 759/49, pp 995-102, 1975.

K-7 Janz, G. J., Molten Salts Handbook, Academic Press, New York, 1967.

APPENDIX L

TRANSIENT THERMAL MODEL FOR THE RECEIVER/THERMAL TRANSPORT SUBSYSTEM

Ford Aerospace &
Communications Corporation
Aeronutronic Division

Ford Road
Newport Beach, California 92663

TECHNICAL REPORT

TR. NO. SPS-016

SOLAR SMALL POWER SYSTEM (SPS) PROGRAM

TITLE: TRANSIENT THERMAL MODEL FOR THE BASELINE RECEIVER/THERMAL TRANSPORT SUBSYSTEM

PREPARED BY	D.B. Osborn - H.J. Haskins D.B. Osborn/H.J. Haskins	ORG NO. L283	CHARGE NO. 2P05-4000
SUPERVISOR APPROVAL	R.M. Grabow	DATE January 17, 1979	
PROGRAM ENGINEER APPROVAL	R.L. Pons	TO Distribution	

SUMMARY

An improved transient thermal model is presented for the baseline subsystem using the USS P-75 Stirling engine. Detailed subsystem responses to normal and inclement operating conditions are also presented. The results demonstrate that the transient performance of the subsystem is stable, well behaved, and has long time constants.

Distribution:

E. D. Avetta
F. P. Boda
T. B. Clark
N. L. Cowden
R. M. Grabow
H. J. Haskins
D. C. Jackson

I. E. Lewis (WDL)

D. B. Osborn (3)
R. L. Pons
R. M. Taylor
H. R. Wahlin
C. C. Wan
D. J. Corn (MTR+3)

1.0 INTRODUCTION

This Technical Report presents the development of an improved transient thermal model for the baseline sodium receiver and thermal transport subsystem. An in-depth transient analysis of the receiver-thermal transport subsystem is necessary in view of the inherent non-steady nature of the solar conversion process. The objective is to characterize the behavior of the subsystem for all operational modes encountered in a solar application. Thus, the preliminary thermal model presented in Reference 1 and an unpublished transport model have been reformulated into a new detailed transient thermal model. This improved transient analysis incorporates the physical and thermal characteristics of the latest baseline design. Subsystem responses to normal and inclement operating conditions are presented for the system using the USS P-75 Stirling engine operating at 1800 rpm.

2.0 METHODS OF ANALYSIS

A schematic of the thermal model is presented in Figure 1. As shown, the energy balance considers the incoming solar power, the thermal power to the engine, and the thermal losses from the subsystem. For computational convenience, conduction losses from the vapor pipe were distributed equally between receiver and engine heater head. Pressure drops throughout the entire subsystem have also been included.

2.1 MODEL IMPROVEMENTS

The following are the major improvements made to the transient thermal model.

- Explicit integration with respect to the time variable.
- Separate differential equations for the pool and head temperatures.
- Deletion of the sodium vapor thermal capacitance since it is negligible.
- Inclusion of vapor transport pressure losses.
- Consideration of various engine, receiver lid, and vapor valve control options.
- Refinement of the solar input heating function to include a clear day profile with arbitrary drop-out.

- Refinement of the engine output function.
- Elimination of the minor numerical instabilities encountered during the development of the model.
- Streamlined computational sequence.
- Refined input/output formats.

2.2 MODEL DEVELOPMENT

The nomenclature and units for the following model are presented in Appendix I. It is assumed that the sodium vapor is saturated (vapor and liquid are in quasi-equilibrium), the vapor volume is approximately constant and that receiver orientation effects are negligible.

Basic energy balance:

$$Q_{SOLAR} = Q_{RR} + Q_{CONV} + Q_{POOL} + Q_{CONDH} + Q_{HEAD} + Q_{ENG}$$

Basic differential equations:

The following two differential equations are solved in the computer code using a library subroutine for numerical solution of simultaneous first-order ordinary differential equations with automatic step change.

$$\frac{d\,T_{POOL}}{dt} = \frac{(Q_{SOLAR} - Q_{RR} - Q_{CONV} - Q_{CONDP} - Q_{TRANS})}{C_{SODIUM} + C_{STRUCTURE} + C_{SALT}}$$

$$\frac{d\,T_{HEAD}}{dt} = \frac{(Q_{TRANS} - Q_{CONDH} - Q_{ENG})}{C_{HEAD}}$$

Solar input heating function:

The following equation generates the solar input power to the receiver.

$$Q_{SOLAR} = f_{DROP}\, A_{DISH}\, \eta_{DSH}\, I_o \exp(-K_{ABS}\, F_{ABS}^{0.7})$$

where: $$F_{ABS} = \frac{1}{\cos L \cos\delta \cos[\pi(1 - t/720)] + \sin L \sin\delta}$$

This solar heating function is based upon the 1976 15 minute Barstow insolation data. A typical uncloudy day was curve-fit to determine the clear sky absorption term. With the present code, the solar input heating can be characterized with any combination of clear, hazy and inclement conditions as a function of solar time.

Heat losses:

Heat loss from the subsystem is characterized by the following equations:

$$Q_{RR} = (\sigma \varepsilon A_R)\ (T_W^4 - T_{SKY}^4)\ f_{LID}$$

$$Q_{CONV} = (h\ A_R)\ (T_W - T_{AMB})\ f_{LID}$$

$$Q_{CONDP} = [G_{POOL} + G_{LID}\ (1 - f_{LID})]\ (T_{POOL} - T_{AMB})$$

$$Q_{CONDH} = [G_{HEAD} + G_{ENG}\ (1 - f_{ENG})]\ (T_{HEAD} - T_{AMB})$$

where:

$$T_W = T_{POOL} + (Q_{SOLAR} - Q_{RR} - Q_{CONV})\ /G_{WALL}$$

$$+ [(Q_{SOLAR} - Q_{RR} - Q_{CONV})\ /G_{Na}]^{1/2.35}$$

The effect of using sky, ambient or zero sink temperature for the re-radiation heat loss term is negligible for the baseline subsystem (only a ± 25W difference).

Power transported:

The thermal power transferred from the receiver pool to the engine heater head is given by the following equation.

$$Q_{TRANS} = \dot{m}_v \, \Delta H_V \, f_{VALVE}$$

where:

$$\dot{m}_v = (\dot{m}_V)_C \times \begin{cases} 1 & \text{for } \dfrac{P_{HEAD}}{P_{POOL}} \leq \left(\dfrac{2}{\gamma+1}\right)^{\frac{\gamma}{\gamma-1}} \\ \left[\left(\dfrac{P_{HEAD}}{P_{POOL}}\right)^{\frac{2}{\gamma}} - \left(\dfrac{P_{HEAD}}{P_{POOL}}\right)^{\frac{\gamma+1}{\gamma}}\right] \Big/ \Gamma' & \text{for } \dfrac{P_{HEAD}}{P_{POOL}} > \left(\dfrac{2}{\gamma+1}\right)^{\frac{\gamma}{\gamma-1}} \end{cases}$$

and

$$(\dot{m}_v)_C = \frac{P_{POOL} \, A_{DUCT} \, g}{C_v^*}$$

$$C_v^* = (ZRgT_{POOL}/\bar{M})^{1/2} / \Gamma$$

$$P_{HEAD} = P_{REF} \exp\left[-T_V\left(\frac{1}{T_{HEAD}} - \frac{1}{T_{REF}}\right)\right] \Big/ \left(\frac{T_{HEAD}}{T_{REF}}\right)^m$$

$$P_{POOL} = P_{REF} \exp\left[-T_V\left(\frac{1}{T_{POOL}} - \frac{1}{T_{REF}}\right)\right] \Big/ \left(\frac{T_{POOL}}{T_{REF}}\right)^m$$

The sodium heat of vaporization is approximated by the following equation:

$$\Delta H_v = 4.9815 \times 10^6 - 1022.7T \qquad (1)$$

$$\Delta H_v \sim \frac{W - sec}{kg}$$

Figure 2 compares equation (1) with the data given in Reference 2. Figures 3 and 4 present the sodium vapor pressure (P_v) and ratio of specific heats (γ) as functions of temperature, respectively. The following equation is used to approximate the sodium gas constant.

$$\frac{ZR}{\bar{M}} = 296.3 + 65.5 \cos \left[\pi/2 \left(\frac{1.5T}{1073} - 0.5\right)\right] \qquad (2)$$

$$\frac{ZR}{\bar{M}} \sim \frac{W - sec}{kg - K}$$

This equation is compared with the exact value in Figure 5.

Engine input power:

The engine power parameters are based upon the analyses of Reference 4 and are presented below.

$$Q_{ENG} = Q_{100} \left(\frac{\bar{P}}{100} \right)^{\ell} (PR)_{HEAD} (PR)_{AMB} f_{ENG}$$

where:

$$(PR)_{HEAD} = \frac{(T_{HEAD} - 273)^{0.2265} - 3.545}{(T_{HEAD} - 273)^{0.2119} - 3.123}$$

$$(PR)_{AMB} = \frac{2.0224 - 0.00355\ T_{COOL}}{1.7978 - 0.00277\ T_{COOL}}$$

and where:

$$T_{COOL} = T_{AMB} + (Q_{ENG} - Q_{OUT})/G_{COOL}$$

and where:

$$Q_{OUT} = \left[Q_o + \beta\ Q_{100} \left(\frac{\bar{P}}{100} \right)^{2} \right] \times f_{ENG}$$

$$\times \left[(T_{HEAD} - 273)^{0.2265} - 3.545 \right]$$

$$\times \left[2.0224 - 0.00355\ T_{COOL} \right]$$

$$= \eta_{ENG}\ Q_{ENG}$$

The Receiver-Thermal Transport Model presented above has been programmed for operation on the Aeronutronic Time-Sharing System (TSS).

3.0 RESULTS

Detailed transient results are presented in this section for the baseline receiver-thermal transport subsystem with the Stirling engine operating at the baseline 1800 rpm condition. Table I presents some of the physical and thermal data of the subsystem used for the present analyses. Both normal and inclement operating conditions have been analyzed.

The following terms are used in this section and are defined as follows: "Idle", "rated" and "equilibrium" power refer to the Stirling engine shaft output power level.

"Idle" power is the low power necessary to stay "on-line".

"Rated" power refers to the power required per engine for the system to generate rated electrical power (1 MW_e) at rated solar conditions ($I_{d,n}$ = 800W/m^2, T_{AMB} = 44.6°C).

"Equilibrium" power is the power level required by the engine controller to maintain the steady-state head temperature.

"Buffer storage" refers to thermal storage added to the subsystem, and is therefore in addition to the inherent thermal capacitance of the subsystem.

- NORMAL START-UP

Figure 6 presents the subsystem temperature response and engine output power during a normal start-up condition. The solar input power profile is based on the 15 minute Barstow insolation data for a typical uncloudy day and includes the effects of both concentrator size and efficiency, thus representing the total power entering the receiver. This solar profile has been used for all start-up cases to facilitate direct comparison between them. In the morning, after normal operation from the previous day and nighttime cool down, the receiver sodium pool temperature is predicted to be approximately 525°C and the engine head at approximately ambient temperature. The receiver lid and vapor valve are opened prior to focusing on the sun. Once the sun is "on", the pool and head temperatures rapidly increase towards the steady-state operating level. After about 3 minutes the engine head temperature has reached the predetermined start temperature (450°C for the present analysis). The engine is then started and operated at a low or "idle" power level consistent with a previously selected helium mean working pressure ($\overline{P}$) for idle conditions (2.5 MPa for the present analysis). When the engine is started, an inflection of the receiver pool and engine head temperature slopes is observed. This occurs because some of the heat, which would normally increase the temperatures is now being removed by the engine. Since the net power to the receiver is increasing, the two temperatures continue to increase while the engine operates at "idle" power. After approximately 8 minutes the engine head reaches the steady-state operating temperature (800°C) and the engine head temperature control mode is activated. At this point the temperature controller moves

the power valve to bring the engine $\overline{P}$ up (and hence the torque level) to an "equilibrium" power level. The power valve is then modulated to maintain the engine head temperature within the control band as the solar flux varies during the day. Reference 5 presents a detailed discussion of the solar-Stirling engine control scheme.

- NORMAL SHUTDOWN

Figure 7 presents the subsystem temperature response during normal shutdown in the evening. For this case, the engine is assumed to be operating at the steady-state temperature and at any "equilibrium" power level above "idle" until the incoming solar power drops to zero. At this time the receiver lid is closed and the engine continues to produce power from the inherent thermal capacitance of the receiver. As energy is removed, the engine head temperature drops below the steady-state level. The engine is then operated at the previously mentioned "idle" power level. After 15 minutes the head temperature reaches the lower operational limit and the engine and valve are shut off. The subsystem temperatures will then slowly soak out to the ambient temperature. Another mode for normal evening shutdown is presented later.

- NORMAL START-UP WITH BUFFER STORAGE

Start-up from the previous day with the subsystem containing 100 kg of buffer storage is presented in Figure 8. Three different eutectic salt melting temperature regions have been investigated in the present analysis (i.e., 790-800°C, 802°C, 803.5°C). Approximately four minutes after the sun is focused upon the receiver the engine head temperature reaches the lower operational limit and the engine is started. An additional twelve minutes is required before the engine is controlled by head temperature for the 802°C and 803.5°C salt melt temperatures. The time required to melt the 100 kg of buffer storage for the 802°C and 803.5°C salt melt temperature cases is 26 and 62 minutes, respectively. For cases where the salt melt temperature is between 790°C and 800°C, approximately eleven minutes of "idle" engine operation is required while the 100 kg of buffer storage is melting. The engine head and receiver pool temperatures rise once again after the eutectic salt is entirely melted. When the head temperature reaches the steady-state operating temperatures of 800°C the "idle" control is shifted to head temperature control. Comparing

Figures 6 and 8 shows that the temperatures rise more slowly with the buffer storage, as is expected. (Note scale change.) For example, three minutes are required for engine start-up for the baseline subsystem and four minutes are required for the subsystem with 100 kg of buffer storage.

- EXTENDED "BAD" WEATHER

Figure 9 presents the subsystem temperature response during normal nighttime and extended "bad" weather conditions. For this case the engine and valve are assumed to be shut off as soon as the solar power becomes zero. With the receiver lid open the pool temperature drops to the sodium freeze temperature (98°C) in about sixteen hours. However, if the receiver lid remains closed, the pool temperature is predicted to stay above freezing in excess of three days. It is interesting to note, based upon the site data, that the sodium pool would not have frozen at any time during 1976 at Barstow. In the absence of additional engine coolant pumping after shutdown, the head is predicted to reach ambient temperature in about a day. The head temperature is independent of the pool temperature response since the closed vapor valve effectively uncouples the head and pool. As shown in Figure 7, the pool and head temperatures at the time of engine shut-off are 545°C and 450°C, respectively. By using these two temperatures as initial conditions, the soak-out (or non-operating cool down) temperature response for the normal nighttime shutdown presented in Figure 7 can easily be obtained from Figure 9.

- START-UP WITH FROZEN POOL

Start-up with a frozen sodium pool can occur after extended "bad" weather conditions or during the initial start-up. The subsystem temperature start-up response for this condition is presented in Figure 10. Engine start-up and switch to head temperature control occur after about 10 and 15 minutes, respectively. As shown, less than one minute is required to melt the sodium pool. As the sodium melts, a liquid layer forms between the heated receiver wall and the still-frozen sodium. This liquid layer rises via capillary action exposing solid sodium to the heated surface. No problems are expected during the melt period based upon the extensive work by the N. V. Philips Company (Reference 6). However, if any problems do occur when the sodium is melted directly by the sun, nichrome heater wires can be placed

between the outer receiver wall and the insulation, and current passed through the wires to slowly melt the entire sodium pool before the receiver is exposed to the sun. This method requires approximately 8.25 kW-hr of electrical energy to raise the receiver temperature from ambient to a level above the sodium melt temperature.

- CLOUD PASSAGE

Figures 11 through 14 present the subsystem temperature response and engine output power during cloud passage conditions. The same solar input power profile (based upon the Barstow insolation data) has been used for all cloud passage cases to facilitate direct comparison between the various cases. Steady-state temperatures and "equilibrium" power conditions are assumed to exist prior to the onset of cloud passage. Cloud passage was assumed to start at 11:00 a.m. for all cases presented.

- 15 MINUTE CLOUD PASSAGE - BASELINE SUBSYSTEM

Figure 11 presents the baseline subsystem temperature response to a fifteen minute cloud passage. As the cloud starts its passage, the solar input power goes to zero, the receiver lid closes and the subsystem temperatures start to decrease. The helium working fluid pressure ($\overline{P}$) will decrease until the pre-selected minimum value is reached resulting in engine operation at a low or "idle" power level. During the fifteen minutes of cloud passage the receiver pool and engine head temperatures decrease while the engine "idle" power remains relatively constant. When the cloud has passed, the solar power returns and the receiver lid is opened allowing the pool and head temperatures to increase. Approximately four minutes is required to heat the subsystem back up to the steady-state operating temperature and return to the "equilibrium" power level. The reheat time in this case is one minute less than for the previously presented normal start-up time because the solar input power is greater for this mid-day case. Thus, a fifteen minute cloud passage causes the baseline system to operate at "idle" (and minimum "on-line") conditions for only nineteen minutes before normal conditions are resumed.

- 30 MINUTE CLOUD PASSAGE - BASELINE SUBSYSTEM

Figure 12 presents the temperature response of the baseline subsystem for a thirty minute cloud passage. This case is identical to the previous case for the first fifteen minutes of cloud passage. After this period, the head temperature reaches the lower operational limit, and engine and valve are shut off. The pool and head temperatures slowly decrease in temperature until the sun returns. When the cloud has passed (and the solar input power returns) the receiver lid and valve are opened. The pool and head temperatures quickly increase to the engine start level (less than one-half minute) where the engine operates at "idle" conditions. From this point on the thirty minute case is identical to the previously described fifteen minute cloud passage case.

- 15 MINUTE CLOUD PASSAGE - BASELINE SUBSYSTEM WITH 100 KG OF BUFFER STORAGE

The temperature response to a fifteen minute cloud passage for the subsystem with 100 kg of buffer storage is presented in Figure 13. The system will operate at "rated" conditions for approximately six minutes from the latent heat of fusion of the eutectic salt. After the buffer storage has completed its constant temperature phase change, the engine will operate at "idle" conditions. The steady-state operating temperature is reached approximately four minutes after the solar power returns. The solar input power that enters the receiver which is in excess of that required to operate the Stirling engine at "rated" conditions is used to melt the eutectic salt storage. Thirteen and one-half minutes of "rated" power operation is required before the engine resumes operating at the "equilibrium" power level. Thus, for a fifteen minute cloud passage, approximately thirteen minutes "idle" opeation occurs for the subsystem with 100 kg of buffer storage.

- 15 MINUTE CLOUD PASSAGE - BASELINE SUBSYSTEM WITH 250 KG OF BUFFER STORAGE

Figure 14 presents the temperature response to a fifteen minute cloud passage for a subsystem containing 250 kg of buffer storage. For this case, the engine will operate at "rated" power for the entire fifteen minutes of cloud cover. However, an additional 33.5 minutes of "rated" power operation is required, once the solar power continues, while the eutectic salt storage "recharges" (melts).

- BUFFER STORAGE

Eutectic salt buffer storage within the receiver subsystem can effectively maintain efficient engine operation during moderate solar drop-out periods. This is accomplished when the salt gives up its stored thermal energy during a constant temperature liquid to solid phase change. A salt with a melting temperature near the steady-state operating temperature is desirable since the Stirling engine operates less efficiently at lower head temperatures. (Reference 4) The analyses of References 7, 8 and 9 suggest NaF/MgF_2 eutectic salt as being an excellent candidate for thermal storage. The selected mole percentages of NaF and MgF_2 are determined by the desired eutectic melting point. A $75NaF/25MgF_2$ eutectic salt has been used for the present analyses.

The effects of adding thermal buffer storage are presented in Figures 15 and 16. These two figures are based upon the analyses of Reference 7 and updated to reflect the effects of operating the Stirling engine at 1800 rpm.

Figure 15 presents the sodium temperature response during engine operation at "rated" and "idle" conditions. Operation was for a subsystem with and without buffer storage as well as for an open and closed receiver lid. The effect of closing the lid is negligible during "rated" power operation since heat lost by radiation and convection out the receiver aperture is small compared to the energy removed by the engine. However, with the engine operating at "idle" power, the reradiation and convection losses are very significant. For example, by simply closing the receiver lid during "idle" conditions, engine operation at $800^{\circ}C$ with 100 kg of buffer storage can be extended from 33 minutes to 60 minutes.

Figure 16 presents the engine operating time with a closed receiver lid as a function of buffer storage mass. As shown, engine operating time during the salt phase change can be increased by 6.0 minutes for each 100 kg of $75\ NaF/25MgF_2$ eutectic salt added to the subsystem. An additional 7.0 minutes of engine operation can be obtained from the entire subsystem sensible heat. However, it may not be desirable to operate at "rated" power below the steady-state head temperature. This is due to the fact that engine efficiency will decrease and warm-up time will increase as the engine head temperature decreases.

Engine operating time is thus gained at the expense of subsystem weight. For example, 250 kg of eutectic salt is required to maintain "rated" output power for a 15 minute solar drop-out period. Although not considered in the present analysis, the weight of encapsulation must also be added to that of the salt. It is desirable to use thin wall containers to minimize structural weight, cost and temperature drops to and from the salt. Fortunately, by incorporating the following two techniques, additional wall thickness for corrosion allowance and pressure differentials is not required. 1) By purifying the salt and using a "getter", e.g. aluminum, the corrosion of 316 stainless steel can be reduced to nil (References 6, 10 and 11). 2) By adding a small amount of sodium to the evacuated salt container, the sodium vapor pressure inside and outside the container are (automatically) nearly equal all the time. (Reference 6)

"On-line" operating time at "idle" power can be extended by two other methods. The first method is by simply increasing the mass of sodium within the receiver. The second is by reducing the "idle" shaft output power level from the present 10 kW level to the minimum level of approximately 1 kW. This would increase "idle" operating time by a factor of three or four.

However, extending the engine operating time beyond that which is possible with the inherent thermal capacitance may not be necessary. A cursory investigation of both the Barstow and Lancaster insolation data indicate that short cloud passages (less than 3 minutes) occurred more than a thousand times at these locations during 1976. Cloud passages on the order of 15 and 30 minutes in length occurred much less frequently (less than 100 times). There were eighteen days in which the total available energy was between 50 percent and 10 percent of the annual mean level. Only eleven days had a total energy level less than 10 percent of the annual mean level. Although it is very difficult to determine the frequency and length of cloud cover from 15 minute insolation data, the above indicates that the duration of a "typical" cloud passage is less than 15 minutes. Thus, buffer storage for a longer period of time may be unnecessary.

- EMERGENCY OPERATION

Figure 17 presents the receiver wall temperature response during an emergency operation in which the engine load suddenly goes to zero. For the conditions listed, the wall temperature increases about 65°C per minute for the baseline subsystem and about 25°C per minute when 100 kg of buffer storage is added to the subsystem. These temperature rates are sufficiently slow to allow defocusing before damage to the receiver can occur.

- SUBSYSTEM RESPONSE CHARACTERISTICS

Figure 18 presents response characteristics for the baseline subsystem during start-up, in addition to those previously presented in Figure 10. In the morning, prior to focusing upon the sun, the receiver lid and vapor valve are opened. The receiver wall and sodium pool temperatures rapidly increase when the solar input power first comes "on". The receiver wall temperature is an average of 23°C higher than the pool temperature during the fifteen minute frozen pool start-up period. The pool and head pressures correspond to the saturated sodium vapor pressure at the respective temperatures. As shown, the pressure magnitudes and differentials are negligible for temperatures below approximately 400°C. As the sodium pool temperature increases above this temperature, the pressure differential and vapor density become great enough to significantly increase the vapor flow to the engine heater head. As a result, the head temperature begins to increase, and the slope of the pool temperature curve decreases. This slope change is a result of the incoming solar power now heating both the pool and head thermal capacitances. The temperatures, pressures, and vapor mass flow rate increase as the solar power continues to enter the system. The Stirling engine is started and operated at "idle" power when the head temperature reaches the start temperature of 450°C. An inflection of the head temperature occurs at this point since some of the power which would normally heat the head is now used to drive the engine. The sodium vapor mass flow rate peaks, and then decreases as the power required by the engine heater head (to increase temperature and drive the engine at "idle" conditions) is reduced. The pool and head temperatures and vapor pressures continue to increase until the 800°C steady-state operating temperature is reached. At this point the engine is controlled to maintain constant head temperature. The helium working pressure is increased, and the

engine is operated at the "equilibrium" shaft output power level. The power that was used to increase the pool and head temperatures is now used for input to the Stirling engine. Thus, the sodium vapor mass flow rate also increases to the "equilibrium" conditions.

4.0 CONCLUSIONS

The development of an improved transient thermal model for the baseline receiver-thermal transport subsystem operating with the USS P-75 Stirling engine has been presented. The two governing differential equations were solved numerically, and detailed results for various transient cases were presented. These results demonstrate that the transient performance of the subsystem is stable and well behaved, and has long time constants. Salient results of the analyses are as follows:

1) For normal morning start-up, only eight minutes are required to heat the system up to the 800°C steady-state operating temperature. In the first three minutes the ambient head temperature is raised up to the 450°C start temperature.

2) Normal start-up to "idle" power requires approximately four minutes for the subsystem with 100 kg of buffer storage. The additional time required to reach "equilibrium" power (and to melt all of the salt) is a function of the salt melt temperature and mass.

3) For start-up with a frozen pool, 10 and 15 minutes are required to reach the start and steady-state operating temperatures, respectively. Less than one minute is required to melt the pool.

4) Due to the inherent thermal capacitance of the subsystem, the engine will operate at "idle" power for fifteen minutes after the solar power goes to zero (evening or cloud passage).

5) If the receiver lid remains closed during extended "bad" weather conditions, the pool temperature is predicted to stay above freezing in excess of three days. With the receiver lid open the pool temperature drops to the sodium freeze temperature in about sixteen hours.

6) The baseline system will stay "on-line" during a fifteen minute cloud passage without adding buffer storage.

7) Approximately 250 kg of buffer storage is required to maintain "rated" power throughout a fifteen minute cloud passage.

8) During an emergency operation, the temperature rise rate is sufficiently slow to allow defocusing before damage to the receiver can occur.

The current transient thermal model is complete, except for any minor changes that may be required as a result of improvements to the receiver, thermal transport duct, and Stirling engine. Additional transient cases will be run for any changes to the baseline system.

TABLE I

Receiver-Thermal Transport Subsystem Data

Steady state operating temperature = 800°C (1472°F)

Engine start temperature = 450°C (842°F)

T_{AMB} = 15°C (59°F)

T_{SKY} = -10°C (14°F)

$T_{MELT-Na}$ = 98°C (208°F)

$T_{MELT-SALT} \approx$ 800°C (1472°F)

Sodium mass = 33 kg (73 lbm)

Structural mass = 150 kg (331 lbm)

Effective head mass = 35 kg (77 lbm)

Salt mass = variable

Salt heat of fusion = 10.578 kW - min/kg (273 Btu/lbm)

Duct diameter = 0.0762m (3.0 inch)

Total transport loss coefficient = 7.0

Insulation conductivity = .03634 W/m-°K (.021 Btu/hr-ft-°F)

$\sigma\varepsilon A_R = 6.389 \times 10^{-12}$ kW/°K^4 (2.077×10^{-9} Btu/hr-°R^4)

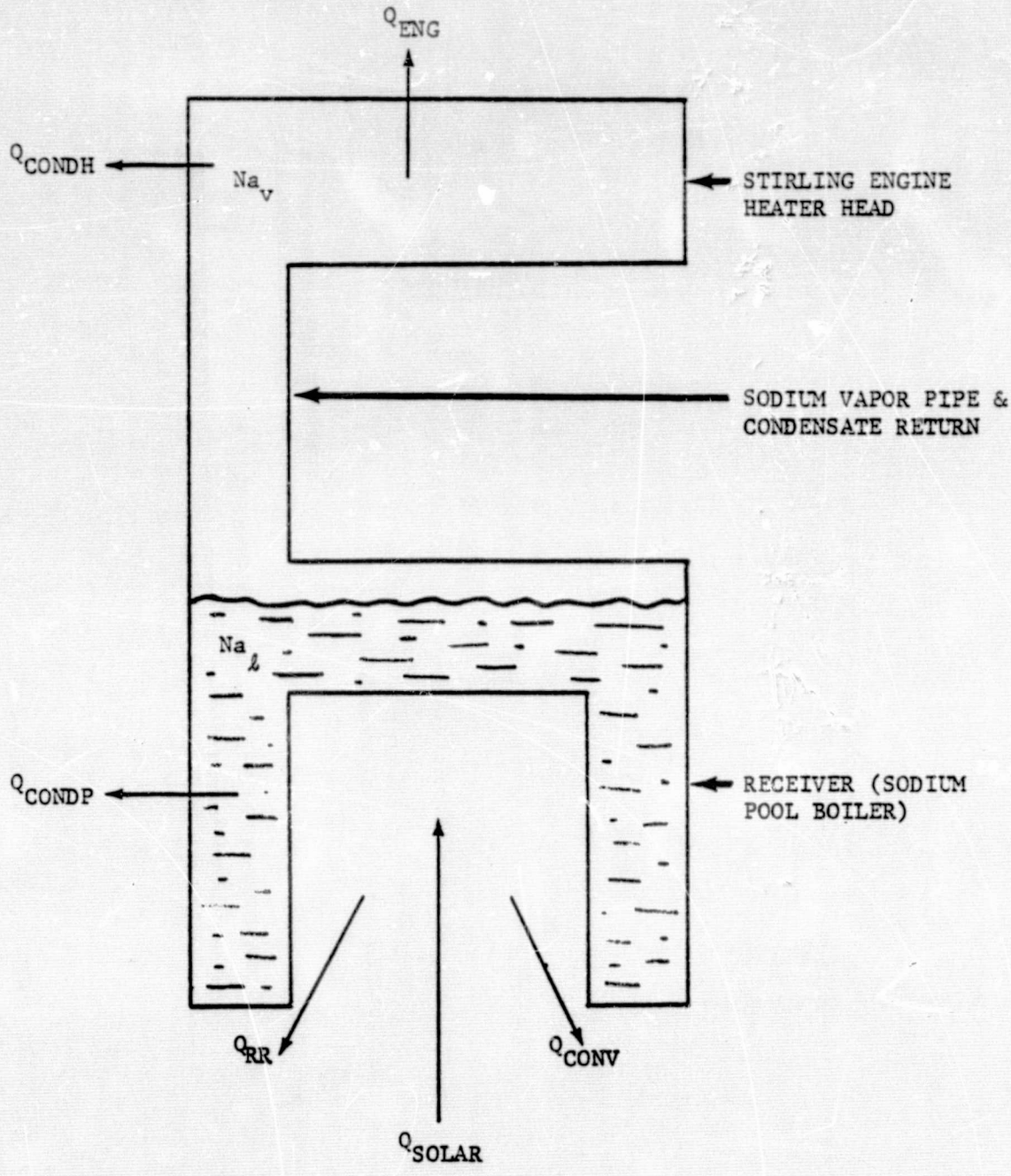
$hA_R = 6.90 \times 10^{-4}$ kW/°K (1.308 Btu/hr-°F)

$\overline{P}_{MIN}$ = 2.5 MPa (25 atm)

$\overline{P}_{MAX}$ = 15.0 MPa (150 atm)

FIGURE 1.

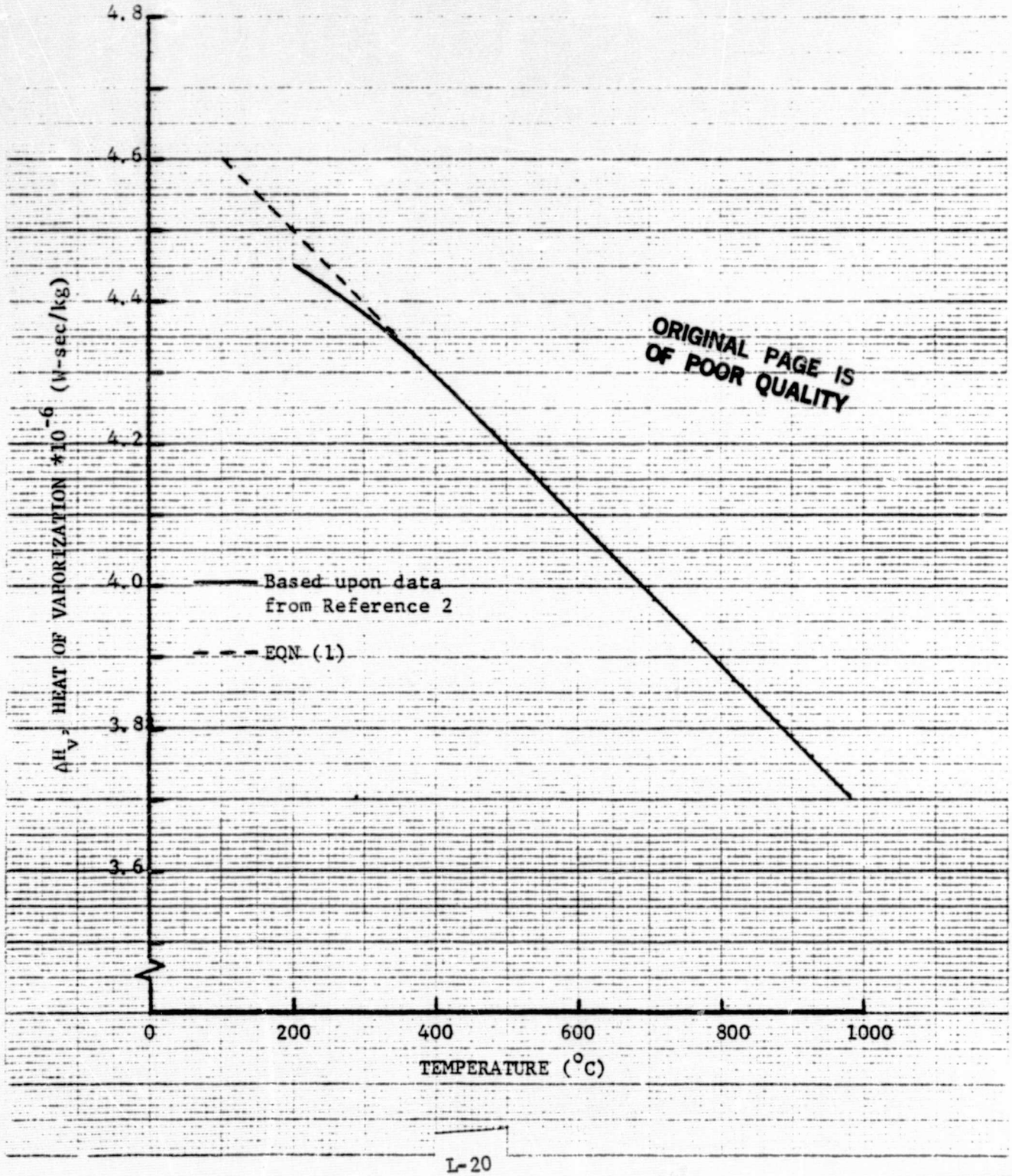
RECEIVER-THERMAL TRANSPORT SCHEMATIC



D.B.D.

FIGURE 2.

SODIUM HEAT OF VAPORIZATION

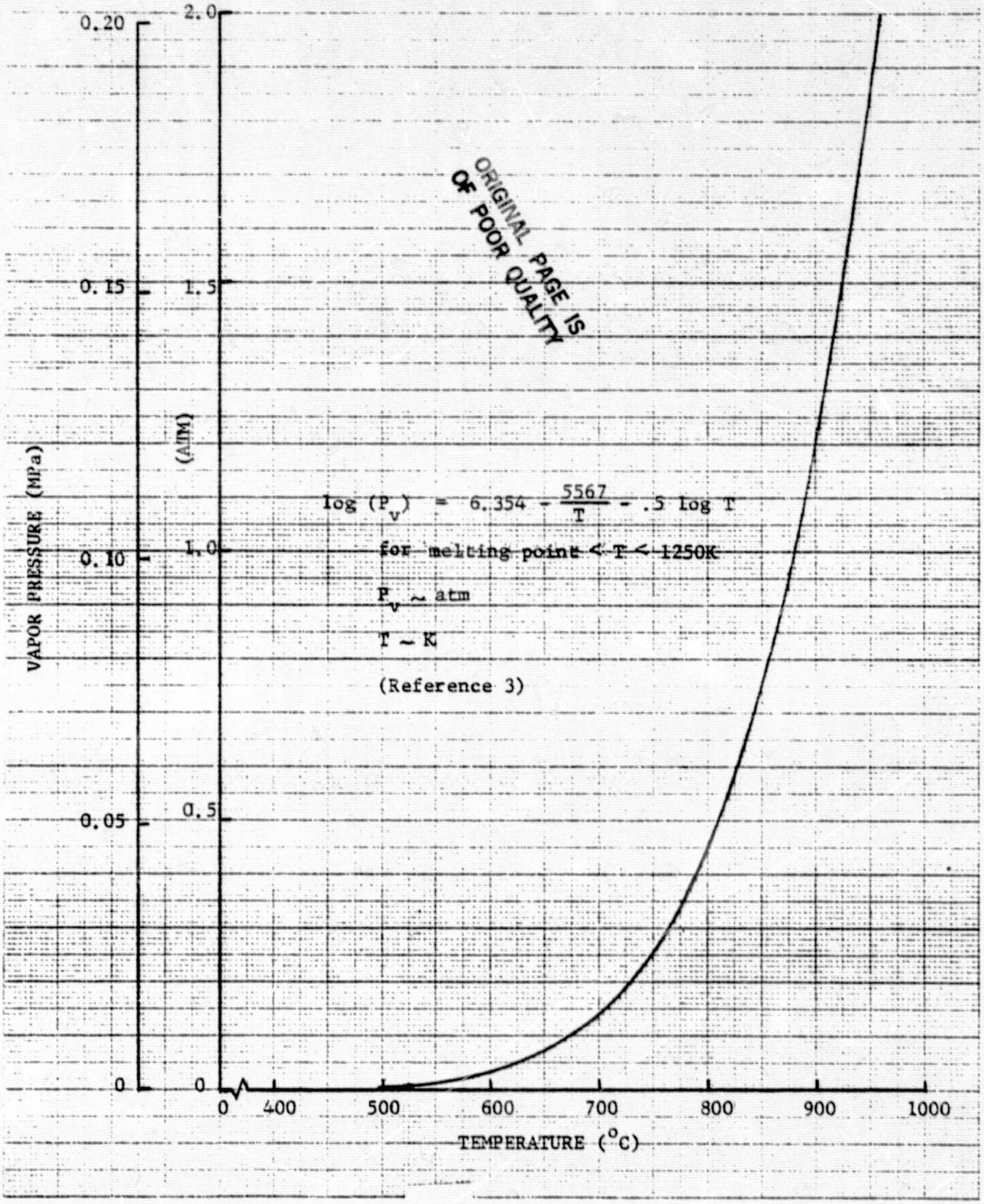


ORIGINAL PAGE IS OF POOR QUALITY

D.B.D.

FIGURE 3

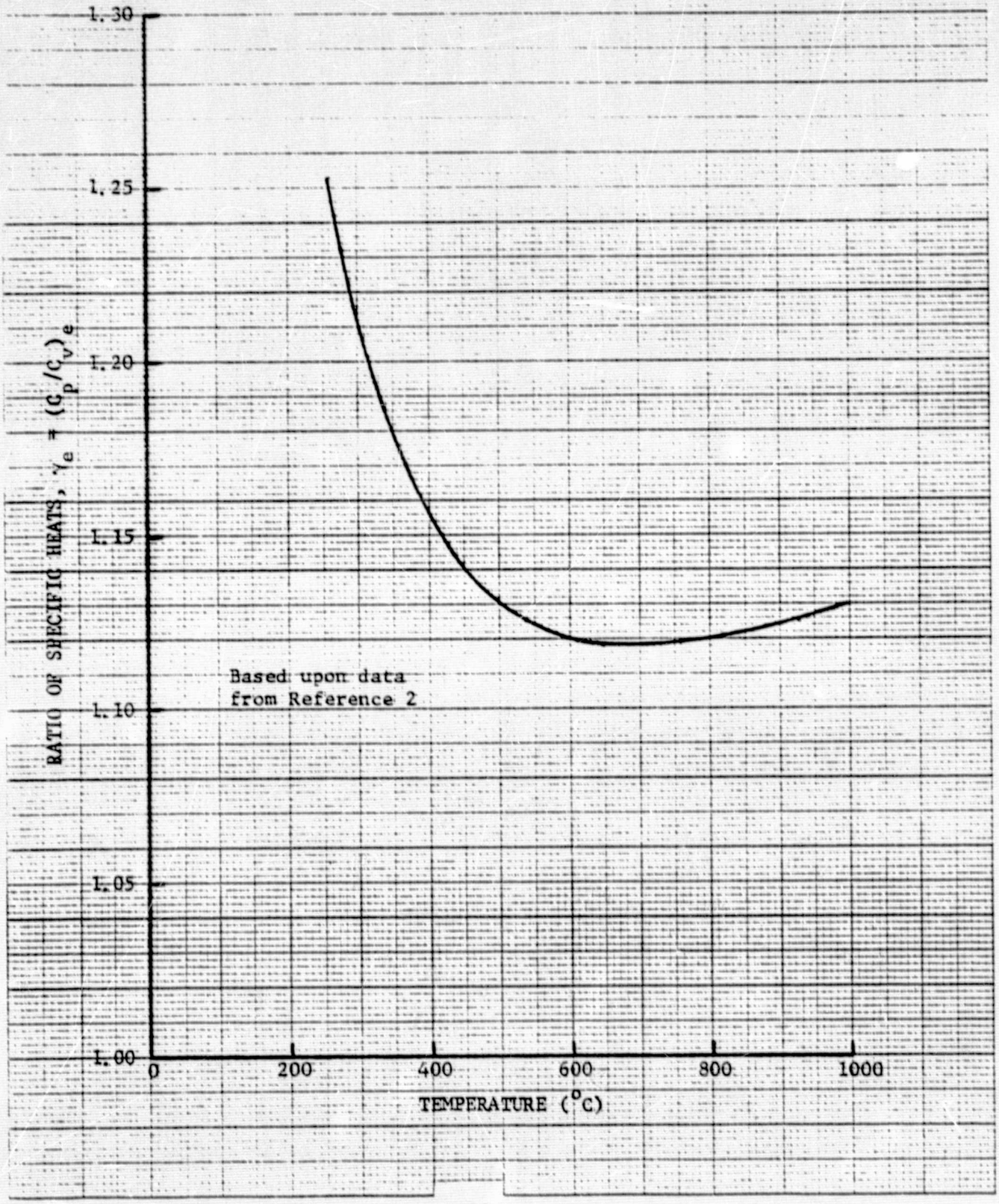
SODIUM VAPOR PRESSURE



D.B.C.

FIGURE 4

RATIO OF SODIUM SPECIFIC HEATS

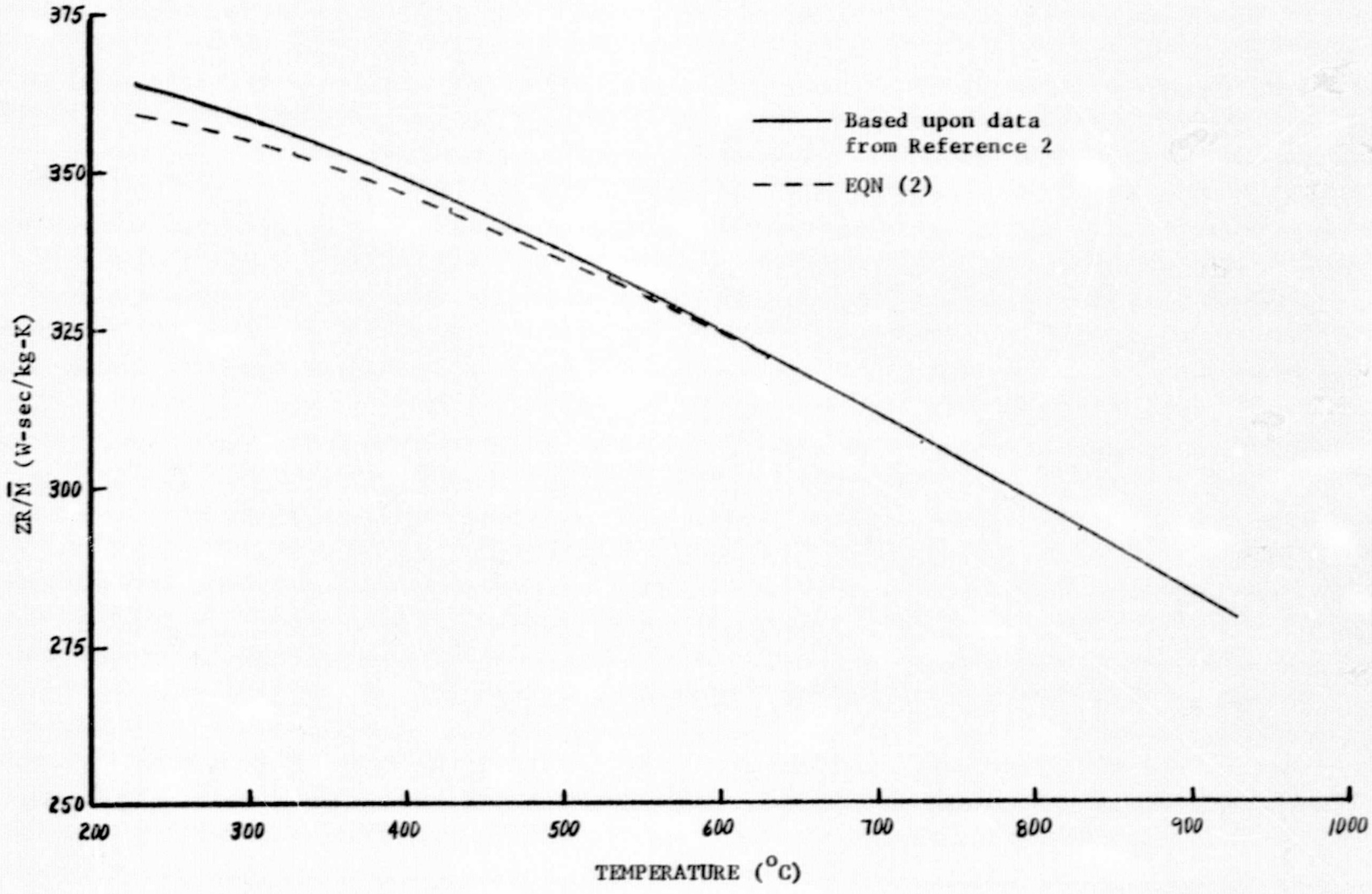


D.O.E.

D.B.Q.

FIGURE 5

SODIUM GAS CONSTANT AND COMPRESSIBILITY FACTOR



D.B.O.

FIGURE 6

THERMAL RESPONSE FOR NORMAL START UP FROM PREVIOUS DAY

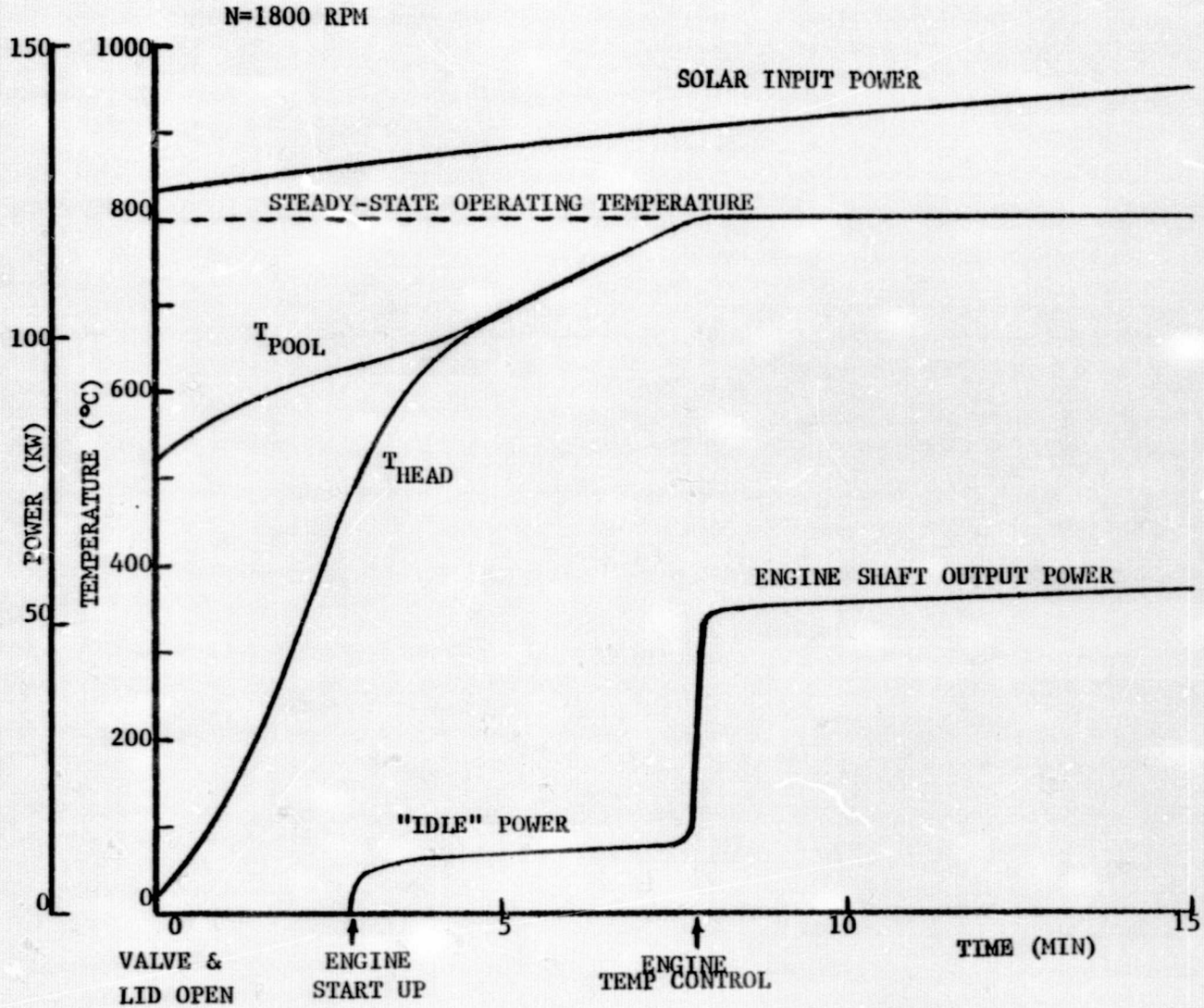


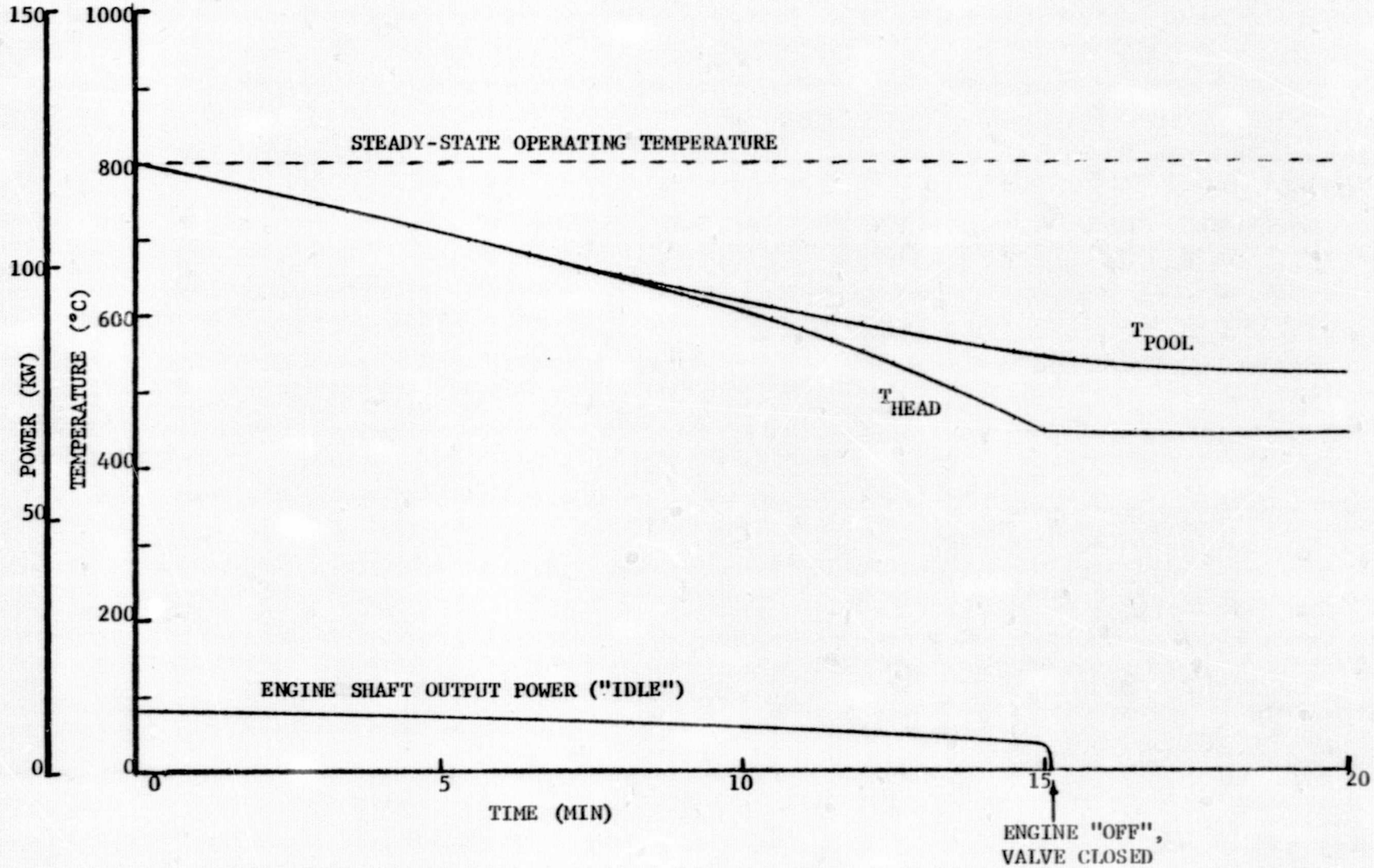
FIGURE 7

THERMAL RESPONSE FOR NORMAL NIGHTTIME SHUTDOWN

N=1800 RPM

$Q_{SOLAR=0}$

CLOSED LID

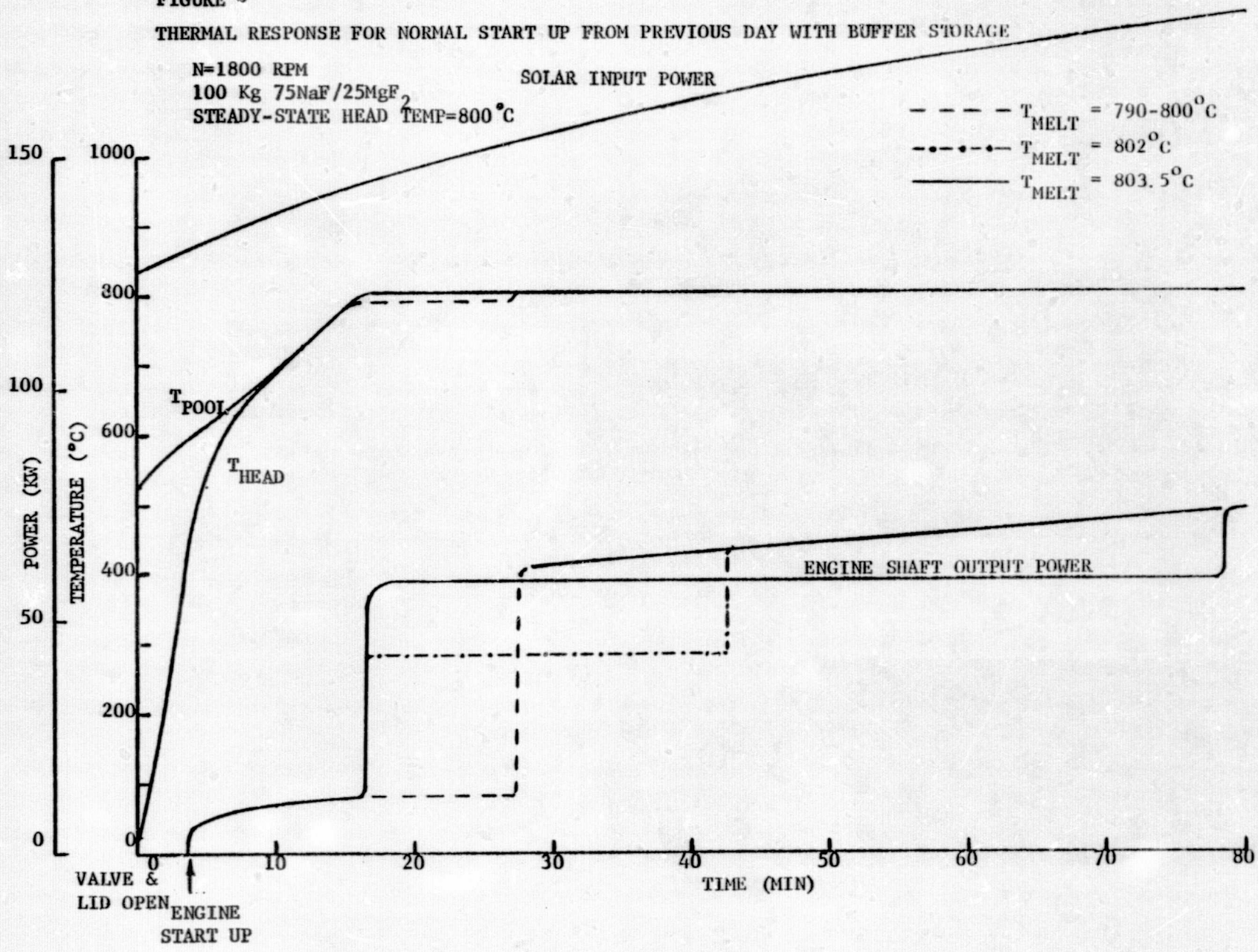


D.B.D.

FIGURE 8

THERMAL RESPONSE FOR NORMAL START UP FROM PREVIOUS DAY WITH BUFFER STORAGE

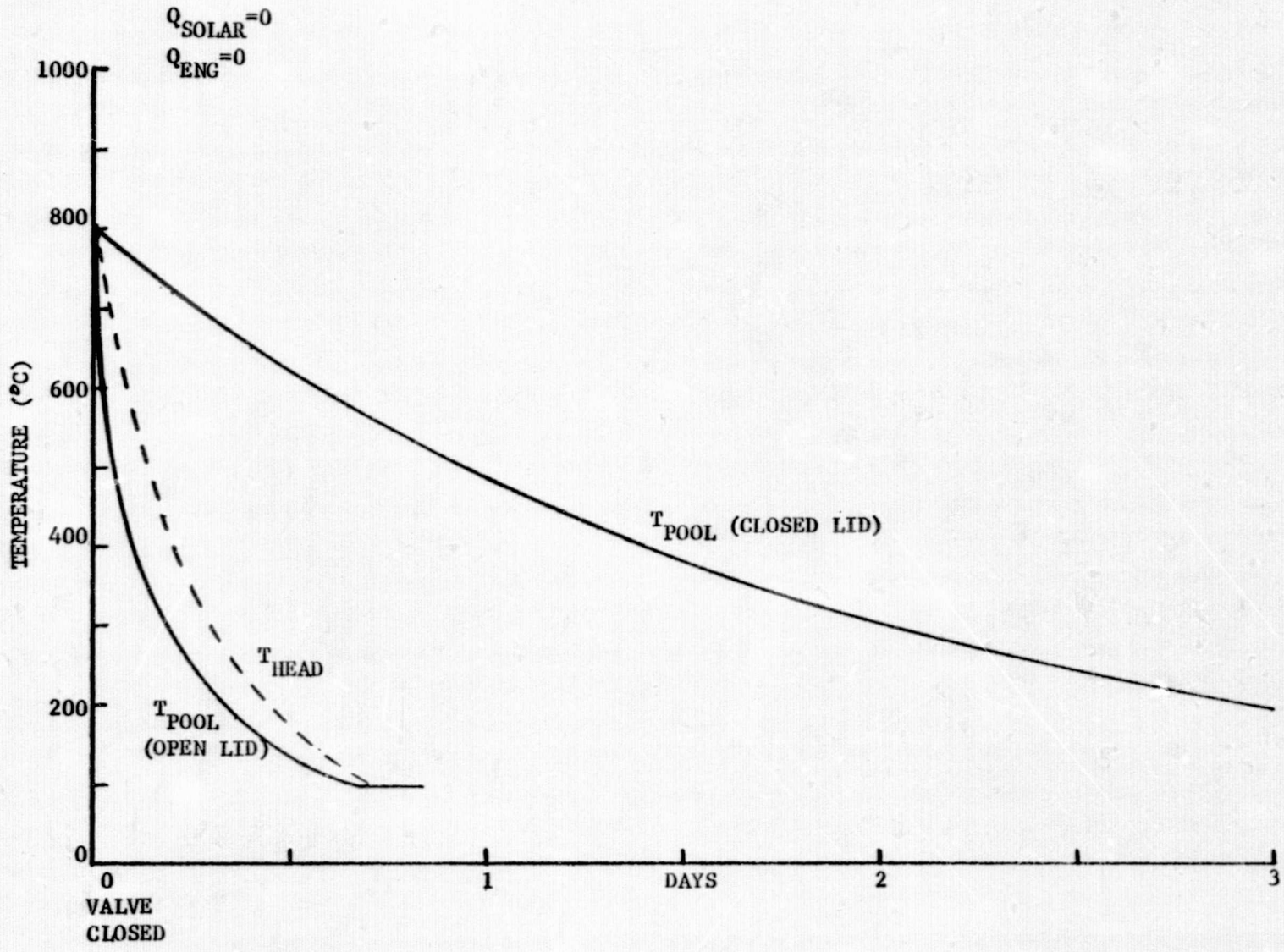
N=1800 RPM
100 Kg 75NaF/25MgF_2
STEADY-STATE HEAD TEMP=800 °C



D.B.O.

FIGURE 9

THERMAL RESPONSE FOR NIGHTTIME AND EXTENDED "BAD" WEATHER



P.B.D.

FIGURE 10

THERMAL RESPONSE FOR START UP WITH FROZEN POOL

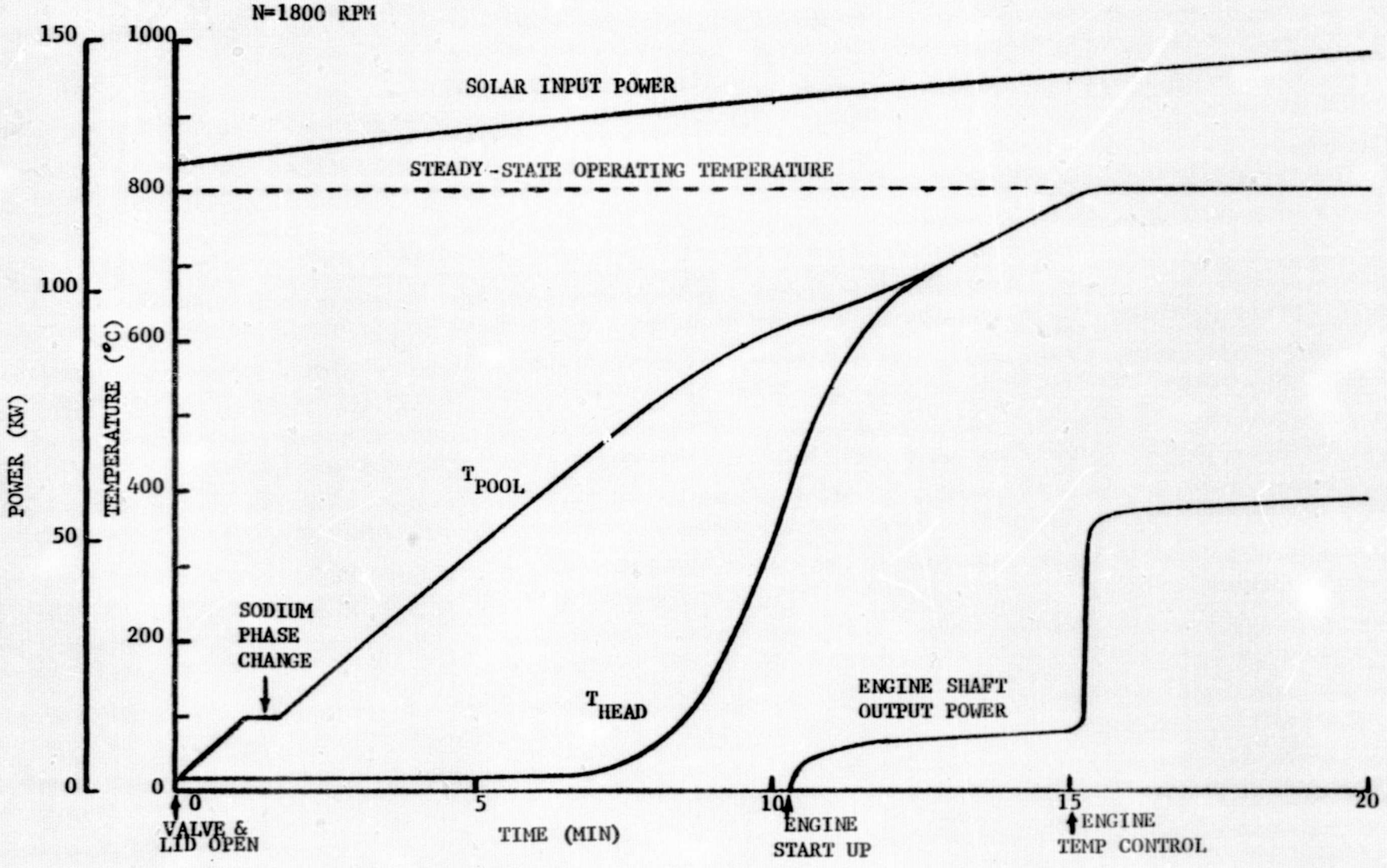
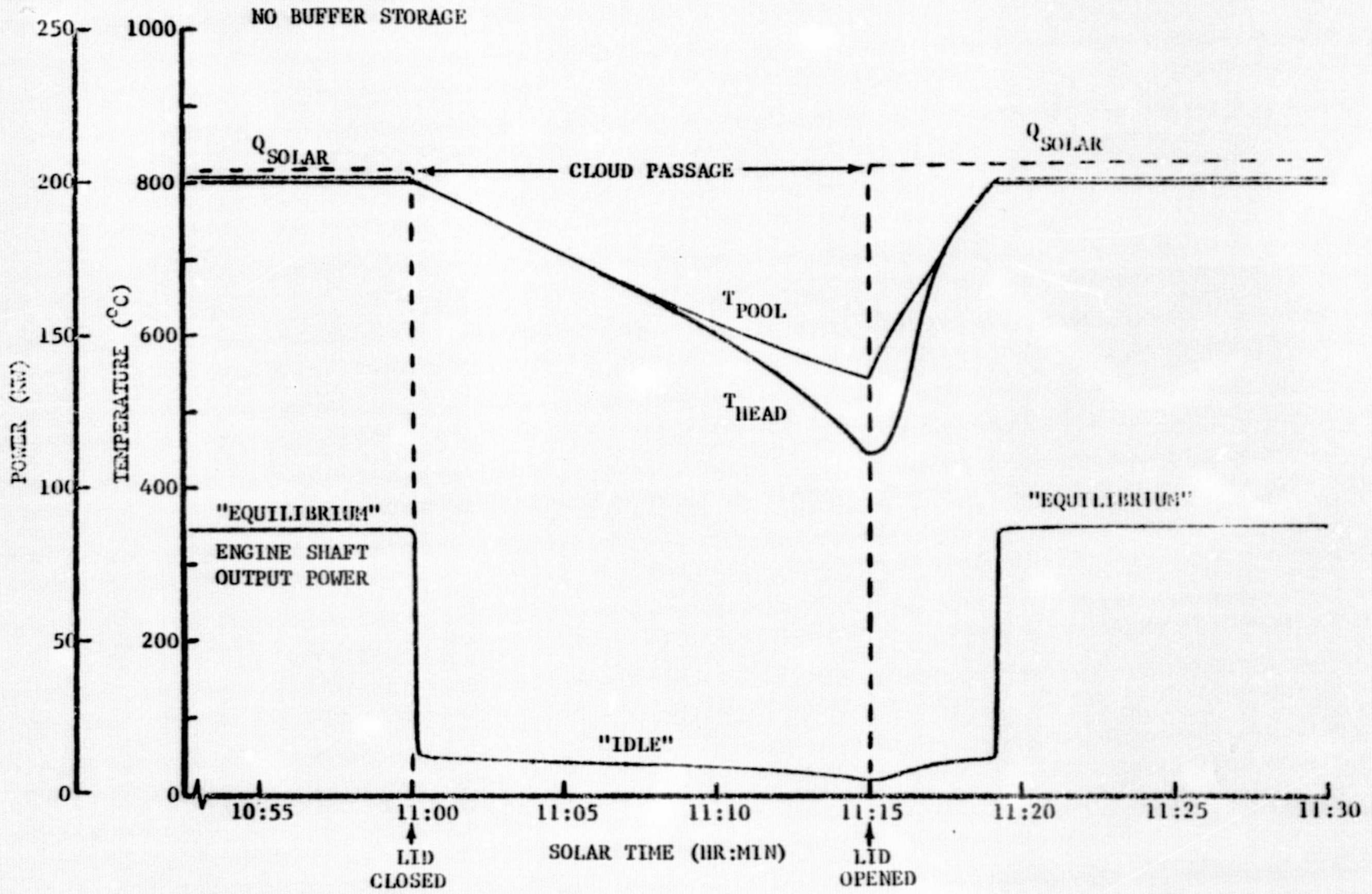


FIGURE 11

SUBSYSTEM TEMPERATURE RESPONSE TO A 15-MINUTE CLOUD PASSAGE



D.E.U.

FIGURE 12

SUBSYSTEM TEMPERATURE RESPONSE TO A 30-MINUTE CLOUD PASSAGE

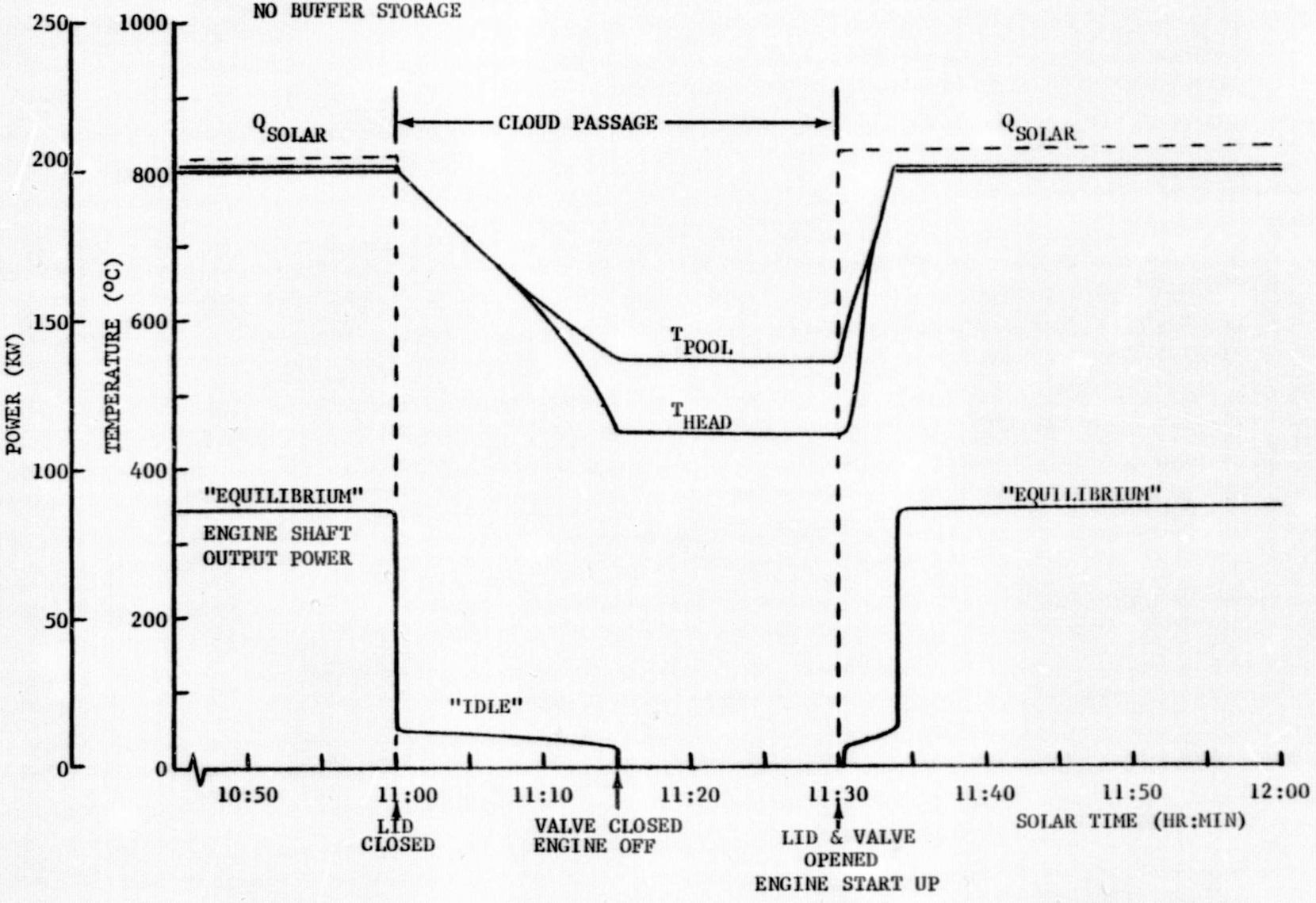


FIGURE 13

SUBSYSTEM TEMPERATURE RESPONSE TO A 15-MINUTE CLOUD PASSAGE WITH 100 KG OF BUFFER STORAGE

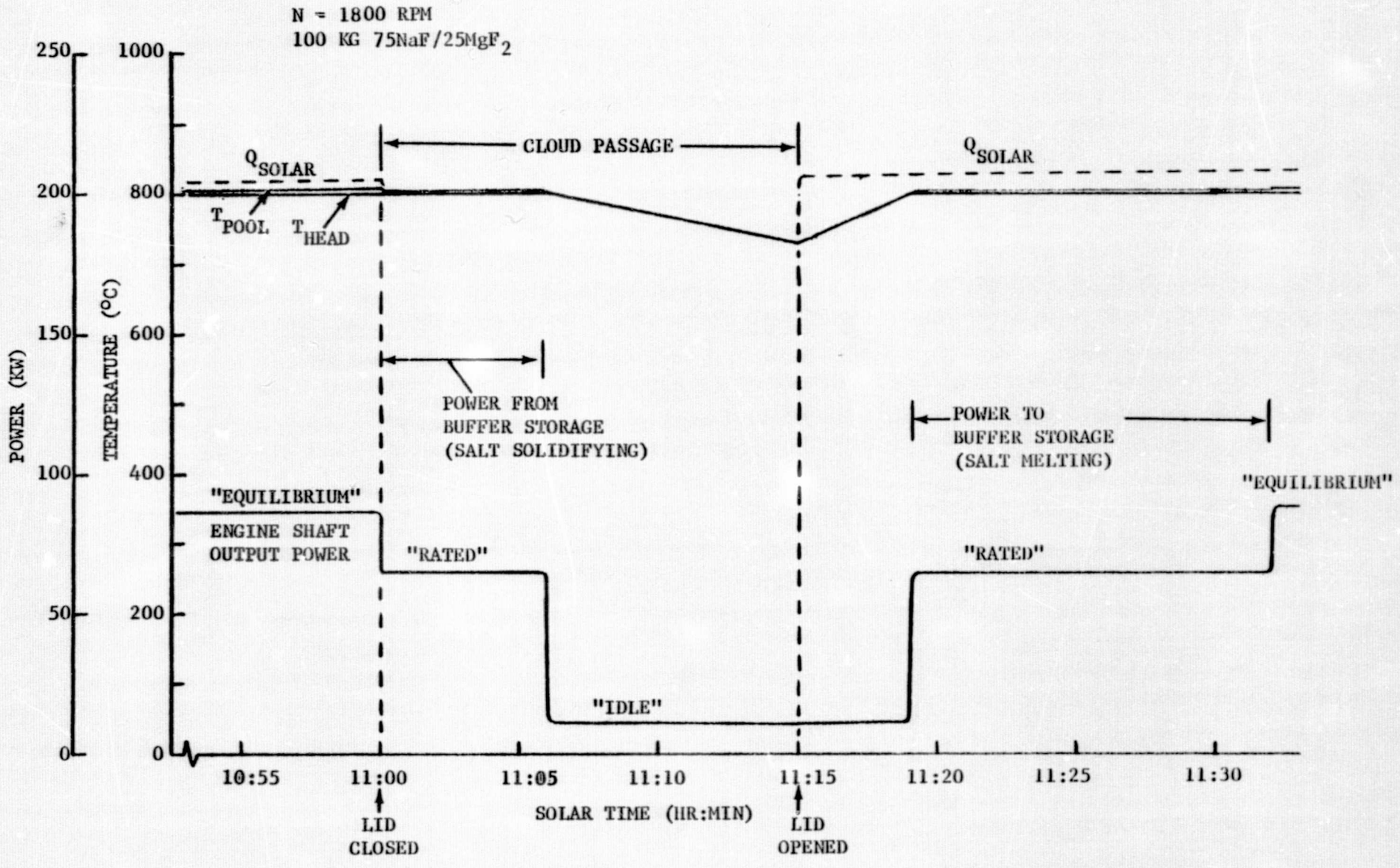


FIGURE 14

SUBSYSTEM TEMPERATURE RESPONSE TO 15-MINUTE CLOUD PASSAGE WITH 250 KG OF BUFFER STORAGE

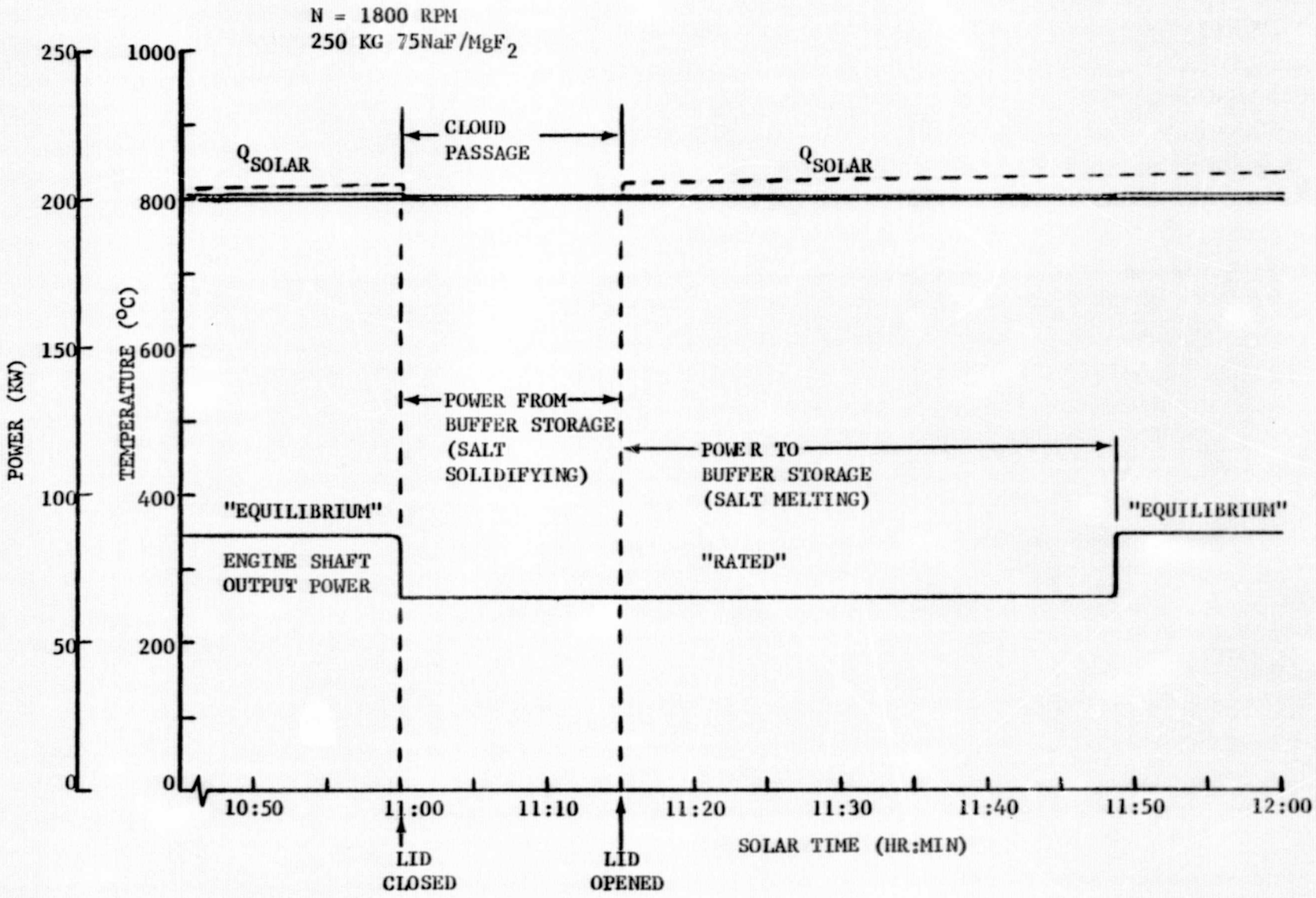


FIGURE 15

SODIUM TEMPERATURE RESPONSE AT RATED & IDLE ENGINE POWER

N=1800 RPM

S_1=Engine at rated power, no buffer storage

S_2=Engine at rated power, 100 Kg buffer storage

S_3=Engine at idle power, no buffer storage

S_4=Engine at idle power, 100 Kg buffer storage

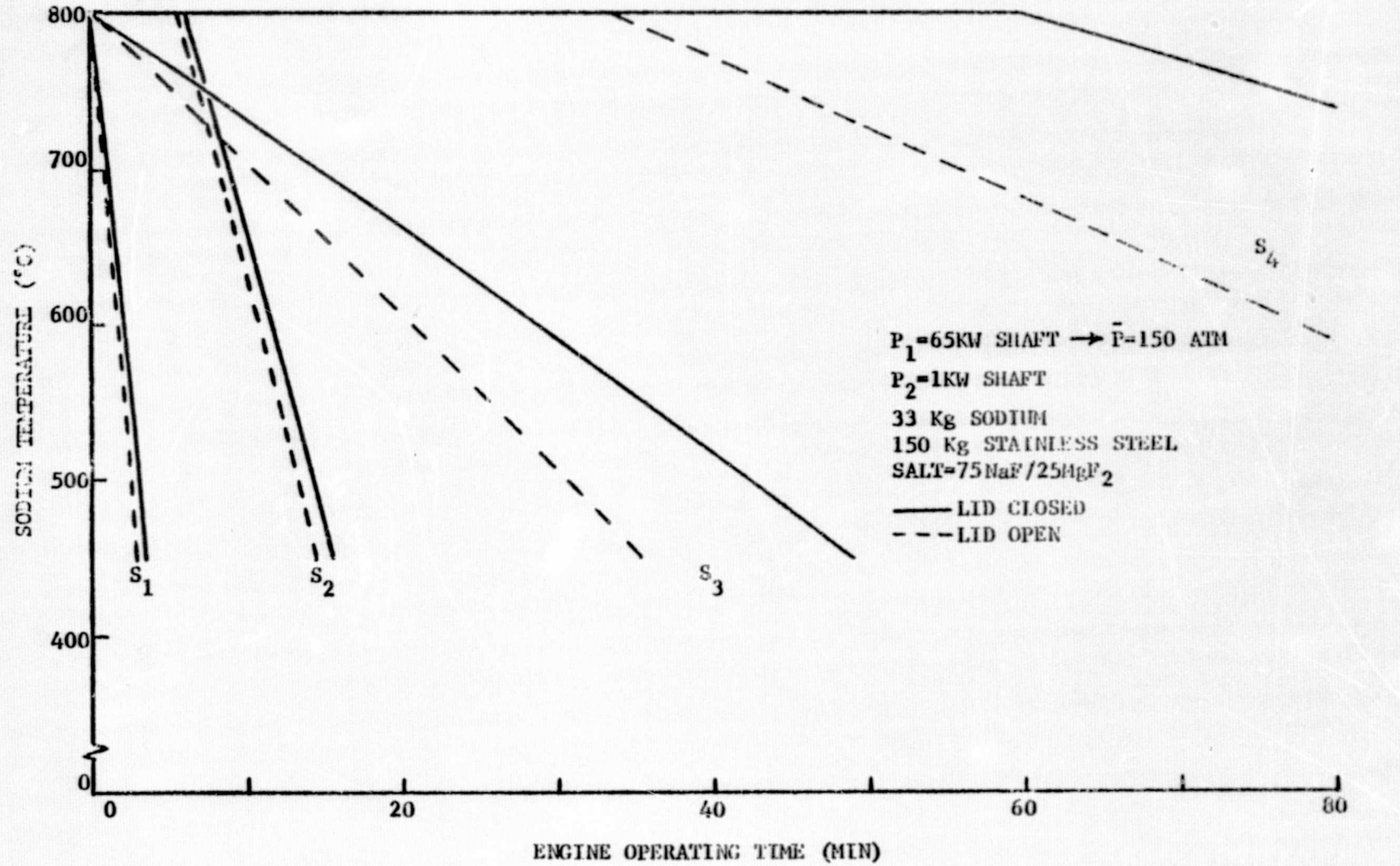
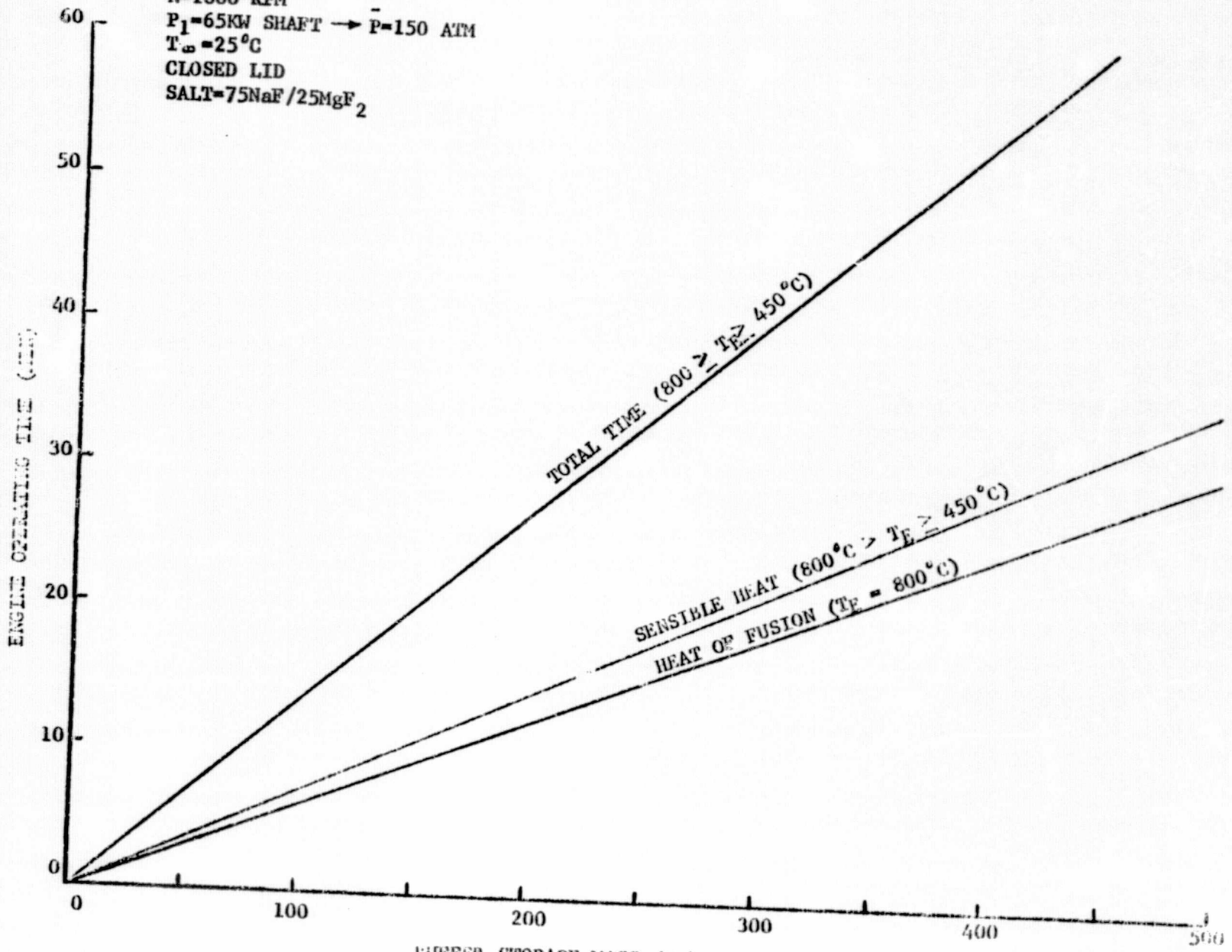


FIGURE 16

ENGINE OPERATING TIME WITH BUFFER STORAGE

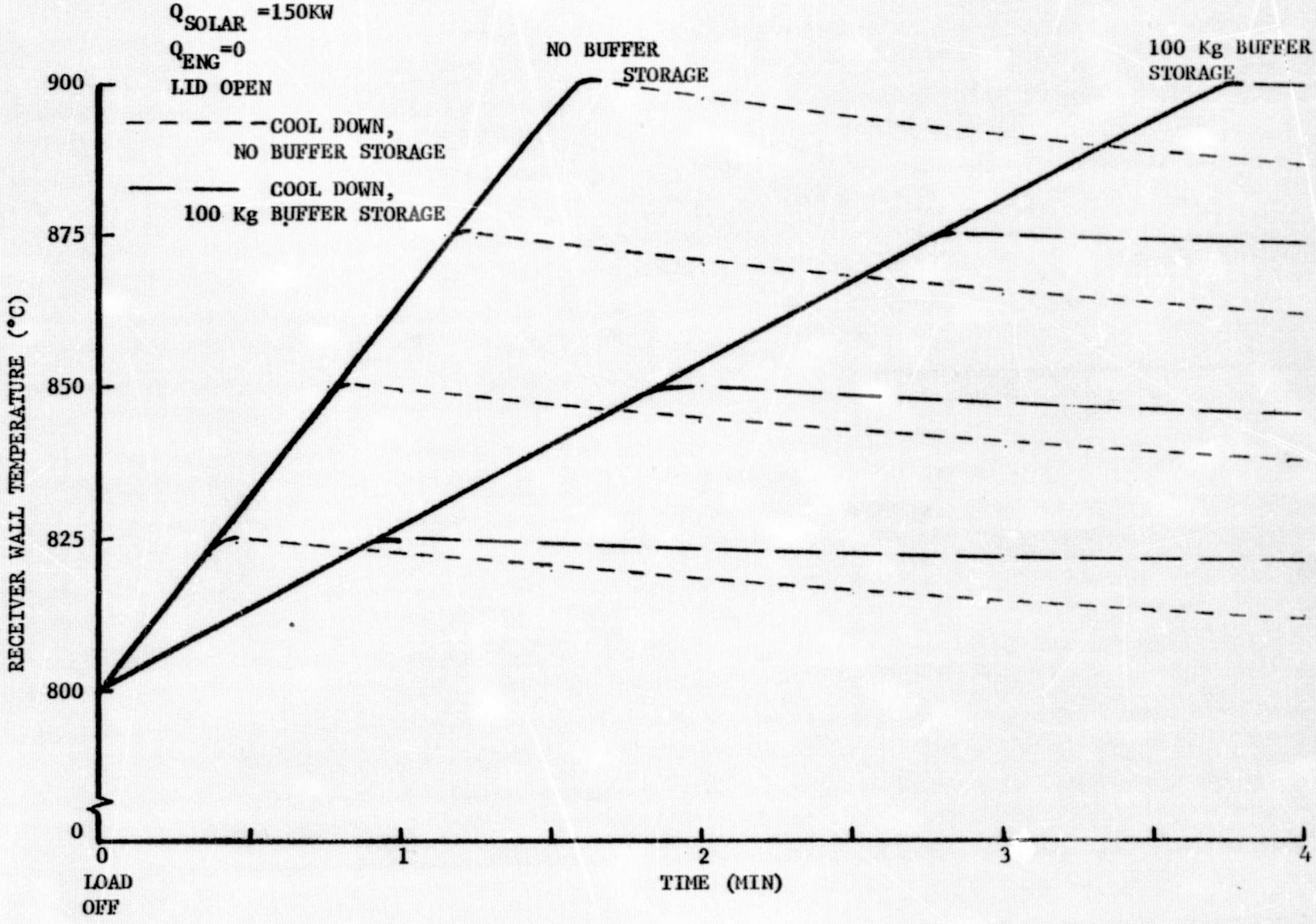
N=1800 RPM
P_1=65KW SHAFT → $\bar{P}$=150 ATM
T_∞=25°C
CLOSED LID
SALT=75NaF/25MgF_2



D.B.Q.

FIGURE 17

THERMAL RESPONSE FOR EMERGENCY OPERATION

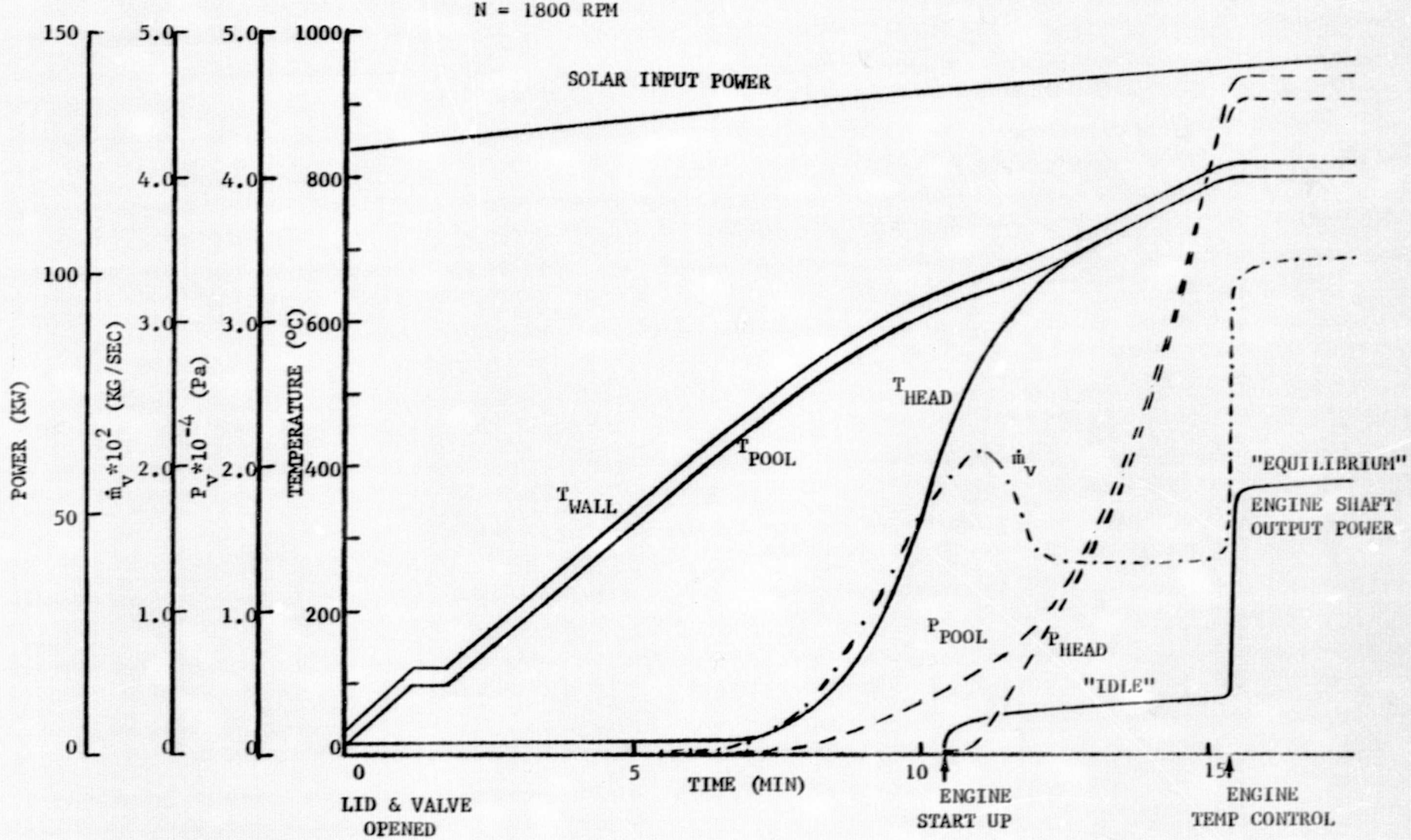


ORIGINAL PAGE IS OF POOR QUALITY

D.B.U.

FIGURE 18

SUBSYSTEM RESPONSE DURING START-UP



REFERENCES

1. Osborn, D.B., "Preliminary Transient Thermal Model for the Baseline Receiver - Transport Subsystem", TR-SPS-004, September 1, 1978, Ford Aerospace & Communications Corporation, Aeronutronic Division, Newport Beach, Ca.

2. Atomic's International, North American Rockwell, Sodium Technology, 1970.

3. Atomic's International, North American Rockwell, FBR Materials Handbook, Chapter VIII, Sodium Properties, release date April 28, 1972.

4. Pons, R.L., "Stirling Engine Performance Model", TR-SPS-001, August 16, 1978, Ford Aerospace & Communications Corporation, Aeronutronic Division, Newport Beach, Ca.

5. Garrigus, W.E., "Solar/Stirling Engine Control Analysis", TR-SPS-012, December 15, 1978, Ford Aerospace & Communications Corporation, Aeronutronic Division, Newport Beach, Ca.

6. Asselman, G.A.A., "Thermal Energy Storage Unit Based on Lithium Fluoride", Energy Conversion, Vol. 16, pp. 35-47, Pergamon Press, 1976.

7. Osborn, D.B., "Preliminary Thermal Analysis for Buffer Storage", TR-SPS-009, October 16, 1978, Ford Aerospace & Communications Corporation, Aeronutronic Division, Newport Beach, Ca.

8. Proposal P-23930, "Preliminary Design Study, 150 KW_e Irrigation Project, Vol. 1, Technical Discussion", November 12, 1976, Ford Aerospace & Communications Corporation, Aeronutronic Division, Newport Beach, Ca.

9. Eichelberger, J.L., "Final Report -- Investigation of Metal Fluoride Thermal Energy Storage Materials, Phase I -- Study of Availability, Cost, and Components", U.S. ERDA Contract No. EY-76-C-02-2990*000, December, 1976, Pennwalt Corporation, King of Prussia, Pa.

10. Boser, O., "Safety Considerations for High Temperature Thermal Energy Storage in Fluoride Salts", 12th IECEC Record, 1977.

11. Schroder, J., "Thermal Energy Storage and Control", ASME paper 74-WA/OcT-1, 1974.

APPENDIX I: NOMENCLATURE AND UNITS

A_{DISH} = collector area (m^2)*

A_{DUCT} = duct cross-sectional area (m^2)*

C_{SALT} = buffer storage capacitance (kW - min/K)*

C_{HEAD} = engine head thermal capacitance (kW - min/K)*

C_{SODIUM} = sodium thermal capacitance (kW - min/K)*

$C_{STRUCTURE}$ = pool and duct structure thermal capacitance (kW - min/K)*

C_V^* = sodium vapor characteristic velocity (m/sec)

F_{ABS} = clear sky absorption path length correction factor

f_{DROP} = solar dropout factor*

$$= \begin{cases} 0 \text{ for cloud passage or night} \\ 1 \text{ for clear sky} \end{cases}$$

f_{ENG} = engine factor*

$$= \begin{cases} 0 \text{ for engine off} \\ 1 \text{ for engine running} \end{cases}$$

f_{LID} = receiver lid factor*

$$= \begin{cases} 0 \text{ for lid closed} \\ 1 \text{ for lid open} \end{cases}$$

f_{VALVE} = sodium valve factor*

$$= \begin{cases} 0 \text{ for valve closed} \\ 1 \text{ for valve open} \end{cases}$$

g = 1 kg m/sec^2/N

G_{COOL} = effective heat transfer coefficient for engine cooling system (kW/K)*

G_{ENG} = conductance for heat loss through the engine when the engine is off (kW/K)*

G_{HEAD} = conductance for engine head conduction loss (kW/K)*

G_{LID} = lid conductance in closed position (kW/K)*

G_{Na} = sodium pool boiling convection coefficient (kW/K)*

G_{POOL} = conductance for receiver conduction loss (kW/K)*

G_{WALL} = receiver cavity wall conductance (kW/K)*

(hA_R) = convection loss coefficient (kW/K)*

I_o = solar flux above earth's atmosphere (kW/m^2)*

K_{ABS} = clear sky absorption for 90^o solar elevation*

L = site latitude*

ℓ = pressure exponent for engine input power*

$\overline{M}$ = sodium vapor mean molecular weight (kg/kg-mole)*

m = vapor pressure exponent*

$\dot{m}_v$ = sodium vapor flow rate (kg/min)*

$(\dot{m}_v)_c$ = sodium vapor flow rate for choked flow through the duct (kg/min)

$\overline{P}$ = engine mean pressure level (atm)*

P_{HEAD} = sodium vapor pressure at engine head (Pa)

P_{POOL} = sodium vapor pressure at the pool (Pa)

P_{REF} = reference vapor pressure (Pa)*

P_v = sodium vapor pressure (Pa)

$(PR)_{AMB}$ = input power ratio for coolant temperature different from 15^oC

$(PR)_{HEAD}$ = input power ratio for head temperature different from 800^oC

Q_{CONDH} = head external conduction loss (kW)

Q_{CONDP} = receiver and duct external conduction loss (kW)

Q_{CONV} = receiver internal convection loss (kW)

Q_{ENG} = power input to the engine (kW)

Q_{HEAD} = net head power (kW)

Q_o = reference engine output power at zero engine pressure (kW)*

Q_{OUT} = engine output power (kW)

Q_{POOL} = net pool power (kW)

Q_{RR} = receiver re-radiation loss (kW)

Q_{SOLAR} = solar heating rate at the receiver (kW)

Q_{TRANS} = power transmitted through the vapor duct (kW)

Q_{100} = reference engine input power at 800°C head temperature and 100 atm engine pressure (kW)*

R = universal gas constant

= 8314.34 (W-sec/kg-mole-K)

t = time variable (min, solar)

T_{AMB} = ambient air temperature (K)*

T_{COOL} = mean temperature of engine coolant (K)

T_{HEAD} = engine head temperature (K)

T_{POOL} = sodium pool bulk temperature (K)

T_{REF} = reference temperature for vapor pressure function (K)*

T_{SKY} = sink temperature for re-radiation (K)*

T_v = vapor pressure constant (K)*

T_w = receiver cavity surface temperature (K)

Z = vapor compressibility factor*

β = slope of engine output vs. input power at 800°C head temp.*

γ = sodium vapor ratio of specific heats*

$$\Gamma = \left[\gamma \left(\frac{2}{\gamma+1} \right)^{\frac{\gamma+1}{\gamma-1}} \right]^{\frac{1}{2}}$$

Γ' = $\left[\frac{\gamma-1}{2}\left(\frac{2}{\gamma+1}\right)^{\frac{\gamma+1}{\gamma-1}}\right]^{\frac{1}{2}}$

δ = solar declination angle*

ΔH_v = sodium heat of vaporization (kW - min/kg)*

η_{DSH} = collector efficiency*

η_{ENG} = engine efficiency

$(\sigma \epsilon A_R)$ = re-radiation coefficient (kW/K^4)*

* denotes input

APPENDIX M

SHADOWING ANALYSIS FOR PARABOLIC CONCENTRATOR FIELDS

APPENDIX M

SHADOWING ANALYSIS FOR PARABOLIC CONCENTRATOR FIELDS

1.0 INTRODUCTION

This Appendix presents the development and results of a shading/shadowing* analysis for a field of parabolic concentrators. A loss of energy occurs whenever solar insolation is prevented from reaching the aperture of a collector. This solar blockage can occur as a result of one (or more) collectors shading another. The percentage of the annual energy which is lost is a function of both the amount of energy available and the percent shading at any given instant which in turn are functions of the site location and the solar time. The amount of shading is also related to the field layout and the collector spacing. Thus, the objective of this study is to evaluate the annual energy loss for various field layouts and collector spacings. The results presented in this study are based upon the 15 minute solar insolation data for Barstow, California for the entire 1976 year. These results were used to optimize the collector arrangement based upon site location, land costs and costs dependent upon plant layout (for example, electrical cabling, fencing, etc.)

2.0 METHODS OF ANALYSIS

The collector shading, as a percentage of the total collector area, is derived from the relationships presented in Section 4. The percent shading is determined for any field of parabolic concentrators given the following information:

NNS = Number of concentrators in the North-South direction.

NEW = Number of concentrators in the East-West direction.

LNS = Ratio of the concentrator spacing (center-to-center) to concentrator diameter in the North-South direction.

LEW = Ratio of the concentrator spacing (center-to-center) to concentrator diameter in the East-West direction.

φ_A = Aximuth angle of the sun (referenced from North).

φ_E = Elevation angle of the sun (referenced from the horizon).

The values of φ_E and φ_E were calculated for each 15 minute time period using the equations presented in Section 5.0.

---

*Shading and shadowing are used interchangibly in the Appendix.

The percent energy loss for fixed values of field layout and sun angles is

$$E_{LOSS} = S_{AVG}\ A_{CONC}\ I_{d,n}$$

where

S_{AVG} = Average shaded area for the entire concentrator field

A_{CONC} = Concentrator area (unity)

$I_{d,n}$ = Solar insolation (direct, normal)

The values of the percent energy loss were compared with the percent loss in Capacity Factor for the baseline system using the P-75 Stirling engine. The difference between the two methods was sufficiently small (less than 3% of the respective values) to permit the use of this approximation. The percent energy loss was calculated for φ_E greater than or equal to 10°. This corresponds to the start-up and shutdown elevation of the baseline system. If the start-up and shutdown elevation was zero, the percent annual energy loss would increase by only about two percent. This is because the solar insolation during the first and last hour of a day are quite low.

The collector packing fraction was determined as follows:

$$\text{Packing Fraction} = \frac{\Sigma A_{CONC}}{A_{FIELD}}$$

where

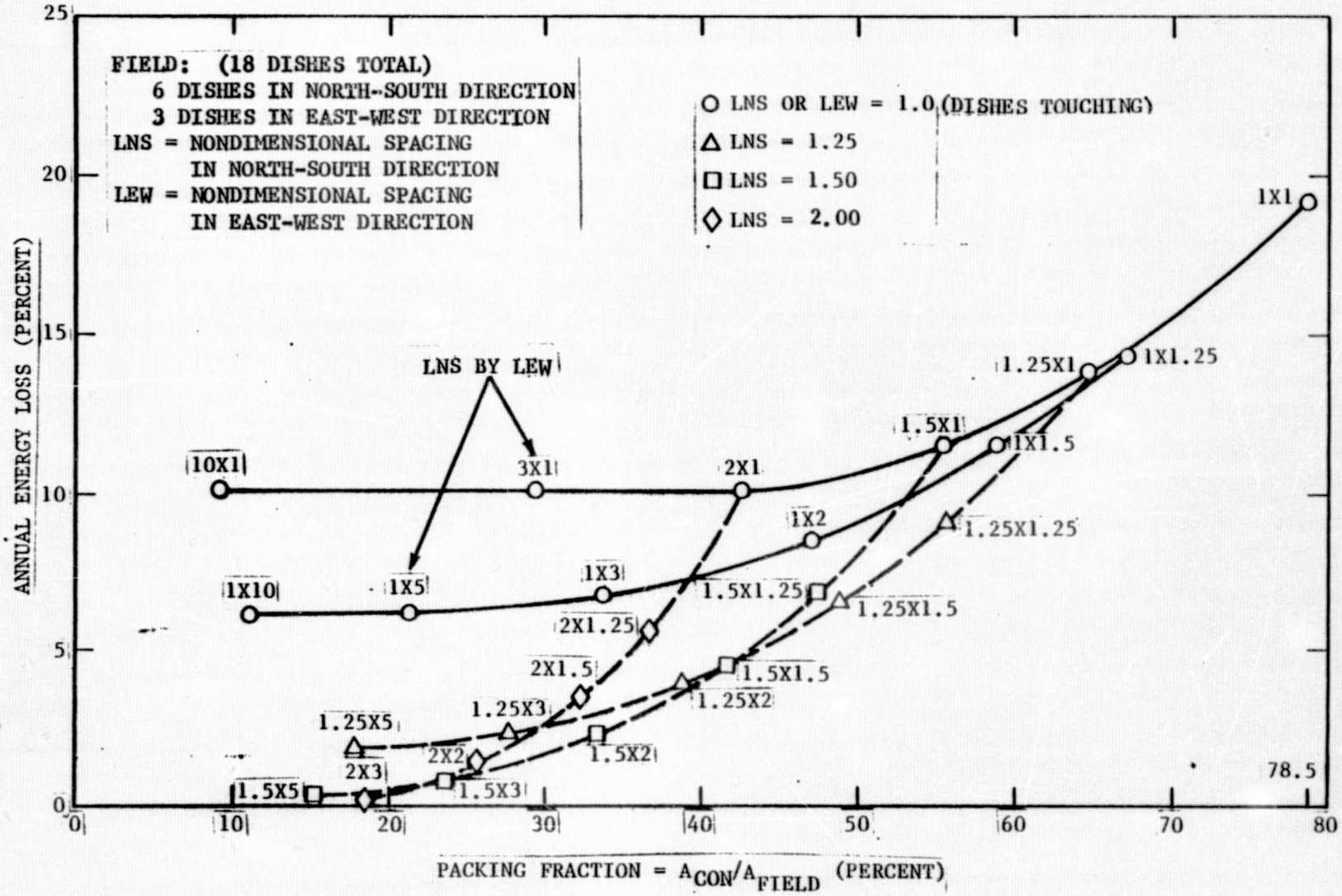
ΣA_{CONC} = Sum of the concentrator areas

A_{FIELD} = Area of the solar field
= ((NNS-1)*LNS+1)*((NEW-1)*LEW+1)

3.0 RESULTS

Figures M-1 through M-4 present the percent annual energy loss due to collector shadowing for various plant layouts of an 18 collector system.

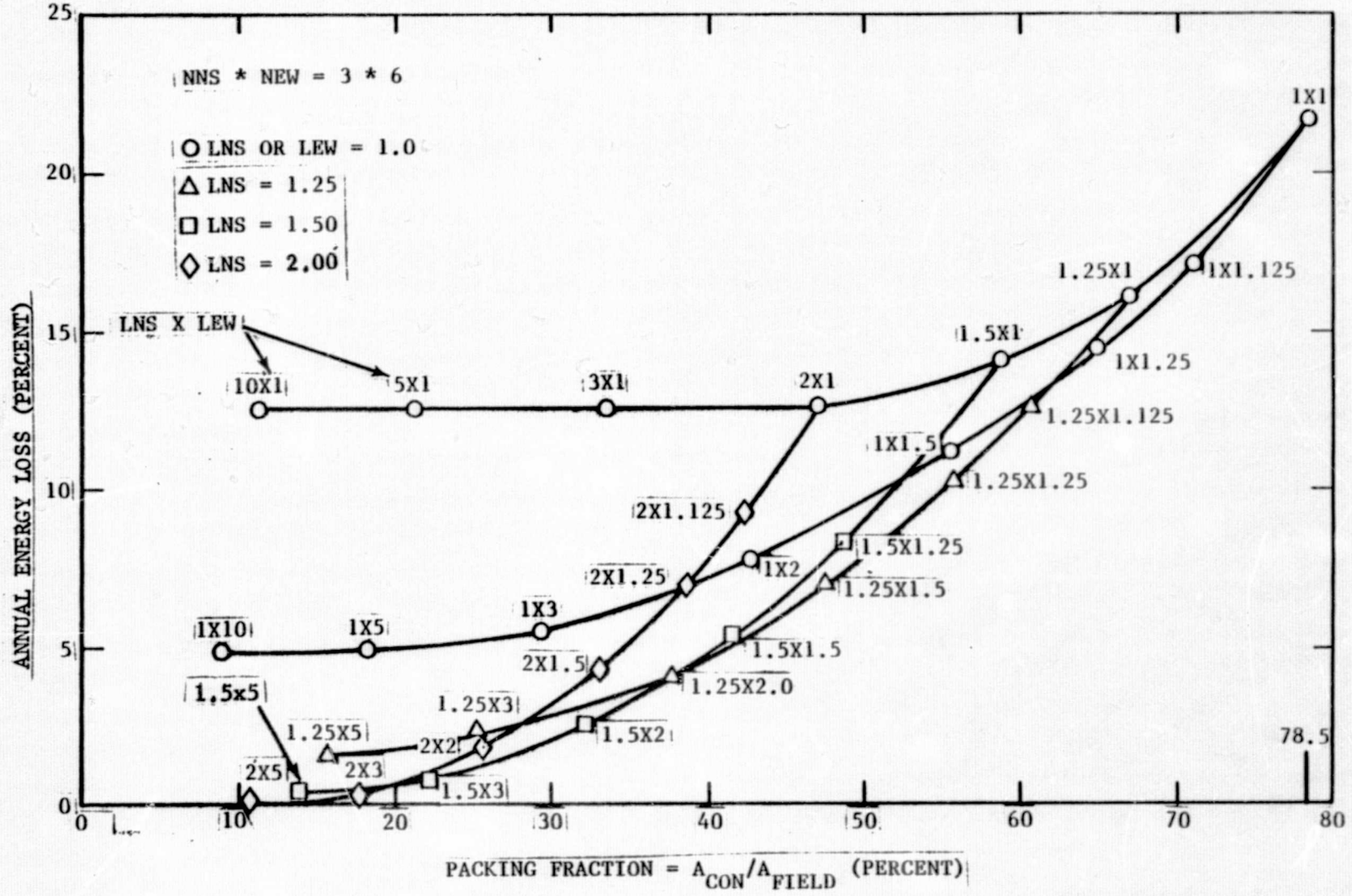
Figure M-1 presents the percent annual energy loss from collector shading, as a function of packing fraction and collector spacing, for a 6 by 3 plant layout. As expected, the energy loss due to shading decreases as the packing fraction decreases (collector spacing increases). However, for a given packing fraction and field configuration there is an optimum collector spacing. Increasing the North-South collector spacing (LNS) beyond about 2 dish diameters is not required since the shadowing (and hence energy loss) in this direction is negligible at greater distances. Likewise, a 5 dish diameter spacing in the East-West direction (LEW) is sufficient to reduce the shadow in this direction to a negligible level. Various combinations of LNS and LEW



94-2-178

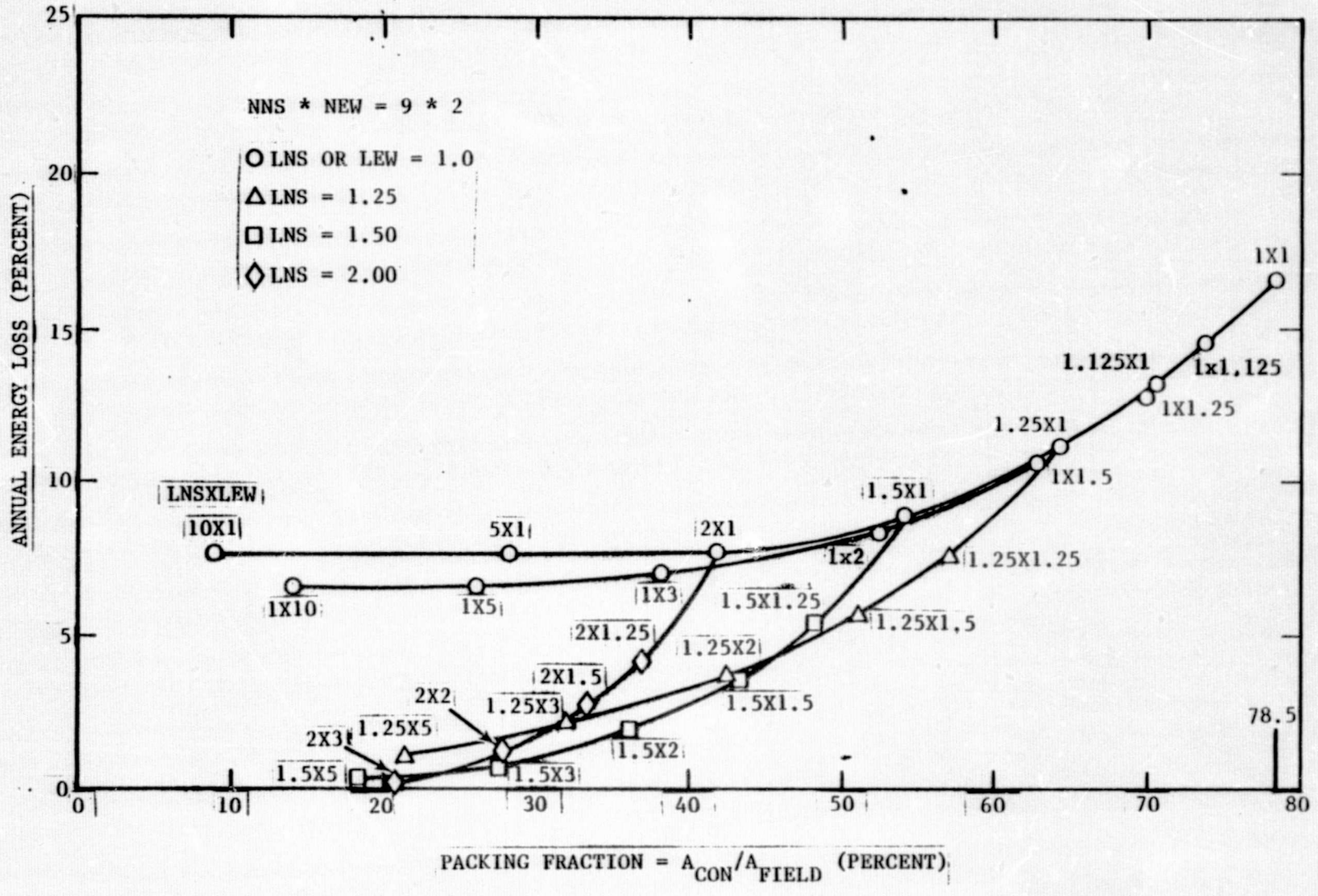
FIGURE M-1. ANNUAL ENERGY LOSS FOR A 6 BY 3 LAYOUT

ORIGINAL PAGE IS OF POOR QUALITY



94-2-179

FIGURE M-2. ANNUAL ENERGY LOSS FOR A 3 BY 6 LAYOUT



94-2-181

FIGURE M-3. ANNUAL ENERGY LOSS FOR A 9 BY 2 LAYOUT

spacing produce the minimum energy loss at a given packing fraction. For example, the baseline system (6 x 3 matrix) with a packing fraction of about 25 percent has a minimum annual energy loss of less than 1 percent. This occurs for collector spacings of approximately 1.5 and 3.0 dish diameters in the North-South and East-West directions, respectively. Similar results are obtained for other collector field arrangements as shown in Figures M-2 through M-4.

4.0 DERIVATION OF THE SHADING RELATIONSHIPS

This section presents the method to determine the percentage of shading that a solar collector experiences as a function of collector spacing and sun position. Figure M-5, which shows the top and side views of a cluster of four collectors, defines the geometry of this analysis. For certain combinations of sun azimuth angle (φ_A), sun elevation angle (φ_E), and collector spacing (L_{NS} and L_{EW}), collector 3 can experience different types of shading from neighboring collectors. Some combinations may yield individual shading by collector 4 (called East-West or 4-3 shading), collector 2 (called North-South or 2-3 shading), or collector 1 (called diagonal or 1-3 shading). Other combinations may produce cross shading when collector 3 is shaded collectively by collectors 1 and 2 (called 1, 2-3 shading) or collectors 1 and 4 (called 1, 4-3 shading). This analysis examines each of these possibilities, and determines the extent of shading that each produces.

a. East-West Shading. Consider first the East-West shading (for example, the shading of collector 4 onto collector 3) as illustrated in Figure M-6.

$$x_{4-3} = L_{EW} \sin(\phi_A)$$
$$= D\ell_{EW} \sin(\phi_A)$$

$$y_{4-3} = L_{EW} \cos(\phi_A)$$
$$= D\ell_{EW} \cos(\phi_A)$$

where

$$\ell_{EW} = L_{EW}/D$$

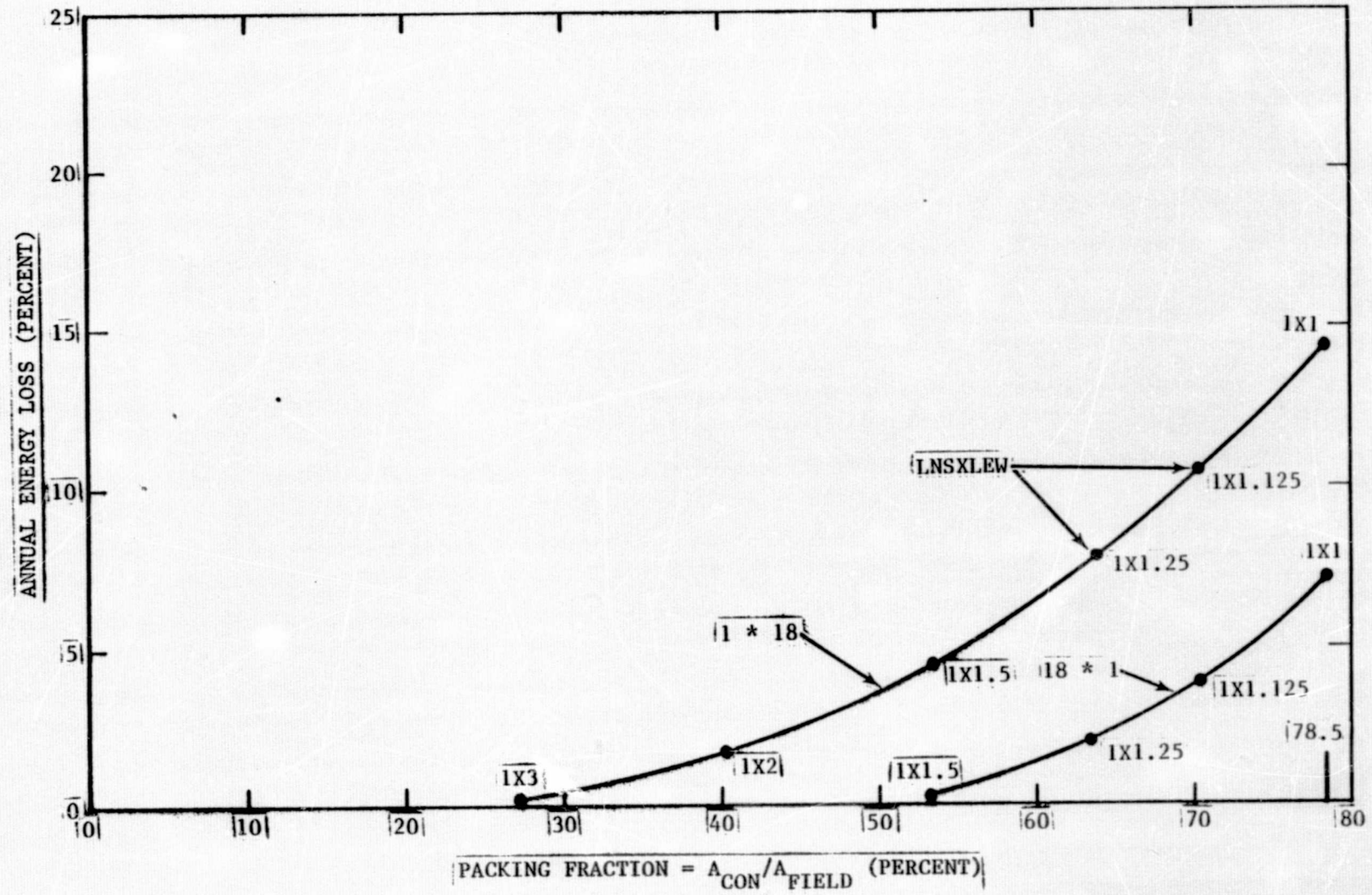
D is the dish diameter

See Figure M-7

$$x'_{4-3} = x_{4-3} \sin(\phi_E)$$
$$= D\ell_{EW} \sin(\phi_A) \sin(\phi_E)$$

See Figure M-8

$$d_{4-3} = \sqrt{(x'_{4-3})^2 + (y_{4-3})^2}$$
$$= D\ell_{EW}\sqrt{\sin^2(\phi_A) \sin^2(\phi_E) + \cos^2(\phi_A)}$$



94-2-180

FIGURE M-4. ANNUAL ENERGY LOSS FOR A 1 BY 18 OR 18 BY 1 LAYOUT

The common area, A_{4-3}, is given by:

$$A_{4-3} = \frac{D^2}{4} (\theta_1 - \sin \theta_1) \quad (1)$$

where the angle, θ_1, can be found as follows:

$$2r\cos\frac{\theta_1}{2} = d_{4-3}$$

$$\theta_1 = 2 \cos^{-1}\left(\frac{d_{4-3}}{D}\right) \quad (2)$$

The following test is used to determine whether or not 4-3 (or East-West) shading exists.

$$\text{If } \frac{d_{4-3}}{D} \begin{cases} \geq 1; \text{ no shading occurs} \\ \quad A_{4-3} = 0, \quad \theta_1 = 0 \\ < 1; \text{ shading occurs} \\ \quad A_{4-3} = \text{eq.(1)}; \ \theta_1 = \text{eq. (2)} \end{cases}$$

b. North-South Shading. Figure M-9 illustrates the case of North-South (or 2-3) shading. The formulation of shading for this case is similar to that used in the East-West shading case.

$$x_{2-3} = L_{NS} \cos(\phi_A) = D\ell_{NS} \cos(\phi_A)$$

$$y_{2-3} = L_{NS} \sin(\phi_A) = D\ell_{NS} \sin(\phi_A)$$

where

$$\ell_{NS} = L_{NS}/D$$

See Figure M-10

$$x'_{2-3} = x_{2-3} \sin(\phi_E) = D\ell_{NS} \cos(\phi_A) \sin(\phi_E)$$

See Figure M-11

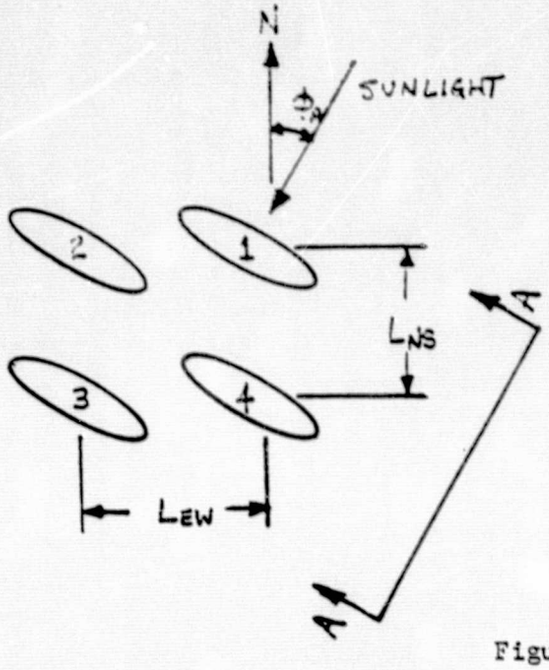
$$d_{2-3} = \sqrt{(x'_{2-3})^2 + (y_{2-3})^2} = D\ell_{NS}\sqrt{\cos^2(\phi_A) \sin^2(\phi_E) + \sin^2(\phi_A)}$$

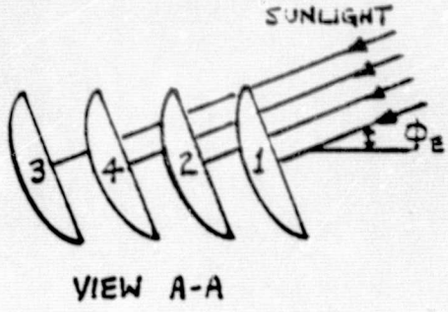
The common area, A_{2-3}, is given by;

$$A_{2-3} = \frac{D^2}{4} (\theta_2 - \sin \theta_2) \quad (3)$$

where the angle, θ_2, is given by;

$$\theta_2 = 2 \cos^{-1}\left(\frac{d_{2-3}}{D}\right) \quad (4)$$





VIEW A-A

Figure M-5

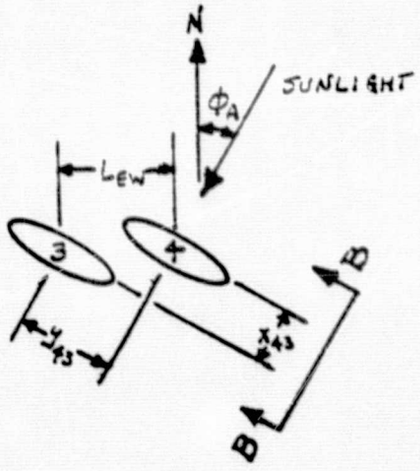
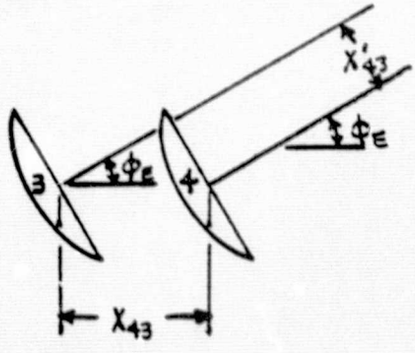


Figure M-6



VIEW B-B

Figure M-7

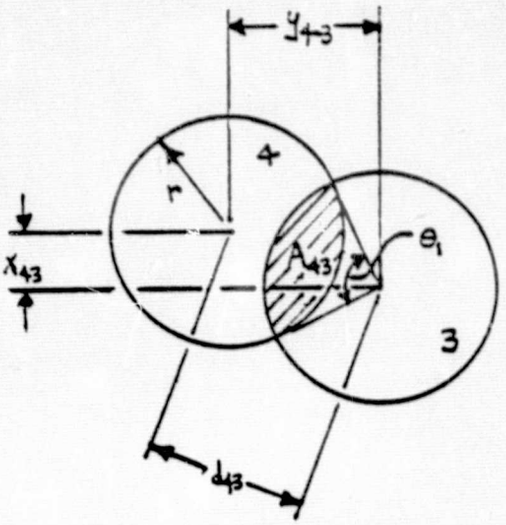


Figure M-8

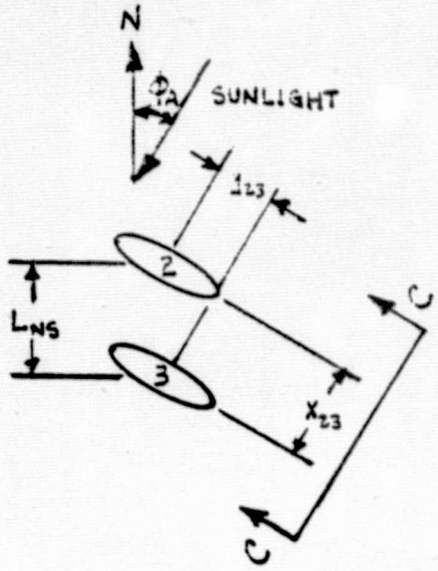
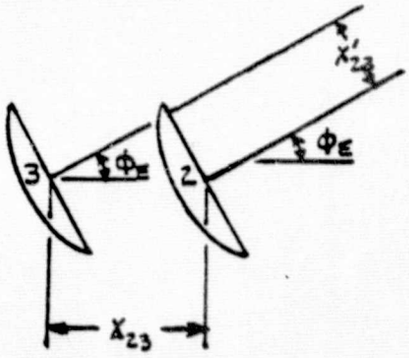


Figure M-9



VIEW C-C

Figure M-10

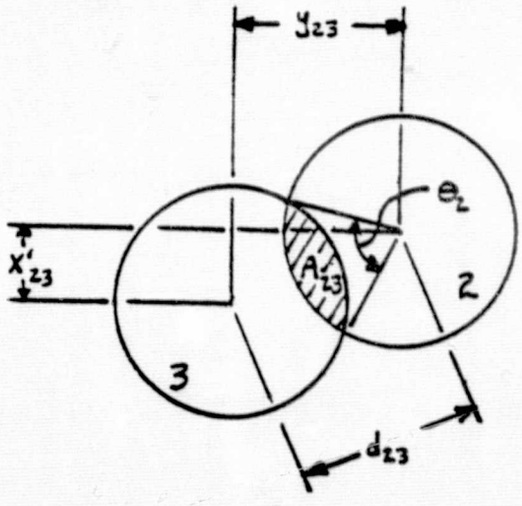


Figure M-11

The following test is applied to determine whether or not 2-3 (or North-South) shading occurs.

$$\text{If } \frac{d_{2-3}}{D} \begin{cases} \geq 1; \text{ no shading occurs} \\ \quad A_{2-3} = 0,\ \theta_2 = 0 \\ < 1; \text{ shading occurs} \\ \quad A_{2-3} = \text{eq.(3)};\ \theta_2 = \text{eq.(4)} \end{cases}$$

c. Diagonal Shading. Consider now the diagonal shading (for example, the shading of collector 1 onto collector 3) as shown in Figure M-12.

$$L_d = \sqrt{L^2_{NS} + L^2_{EW}}$$

$$x_{1-3} = L_d \cos \beta$$

$$y_{1-3} = L_d \sin \beta$$

where

$$\beta = \frac{\pi}{2} - \theta_A - 2$$

$$\alpha = \tan^{-1}\left(\frac{L_{NS}}{L_{EW}}\right)$$

Therefore,

$$x_{1-3} = D\sqrt{\ell^2_{NS} + \ell^2_{EW}} \cos\left[\frac{\pi}{2} - \phi_A - \tan^{-1}\left(\frac{L_{NS}}{L_{EW}}\right)\right]$$

$$y_{1-3} = D\sqrt{\ell^2_{NS} + \ell^2_{EW}} \sin\left[\frac{\pi}{2} - \phi_A - \tan^{-1}\left(\frac{L_{NS}}{L_{EW}}\right)\right]$$

See Figure M-13

$$x'_{1-3} = x_{1-3} \sin(\phi_E)$$

$$= D\sqrt{\ell^2_{NS} + \ell^2_{EW}} \cos\left[\frac{\pi}{2} - \phi_A - \tan^{-1}\left(\frac{L_{NS}}{L_{EW}}\right)\right] \sin(\phi_E)$$

See Figure M-14

$$d_{1-3} = \sqrt{(x'_{1-3})^2 + (y_{1-3})^2}$$

$$= D\sqrt{(\ell^2_{NS} + \ell^2_{EW})\left\{\cos^2\left[\frac{\pi}{2} - \phi_A - \tan^{-1}\left(\frac{L_{NS}}{L_{EW}}\right)\right] \sin^2(\phi_E) + \sin^2\left[\frac{\pi}{2} - \phi_A - \tan^{-1}\left(\frac{L_{NS}}{L_{EW}}\right)\right]\right.}$$

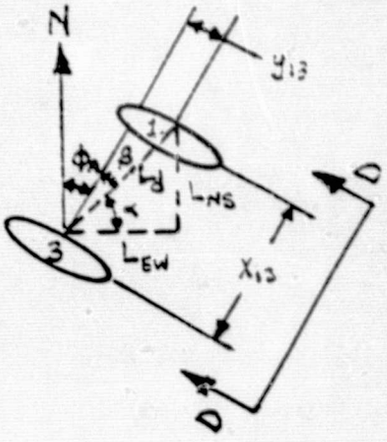


Figure M-12

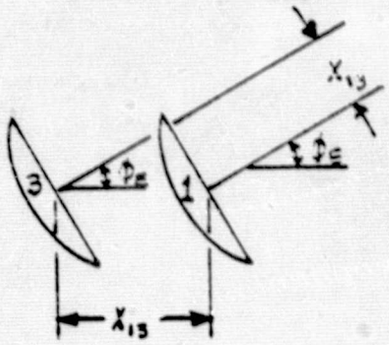


Figure M-13

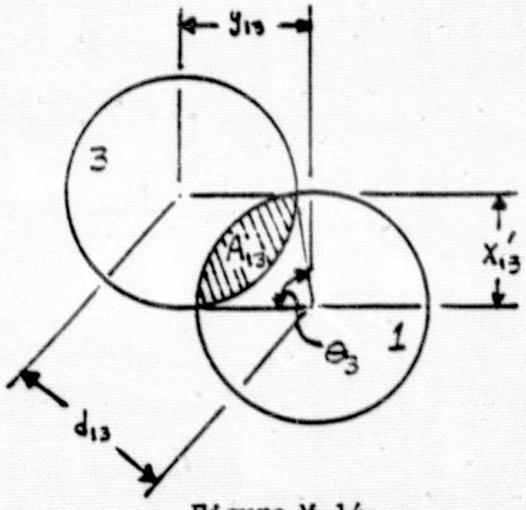


Figure M-14

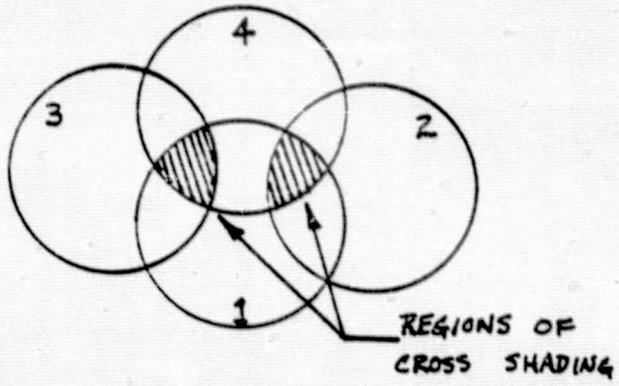


Figure M-15

The common area, A_{1-3}, is given by;

$$A_{1-3} = \frac{D^2}{4} (\theta_3 - \sin \theta_3) \tag{5}$$

where

$$\theta_3 = 2 \cos^{-1} \left(\frac{d_{1-3}}{D} \right) \tag{6}$$

The following test is used to determine whether or not diagonal (or 1-3) shading exists.

$$\text{If } \frac{d_{1-3}}{D} \begin{cases} \geq 1; \text{ no shading occurs} \\ \quad A_{1-3} = 0; \ \theta_3 = 0 \\ < 1; \text{ shading occurs} \\ \quad A_{1-3} = \text{eq (5)}; \ \theta_3 = \text{eq (6)} \end{cases}$$

d. Cross Shading. Cross shading on any given collector occurs whenever two shadows, cast by other collectors, intersect and share a common area. Figure M-15 shows how collectors 1 and 2 may cross shade collector 3 and how collectors 1 and 4 may cross shade collector 3.

Figure M-16 is an enlarged drawing of the condition where collector 3 is double shaded by collectors 1 and 2.

From the law of cosines;

$$S_1 = \cos^{-1} \left(\frac{d^2_{1-2} + d_{1-3}{}^2 - d^2_{2-3}}{2 d_{1-2} \, d_{1-3}} \right)$$

$$S_2 = \cos^{-1} \left(\frac{d^2_{2-3} + d^2_{1-2} - d^2_{1-3}}{2 d_{2-3} \, d_{1-2}} \right)$$

$$S_3 = \cos^{-1} \left(\frac{d^2_{1-3} + d^2_{2-3} - d^2_{1-2}}{2 d_{1-3} \, d_{2-3}} \right)$$

where

$$d_{1-2} = d_{4-3}$$

From the geometry of the figure, it can be shown that,

$$\gamma_1 = \tfrac{1}{2} (\theta_3 + \theta_2) - \delta_1$$
$$\gamma_2 = \tfrac{1}{2} (\theta_2 + \theta_1) - \delta_2$$
$$\gamma_3 = \tfrac{1}{2} (\theta_1 + \theta_3) - \delta_3$$

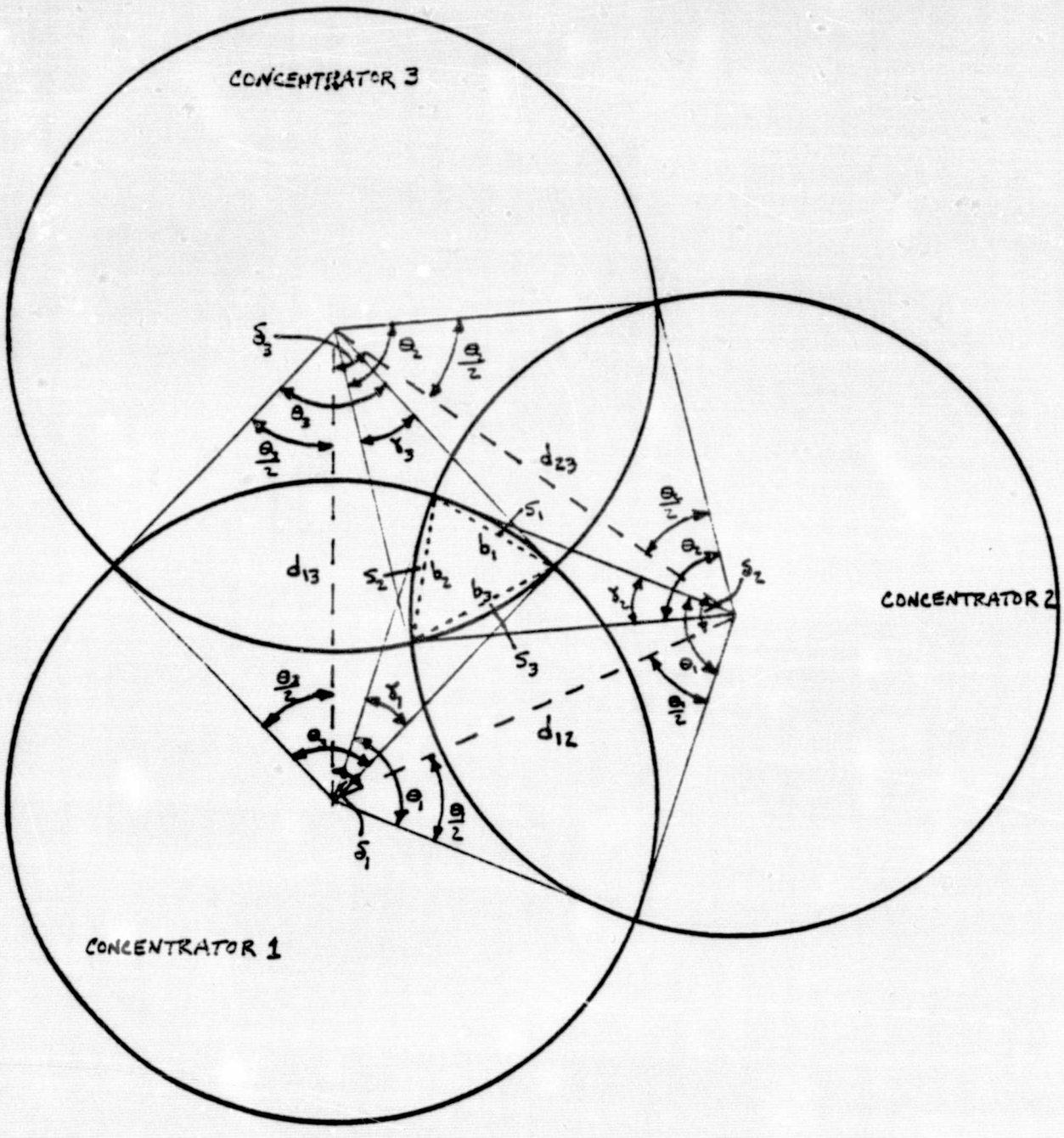


Figure M-16. Cross Shading of Collectors 1 and 2 onto Collector 3.

The areas of the segments S_1, S_2, and S_3 are given by;

$$S_1 = \frac{D^2}{8} (\gamma_1 - \sin \gamma_1)$$

$$S_2 = \frac{D^2}{8} (\gamma_2 - \sin \gamma_2)$$

$$S_3 = \frac{D^2}{8} (\gamma_3 - \sin \gamma_3)$$

The chord lengths b_1, b_2, and b_3 are expressed by,

$$b_1 = D \sin (\tfrac{1}{2}\gamma_1)$$

$$b_2 = D \sin (\tfrac{1}{2}\gamma_2)$$

$$b_3 = D \sin (\tfrac{1}{2}\gamma_3)$$

The area of the triangle enclosed by chords b_1, b_2, and b_3 is;

$$A_{tri} = \sqrt{x\ (x - b_1)\ (x - b_2)\ (x - b_3)}$$

where

$$x = \tfrac{1}{2}\ (b_1 + b_2 + b_3)$$

The area of the region common to all three circles, $A_{1,\ 2\text{-}3,}$ is given as;

$$A_{1,\ 2\text{-}3} = S_1 + S_2 + S_3 + A_{tri} \qquad (7)$$

The following test is used to determine the extent of cross shading onto collector 3 due to collectors 1 and 2.

$$\text{If } \gamma_1 \begin{cases} \leq 0; \text{ no cross shading exists} \\ \quad A_{1,\ 2\text{-}3} = 0 \\ > 0; \text{ cross shading exists} \\ \quad A_{1,\ 2\text{-}3} = \text{eq. (7)} \end{cases}$$

The analysis for 1, 4-3 diagonal shading is identical to that of 1, 2-4 shading except $d_{1\text{-}4}$ is used in place of $d_{1\text{-}2}$, and $d_{4\text{-}3}$ is used in place of $d_{2\text{-}3}$.

5.0 SOLAR ANGLE RELATIONSHIPS

The azimuth and elevation angles of the sun are determined by the following expressions*:

---

*Anon., "On The Nature and Distribution of Solar Radiation", Prepared for the U.S. Department of Energy, HCP/T2552-01, March 1978.

$$\varphi_E = \sin^{-1}\left[\cos L \cos\delta \cos h + \sin L \sin\delta\right]$$

$$\varphi_A = \cos^{-1}\left[(\sin\delta - \sin L \sin\varphi_E)\Big/(\cos L \cos\varphi_E)\right]$$

$$h = 15(H_S - 12)$$

$$\delta = 23.45 \sin\left[1.008(n-80)\right] \qquad 1 \leq n \leq 80$$

$$\delta = 23.45 \sin\left[.965(n-80)\right] \qquad 81 \leq n \leq 266$$

$$\delta = -23.45 \sin\left[.975(n-266)\right] \qquad 267 \leq n \leq 366$$

where

L = site latitude (degrees)

S = solar declination (degrees)

h = hour angle about noon (degrees)

H_S = true solar time (hours)

n = number of the day of the year

APPENDIX N

STUDY OF SODIUM FOR HIGH TEMPERATURE APPLICATIONS

Ford Aerospace & Communications Corporation
Aeronutronic Division

Ford Road
Newport Beach, California 92663

TECHNICAL REPORT

TR. NO. SPS-019

SOLAR SMALL POWER SYSTEM (SPS) PROGRAM

TITLE: STUDY OF SODIUM FOR HIGH TEMPERATURE APPLICATIONS

PREPARED BY: D.C. Jackson	ORG NO. L284	CHARGE NO. 2205-5000
SUPERVISOR APPROVAL: R.M. Taylor	DATE 3/2/79	
PROGRAM ENGINEER APPROVAL: R.L. Pons	TO DISTRIBUTION	

SUMMARY

An in-depth study of the prior use of metallic sodium in high temperature applications is presented. The areas which have been investigated include:

- Commercial applications of metallic sodium.
- Hardware used in sodium systems which includes filtering devices, pumps, and valves.
- The corrosion behavior of 300 series stainless steels and nickel base alloys in high temperature sodium.
- Sodium handling including preparing and filling containers to minimize trapped impurities.

DISTRIBUTION

E. D. Avetta
W. C. Barnum
F. P. Boda
T. B. Clark
N. L. Cowden (2)
R. M. Grabow
H. J. Haskins
D. C. Jackson (2)
I. E. Lewis (WDL)
R. A. Maxwell
D. B. Osborn
W. B. Sweningsen
R. M. Taylor
C. C. Wan
D. J. Corn (3+MTR)

ORIGINAL PAGE IS
OF POOR QUALITY

1.0 INTRODUCTION AND BACKGROUND

The baseline receiver coupled with the Stirling Cycle Engine utilizes metallic sodium (Na) as a heat-transfer medium. The excellent physical properties of the liquid-metal (sodium) make it possible to design a simple and efficient heat-exchanger (boiler) which transfers concentrated sun energy into hot sodium vapor. This hot vapor at less than atmospheric pressure is then used to operate a Stirling Engine. The high heat transfer coefficient of sodium and its relatively low operating pressure at high temperatures are only two of the favorable properties.

Figure 1 shows a sketch of the baseline system. The major components of the system are receiver core filled with sodium, cavity door, butterfly blocking valve, expansion bellows, vapor pipe, Stirling Engine, and generator. The entire system up to and including the engine head is covered with thermal insulation. The receiver core contains approximately 33 Kg (73 pounds) of sodium which is heated to approximately 800°C. The hot sodium vapor from the receiver core is ducted by a vapor pipe through a butterfly valve and bellows to the engine head. During the night-time shut-down periods the butterfly valve is closed to block vapor flow to the engine, and the cavity door is closed to minimize heat loss. The complete baseline system shown in Figure 1 has a total weight of approximately 1088.6 Kg (2400 pounds).

This report presents summarized results from an in-depth study of metallic sodium. The topics presented are commercial applications of metallic sodium, hardware found in sodium systems, corrosion of materials (stainless steel and nickel-base alloys) exposed to liquid sodium, and sodium handling.

2.0 COMMERCIAL APPLICATIONS OF METALLIC SODIUM

Presently, the applications of metallic sodium are divided into two major categories -- those based on the physical properties of sodium and those based on the chemical reactions of sodium. This report will be confined to the uses based on physical properties and will neglect the uses based on inorganic and organic chemical reactions.

Probably the best known use of sodium is as a heat transfer medium. This application is very evident if the heat transfer coefficients (boiling, condensing, and convection) of sodium are compared to other working fluids. The ability of the sodium to rapidly transfer heat at high temperatures makes it very useful

for solar heating applications where high temperature transients are encountered. Other unique properties of sodium which make it a very desirable working fluid includes:

a) Low operating vapor pressure over a wide temperature range. (This quality is very important for mechanical design and fabrication of heat exchangers).

b) Sodium has previously been used in a Stirling engine. (Reference 1)

c) High boiling point.

d) Relatively high merit number over a wide temperature range.

A few examples follow which describe commercial applications of metallic sodium.

2.1 ENGINE VALVES

For many years sodium has been used as a heat transfer medium in sodium-cooled valves in trucks, cars, and aircraft engines. Sodium is contained within a hollow space inside the valve. Heat is transferred from the head of the valve to the stem by the splashing of the liquid sodium as the valve moves up and down during engine operation. Figure 2 shows operating temperatures for a conventional solid stem valve and a hollow stem sodium-filled valve. Figure 2 shows that with 60 percent of the hollow valve stem filled with sodium the operating temperature of the valve neck and stem is reduced approximately 190°C. This substantial reduction of operating temperature of the valve material prolongs valve life.

2.2 NUCLEAR POWER PLANTS

Because of the very desirable properties of sodium, it is an ideal heat transfer medium for nuclear power plants. These properties include:

- Low neutron absorption
- High boiling point
- High heat-transfer efficiency
- Extreme thermal stability
- Ease of pumping
- Freedom from corrosion in the absence of impurities
- High temperature operation at low vapor pressure

Typically, the heat removed from the reactor core is transferred to a steam generator through two separate sodium loops; a primary and secondary system. This dual system is necessary to prevent radioactive sodium in the primary loop from coming into contact with the fluid used to drive the steam generator. Therefore, the radioactive primary loop is separated from the water system by means of a secondary sodium system.

For several years a sodium-cooled nuclear reactor built by Atomics International at Santa Susanna, California, has supplied heat to generate electricity for a commercial grid. Because liquid metal (sodium) has such good heat-transfer capability and low operating pressures at high temperature, this nuclear power plant is operated safely and efficiently.

A few of the many other non-chemical applications of liquid sodium are listed below:

- Liquid sodium has been used as a heat-treating medium to provide uniform temperature distributions.
- In the die-casting of magnesium, sodium is used for core cooling of casting machines.
- Another instance of the successful application of sodium to an industrial heat-transfer problem is in shale oil retorting. Special plows which distribute shale are exposed to 1200°C operating temperatures and cooled by sodium.
- For the control of glass mold temperatures. Sodium is used to absorb heat during the glass molding cycle, and also preheat empty molds.
- Liquid metal (sodium) is used in the reheat cycle of large steam plants. Liquid metal heaters, located in the boiler, carry hot sodium to the second stage turbine reheater. Superheated steam, which has expanded through a high pressure primary stage turbine, is then reheated before passage through the second turbine.

3.0 SODIUM SYSTEMS HARDWARE

3.1 PUMPING/TRANSFERRING LIQUID SODIUM

Both mechanical and electromagnetic pumps have been used with relatively good success as a means of pumping molten sodium. The primary problem in designing pumps used to transfer sodium (as with valves) is to provide satisfactory seals. Currently there are various types of pump seals being used -

a frozen seal, gas-sealed, and mechanical seals. Examples of these types of seals are shown in Figure 3.

Electromagnetic pumps have been used successfully for liquid sodium recirculation systems. These pumps are totally sealed with no moving parts, and provide long periods of trouble-free service. A wide range of pump models providing different flow rates and pressure outputs are available. Figure 4 shows a diagram of a D-C Faraday-Type pump.

Mechanical pumps that have been used successfully to transfer liquid sodium are the gas-sealed submerged centrifugal pumps, piston and diaphram pumps, and rotary gear-type pumps. These pumps have high operating efficiencies and are capable of maintaining high system pressure for continuous service. A large number of pumps with a variety of flow rates and pressure outputs are available from commercial pump companies. A single stage centrifugal pump and a gas-sealed type centrifugal pump are shown in Figure 5.

For many operations, liquid sodium can be transferred by differential-pressure methods. One method used for inducing sodium flow is to establish a vacuum in the receiving tank or equipment. A low-pressure nitrogen atmosphere is maintained in the tank from which the sodium is being withdrawn. The pressure differential thus creates sodium flow. A simple air-cooled, reciprocating vacuum pump can be used to produce the necessary vacuum. To prevent drawing liquid sodium into the vacuum pump, it is common practice to install a barometric loop ahead of the pump.

3.2 FILTERS/COLD TRAPS

Raw sodium from the manufacturer contains small quantities of impurities such as oxides, chlorides, and calcium metals. However, because the solubility of these impurities is reduced at low temperatures, the sodium can be purified by filtration. A number of devices and techniques have been employed for removal of these impurities from molten sodium. These include:

- Chemical "getting" of oxygen by calcium or titanium.
- Filtration.
- Cold-trapping.

Chemical purification by "getting agents" is used primarily for oxygen content reduction. Two of the more common gettering agents are calcium and titanium. The calcium getter material is soluble in sodium and forms an oxide

with limited solubility. These oxides are then reacted with impurity materials soluble in sodium and removed by filtration.

The second gettering agent, titanium, is insoluble in sodium. The titanium getter reduces sodium oxides to insoluble getterer oxide which is removed from the system by filtration.

The second technique commonly used to purify sodium is by filtering at approximately 150°C through Micro Metallic filters. These filters have a pore size of approximately 15-microns and are constructed of sintered stainless steel. This type of filtering can provide an oxide content as low as 10 parts per million (ppm). This oxide level was found to be satisfactory for the proposed FACC baseline sodium receiver.

A cold trap is a basic purification device for flowing sodium systems. In this unit, sodium is cooled down to a temperature of approximately 170°C. At this reduced temperature, oxides and other impurities become insoluble and precipitate out of the sodium. Under these conditions, the trapped impurities can be permanently removed from the sodium system. In this form of purification, the oxide content of a sodium system can be maintained as low as about 5 to 10 parts per million. This level is satisfactory for most systems constructed of stainless steel material.

A typical cold trap, shown in Figure 6, would consist of a canister containing 10-15 micron pore size stainless steel wool sized such that the flowing sodium would be kept at approximately 170°C. Maintenance of a cold trap would involve periodically replacing the contaminated stainless steel wool. Since the FACC baseline sodium receiver operates isothermally, cold trap devices are not necessary for sodium filtering.

3.3 VALVES

Typical valves found in sodium systems are blocking valves, throttle-type valves, and ball-type check valves. These valves are designed to perform specific tasks and meet the general requirements to provide safe and efficient operation.

The general requirements for valves for liquid sodium systems are:

- Zero valve stem leakage.
  All valves must be specifically constructed for zero leakage to the surroundings to prevent impurities, such as oxygen, from entering the system. This type of leakage prevention requires all-welded constructions of valves with either bellows seals or freeze seals.

- Corrosion Resistance.
  Corrosion resistance materials are used in all valves. Typically, the standard materials used are types 304 and 316 stainless steels. However, valve seats, discs, and other wearing parts should be constructed with hard facing materials in order to prevent galling. The possibility of intergranular corrosion requires that special precautions be taken to insure sound metal parts with no porosity. The stringent requirements make the use of forged valve bodies very desirable.
- Thermal Shock.
  Valves must be designed to resist the pipe stresses resulting from thermal cycling and shock. Precautions should be taken in valve design to prevent binding due to thermal expansion.

A typical ball check valve is shown in Figure 7. This valve permits flow in only one direction and is operated by the pressure difference across the valve. Figure 8 shows a cross-section view of a piston-operated blocking valve. The FACC baseline receiver will utilize a butterfly valve similar to the valve shown in Figure 9.

4.0 CORROSION OF MATERIALS

This section of the report will focus on the corrosion behavior of stainless steels (300 series) and nickel base alloys in high temperature sodium. The various parameters which affect the rate of mass transfer, rates of material loss, and carbonization of stainless steels, have been studied. These parameters include the effect of temperature in the range 600 to 900°C, the effect of impurity content of the liquid metal (oxygen, sulfur, hydrogen, carbon) and the effect of alloying content such as high percentages of nickel. The effect of fluid flow rate will not be considered because it is not applicable to the FACC baseline sodium receiver.

Each of the above parameters will be discussed separately and comparisons, where appropriate, are made between various references.

4.1 MASS TRANSFER

A common mechanism of corrosion in liquid-metal systems is mass transport. Mass transport results from a coexistence of a temperature differential and an appreciable thermal coefficient of solubility. Corrosion deposits from the

structure materials will tend to dissolve in regions of high chemical activity (hot areas), and will tend to deposit from solution in regions of low chemical activity (cold areas). This continued transfer of material in the system can accelerate corrosion attack in the areas of high activity. The precipitated material will accumulate in cooler regions of the system and may eventually cause plugging of flow tubes. At present most sodium pumped systems utilize "cold trapping" as a means of continually filtering the flowing sodium. These cold traps, which maintain a temperature of approximately 170°C, provide the necessary cold area for material deposit.

Mass transport of impurity substances virtually does not exist in the FACC baseline sodium receiver design. The temperature differential within the sodium boiler is not sufficient to cause the impurities held in suspension to precipitate out of the sodium. The rate of material loss and corrosion of receiver material are therefore minimized.

4.2 EFFECTS OF TEMPERATURE AND OXYGEN CONTENT

Typically, corrosion experiments involving high-temperature sodium are conducted using electromagnetically pumped sodium loops. These loops employ flowmeters to monitor fluid velocity through hot-and-cold-leg sections. Heat is supplied to the system by wound heaters placed around the hot-leg section. The cold-leg consists of a cold trap which collects material deposits during the time of system operation. Measurements of mass transfer rates are determined by gravimetric and metallographic analysis of the cold trap deposits. The corrosion rate data presented in the following paragraphs is based on operating systems and measuring techniques described above.

The mass transfer rates of nickel-base materials (Hastelloy, Inconel) and 300 series stainless steel are presented in Figure 10 as a function of temperature. Figure 10 shows a marked temperature dependence of mass transfer in Inconel and Hastelloy materials between 648° and 816°C. The mass transfer rate of the nickel-base alloys is very much higher at 816°C compared to 300 series stainless steels under comparable conditions. Similar findings were noted by Russian investigators (Reference 3) in comparable high temperature evaluations.

The cold-leg deposits in both the Inconel and Hastelloy systems were composed primarily of nickel with small amounts of chromium and virtually no iron. The depth of intergranular penetration measured after 2000 hours between

704 and 816°C was 1 to 2 mils. Extrapolation of time would result with approximately 6.57 mils/year material loss.

The deposits found in the stainless steel systems were composed predominantly of chromium with small equal amounts of iron and nickel. The steels containing 18% chromium and 10% nickel (types 304 and 316) were the most corrosion resistant of the various types tested. Test results from Reference 2 indicated a corrosion rate at 816°C of approximately 2.92 mils/year.

Of equal importance when selecting materials for sodium service concerns the effect of oxygen contamination on corrosion. Contrary to the high mass transfer rates of nickel-base alloys resulting from high temperature levels (816°C), increases in oxygen content levels up to 500 ppm had no measurable affect on the material corrosion rates. However, for stainless steel, the oxygen content of the sodium is one of the most important parameters. Test results (Reference 3) indicate that if the oxygen level is reduced from 25 to 10 ppm the corrosion rate is reduced by 50% at 650°C. For an oxygen content level of 10 ppm the corrosion rate of stainless steel is approximately 2.64 mils/year. (This material loss rate was used for the FACC baseline sodium receiver analysis at an operating temperature of 816°C.) Therefore, this study implies that a greater latitude in sodium purity can be permitted for nickel-base alloys than for stainless steels.

Figure 11 presents a comparison of corrosion rates (mils/year) for 300 series stainless steels from References 1 and 2. For an oxygen content of 10 ppm and a temperature range from 700 to 816°C, good data correlation can be seen. The corrosion rate curves from the two references at 25 ppm oxygen content correlate at 650°C only, and differ by 8 mils/year at an operating temperature of 816°C. An oxygen content of 10 ppm was assumed for the baseline receiver design analysis.

4.3 CARBURIZATION OF STAINLESS STEEL

Research studies indicate that a reduction of room temperature ductility of 304 and 316 stainless steel is likely with increases in carbon content when the materials are exposed to liquid sodium. This carbon increase can be attributed to the following:

- Carbon dioxide (CO_2) impurities in the system are reduced by the molten sodium to form carbon and oxides.

- Higher than normal carbon percentages present in the material following manufacture.
- Small amounts of carbon present in the sodium.

Long term sodium loop tests (Reference 2) at 650°C show that the average carbon levels in both stainless materials (304 and 316) increased approximately .25%. Both material specimens contained carbon gradients through their cross-sections. The carbon levels that resulted did not materially affect the high temperature ductility of the materials. The type of carbide resulting from the carburization of the steel surface was identified as Fe_4Mo_2C, which is dispersed in the steel matrix.

By contrast, data presented in Reference 3 showed only small increases in the carbon content. For long term exposure (1300 hours) the exposed samples indicated that the carbon content increased slightly to approximately .036%. Further testing (Reference 4) was conducted to evaluate the room temperature mechanical properties of the stainless steel specimens. These test results indicated that the tensile strength of the exposed sample was above the minimum value specified by the ASTM for type 304 stainless steel pipe, whereas the yield strength was at the minimum value specified.

The filling procedure for the baseline sodium receiver is outlined in a later section of this report titled "Sodium Handling". The handling, cleaning, and filling procedure described therein will ensure very low levels of impurities trapped within the system after filling. Therefore, we are not anticipating carburization (decrease in ductility) of the stainless steel receiver material.

5.0 SODIUM HANDLING

Commercial sodium is available and can be purchased in brick form (1, 25, 5, 12 pound sizes) and cast solid form. These forms are available in regular purity and argon (reactor) purity grades. The argon (reactor) grade sodium has fewer impurities than the regular grade, and will be used in the baseline receiver tank.

The brick forms of sodium are packed and delivered in returnable 55-gallon steel barrels. These barrels are fitted with airtight covers to maintain a protective nitrogen atmosphere. Cast solid sodium is available in 55-gallon steel drums and in 5-gallon steel pails. Sodium delivered in these non-

returnable containers can be heated directly and dispensed as a liquid. Figure 12 shows a sodium-filling system which is currently being used at FACC to service experimental sodium/sulfur battery cells. This system will be utilized to fill the baseline sodium receiver tank. (The filling procedure is discussed in the section 5.1 of this report). The closed-filling-system illustration shown in Figure 12 reduces handling costs and eliminates oxide formation during the filling procedure. The empty 5-gallon sodium pails must be cleaned free of sodium before disposal or other use. Tech-Report 015 describes safety precautions which pertain to container cleaning.

5.1 RECEIVER PREPARATION AND FILLING

The corrosion data presented in the previous sections of this report indicates the importance of minimizing the oxygen level (ppm) and oxides formed when filling the sodium (baseline) receiver. In an effort to minimize these corrosion reactants the following surface cleaning treatment and filling procedure is recommended:

1. Vapor degrease component parts of receiver tank prior to welding with trichloracthlyene for 45 minutes.
2. Abrasive cleaning of all welded joints by impinging with Aluminum oxide material (#60). This process should be done during the assembly sequence to all welds exposed to sodium.
3. Nitric acid (technical grade) dip of completely assembled receiver tank.
4. Rinse receiver in distilled water and then in ethylene alcohol.
5. Dry receiver in oven.

After the above steps are completed the receiver tank is ready to be filled. To eliminate and remove oxides, the following filling procedure is recommended:

(Refer to Figure 12)

1. Remove trapped air in the system - Close valve D first, then, in the following sequence, open valves C, B, and A. This will allow the entire system to be evacuated by the vacuum accumulator.
2. Fill bellows with Molten sodium - Close all valves except valve D. The volume of molten sodium flowing into the bellows is indicated by the position indicator. When the bellows maximum capacity is reached valve D is closed.

3. Remove trapped air inside receiver tank - The receiver tank is connected to the system fill line shown in the Figure 12. To evacuate the tank valves B and C remain closed and valve A is opened.
4. Fill receiver tank with molten sodium - Close valves A and D, actuate bellows with nitrogen gas pressure and pump molten sodium into tank. To obtain the required sodium purity the sodium is pumped through a 30 micron and 10 micron filter.

After the receiver tank is filled to the correct level the intake pipe is capped-off and the tank is agitated for approximately 15 minutes. During this time, the oxide layer on the inside surface of the receiver will be removed by the hot sodium and carried in suspension. After approximately 30 minutes the hot sodium and oxide impurities are removed from the receiver tank leaving an oxide-free surface. The sodium removed from the receiver tank can be filtered and reused. After completing steps C and D once again, the receiver tank is filled and ready to be mated with the other components.

6.0 CONCLUSIONS

1. Sodium has been in extensive use as a heat transfer medium throughout the United States and Europe for many years.
2. The high heat transfer coefficient of sodium and low vapor pressure (less than 1 atmosphere) make it possible to design a simple and efficient solar receiver.
3. The corrosion behavior of stainless steel alloys in hot sodium is well studied and very predictable. The low corrosion rates of stainless steel make it an excellent material for a long life (15 years) solar receiver. In addition, stainless steel material is relatively inexpensive and readily available.
4. The handling, filling, filtering, and operating procedures associated with hot sodium are very well established. The impurity level in the FACC baseline receiver can be held to as low as 10 ppm.
5. Technical Report number 015 shows that hot sodium is a very safe medium when handled properly.

References

1. McKisson, R.L., "Corrosion and Mass Transfer", Sodium Technology, Atomics International, 1970.

2. Thorley, A.W., Tyzack, C., "Corrosion Behavior of Steels and Nickel Alloys in High-Temperature Sodium", Alkai-Metal Coolants, Proceedings of Symposium, Vienna Austria, 1967.

3. Devan, J.H., "Corrosion of Iron-and Nickel-Base Alloys in High-Temperature Sodium and NAK", Alkai-Metal Coolants, Proceedings of Symposium, Vienna Austria, 1966.

4. Ratz, G.A., "Effect of Liquid Sodium on Welded AISI type 304 Stainless Steel Pipe", Nucl. Appl. V17, No. 2,1973.

5. "Sodium (NAK) Supplement", Liquid-Metals Handbook, C.B. Jackson, Ed., U.S. Atomic Energy Commission 1955.

6. "Handling Metallic Sodium on A Plant Scale", U.S. Industrial Chemicals Co. Third Ed. 1959.

7. Sittig, M., Sodium Its Manufacture, Properties and Uses, Reinhold Publishing Corp., 1956.

8. Kay, R.E., "Application of Sodium Wicking Materials to the Sodium/Sulfur Cell", In-house Preliminary Report, 1979.

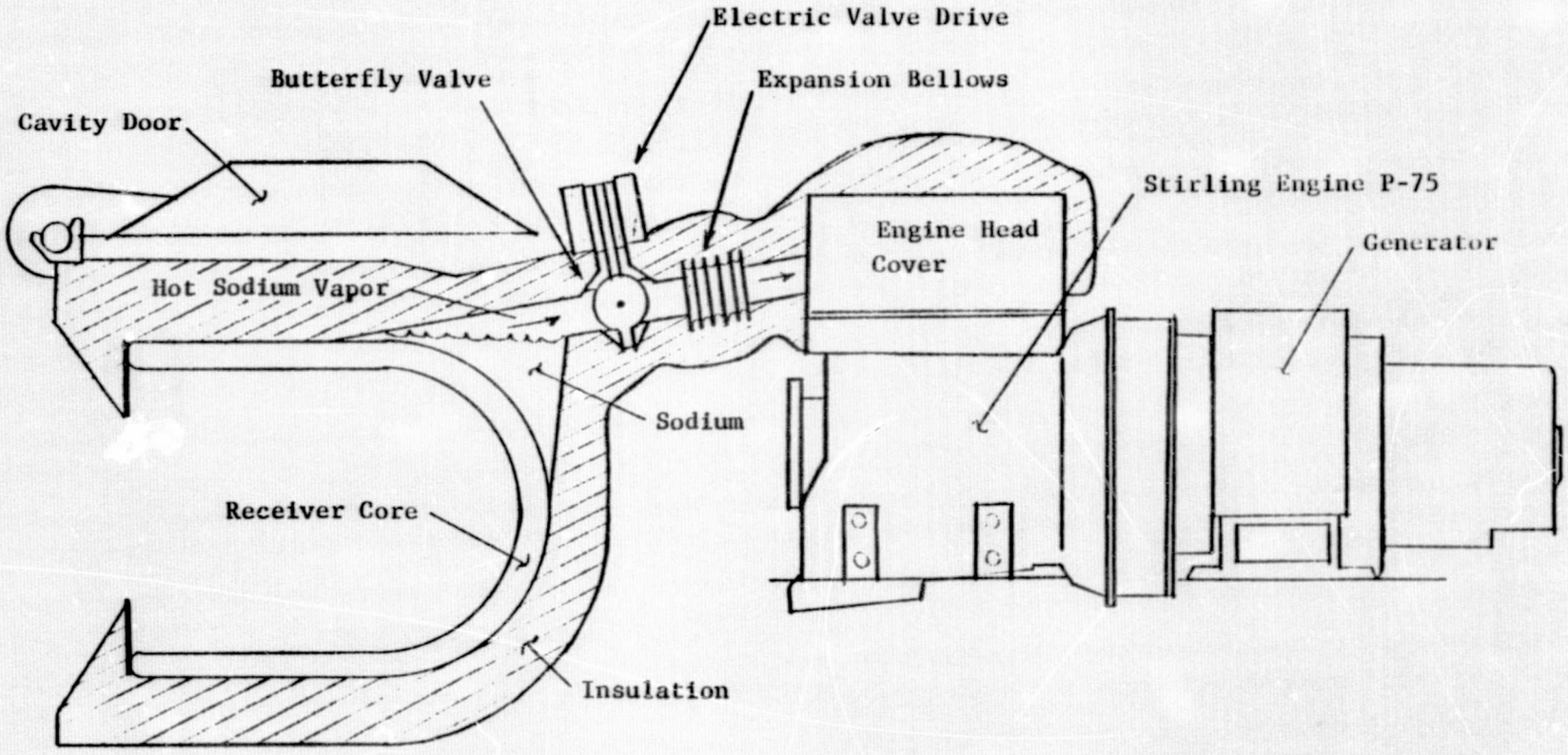
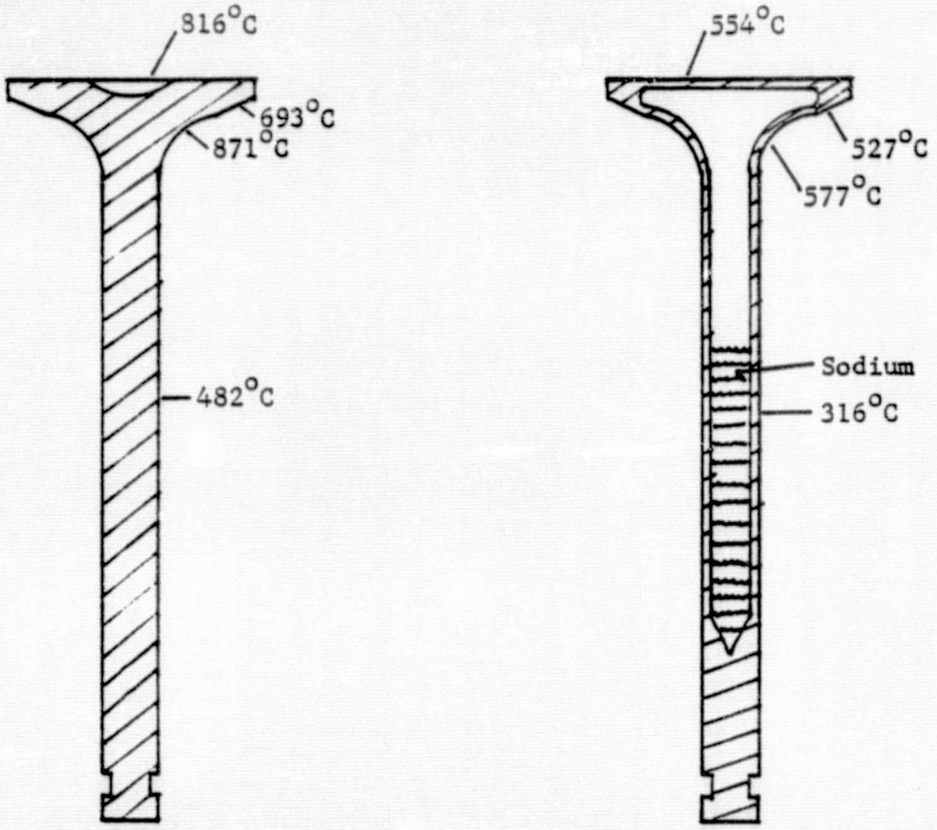


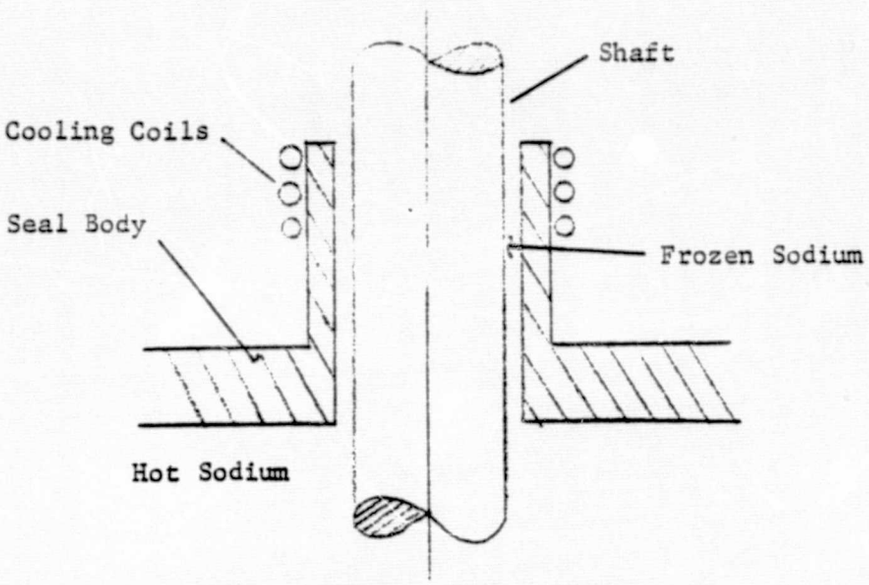
FIGURE 1. BASELINE SYSTEM



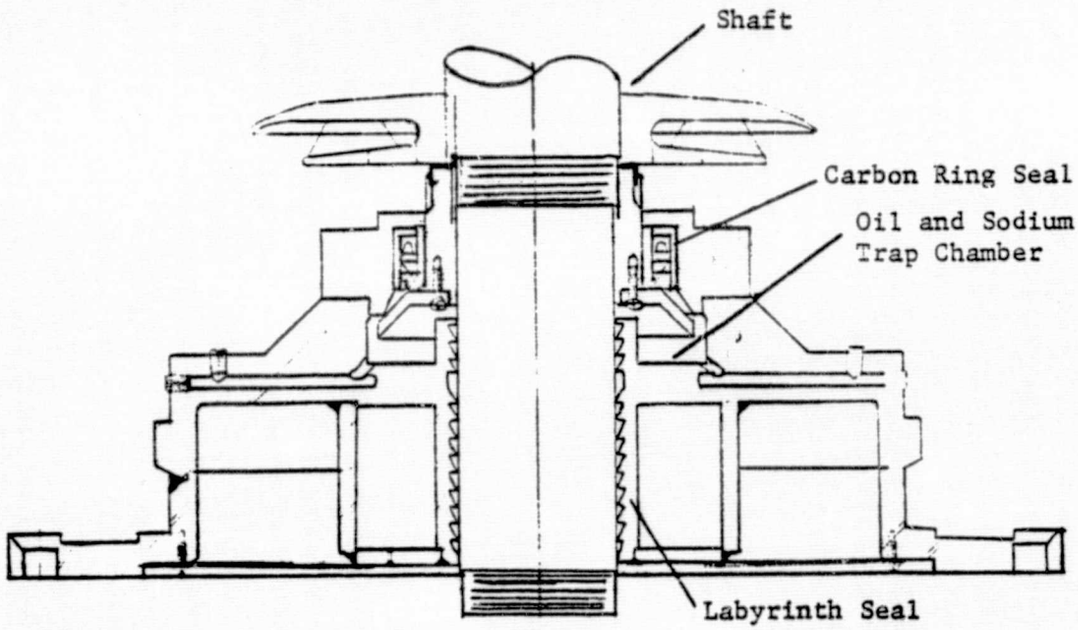
Solid Stem

Hollow Stem and Head
(sodium filled)

Figure 2. Cross-sections of Automotive Valves Showing Temperature Comparisons (Reference 7)



Cross-Section Of Frozen Seal



Cross-Section Of Gas Seal

Figure 3. TYPICAL SEALS USED WITH SODIUM

(Reference 5)

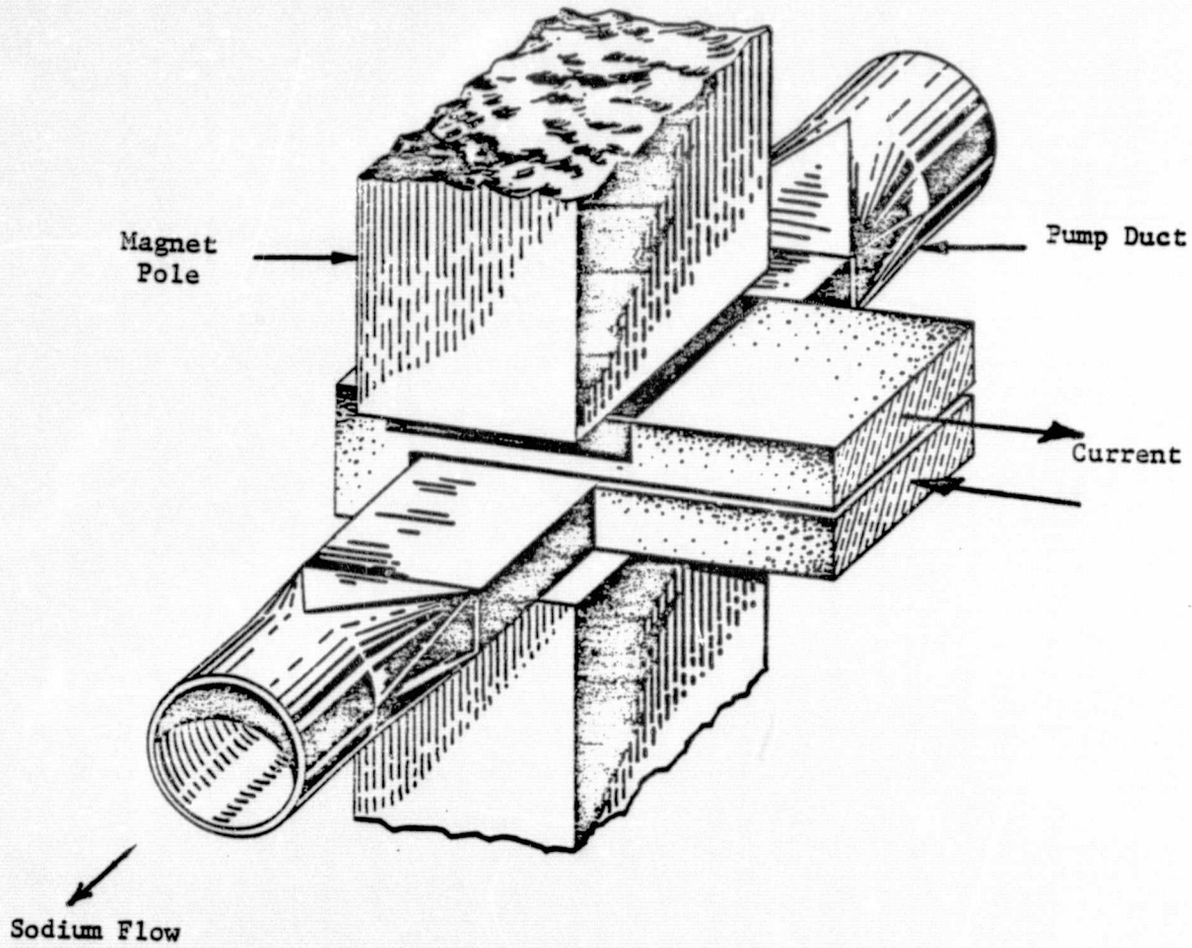
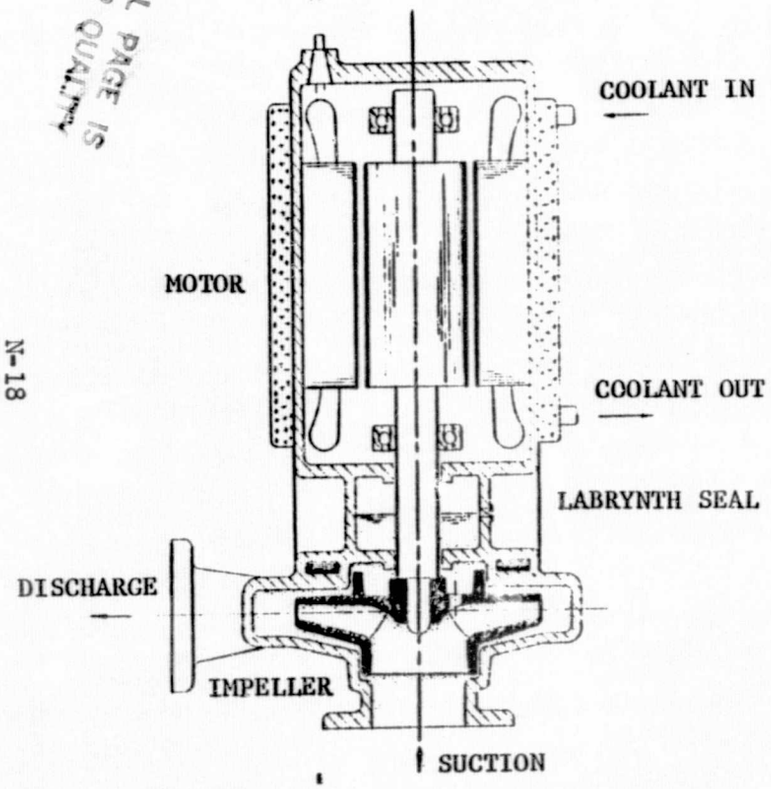


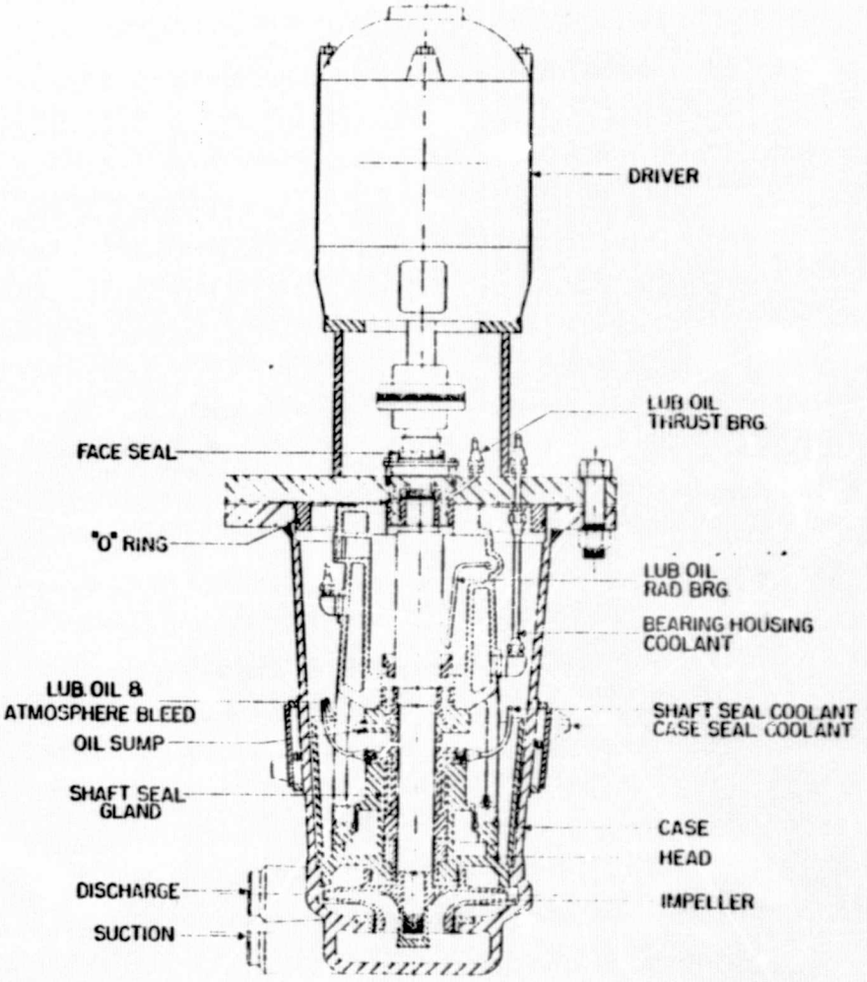
Figure 4. D.C. FARADAY-TYPE PUMP
(Reference 5)

ORIGINAL PAGE IS
OF POOR QUALITY

ORIGINAL PAGE IS OF POOR QUALITY



Gas-Sealed Centrifugal Pump



Single Stage Centrifugal Pump

Figure 5. Typical Mechanical Pumps

(Reference 5)

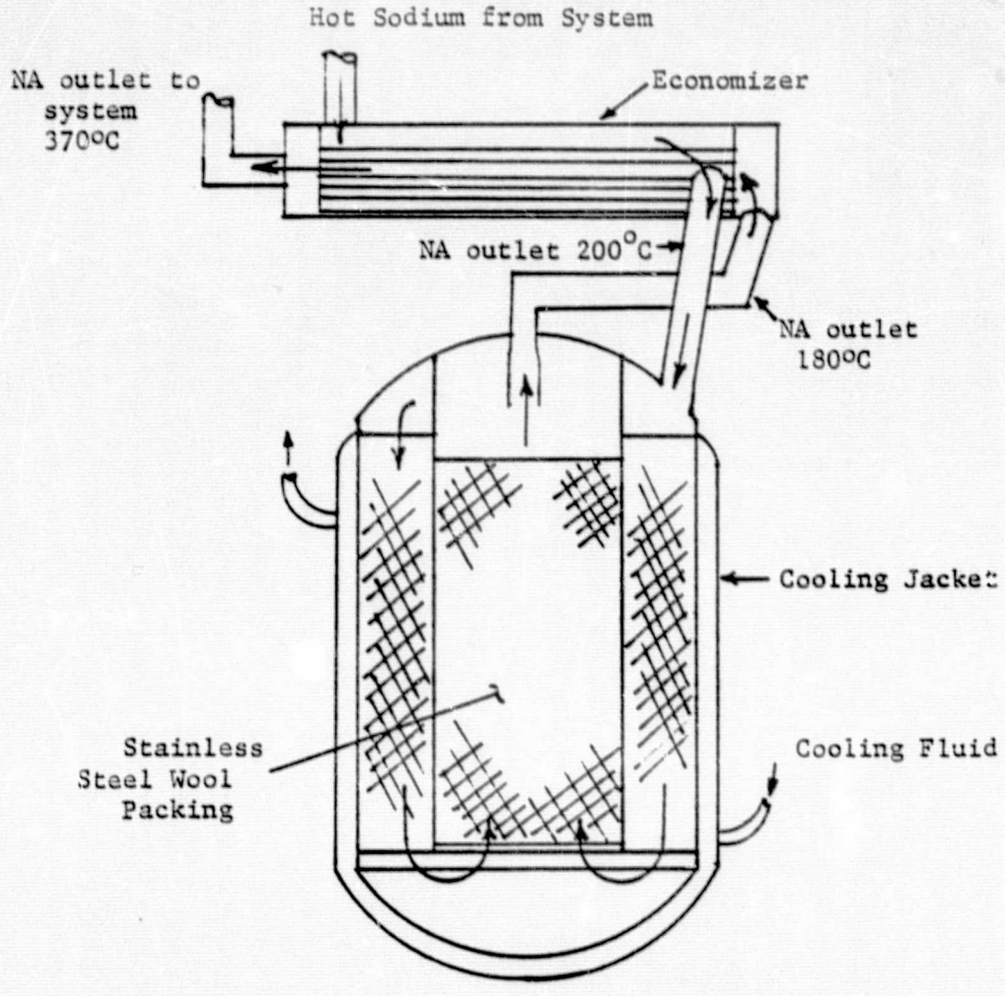


Figure 6. Cross-Section of Cold Trap (Reference 7)

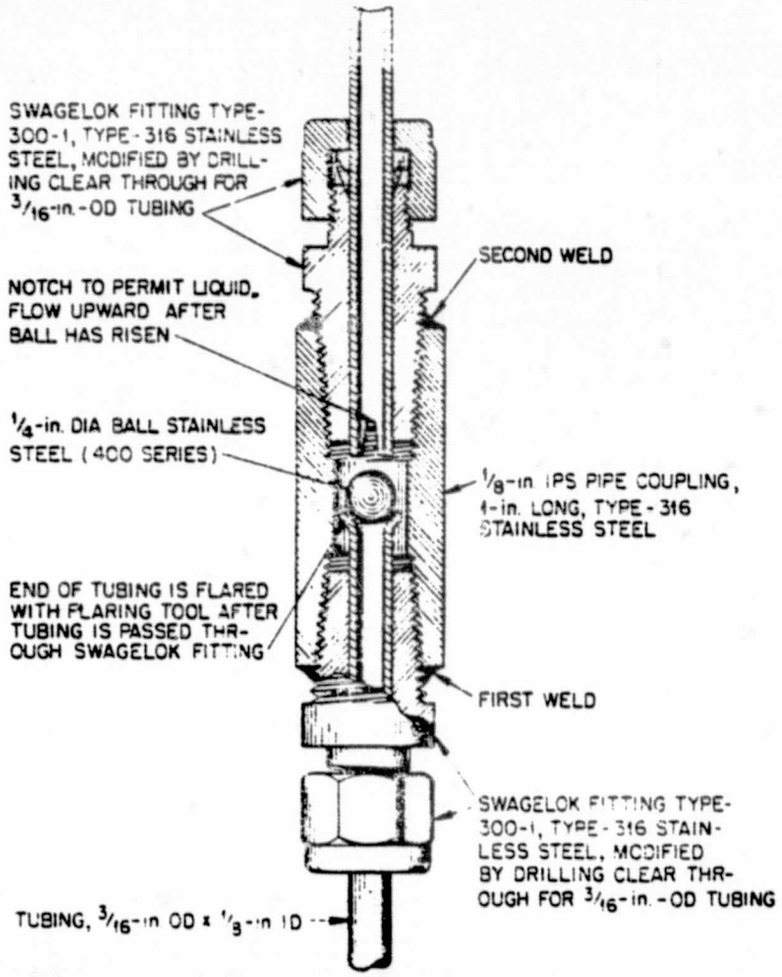
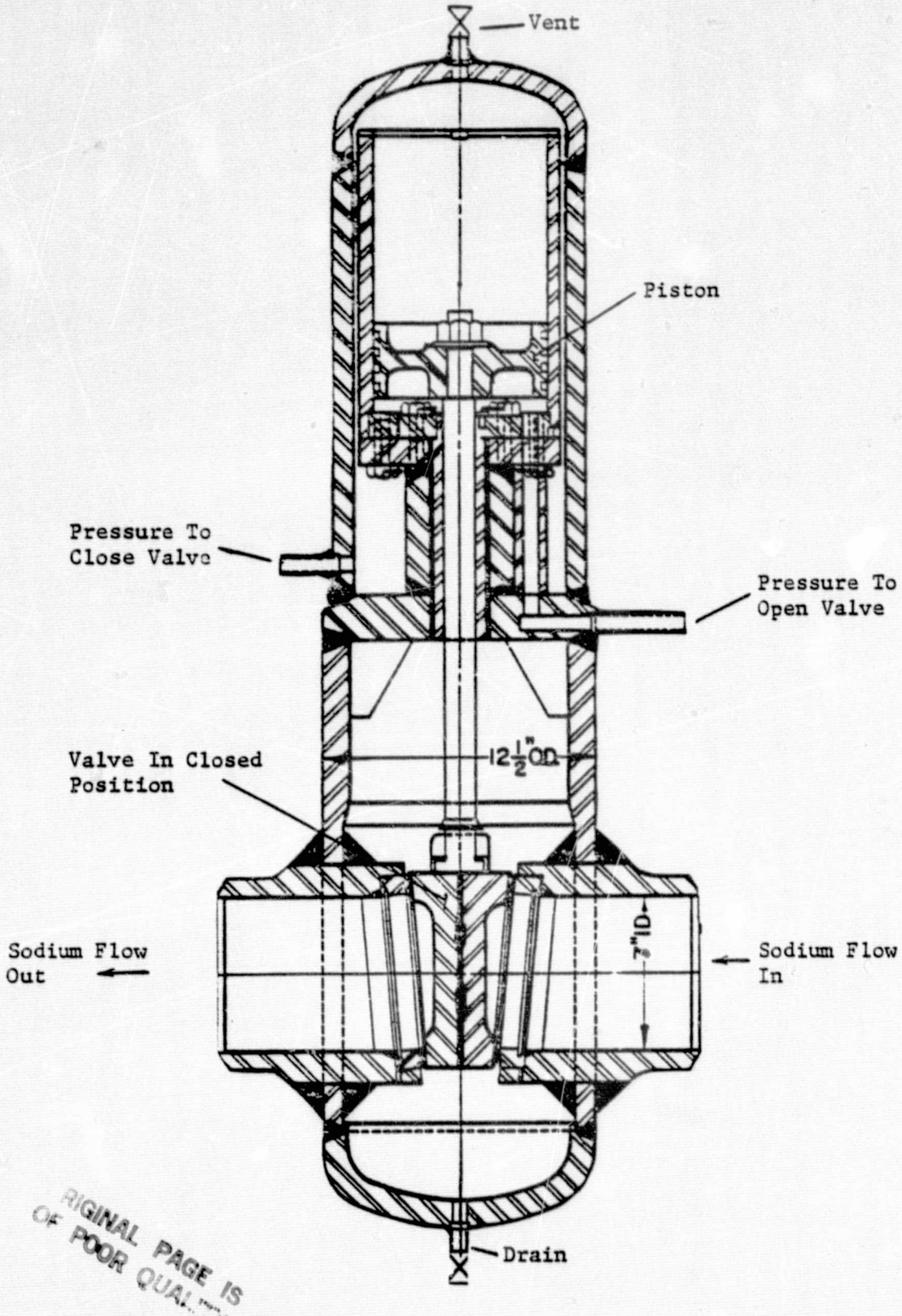


Figure 7. BALL CHECK VALVE
(Reference 5)



RIGINAL PAGE IS
OF POOR QUAL

Figure 8. PISTON OPERATED SODIUM VALVE
(Reference 5)

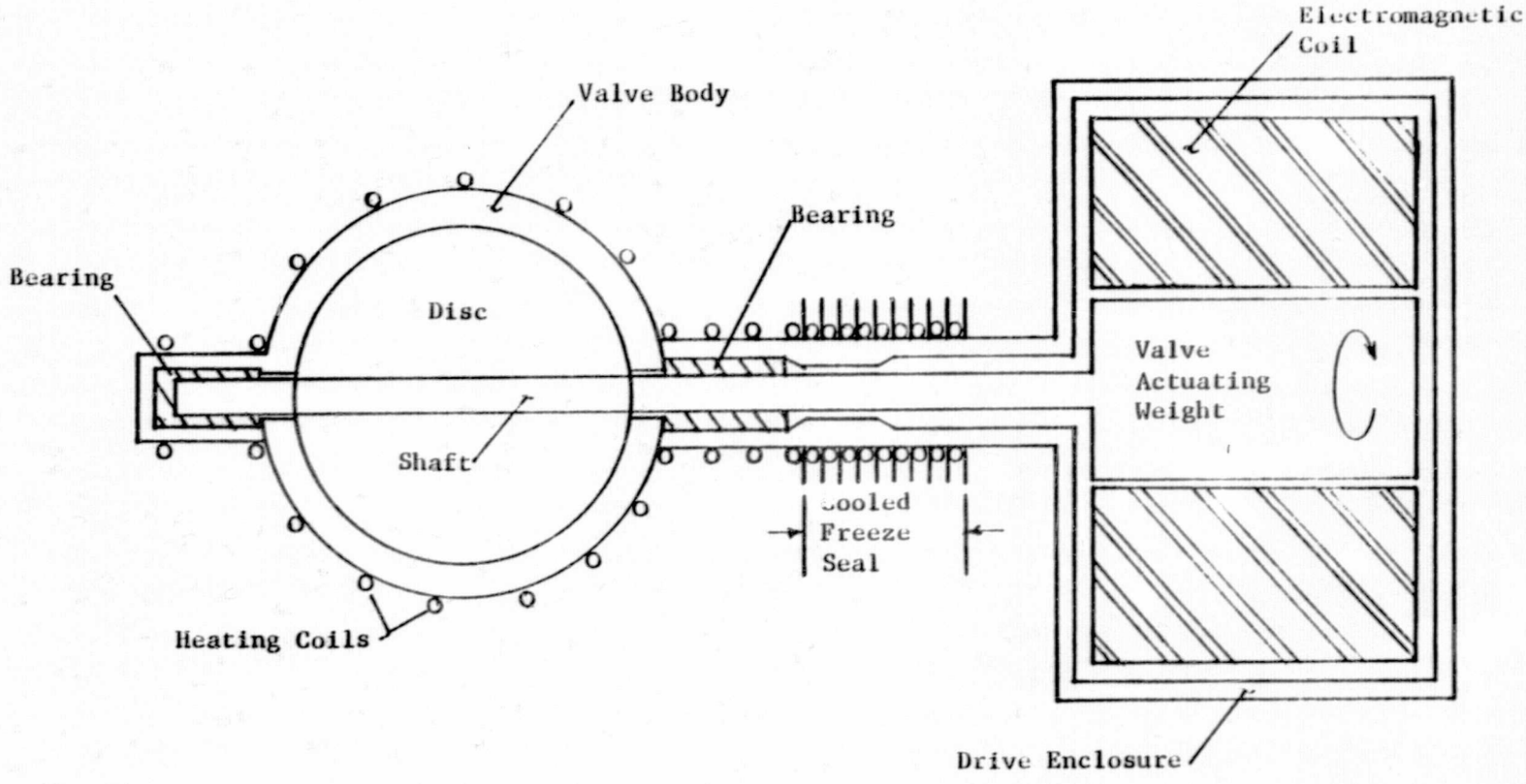


Figure 9. SODIUM BUTTERFLY VALVE

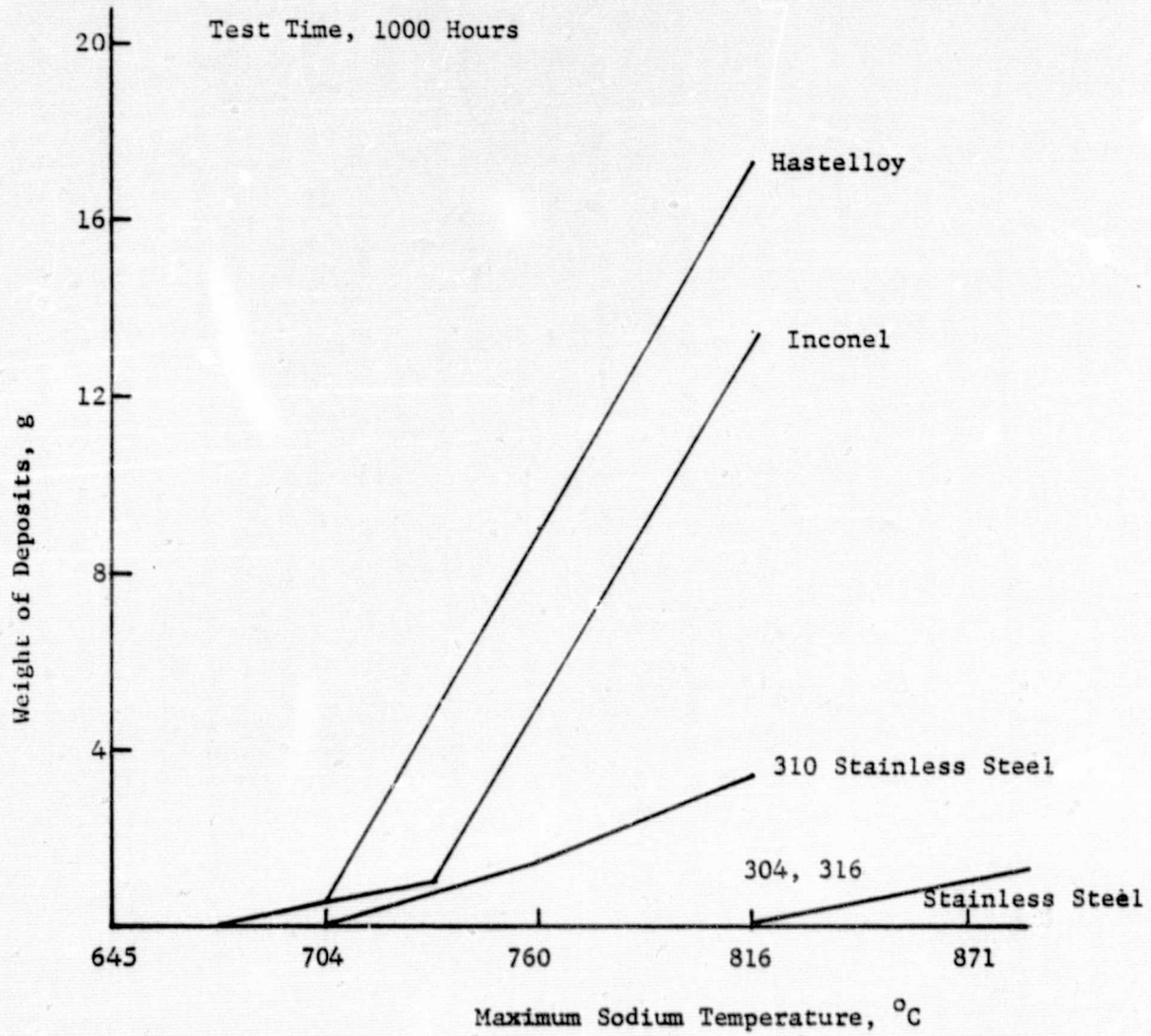


Figure 10 Mass Transfer Rates of Nickel-base Alloys and Stainless Steel

(Reference 3)

FIGURE COMPARISON OF SODIUM CORROSION DATA
300 SERIES STAINLESS STEEL

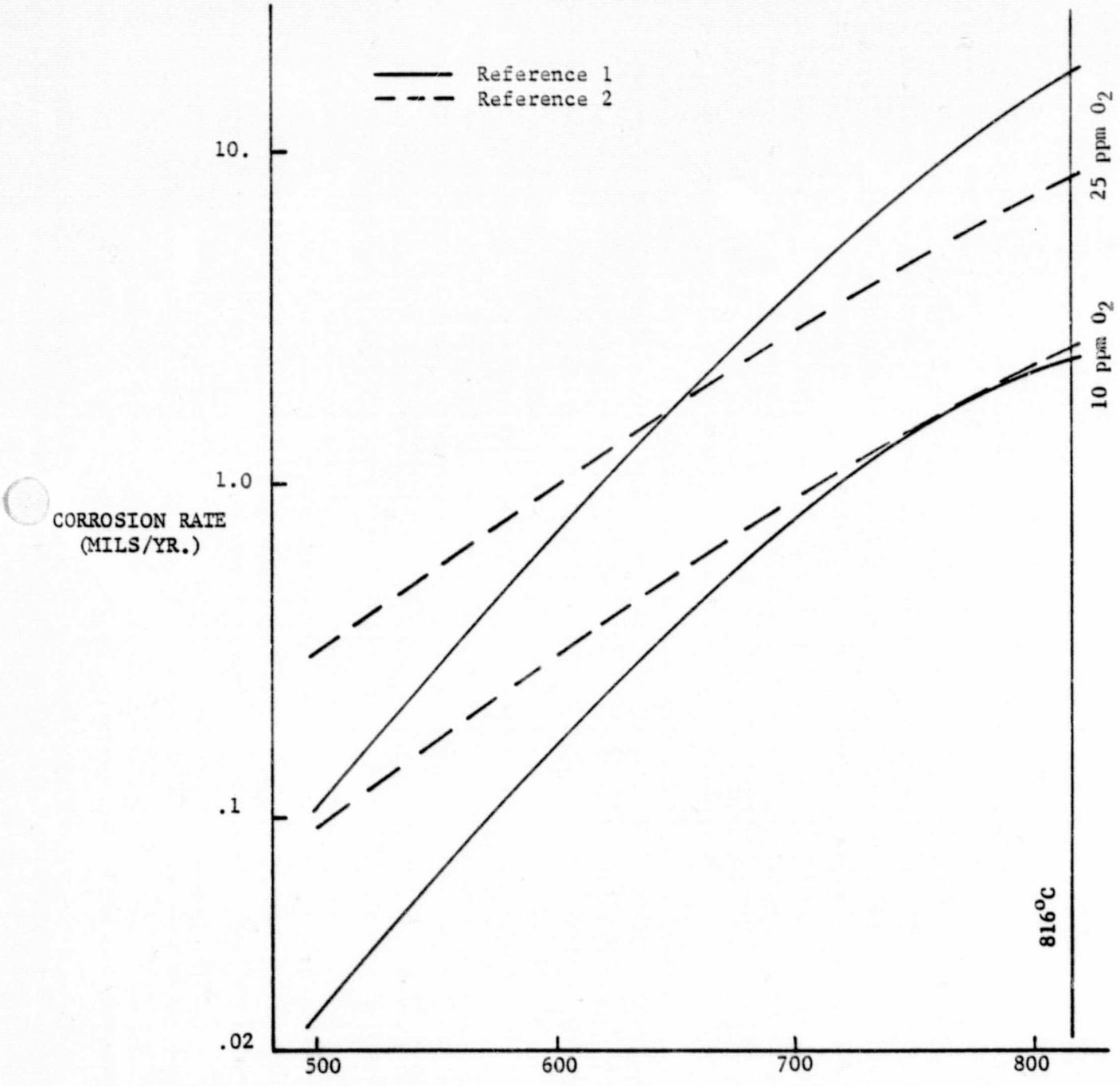


Figure 11. SODIUM TEMPERATURE, (°C)

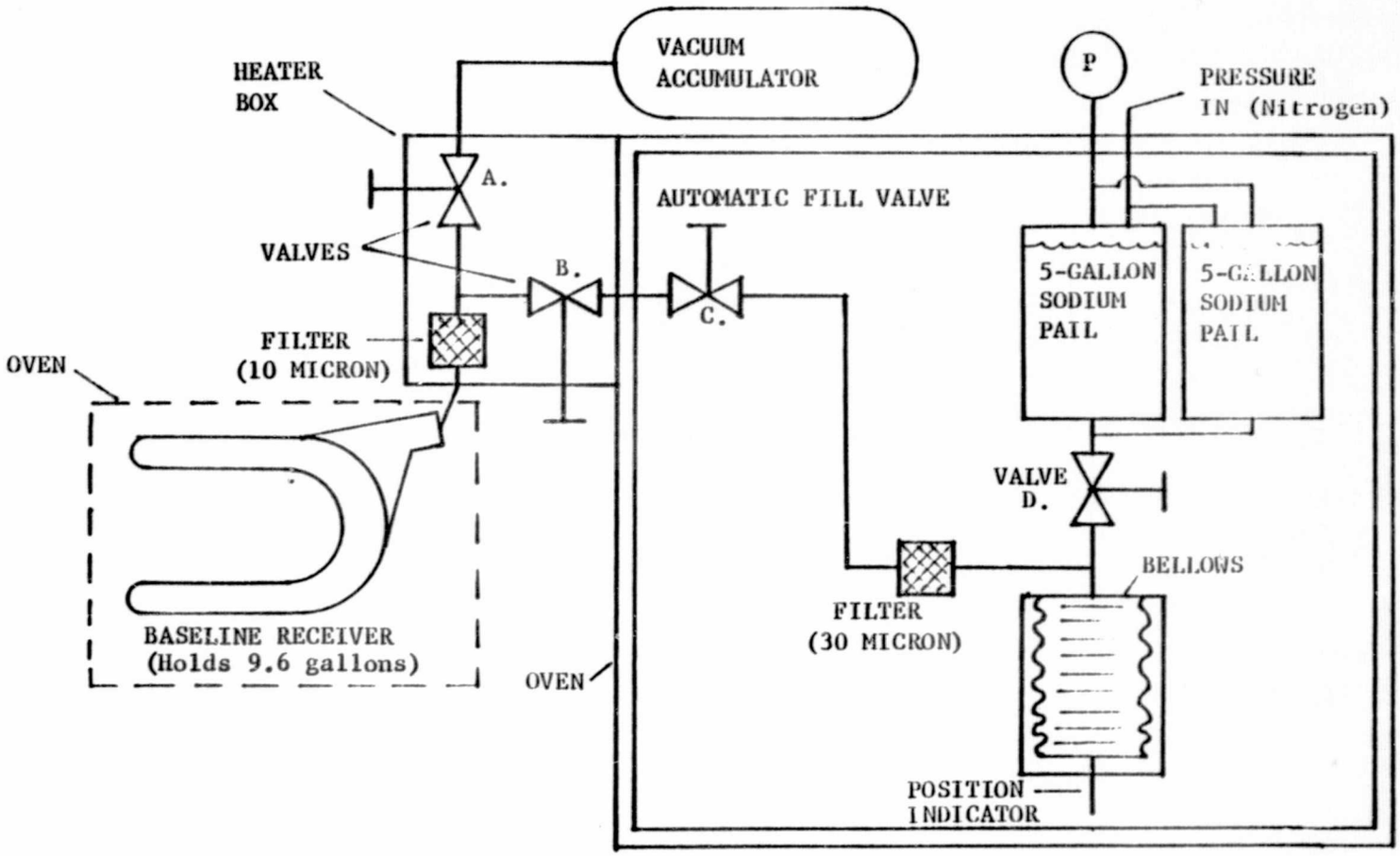


Figure 12. SODIUM-FILLING SYSTEM